National Library of Canada
Bibliothèque nationale du Canada

Canadian Theses Service
Service des thèses canadiennes

Ottawa, Canada
K1A 0N4

NOTICE

The quality of this microform is heavily dependent upon the quality of the original thesis submitted for microfilming. Every effort has been made to ensure the highest quality of reproduction possible.

If pages are missing, contact the university which granted the degree.

Some pages may have indistinct print especially if the original pages were typed with a poor typewriter ribbon or if the university sent us an inferior photocopy.

Previously copyrighted materials (journal articles, published tests, etc.) are not filmed.

Reproduction in full or in part of this microform is governed by the Canadian Copyright Act, R.S.C. 1970, c. C-30.

AVIS

La qualité de cette microforme dépend grandement de la qualité de la thèse soumise au microfilmage. Nous avons tout fait pour assurer une qualité supérieure de reproduction.

S'il manque des pages, veuillez communiquer avec l'université qui a conféré le grade.

La qualité d'impression de certaines pages peut laisser à désirer, surtout si les pages originales ont été dactylographiées à l'aide d'un ruban usé ou si l'université nous a fait parvenir une photocopie de qualité inférieure.

Les documents qui font déjà l'objet d'un droit d'auteur (articles de revue, tests publiés, etc.) ne sont pas microfilmés.

La reproduction, même partielle, de cette microforme est soumise à la Loi canadienne sur le droit d'auteur, SRC 1970, c. C-30.

NL-339 (r. 88/04)

Canada

THE UNIVERSITY OF ALBERTA

REACTION RATE MULTIPLICITY DURING THE REDUCTION OF N_2O AND NO BY CO ON PLATINUM

by

Jing Ye

A THESIS

SUBMITTED TO THE FACULTY OF GRADUATE STUDIES AND RESEARCH
IN PARTIAL FULFILMENT OF THE REQUIREMENTS FOR THE DEGREE
OF MASTER OF SCIENCE

DEPARTMENT OF CHEMICAL ENGINEERING

EDMONTON, ALBERTA
FALL 1988

Permission has been granted to the National Library of Canada to microfilm this thesis and to lend or sell copies of the film.

The author (copyright owner) has reserved other publication rights, and neither the thesis nor extensive extracts from it may be printed or otherwise reproduced without his/her written permission.

L'autorisation a été accordée à la Bibliothèque nationale du Canada de microfilmer cette thèse et de prêter ou de vendre des exemplaires du film.

L'auteur (titulaire du droit d'auteur) se réserve les autres droits de publication; ni la thèse ni de longs extraits de celle-ci ne doivent être imprimés ou autrement reproduits sans son autorisation écrite.

ISBN 0-315-45774-0

THE UNIVERSITY OF ALBERTA

RELEASE FORM

NAME OF AUTHOR Jing Ye

TITLE OF THESIS REACTION RATE MULTIPLICITY DURING THE REDUCTION OF N_2O AND NO BY CO ON PLATINUM

DEGREE FOR WHICH THESIS WAS PRESENTED MASTER OF SCIENCE

YEAR THIS DEGREE GRANTED FALL 1988

Permission is hereby granted to THE UNIVERSITY OF ALBERTA LIBRARY to reproduce single copies of this thesis and to lend or sell such copies for private, scholarly or scientific research purposes only.

The author reserves other publication rights, and neither the thesis nor extensive extracts from it may be printed or otherwise reproduced without the author's written permission.

(SIGNED) ...Jing...Ye.........

PERMANENT ADDRESS:

...#1..Xiao.Long.st......
...Dalian..................
...P..R..of.china.........

DATED ..Oct.12...........1988

THE UNIVERSITY OF ALBERTA

FACULTY OF GRADUATE STUDIES AND RESEARCH

The undersigned certify that they have read, and recommend to the Faculty of Graduate Studies and Research, for acceptance, a thesis entitled REACTION RATE MULTIPLICITY DURING THE REDUCTION OF N_2O AND NO BY CO ON PLATINUM submitted by Jing Ye in partial fulfilment of the requirements for the degree of MASTER OF SCIENCE in CHEMICAL ENGINEERING.

David T. Lynch
D. T. Lynch (Supervisor)

I. G. Dalla Lana
I. G. Dalla Lana

N. O. Egiebor

Date: September 26, 1988

ABSTRACT

The reduction reactions of N_2O by CO and NO by CO on $Pt/\gamma\text{-}Al_2O_3$ were studied using an external recycle reactor. The catalyst contained 0.5 wt% platinum, with the Pt located in a thin shell on the external portion of cylindrical pellets. The initial objectives of the study were to investigate the occurrence of multiplicity behavior for the N_2O+CO reaction and to use such behavior to discriminate among several mechanisms. The study was later extended to include an examination of the NO+CO reaction system.

It was observed that the N_2O+CO reaction displays multiplicity behavior over the temperature range 170 to 246°C for a total reaction pressure at 1 atm, with N_2O and CO feed compositions in the range 0.1 to 2.0%. It was found that N_2O+CO reaction behavior can be quantitatively described by a Langmuir-Hinshelwood type reaction mechanism with a self-exclusion effect for CO adsorption. Reaction multiplicity behavior for NO+CO was also observed under the experimental conditions. The main reaction products were N_2O, N_2 and CO_2. The distribution of nitrogen containing products (N_2O/N_2) depended strongly on the reactant conversion. High ratios of N_2O to N_2 were achieved when the conversion was high, with low ratios obtained for low conversions. Both the experimental results and the model discrimination study indicated that N_2O is an intermediate in the overall reaction. However, it was not ruled out that part of the N_2 was formed directly from NO decomposition.

ACKNOWLEDGMENTS

The author would like to express her thanks and appreciation to Dr. D. T. Lynch, for his patience, support and guidance throughout the course of this work. The author also wants to thank the DACS center personnel for their assistance in the use of the university computing facilities. Thanks are extended to graduate students for their many helpful discussions and friendship over the two past years. Most of all, the author wishes to thank her parents for their love, encouragement and support.

Table of Contents

Chapter Page

1. INTRODUCTION AND REVIEW OF LITERATURE 1

1.1 Introduction 1

1.2 Literature Review 4

1.2.1 CO Adsorption 4

1.2.2 CO Desorption 5

1.2.3 CO Oxidation 6

1.2.4 N_2O Adsorption 7

1.2.5 N_2O Desorption 8

1.2.6 N_2O Decomposition 9

1.2.7 Formation of N_2O 13

1.2.8 Formation of N_2 15

1.2.9 Mechanisms of N_2O+CO 16

1.2.10 NO Adsorption 19

1.2.11 NO Decomposition 22

1.2.12 Mechanisms of NO+CO 24

1.2.12.1 Unimolecular Mechanism 25

1.2.12.2 Bimolecular Mechanism 25

1.2.12.3 Disproportionation Mechanism ...26

2. DESCRIPTION OF THE EXPERIMENTAL APPARATUS 28

2.1 Feed Stream Regulation 28

2.2 Preheat Compartment 30

2.3 Catalytic Reactor 32

2.4 Experimental Materials 34

2.5 Preliminary Reactor Tests 35

3. EXPERIMENTAL OBSERVATIONS FOR THE N_2O+CO REACTION ...37

3.1 Introduction 37

3.2 Experimental Observations 37
3.2.1 Reactor Behavior at 190°C 38
3.2.2 Reactor Behavior at 210°C 43
3.2.3 Reactor Behavior at 246°C 46
3.2.4 Adsorption Inhibition Effects 49
3.2.5 Formation of Molecular Oxygen 50
3.2.6 Transition Boundary 52
3.3 Inter- and Intraparticle Mass Transfer Effects .56
3.4 Summary 60
4. EXAMINATION OF MECHANISMS FOR THE N_2O+CO REACTION ...61
4.1 Introduction 61
4.1.1 Oxygen Desorption (step 4.3) 62
4.1.2 Nitrous Oxide Adsorption (step 4.4) 63
4.1.3 Remaining Reaction steps 63
4.2 Mechanism 1 65
4.3 Mechanism 2 66
4.4 Mechanism 3 72
4.5 Mechanism 4 75
4.6 Mechanism 5 76
4.7 Mechanism 6 78
4.8 Mechanism 7 79
4.9 Mechanism 8 81
4.10 Mechanism 9 84
4.11 Mechanism 10 87
4.12 Mechanism 11 97
4.13 Summary 104
4.14 Nomenclature 104

5. EXPERIMENTAL OBSERVATIONS FOR THE NO+CO REACTION ...106

  5.1 Preliminary 106

  5.2 Effect of Reaction Temperature on the Reactor Behavior 108

    5.2.1 CO Conversion 108

    5.2.2 NO Conversion 113

    5.2.3 CO_2 Formation Rate 117

    5.2.4 Nitrous Oxide in the Reactor 121

  5.3 Effect of Total Flow Rate on the Reactor Behavior 121

  5.4 Selectivity 125

  5.5 Summary 136

6. EXAMINATION OF MECHANISMS FOR THE NO+CO REACTION ...138

  6.1 Introduction 138

  6.2 Reaction Steps 139

  6.3 Mechanism 1 141

  6.4 Mechanism 2 144

  6.5 Mechanism 3 146

  6.6 Mechanism 4 150

  6.7 Summary 152

  6.8 Nomenclature 156

7. CONCLUSIONS 158

BIBLIOGRAPHY 159

APPENDIX 1. CALIBRATION CURVES 165

APPENDIX 2. EXPERIMENTAL DATA FOR N_2O+CO 170

APPENDIX 3. CALCULATIONS FOR THE N_2O+CO REACTION 184

APPENDIX 4. EXPERIMENTAL DATA FOR THE NO+CO REACTION 199

APPENDIX 5. BALANCE EQUATIONS FOR N_2O+CO 220

APPENDIX 6. BALANCE EQUATIONS FOR NO+CO 224
APPENDIX 7. COMPUTER PROGRAMS 228

List of Tables

Table Page

4.1 Values of Parameters for Mechanisms 69

4.2 Reaction Steps Involved in Mechanisms 69

4.3 Values of Parameters for Predictions in Figure 4.8 to 4.10 94

4.4 The Values of Kinetic Parameters for Mechanism 11 102

6.1 Values of Parameters for Mechanisms 145

List of Figures

Figure Page

2.1 Overall Equipment Schematic 29

2.2 Preheat Compartment Schematic 31

3.1 CO_2 Formation Rate for N_2O+CO at 190°C 39

3.2 CO Conversion for N_2O+CO at 190°C 42

3.3 CO_2 Formation Rate for N_2O+CO at 210°C 44

3.4 CO Conversion for N_2O+CO at 210°C 45

3.5 CO_2 Formation Rate for N_2O+CO at 246°C 47

3.6 CO Conversion for N_2O+CO at 246°C 48

3.7 Effect of the N_2O Concentration on the Reaction Rate 51

3.8 Calculated O_2 Concentrations in the Reactor Exit 53

3.9 Effect of Temperature on the Multiplicity Behavior 54

4.1 CO Conversion Predictions from Mechanism 2 70

4.2 CO Conversion Predictions from Mechanism 3 74

4.3 CO Conversion Predictions from Mechanism 5 77

4.4 CO Conversion Predictions from Mechanism 6 80

4.5 CO Conversion Predictions from Mechanism 7 82

4.6 CO Conversion Predictions from Mechanism 8 83

4.7 CO Conversion Predictions from Mechanism 9 86

4.8 CO Conversion Predictions from Mechanism 10 at 210°C 88

4.9 CO Conversion Predictions from Mechanism 10 at 190°C 90

Figure Page

4.10 CO Conversion Predictions from Mechanism 10 at 246°C 91

4.11 Arrhenius Analysis for Activation Energies 92

4.12 Overall Predictions from Mechanism 10 at 210°C 95

4.13 Overall Predictions from Mechanism 10 at 246°C 96

4.14 CO Conversion Predictions from Mechanism 11 at 210°C 99

4.15 CO Conversion Predictions from Mechanism 11 at 190°C 100

4.16 CO Conversion Predictions from Mechanism 11 at 246°C 101

4.17 Arrhenius Analysis for Mechanism 11 Parameters 103

5.1 CO Conversion for NO+CO at 150°C, 200 SCCM 109

5.2 CO Conversion for NO+CO at 170°C, 200 SCCM 111

5.3 CO Conversion for NO+CO at 190°C, 200 SCCM 112

5.4 NO Conversion for NO+CO at 150°C, 200 SCCM 114

5.5 NO Conversion for NO+CO at 170°C, 200 SCCM 115

5.6 NO Conversion for NO+CO at 190°C, 200 SCCM 116

5.7 CO_2 Formation Rate for NO+CO at 150°C, 200 SCCM 118

5.8 CO_2 Formation Rate for NO+CO at 170°C, 200 SCCM 119

5.9 CO_2 Formation Rate for NO+CO at 190°C, 200 SCCM 120

5.10 N_2O Formation Rate for NO+CO at 150°C, 200 SCCM 122

Figure Page

5.11 N_2O Formation Rate for NO+CO at 170°C, 200 SCCM 123

5.12 N_2O Formation Rate for NO+CO at 190°C, 200 SCCM 124

5.13 CO Conversion for NO+CO at 170°C, 100 SCCM 126

5.14 CO Conversion for NO+CO at 170°C, 400 SCCM 127

5.15 NO Conversion for NO+CO at 170°C, 100 SCCM 128

5.16 NO Conversion for NO+CO at 170°C, 400 SCCM 129

5.17 CO_2 Formation Rate at 170°C, 100 SCCM 130

5.18 CO_2 Formation Rate at 170°C, 400 SCCM 131

5.19 N_2O Formation Rate at 170°C, 100 SCCM 132

5.20 N_2O Formation Rate at 170°C, 400 SCCM 133

5.21 Selectivity for NO+CO at 170°C, 100 SCCM 134

5.22 Selectivity for NO+CO at 190°C, 200 SCCM 135

6.1 Selectivity Predictions from Mechanism 1 143

6.2 Selectivity Predictions from Mechanism 2 147

6.3 Selectivity Predictions from Mechanism 3 149

6.4 Selectivity Predictions from Mechanism 4 151

6.5 CO Conversion Predictions from Mechanism 4 153

6.6 NO Conversion Predictions from Mechanism 4 154

6.7 N_2O Concentration Predictions from Mechanism 4 155

1. INTRODUCTION AND REVIEW OF LITERATURE

1.1 Introduction

The increasingly stringent regulations for automobile emissions have resulted in many recent studies being performed which have investigated the catalytic elimination of these pollutants. These studies have been primarily concerned with the oxidation of carbon monoxide (CO) and hydrocarbons, and with the reduction of the various oxides of nitrogen (NO_x, i.e. NO, N_2O, NO_2, etc.). The partitioning of CO in automobile emissions between the reduction reaction with NO, and the oxidation reaction with molecular oxygen (O_2) lies at the heart of the three-way catalytic converter systems (Summers and Hegedus, 1979). The proper operation of these systems requires that O_2 be present in approximately stoichiometric quantities, thus necessitating the use of computer control systems for monitoring and controlling the air to fuel ratio. The catalysts customarily used in these reactors are composed of various noble metals (Pt, Pd, Rh, Ru, etc.) supported on a high surface area carrier, typically γ-Al_2O_3.

The design and operation of these catalytic reaction systems are by no means simple or straightforward tasks. For example, the platinum catalyzed reduction of NO by CO, even in the absence of molecular oxygen, has been shown to display very complex behavior such as self-sustained composition oscillations (Adlhoch and Lintz, 1976; Adlhoch et al., 1981; Lesley and Schmidt, 1985; Schwartz and Schmidt, 1987) and steady-state multiplicity (Bolten et al., 1985; Adloch and Lintz, 1978). The mechanisms underlying these phenomena are not at present fully understood, but it is believed that a catalyst surface reconstruction process for Pt(100) could be responsible for some of the observed complex behavior. Such a process has recently been used to quantitatively explain similar phenomena for $CO+O_2$ oxidation on platinum (Lynch et al., 1986).

In studies concerned with the reduction of NO, it has often been found that nitrous oxide (N_2O) is formed in varying quantities (Shelef et al., 1968; Lambert and Comire, 1974; Pirug and Bonzel, 1977; Lorimer and Bell, 1979; Adlhoch and Lintz, 1978; Klein et al., 1985; Lim et al., 1986). While the exact mechanism by which NO is reduced by CO is still a matter of considerable controversy (Lorimer and Bell, 1979; Adlhoch and Lintz, 1978; Klein et al., 1985; Lim et al., 1986), it is thought that, for temperatures less than 300°C, N_2O is an intermediate in the overall reaction (Shelef et al., 1968). This view is supported by the observation that N_2O was the only product observed when nitrogen atoms reacted with chemisorbed oxygen on platinum (Halpern et al., 1981), even though it was initially expected that the simpler molecule NO would be the main product.

At the higher temperatures (500-600°C) encountered in a catalytic converter after the warm-up period, N_2O is not commonly observed in significant quantities either due to the increased rate of a surface reaction between N_2O and CO, or due to the increased importance of the N_2O decomposition reaction at high temperatures. This decomposition reaction on platinum has been studied a number of times (Redmond, 1963; Alnot et al., 1974; Takoudis and Schmidt, 1983; Lintz and Riekert, 1984), but even for this apparently simple reaction, questions remain concerning the mechanism.

Despite these observations of N_2O formation and reaction during NO reduction by CO, the reaction of N_2O with CO on platinum has only rarely been the primary focus of an investigation (Adlhoch et al., 1980). However, a thorough study of this reaction could provide information about the elementary steps in the related reactions of N_2O decomposition, and NO reduction by CO. This is one of the objectives of this study. The amount of information provided by such a study, and the ability to discriminate among various mechanisms are vastly increased when the reaction system displays multiplicity behavior, as has recently been shown for the case of CO oxidation by O_2 (Graham and Lynch, 1987). In particular, in the neighborhood of a transition point from low to high conversion, the extremely nonlinear response of the reaction rate to the concentration change enables a very sensitive discrimination to be made among rival reaction mechanisms. Thus, an additional objective of this study is to investigate the possibility of the occurrence of multiplicity behavior for the N_2O+CO reaction, and to use such behavior to discriminate among several potential mechanisms.

Following the development of a satisfactory description of the kinetics of CO oxidation by N_2O, this model will then be extended to encompass the related reduction of NO by CO.

1.2 Literature Review

1.2.1 CO Adsorption

The adsorption, desorption and oxidation (with O_2) of CO on noble metal catalysts have been extensively reviewed (Engel and Ertl, 1979). Carbon monoxide adsorbs very strongly on a platinum surface. Compared to nitrous oxide, carbon monoxide has a much higher sticking probability on metal surfaces. It is believed that adsorbed CO on a platinum surface has two main configurations, namely, linear and bridged forms.

The saturation coverage of CO on platinum depends on the size of the metal crystallites. Freel (1972), Dorling and Moss (1967), and Yao et al. (1979) have determined that for supported Pt with a small average particle size (less than 5 nm), the maximum ratio of adsorbed CO molecules to Pt surface atoms is 0.87±0.07. For a catalyst with a large crystallite size, the ratio of CO:Pt can be as low as 1:3. These observations have usually been explained by assuming bridge bonding on large crystallites and linear bonding on highly dispersed platinum.

In the classical Langmuir-Hinshelwood adsorption/-desorption model, an adsorbed CO molecule occupies one surface Pt atom, and every Pt atom is available for the CO adsorption. Because the fractional saturation coverage is usually less than unity on a Pt surface, models using a self-exclusion effect (Herz and Marin, 1980; Graham and Lynch, 1987) have been proposed for both oxygen and CO adsorption on Pt. This effect means that an adsorbed CO molecule excludes other CO from an area equivalent in size to N_{CO} surface Pt atoms, where the rate of CO adsorption would be given as follows:

$$R_{CO,ads} = k_1 \; [CO] \; (1-\Sigma\theta_i) \; \frac{(1 - N_{CO}\theta_{CO})}{(1 - \theta_{CO})} \tag{1.1}$$

N_{CO} is in the range of 1.0 to 1.25 on highly dispersed catalysts, with N_{CO}=1.0 giving the standard Langmuir-Hinshelwood approach. It has been reported that an elementary-step model incorporating a carbon monoxide self-exclusion effect could quantitatively describe the steady-state rates and the multiplicity regions for the $CO+O_2$ reaction on supported Pt (Graham and Lynch, 1987).

1.2.2 CO Desorption

From thermal desorption studies, numerous investigations (Bonzel and Ku, 1973; Engel, 1978; Engel and Ertl, 1979) have reported that the CO desorption rate can be expressed as:

$$R_{CO,des} = k_{-1} \; EXP(- \frac{E_{-1}}{RT}) \; \theta_{CO} \tag{1.2}$$

where E_{-1}/R is in the range 12600 to 17100 K. Multimodal desorption patterns have often been observed and these have been explained by assuming that CO is present in several adsorbed states.

1.2.3 CO Oxidation

It is believed that the CO oxidation reaction proceeds via a bimolecular Langmuir-Hinshelwood (L-H) surface reaction between adsorbed carbon monoxide and adsorbed oxygen, and/or an Eley-Rideal type reaction (E-R) involving gas phase carbon monoxide and adsorbed oxygen. The reaction product is carbon dioxide. These mechanisms are described by the following elementary steps:

$$CO(g) + M \rightleftharpoons CO\text{-}M \tag{1.3}$$

$$CO\text{-}M + O\text{-}M \longrightarrow CO_2(g) + 2\,M \tag{1.4}$$

$$CO(g) + O\text{-}M \longrightarrow CO_2(g) + M \tag{1.5}$$

Carbon dioxide does not appreciably adsorb on platinum (Conrad et al., 1978), but it does adsorb strongly on catalyst supports such as Al_2O_3. Of course, the adsorption of CO_2 on a support has no effect on the reaction rates.

1.2.4 N_2O Adsorption

N_2O is an unusual molecule among the A_2B family. It is asymmetric and best described by the two canonical structures, $^-N=N^+=O$ and $N\equiv N^+-O^-$. As an adsorbent, this raises the question of whether bonding occurs through the terminal N or O ends of the molecule.

On the basis of electron energy loss spectroscopy (EELS) and thermal desorption spectroscopy (TDS), Avery (1983) reported that, on Pt(111) at a temperature of 78 K, molecular adsorption occurs by bonding through the N end. The linear N_2O molecule is inclined at an angle estimated to be about 35° to the surface. No evidence for N_2O dissociation was found on this surface at 78 K. Weinberg (1973) used the bond energy bond order model of chemisorption to describe the interaction of N_2O with both clean and carbon covered Pt surfaces. The similar conclusion was reached that N_2O binds to the Pt surface through the nitrogen atom.

Umbach and Menzel (1981) and Madey et al. (1983) determined the configuration of N_2O on a Ru surface. From these studies, the evidence indicated that N_2O was bound to ruthenium via the terminal N atom (Ru-N-N-O). However, based on the IR spectra and a force constant calculation, Diamantis and Sparrow (1974) claimed that the bond is through the O atom (Ru-O-N-N).

The adsorption of N_2O on other catalysts, such as Ag(111) (Tan et al., 1987), Cu(110) (Habraken and Bootsma, 1979), Rh (Gasser and Marsay, 1970) and Ru(001) surfaces

(Madey et al., 1983), has also been investigated. In a study of the interaction of N_2O with a Cu(110) surface (Habraken and Bootsma, 1979), it was shown that the fractional saturation coverage of N_2O is 0.5 monolayer for an exposure of 10^5L at a temperature of 400°C. As saturated oxygen coverage on the same catalyst is also 0.5 monolayer, they believed that this phenomenon supports the idea that bonding occurs through the O end.

Alnot et al. (1974) compared adsorption of N_2O with O_2 on platinum polycrystalline ribbons. The adsorption of N_2O was accompanied by the evolution of molecular N_2 in the gas phase, even in the 300-500 K range. They found that the N_2O sticking coefficient varied with the surface coverage. The sticking coefficient was constant when N_2O coverage was less than 0.3 to 0.4×10^{14} atom/cm²; thereafter it decreased linearly with increasing coverage.

1.2.5 N_2O Desorption

A general desorption rate expression for N_2O has been written as:

$$-\frac{d\theta}{dt} = \nu(\theta)\ \theta^x\ \mathrm{EXP}(-E(\theta)/RT) \qquad (1.6)$$

where x is the order, and $\nu(\theta)$ and $E(\theta)$ are the generalized coverage dependent preexponential factor and heat of desorption, respectively. Avery (1983) examined N_2O desorption on a Pt(111) surface and constructed an Arrhenius plot at constant fractional coverage, θ. The plot indicated that the heat of desorption increased monotonically from 16 kJ/mol at θ_{N_2O}=0.2 to 26 kJ/mol at θ_{N_2O}=0.7. An attempt to determine x and $\nu(\theta)$ directly from the experimental data was not feasible due to the large extrapolation required (Soler and Garcia, 1983). It was suggested that the desorption is first order, and the preexponential factor was taken as 10^{13} s^{-1} and was independent of coverage. The desorption rate expression was then given by

$$- \frac{d\theta_{N_2O}}{dt} = \nu \ \theta_{N_2O} \ \mathrm{EXP}(- \frac{5600+450\theta_{N_2O}}{RT}) \qquad (1.7)$$

However, Alnot et al. (1974) claimed that on recrystallized platinum ribbons, the desorption curve of N_2O is very similar to that of O_2, i.e. the desorption rate is second order with respect to the N_2O surface coverage. Both the preexponential factor and the heat of adsorption depended on coverage.

1.2.6 N_2O Decomposition

Since the early work by Hinshelwood and Prichard (1925), the decomposition of N_2O on platinum surfaces has been studied several times (Steacie and McCubbine, 1934; Redmond, 1963; Winter, 1969; Takoudis and Schmidt, 1983). Lintz and Riekert (1984) compared the reaction probability (b_{N_2O}) of N_2O decomposition from several studies, and they concluded that the observations regarding the N_2O-Pt system were quite reproducible and all studies were in accord with an oxygen inhibition effect on N_2O decomposition. However, the complete mechanism of N_2O decomposition is still uncertain.

In the recent study made by Takoudis and Schmidt (1983) using polycrystalline platinum, it was proposed that the reaction mechanism is described by:

$$N_2O(g) + M \rightleftharpoons N_2O\text{-}M \tag{1.8}$$

$$N_2O\text{-}M \longrightarrow N_2(g) + O\text{-}M \tag{1.9}$$

$$2\ O\text{-}M \rightleftharpoons O_2(g) + 2\ M \tag{1.10}$$

where the rate-limiting step was assumed to be the decomposition of adsorbed nitrous oxide. Based on this mechanism, a single L-H rate expression was established and it correlated all rate data within ±10%, at temperatures from 400 to 1200°C and pressures from 0.01 to 0.50 Torr. In the work, they suggested that the coverage of N_2O is equal to unity at low temperatures. However, in a later study, Schmidt et al. (1985) reported that N_2O does not appear to chemisorb on Pt in UHV experiments (at temperatures between 800 to 1600 K), although it reacts readily with a high apparent adsorption heat.

The above mechanism has also been proposed by other authors (Redmond, 1963; and Weinberg, 1973; Hardee and

Hightower, 1984). Redmond (1963) studied N_2O decomposition on a platinum filament, and also supported the mechanism, although he believed that the surface is mainly covered with adsorbed oxygen. In addition, he pointed out that the observed N_2O decomposition kinetics are consistent with either the adsorption of nitrous oxide or the dissociative chemisorption of nitrous oxide as the rate-limiting step.

Alnot et al. (1974) claimed that N_2O dissociates on a Pt surface into adsorbed oxygen and molecular nitrogen according to:

$$N_2O(g) + M \longrightarrow N_2(g) + O\text{-}M \tag{1.11}$$

This mechanism is also supported by the evidence of N_2O decomposition on other metal surfaces, such as Ag, Cu and Ru (Habraken and Bootsma, 1979; Madey et al., 1983; Tan et al., 1987).

Over an Fe-Y zeolite Fu et al. (1981) used isotopic tracers to identify the reaction

$$N_2O(g) + O\text{-}M \longrightarrow N_2(g) + O_2(g) + M \tag{1.12}$$

as a major step for catalytic reduction. However, Hardee and Hightower (1984) did not believe that this reaction step correctly describes the reaction on noble metal catalysts, since Equation (1.12) implies that the presence of oxygen would have a beneficial effect on the reaction rate, which is contrary to the observations made by Lintz and Riekert (1984) and Takoudis and Schmidt (1983).

Although all evidence shows that the presence of oxygen inhibits N_2O decomposition on noble metals, there is disagreement as to whether the effectiveness of added oxygen as a poison is the same as that of the oxygen produced by the decomposition reaction. Steacie and McCubbine (1934) found that the reaction rate constant was reduced by adding oxygen, whereas Redmond (1963) indicated that both added oxygen and product oxygen had the same effect on the reaction. Hardee and Hightower (1984) found that addition of only a small amount of oxygen decreased the initial N_2O decomposition rate by about a factor of 3. However, the rate was not further decreased as the O_2 pressure was increased from 6.7×10^2 to 8.7×10^3 N/m². It was reported that adsorbed oxygen from N_2O decomposition exists only in the β state whereas the desorption curves after O_2 adsorption at 300 and 500 K exhibit three different binding states (Alnot et al., 1974). However, Alnot and his co-workers did not investigate the oxygen inhibition effect on N_2O decomposition.

Nitric oxide also has an inhibition effect on N_2O decomposition (Hardee and Hightower, 1984). NO apparently competes for the same active sites with N_2O on Rh/Al_2O_3 catalysts. They believed that, this poisoning effect by NO may explain why N_2O was the product in NO reduction and decomposition reactions and why various quantities of N_2O were observed during the reduction of NO by CO.

1.2.7 Formation of N_2O

A fundamental question about NO decomposition and reduction concerns the manner by which nitrous oxide is formed during the reduction of NO by CO. Some studies have shown that adsorbed N_2O is an exclusive intermediate in the formation of nitrous oxide, which is formed by disproportionation of two NO molecules; while others have indicated that an adsorbed NO reacts with a N atom, or gas phase NO, and N_2O is produced. The true mechanism of N_2O formation remains unclear.

Halpern et al. (1981) studied the reaction between a molecular beam of nitrogen atoms and pre-adsorbed oxygen atoms using a Pt surface. Unexpectedly, nitrous oxide was formed during the reaction, although initially nitric oxide was expected to be the product. They thought that adsorbed NO is an intermediate species in the production of N_2O on a Pt surface.

The fact that adsorbed N_2O is an exclusive intermediate in the reduction of NO by CO is supported by isotopic tracer experiments using a Rh/Al_2O_3 catalyst, which were carried out by Hardee and Hightower (1984) and Hu and Hightower (1976). The results illustrated that N_2O is not an exclusive gas-phase intermediate in the N_2 formation, and that adsorbed N_2O might be an exclusive surface intermediate. According to their observations, a possible process for the formation of gaseous N_2O is as below:

$$2\ NO\text{-}M \longrightarrow N_2O\text{-}M + O\text{-}M \qquad (1.13)$$

$$N_2O\text{-}M \longrightarrow N_2(g) + O\text{-}M \qquad (1.9)$$

Two adsorbed NO molecules disproportionate to form an adsorbed oxygen and the surface intermediate. Adsorbed N_2O-M either desorbs as N_2O or decomposes to N_2 and O-M.

However, low-pressure studies by Lambert and Comrie (1974) have indicated that N_2O is formed by a surface reaction between adsorbed NO and an adsorbed nitrogen atom.

$$NO\text{-}M + N\text{-}M \longrightarrow N_2O(g) + 2\ M \qquad (1.14)$$

Pirug and Bonzel (1977) suggested that in addition to reaction (1.14), an Eley-Rideal step also involved,

$$NO(g) + N\text{-}M \longrightarrow N_2O(g) + M \qquad (1.15)$$

This mechanism was also suggested by Hendershot and Hansen (1986) and Hecker and Bell (1983) (on a Rh(100) single-crystal surface and silica-supported Rhodium, respectively). The inclusion of reaction (1.15) is based upon the theoretical work of Weinberg and Merrill (1975), which suggested that at moderate NO partial pressures reaction (1.15) should be favored over reaction (1.14). During the study of reaction kinetics for NO+CO, Lorimer and Bell (1979) employed both of the processes in the reaction mechanism and claimed that reaction (1.14) provides a more satisfactory description of N_2O formation than reaction (1.15).

Other proposed steps for N_2O formation are the reaction between adsorbed NO and gas phase NO on carbon supported platinum (Lim et al., 1986):

$$NO(g) + NO\text{-}M \longrightarrow N_2O(g) + O\text{-}M \qquad (1.16)$$

and the Eley-Rideal type oxidation of adsorbed CO by two NO molecules (Brown and Gonzalez, 1976):

$$2\ NO(g) + CO\text{-}M \longrightarrow N_2O(g) + CO_2(g) + O\text{-}M \qquad (1.17)$$

1.2.8 Formation of N_2

During the study of NO decomposition, two N_2 peaks were found by Chin and Bell (1983). They thought that the formation of molecular nitrogen occurs via two processes; a low temperature process:

$$NO\text{-}M + N\text{-}M \longrightarrow N_2(g) + O\text{-}M + M \qquad (1.18)$$

and a high temperature process:

$$2\ N\text{-}M \longrightarrow N_2(g) + 2\ M \qquad (1.19)$$

Pirug and Bonzel (1977) carried out experiments concerned with NO dissociation over a temperature range of 640 to 843 K over polycrystalline Pt. The ratio of the partial pressures P_{N_2}/P_{NO} could be described by a rate expression based on step (1.19) in conjunction with a mechanism for NO dissociation. They suggested that the formation of molecular nitrogen during the NO+CO reaction over a Pt surface proceeds through a surface reaction between two adsorbed nitrogen atoms. These two steps are supported by other works (Klein et al., 1985; Lim et al., 1986). However, Hendershot and Hansen (1986) suggested an Eley-Rideal type path to form N_2:

$$N_2O(g) + CO\text{-}M \longrightarrow N_2(g) + CO_2(g) + M \qquad (1.2)$$

In their work, this is the only route to form molecular nitrogen.

1.2.9 Mechanisms of N_2O+CO

The reaction between N_2O and CO has received much attention mainly from its relevance in laser applications as a source of vibrationally excited CO_2. These investigations have been carried out in a shock tube at high temperatures (Milks and Matula, 1972; Loriat et al., 1983; non-catalytic). Meanwhile, since the reaction of nitrous oxide with carbon monoxide plays an important role in the control of automotive emissions, kinetic and mechanistic studies (Lorimer and Bell, 1979; Adloch et al., 1980; Hecker and Bell, 1984; Hendershot and Hansen, 1986) have been performed for the reduction of nitrous oxide with carbon monoxide on noble metal catalysts.

Several N_2O+CO reaction mechanisms have been proposed for noble metal catalysts (Lorimer and Bell, 1979; Lintz, 1981; Hardee and Hightower, 1984). These mechanisms can be classified into two categories: one involves the dissociative chemisorption of N_2O, the other involves the decomposition of adsorbed N_2O.

Lintz (1981) claimed that the reaction involved four elementary steps:

$$CO(g) + M \rightleftharpoons CO\text{-}M \tag{1.3}$$

$$N_2O(g) + M \longrightarrow N_2(g) + O\text{-}M \tag{1.9}$$

$$CO\text{-}M + O\text{-}M \longrightarrow CO_2(g) + 2\,M \tag{1.4}$$

$$CO(g) + O\text{-}M \longrightarrow CO_2(g) + M \tag{1.5}$$

In this mechanism, the dissociative chemisorption of N_2O results in the production of molecular nitrogen. It was found that the reaction probability of this process is very low (at 500 K). At temperatures higher than 650 K when the reaction is no longer inhibited by CO adsorption, the overall reaction rate is therefore determined by the N_2O decomposition rate.

A different mechanism has been proposed by Winter (1969), in which the dissociative chemisorption of N_2O is used in the preceding mechanism with step (1.9) not used, i.e.

$$N_2O(g) + M \rightleftharpoons N_2O\text{-}M \tag{1.8}$$

$$N_2O\text{-}M \longrightarrow N_2(g) + O\text{-}M \tag{1.9}$$

It was assumed that the decomposition of the N_2O surface complex is the rate-limiting step. Hardee and Hightower (1984), who examined the NO+CO catalytic reaction on a Rh/Al_2O_3 catalyst, suggested that N_2O is a primary product for this reaction and this mechanism could describe the experimental observations.

The Eley-Rideal type reaction:

$$N_2O(g) + CO\text{-}M \longrightarrow N_2(g) + CO_2(g) + M \tag{1.20}$$

was identified by Fu et al. (1981). However, Hardee and Hightower (1984) disagreed with this idea, because this reaction implies that the presence of oxygen would be beneficial for the overall reaction.

Yet another surface reaction has been proposed by Hendershot and Hansen (1986), who investigated the reduction of nitric oxide with carbon monoxide on a Rh(100) single crystal surface. They assumed that an adsorbed nitrous oxide intermediate was involved in the reaction process. The surface nitrous oxide reacts with adsorbed carbon monoxide, with gas phase nitrogen and carbon dioxide as the products.

$$N_2O\text{-}M + CO\text{-}M \longrightarrow N_2(g) + CO_2(g) + 2\ M \qquad (1.21)$$

They showed that this step was consistent with both steady-state kinetics and surface characterization results.

Because so many different mechanisms have been proposed for the reduction of N_2O by CO, it is possible that there is not a single rate-controlling step for all conditions. Alternatively, it should always be remembered that the fact that a derived rate expression is consistent with experimental data provides only a necessary, but not a sufficient, condition that a model is based on the correct reaction mechanism. Often very good agreement is possible solely because rate functions of the Langmuir-Hinshelwood-Hougen-Watson type are very adept at fitting data.

An additional interesting observation is that despite the similarity of the N_2O+CO reaction to the O_2+CO system, there are apparently as of yet no reports in the literature of multiplicity behavior for the N_2O+CO reaction on noble metal catalysts.

1.2.10 NO Adsorption

Because of the interest in the removal of NO as an air pollutant, NO adsorption and decomposition on platinum metals have been studied extensively. However, in spite of considerable effort, many aspects of the bonding and reactivity of NO on Pt remain unclear. Generally speaking, a high-frequency IR band (1700-1820 cm^{-1}) which has been most prominent at high surface coverages has been assigned to NO adsorbed as a linear species, whereas the low-frequency band (1400-1660 cm^{-1}) which is relatively more prominent at low surface coverages, has been assigned to NO adsorbed either in a bent configuration or as NO bridge bonded to two Pt atoms.

Many investigations of NO adsorption have been carried out on both supported noble metal catalysts and on well-defined Pt surfaces, such as Pt(100), Pt(110) and Pt(111) (Pirug and Bonzel, 1977; Lorimer and Bell, 1979; Gland and Sexton, 1980; Gorte and Schmidt, 1981; Hecker and Bell, 1983; Lesley and Schmidt, 1985; Morrow et al., 1985). However, even for these low index surfaces, the process of NO adsorption is very complicated due to surface reconstruction during adsorption (Lambert and Comrie, 1974; Gorte and Schmidt, 1981). In addition, many investigations have shown that during NO adsorption on Pt and Ru surfaces an isocyanate species is formed (Brown and Gonzalez, 1976; Solymosi et al., 1978; Lorimer and Bell, 1979; Hecker and Bell, 1984). A clear mechanistic role for the isocyanate structure has not been established.

From EELS measurements, Lambert and Comrie (1974) observed that on a Pt(111) surface NO adsorbed into a single binding state, while on the clean, reconstructed Pt(111)-(1×2) surface species adsorbed with rearrangement of the Pt substrate back to (1×1) to produce two distinct states (α and β). The α state appeared only at high coverages. For the Pt(100) surface the clean crystal gives a (5×20) LEED with NO adsorption (Gorte and Schmidt, 1981). This reconstruction relaxes to a (1×1) surface structure during NO adsorption. There are at least three primary NO desorption peaks on this surface.

The co-adsorption of NO and CO leads to the appearance of new CO and NO binding states (Comire, 1974). For CO adsorption on Pt(111), two new states appeared in addition to the original β state. On Pt(110) an α_1 state also appeared in addition to the original α_2 and β states. In the case of NO, no new states appeared on the Pt(110), but on Pt(111) an α state was formed in addition to the original β state.

Lambert and Comrie (1974) found that large exposures to CO appeared to suppress the yield by a mechanism other than that of simply denying adsorption sites to NO. That is, large CO exposure was considerably more effective at suppressing the reaction than large NO exposure despite the comparable sticking probabilities of the two molecules. They believed that such an effect is due to actual displacement of adsorbed NO by incident CO molecules.

$$CO(g) + NO\text{-}M \longrightarrow NO(g) + CO\text{-}M \qquad (1.22)$$

Brown and Gonzalez (1976) investigated NO adsorption on Pt/SiO_2. A sample with monolayer CO coverage was exposed to excess NO for an extended period of time. They observed a slight decrease in the intensity of the CO band at 2070 cm^{-1} and noted the appearance of a weak NO band at 1760 cm^{-1}. The results indicated that chemisorbed CO was not displaced from the Pt surface by NO, but rather it was oxidized by excess NO to CO_2.

$$2\,NO(g) + CO\text{-}M \longrightarrow N_2O(g) + CO_2(g) + M \qquad (1.17)$$

1.2.11 NO Decomposition

For NO decomposition, it is still uncertain whether nitric oxide dissociates into adsorbed nitrogen and adsorbed oxygen, or disproportionates into an adsorbed N_2O intermediate and adsorbed oxygen.

In 1974 Lambert and Comrie (1974) studied the adsorption of NO at low pressures on single crystals of Pt(111) and Pt(110). They found evidence for NO dissociation from a flash-desorption study. Since then, the fact that NO dissociates on Pt has been the subject of many papers and the inhibition of NO dissociation by oxygen has also been investigated (Amirnazmi and Boudart, 1975; Pirgun and Bonzel, 1977; Mummey and Schmidt, 1981). All the observations of NO dissociation are in agreement, i.e., NO dissociates on a Pt(100) surface, but this is not true on a Pt(111) surface

(Gorte and Schmidt, 1981). The dissociative state can only be reached through the molecular adsorbed state, not directly from the gas phase.

Lambert and Comrie (1974) claimed that significant dissociation of NO occurred prior to desorption when the adlayer was heated. Amounts of NO, N_2, N_2O and O_2 were recorded as a function of temperature. No trace of NO_2 was observed. At low NO coverage, the major amount of gas desorbed was N_2 while at high NO coverage a large amount of NO was observed in addition to N_2. The occurrence of N_2O was noted particularly for intermediate and high initial NO coverage. They believed that the N_2 and N_2O formation steps are not rate-limiting steps. N_2 and N_2O are direct measures of the rate of NO dissociation.

Gorte and Schmidt (1981) reported that there are at least three primary NO desorption peaks on Pt(100). A significant amount of dissociation also occurs during an adsorption-desorption experiment. Enough O_2 desorbed from the surface to balance the N_2 product. A small amount of N_2O also desorbed at about 500 K, but this accounts for less than 2% of the total nitrogen desorbed.

NO decomposition was investigated over a supported Pt catalyst at a temperature of 350°C by Hu and Hightower (1976). They observed that the reaction is initially fast over a reduced surface, but it rapidly slows down and almost completely stops after a short period of time. From the deficiency of oxygen atoms among the gaseous products, the poisoning must be due to the build-up of oxygen atoms on the catalyst surface. This is supported by the fact that the catalyst activity is much lower on an oxidized surface than on a reduced surface.

Other studies (Amirnazmi and Boudart, 1975; Pirug and Bonzel, 1977; Mummey and Schmidt, 1981) also reported that the presence of oxygen inhibits the NO dissociation. However, the adsorbed atomic oxygen did not inhibit NO adsorption (Gorte and Schmidt, 1981) on a Pt(111) surface, but did inhibit the decomposition reaction. They suggested that this inhibition of NO decomposition could be caused by a kinetic limitation on the decomposition reaction and/or a shift in the decomposition equilibrium caused by an increased oxygen surface concentration. Hu and Hightower(1976) found that a triple-site Langmuir-Hinshelwood rate expression accounted for the disappearance of NO when reduced by methane over Pt/Al_2O_3. Using isotropic tracers they deduced that the mechanism of NO reduction involves a disproportionation of NO into adsorbed $(N_2O)_a$ and adsorbed oxygen. Hardee and Hightower (1984) also claimed that adsorbed N_2O perhaps is an exclusive surface intermediate in NO reduction.

1.2.12 Mechanisms of NO+CO

Initially, it was believed that the reaction of NO+CO proceeded via a unimolecular mechanism. In recent investigations, the evidence indicates that a surface reaction between adsorbed NO and adsorbed CO might be the rate-limiting step. Based on that, a bimolecular mechanism has been proposed. In addition, it was also suggested that a mechanism involving NO disproportionation could describe the experimental results. No consensus on detailed rate expressions or mechanisms has emerged.

1.2.12.1 Unimolecular Mechanism

A unimolecular mechanism for the reduction of nitric oxide by carbon monoxide on platinum and other noble metals has been proposed by many authors (Lambert and Comrie, 1974; Lorimer and Bell, 1979; Hecker and Bell, 1983). This mechanism is a sequence initiated by the dissociation of an adsorbed NO, followed by CO scavenging of co-adsorbed oxygen which would otherwise poison the surface for further adsorption and reaction. It was assumed that the dissociation of chemisorbed NO is the rate-limiting step for the reduction of NO. It was also claimed that based on the above mechanism, the rate expression could predict reaction rates within ±15%. In addition, the mechanism could describe the observed trends in N_2O selectivity with respect to the gas composition (Lorimer and Bell, 1979).

1.2.12.2 Bimolecular Mechanism

In 1985, Klein et al. (1985) proposed that NO reduction by CO proceeds through a surface bimolecular reaction between adsorbed NO and adsorbed CO. The NO+CO reaction was carried out on polycrystalline Pt at temperatures between 300 K and 1200 K, and pressures between 10^{-8} and 1 torr. For these reaction conditions, it was found that the rate of N_2O formation was only a few percent of the N_2 formation rate. They used rate expressions based on both unimolecular and bimolecular mechanisms to fit the experimental data. By comparing the predictions from the different mechanisms, they suggested that the reaction follows a bimolecular mechanism.

1.2.12.3 Disproportionation Mechanism

Hu and Hightower (1976) studied nitric oxide reduction by methane over a platinum catalyst. They found that during both NO decomposition and reduction, N_2O is a prominent reaction product. In their opinion, N_2O is in fact an exclusive intermediate in the route to N_2 formation in both of these reactions. N_2O-M might be an exclusive surface species formed through the disproportionation of two NO molecules. Such a species could simply be desorbed as N_2O or could react with CH_4 by dissociating to form adsorbed oxygen and gaseous N_2.

Hardee and Hightower (1984) suggested a possible mechanism for NO reduction by CO on supported Rh. The key assumptions of the mechanism are that two NO molecules disproportionate on the catalyst to form adsorbed N_2O and adsorbed oxygen. The adsorbed N_2O either desorbs to form gaseous N_2O or decomposes to form N_2O and adsorbed oxygen. The role of the CO is to remove the adsorbed oxygen which keeps the catalyst in an active reduced state. In this mechanism, the rate limiting step in the reduction of NO by CO involves the surface reaction of two NO molecules:

$$2\ NO\text{-}M \longrightarrow N_2O\text{-}M + O\text{-}M \qquad (1.13)$$

2. DESCRIPTION OF THE EXPERIMENTAL APPARATUS

In this investigation, all experimental measurements of reaction rate were carried out by using a modification of an external recycle reactor system which has previously been described by Lynch (1981). The apparatus consisted of four main parts, a tubular reactor for holding the catalyst, a heated compartment containing the recycle pump and associated tubing, an infrared spectrophotometer for composition analysis, and mass flow controllers for feed flow rate and composition regulation. A schematic description of the overall reactor system is shown in Figure 2.1. A detailed description of each part of the apparatus will be given in the following.

2.1 Feed Stream Regulation

The feed composition and flow rates were controlled by three Matheson model 8250 mass flow controllers. One of the flow controllers was always used to regulate the amount of CO sent to the reactor, while a second flow controller was used either for N_2O or NO depending on the reaction system under investigation. A third flow controller was used to hold the total flow rate to the reactor constant at any specified value by the addition of nitrogen. The total flow rate was typically 200 cm^3/min. (21°C, 101.3 kPa, i.e. 138 μmol/s) for the N_2O+CO reaction, and 100, 200 or 400 cm^3/min. for the NO+CO system. The flow sensors for the flow meters were interchangeable so that each feed component

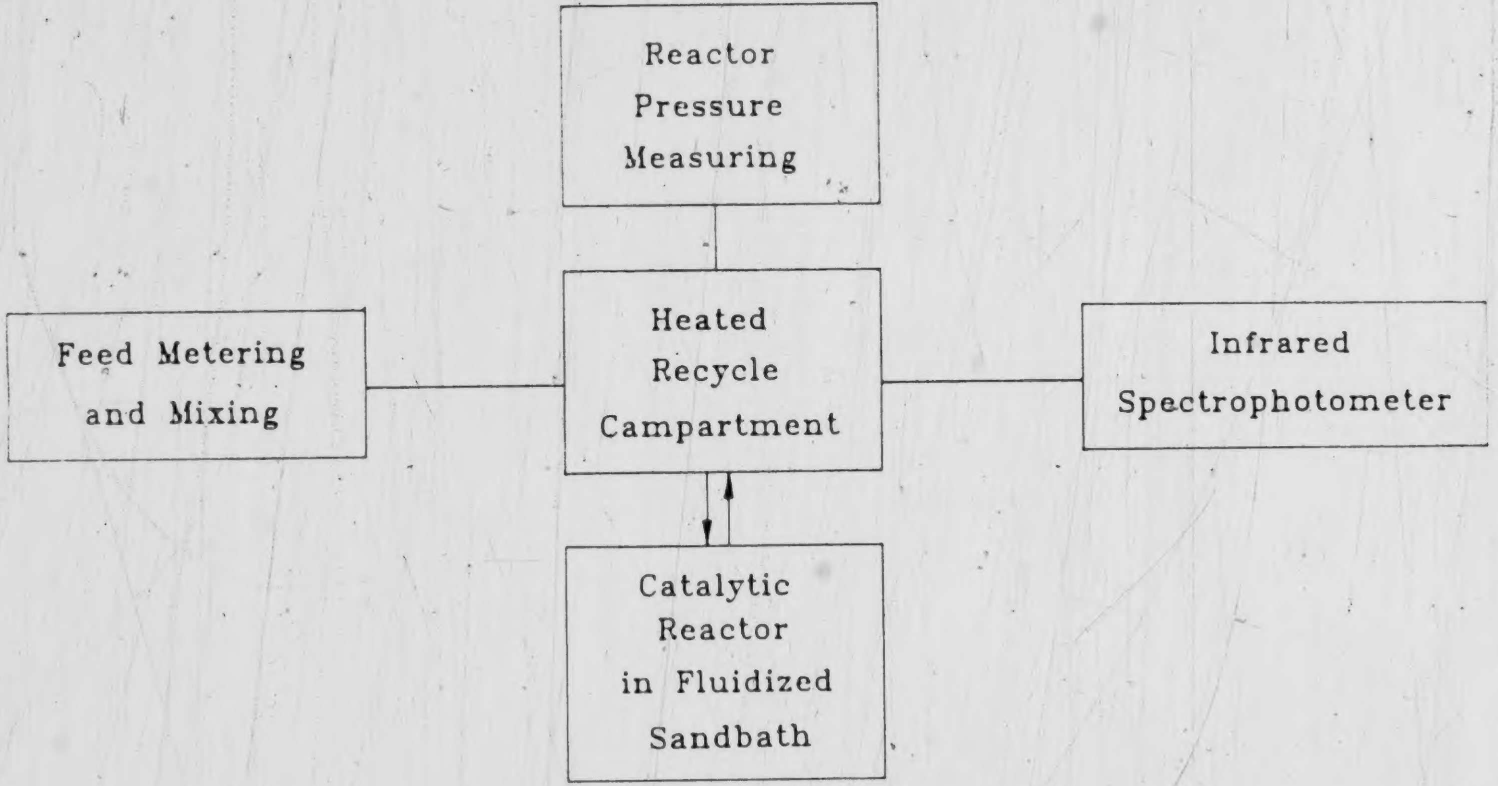
Reactor
Pressure
Measuring
Feed Metering
and Mixing
Heated
Recycle
Campartment
Infrared
Spectrophotometer
Catalytic
Reactor
in Fluidized
Sandbath

Figure 2.1 Overall Equipment Schematic

could be regulated with maximum precision. Thus, the achievable feed compositions were limited only by the compositions of the high pressure cylinders from which the feed gases were supplied. Calibration curves for the flow meters were determined by routing the effluent gas from the flow controllers to a bubble flow meter. These curves are presented in Appendix 1.

2.2 Preheat Compartment

The combined feed from the mixing section was routed either to the infrared spectrophotometer or bubble flow meter for calibration purposes, or to the reactor preheat compartment for the carrying out of reaction studies. This compartment, shown schematically in Figure 2.2 contained the equipment for recycling the reaction product stream, heating the compartment and regulating the reaction pressure. A Metal Bellows Corporation model MB-118HT (Ser. #1622) bellows compressor which was driven by a one horsepower Reliance V5D motor was employed to recycle the reaction gases. This motor was manually controllable over the range 300 to 2000 RPM by means of an associated electronic speed controller. A gas filter was located on the suction side of the recycle pump in order to protect the metal bellows. The installed flow rate delivered by this compressor was approximately 500 cm^3/s at a system pressure of 101.3 kPa (Graham and Lynch, 1987). Thus, for a feed rate of 200 $cm^3/min.$ a recycle ratio of approximately 150 can be achieved.

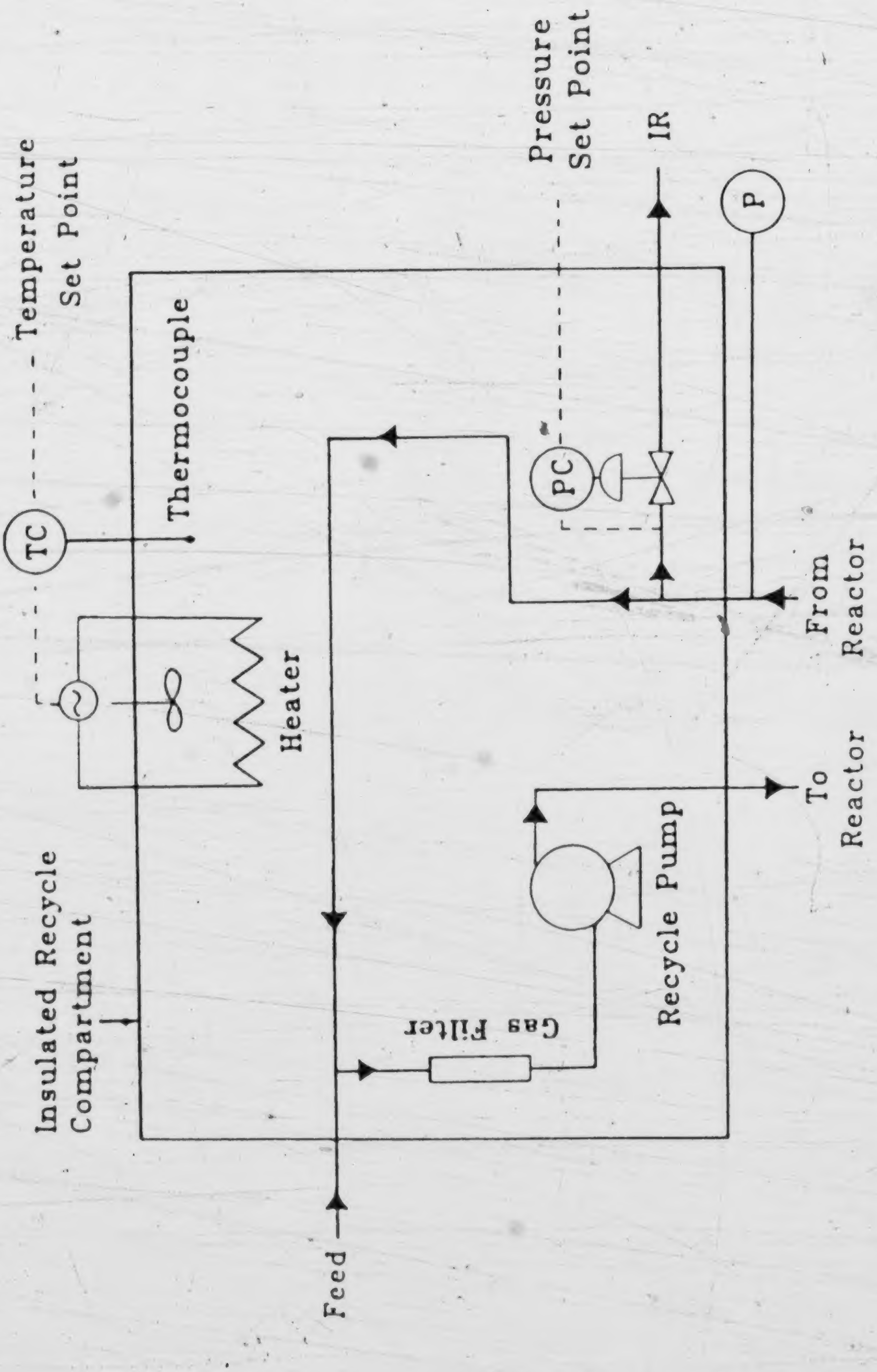
Temperature Set Point
TC
Thermocouple
Heater
Insulated Recycle Compartment
Gas Filter
Recycle Pump
Feed
To Reactor
From Reactor
PC
Pressure Set Point
IR
P

Figure 2.2 Preheat Compartment Schematic

The temperature of the preheat compartment was normally maintained at a level somewhat lower than the reactor temperature. The maximum temperature in the compartment is limited by the softening temperature of the Teflon™ seals in the bellows compressor. Heat loss from the compartment was minimized through the use of fiberglass insulation on the inside walls. The temperature in the compartment was measured with an iron-constantan thermocouple and controlled with a Honeywell model R 7161J temperature controller which supplied electrical current to a resistance heater.

Also located in the preheat compartment was a Moore model 63SUI (Ser. #PC-5402) differential flow controller. This flow controller manipulated the effluent flow rate such that the pressure in the recycle line was kept equal to an externally applied pressure. The reaction was normally carried out at 0.1 MPa, and the reactor pressure was measured by a Heise model 7108B (Ser. #S7-14023) digital pressure gauge.

2.3 Catalytic Reactor

After passing through the recycle compressor, the combined fresh feed and recycled stream passes out of the preheat compartment and into the reactor vessel which contains the catalyst. This vessel was a piece of stainless steel tubing 2.5 cm in diameter with a total free volume of 47 cm^3. This limited the maximum catalyst charge to approximately 50 g. The reactor was normally filled with 20 g of catalyst with the remaining volume filled with inert glass spheres, which were thoroughly mixed with the catalyst pellets. The total volume of the empty reactor, recycle compressor and associated tubing has previously been determined to be approximately 245 cm^3 (Graham and Lynch, 1987).

The catalytic reactor was set in a fluidized sandbath, with a resistance heating element wound around the outside of the sandbath. The reaction temperature was measured by two thermocouples. One monitored the gas phase temperature at the top of the reactor, while the second was welded to the center of the wall of the reactor. The voltages of both thermocouples were continuously recorded by a two-pen chart recorder (Varian Model A-25). The temperature of the thermocouple located in the gas stream was used as the control temperature for the sandbath resistance heater. A THERMOELECTRIC model 400 (Ser. #56486-118) temperature controller was used. The reactor was normally operated in the 150°C to 250°C temperature range.

Due to the thermal capacity of the sandbath and reactor system, a warm-up period of approximately 2 hours was always used in order to allow the system to approach steady-state thermal operating conditions following any change to the temperature setpoint. However, following any change to the feed composition, a shorter period of approximately 30 minutes was provided for the reactor to approach the new steady-state operating conditions. This amount of time was considered to be sufficient given that the space time of the reactor system was in the range 0.3 to 1.5 minutes for the conditions used in this study. The adequacy of this period of time was normally verified by sequential analyses of the product composition.

A Pye Unicam ratio-recording infrared spectrophotometer was used for analysis of the reactor effluent. The IR was set at 2355 cm^{-1} or 2235 cm^{-1}, respectively, to measure CO_2 or N_2O concentrations. While CO and NO concentrations could also be determined with the IR, the measurements are very imprecise due to the low sensitivity of the IR for these components relative to CO_2 or N_2O. Thus, the concentrations of components other than CO_2 and N_2O were calculated by mass balance equations.

2.4 Experimental Materials

All gases used in this study were either Matheson ultrahigh purity grade, or special mixtures of N_2O/N_2, NO/N_2 and CO/N_2 prepared by Matheson and/or Linde and used without further purification. The compositions of the gas mixtures used were (volume percent): 2.00% or 2.30% N_2O in N_2, 2.29% or 6.13% NO in N_2, and 2.02% or 10.0% CO in N_2. Nitrogen was always used as the inert gas.

The catalyst used in all of the experiments was purchased from Aldrich. It contained 0.5 wt% Pt supported on γ-Al_2O_3 with an estimated Pt dispersion of 0.5 to 0.6 from hydrogen adsorption measurements. The BET area of the catalyst support was 108 m^2/g, and the support had a 3 nm average pore radius (Graham and Lynch, 1987). It was an egg-shell kind of catalyst with all of the platinum deposited in a thin layer on the exterior of the pellets. The catalyst pellets were cylindrical in shape, with a length of 3.2 mm and a diameter of 3.2 mm.

2.5 Preliminary Reactor Tests

Preliminary tests were carried out in order to verify that the reactor system was not catalytically active for the reactions of interest. For example, feed streams containing various amounts of N_2O and CO were passed through the reactor which was operated at 210°C and which contained a bed of γ-Al_2O_3 mixed with glass beads (no platinum catalyst). Essentially no CO_2 production was observed thus ruling out the possibility of the reactor system or the support materials possessing catalytic activity for the reduction of N_2O by CO.

Experiments were also carried out to determine if N_2O or CO decomposition reactions occurred when the platinum catalyst was placed in the reactor. For example, when a feed stream of N_2O in N_2 was fed to the reactor, which was operated at 246°C and which contained the platinum catalyst, no decomposition of N_2O was observed (N_2O exit concentration was identical to the N_2O inlet concentration). In a similar fashion, when a feed stream of CO in N_2 was passed over the catalyst (at 210°C), no CO_2 production was observed thus eliminating the possibility of a CO disproportionation reaction which would result in the production of CO_2 plus coke.

In addition, coke formation under reaction conditions was ruled out by the observation that the catalyst activity remained constant during the duration of the experimental program.

3. EXPERIMENTAL OBSERVATIONS FOR THE N_2O+CO REACTION

3.1 Introduction

As mentioned in the introductory chapter, N_2O is potentially an intermediate for the NO+CO reaction. In order to better understand NO+CO reaction kinetics, the present work was divided into two separate parts. The first part, contained in Chapters 3 and 4, is concerned with observing and describing N_2O+CO reaction kinetics. In the second part, presented in Chapters 5 and 6, the NO+CO reaction system is examined, and the reaction mechanism is developed as an extension of the N_2O+CO reaction system.

3.2 Experimental Observations

The experimental investigations of nitrous oxide reduction by carbon monoxide were concerned with examining the steady-state multiplicity behavior at reaction temperatures of 170°C, 190°C, 210°C and 246°C, with a total flow rate of 200 SCCM to the reactor. To achieve this purpose, each experimental run was carried out at a constant temperature, with the feed concentration of one reactant (CO or N_2O) varied, while maintaining the other feed concentration constant (N_2O or CO). The initial feed composition for each experimental run was set such that either the %CO or the %N_2O was in large excess. As the experiment proceeded, the feed concentration of one reactant was increased or decreased, with the other held constant. The CO_2 and the N_2O

concentrations in the reactor were analyzed directly by measuring the IR absorbance of the effluent gases. The measurements were made under steady-state conditions.

3.2.1 Reactor Behavior at 190°C

Shown in Figure 3.1 are experimental observations of the reaction rate collected at a reaction temperature of 190°C. The investigations were made for four constant N_2O feed compositions, 0.2%, 0.406%, 0.70% and 1.035%, while varying the CO feed concentration. In Figure 3.1, each type of symbol, both filled and unfilled, represents the experimental observations for a particular %N_2O value in the feed.

It was found (see Figure 3.1) that the reaction has two CO_2 formation rate curves for a specified N_2O feed composition, a high rate curve and a low rate curve. The high CO_2 formation rates (filled symbols) were obtained when the experiments were started with a very low CO feed composition, with the CO composition to the reactor subsequently increased step by step. The low CO_2 formation rates (empty symbols) were observed when the sequence was started with excess carbon monoxide in the feed, with the CO concentration subsequently reduced as the reaction was carried out.

The high CO_2 formation rates were obtained in the low CO concentration region. In this region, all filled symbols fall in one line, in spite of the differing N_2O feed concentration. The high CO_2 formation rate increases linearly with increasing CO concentration. It was not affected by the N_2O

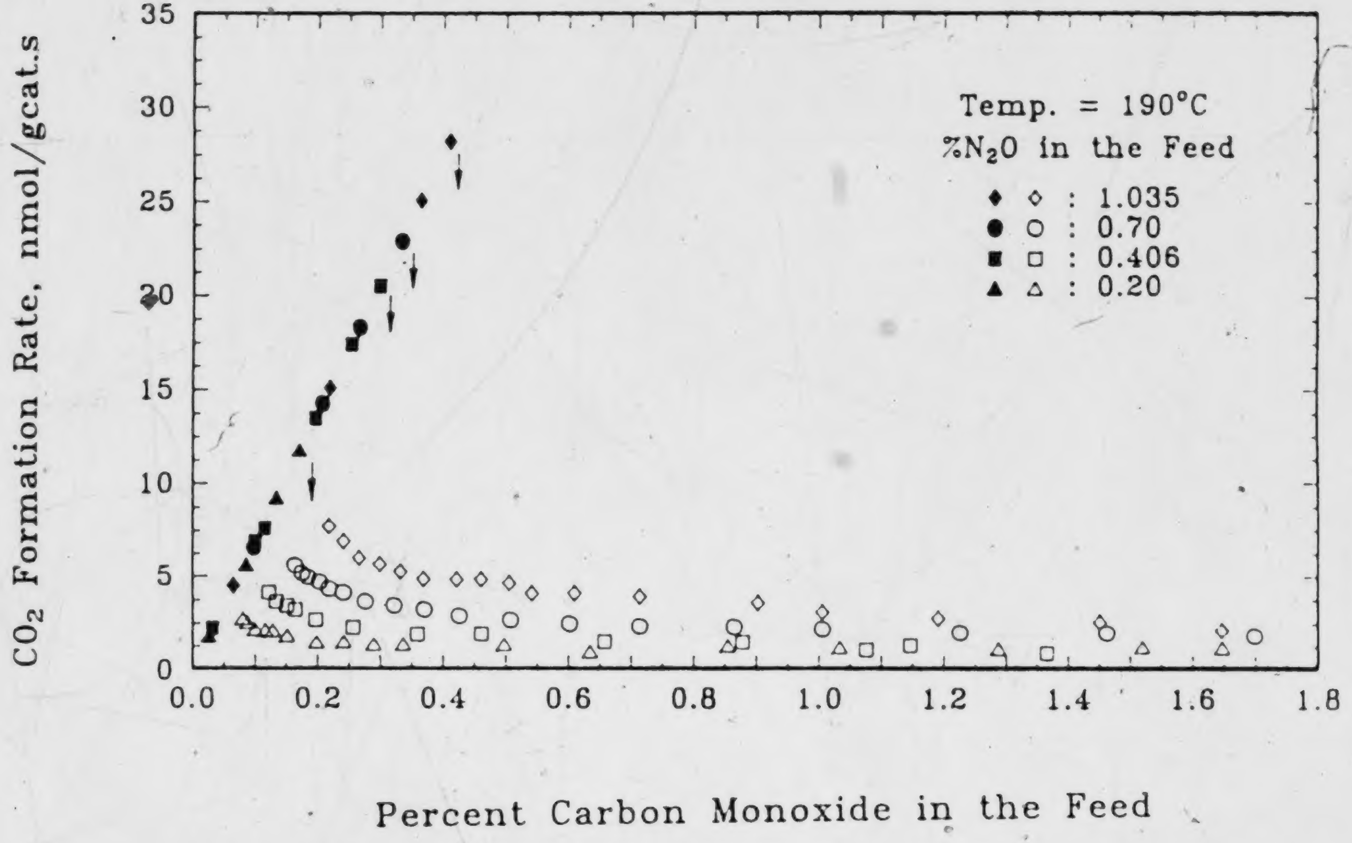

Figure 3.1 CO_2 Formation Rate for N_2O+CO at 190°C

feed concentration. When the CO feed concentration reaches a certain value, the CO_2 formation rate drops to the low rate curve. The locations of the transition boundaries are indicated by arrows in Figure 3.1. The transition boundaries are located at 0.2% CO for %N_2O=0.2, and at 0.41% CO for %N_2O=1.035.

When the reaction is carried out in the very high feed CO concentration region, the CO_2 formation rate is barely affected by the CO feed concentration. Only when the CO concentration is close to the corresponding transition boundary, does the CO_2 formation rate increase gently with decreasing %CO in the feed. When the CO feed concentration reaches the transition point, the reaction rate switches to a high CO_2 formation rate. Further decreasing the CO feed composition leads to the CO_2 formation rates following the upper rate curve. Both transition boundaries (from the low to high rate, or from the high to low rate) are affected by the N_2O feed concentration. Increasing the N_2O feed concentration shifts the boundaries towards higher CO concentrations.

Therefore, at intermediate CO concentrations, the reaction has two observable steady-state rates, a high reaction rate and a low reaction rate. The observed reaction rate in this region is totally dependent upon the initial reaction conditions. That is, if the reaction starts in the low CO concentration region, then the high rates will be obtained in the multiplicity region. If the reaction starts in the high CO concentration region, then the reaction rate in the multiplicity region will be low.

The experimental results in Figure 3.1 can be plotted as the CO conversion versus the CO feed concentration as shown in Figure 3.2. As with the rate curves, over an intermediate range of CO concentrations, the reaction has two CO conversion curves for a specified N_2O feed composition: a high CO conversion curve and a low CO conversion curve. It is seen from Figure 3.2 that at low CO concentrations, CO is completely oxidized to CO_2 for all N_2O feed compositions and the CO conversion is influenced neither by the CO feed composition nor by the N_2O feed composition. When the CO concentration to the reactor reaches the transition point (from the multiplicity region to the low conversion region), the CO conversion drops to the low conversion curve.

At very high CO concentrations, CO conversion is about a few percent and both CO and N_2O concentrations have little effect on the value of the CO conversion. However, in the multiplicity region, the low CO conversion increases significantly with decreasing CO concentration in the feed. When the CO feed composition is very close to the transition boundary, the CO conversion increases dramatically, and eventually it reaches complete conversion.

It is seen in Figure 3.2 that with increasing the $\%N_2O$ in the feed, both transition boundaries (from low conversion to high conversion, or from high conversion to low conversion) are shifted towards the direction of higher CO

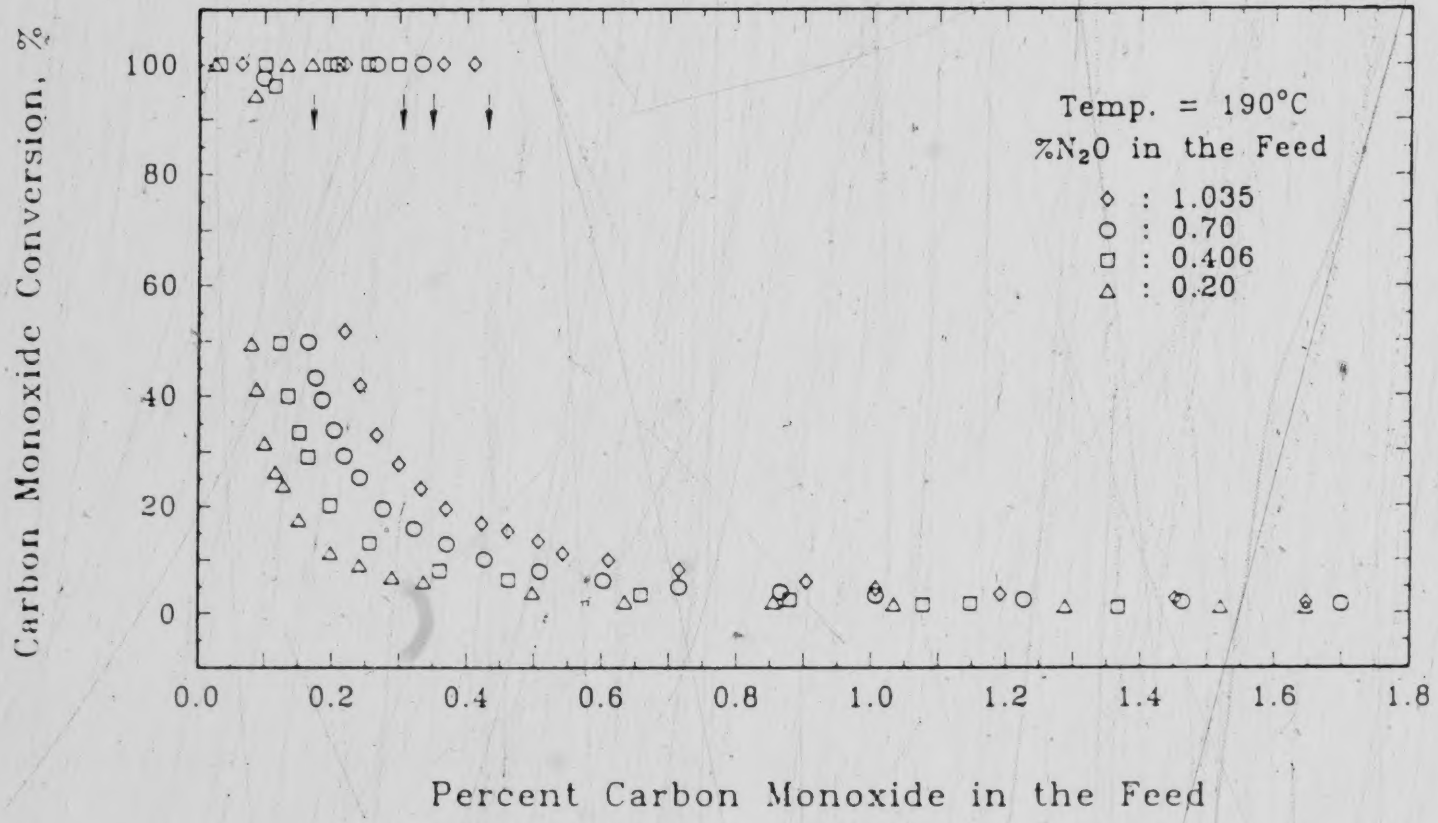

Figure 3.2 CO Conversion for N_2O+CO at 190°C

concentrations. Increasing the N_2O concentration to the reactor also increases the width of the multiplicity region. The multiplicity region ranges from 0.08% CO to 0.18% CO in the feed for $\%N_2O = 0.2$, while for $\%N_2O=1.035$, the multiplicity region is between CO feed compositions of 0.20% to 0.41%.

According to these results, it can be concluded that nitrous oxide reduction by carbon monoxide displays multiplicity behavior at a reaction temperature of 190°C. The location of the multiplicity region is influenced by the N_2O feed composition. In the following section, the effect of reaction temperature and the CO feed composition on the multiplicity behavior will be examined.

3.2.2 Reactor Behavior at 210°C

Similar experimental runs were also carried out at a temperature of 210°C, in order to investigate the effect of temperature on this reaction. The results are presented in Figures 3.3 and 3.4. It is seen that the observations are qualitatively identical with those made at 190°C. The reaction has one unique steady state at low and high CO concentrations, while for intermediate CO concentrations, the reaction has two observable steady states.

The main differences between the 210°C and the 190°C observations are that the transition boundaries and multiplicity region are shifted towards higher CO concentrations for the 210°C situation, and in addition, the rates and the

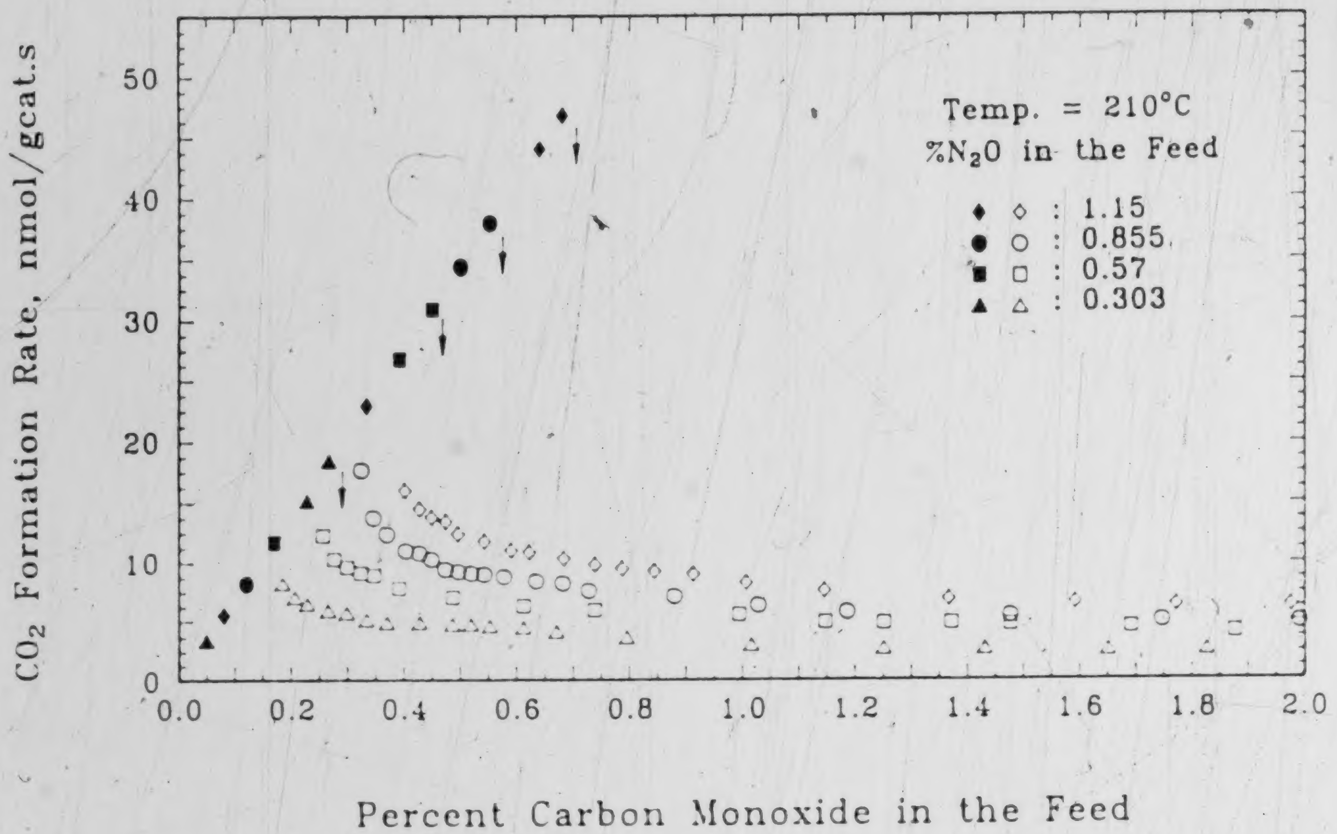

Figure 3.3 CO$_2$ Formation Rate for N$_2$O+CO at 210°C

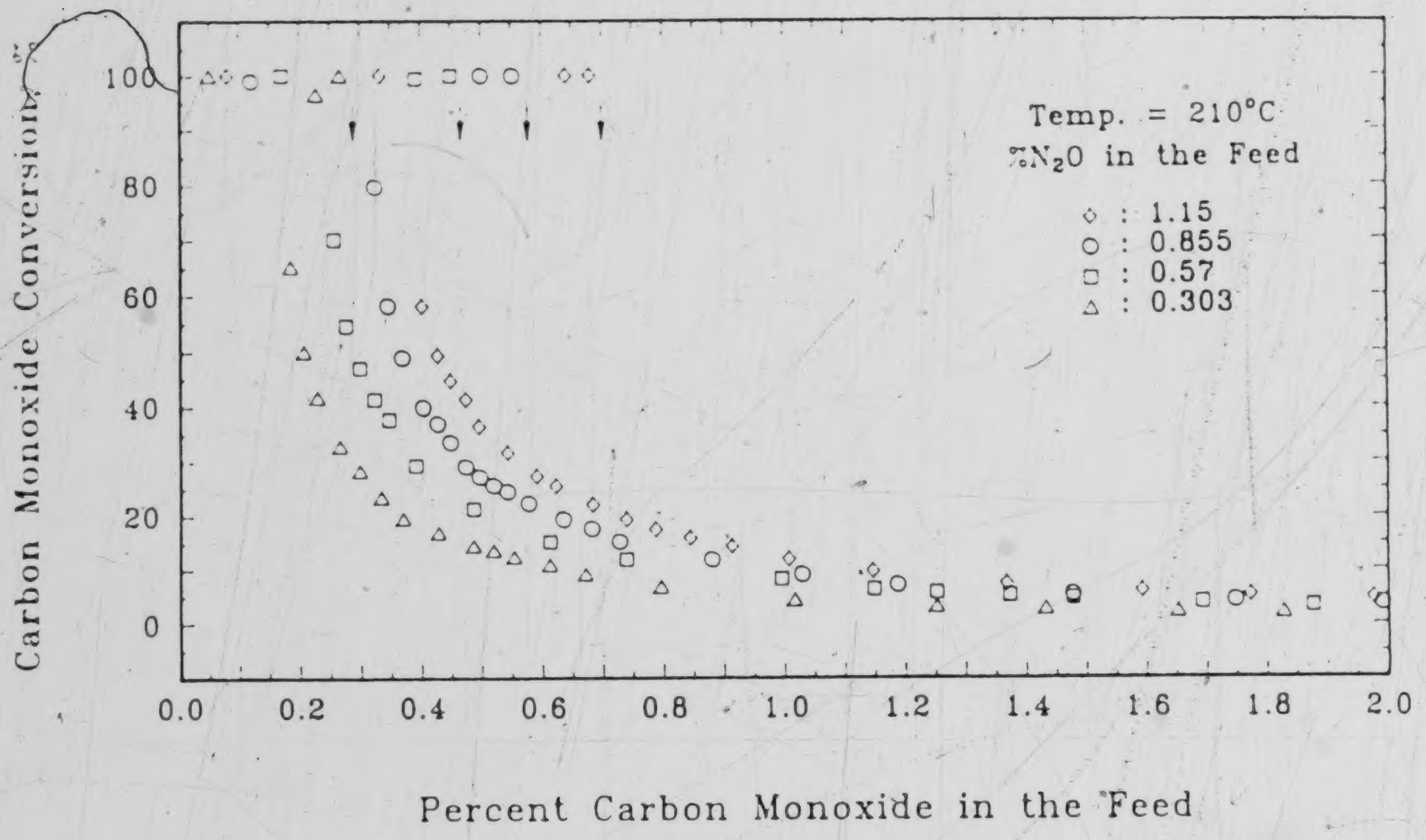

Figure 3.4 CO Conversion for N_2O+CO at 210°C

CO conversions are higher in the high CO concentration region, for corresponding values of the %N_2O and %CO in the feed. The CO_2 formation rate in the low conversion region is doubled by the increase of 20°C in the reaction temperature. For the high rate curves the CO_2 formation rate is limited by the CO feed concentration.

3.2.3 Reactor Behavior at 246°C

The locations of the multiplicity regions were also determined at 246°C. However, for these observations the roles of N_2O and CO were reversed, i.e. the N_2O feed concentration was varied while holding the %CO in the feed constant for each experimental run. As in the previous experiments, the initial reaction condition was set with either excess %CO over %N_2O in the feed, or vice versa. The results are presented in Figures 3.5 and 3.6.

In Figure 3.5, the low CO_2 formation rates were obtained when the experiment was started with the %CO in excess over the %N_2O in the feed . The data show that increasing the N_2O feed concentration results in an increase in the CO_2 formation rate. The high rate curves were obtained when the N_2O feed concentrations were much higher than the CO feed concentrations. In this region, the high CO_2 formation rates are determined by the CO feed concentrations because all of the CO is completely oxidized to CO_2. Figure 3.6 has a totally different appearance when compared to Figures 3.2 and 3.4. In fact, however, the appearance of

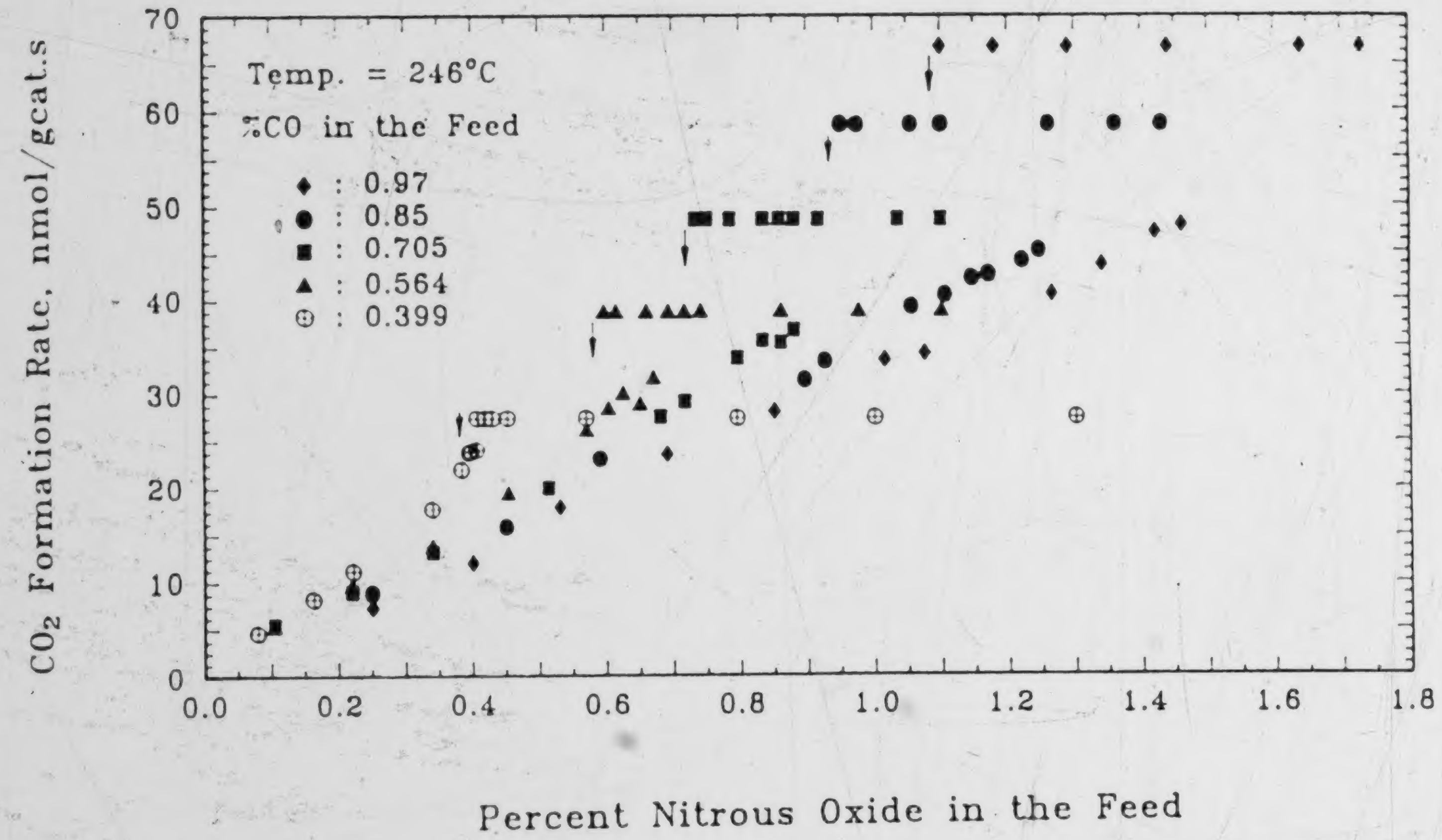

Figure 3.5 CO_2 Formation Rate for N_2O+CO at 246°C

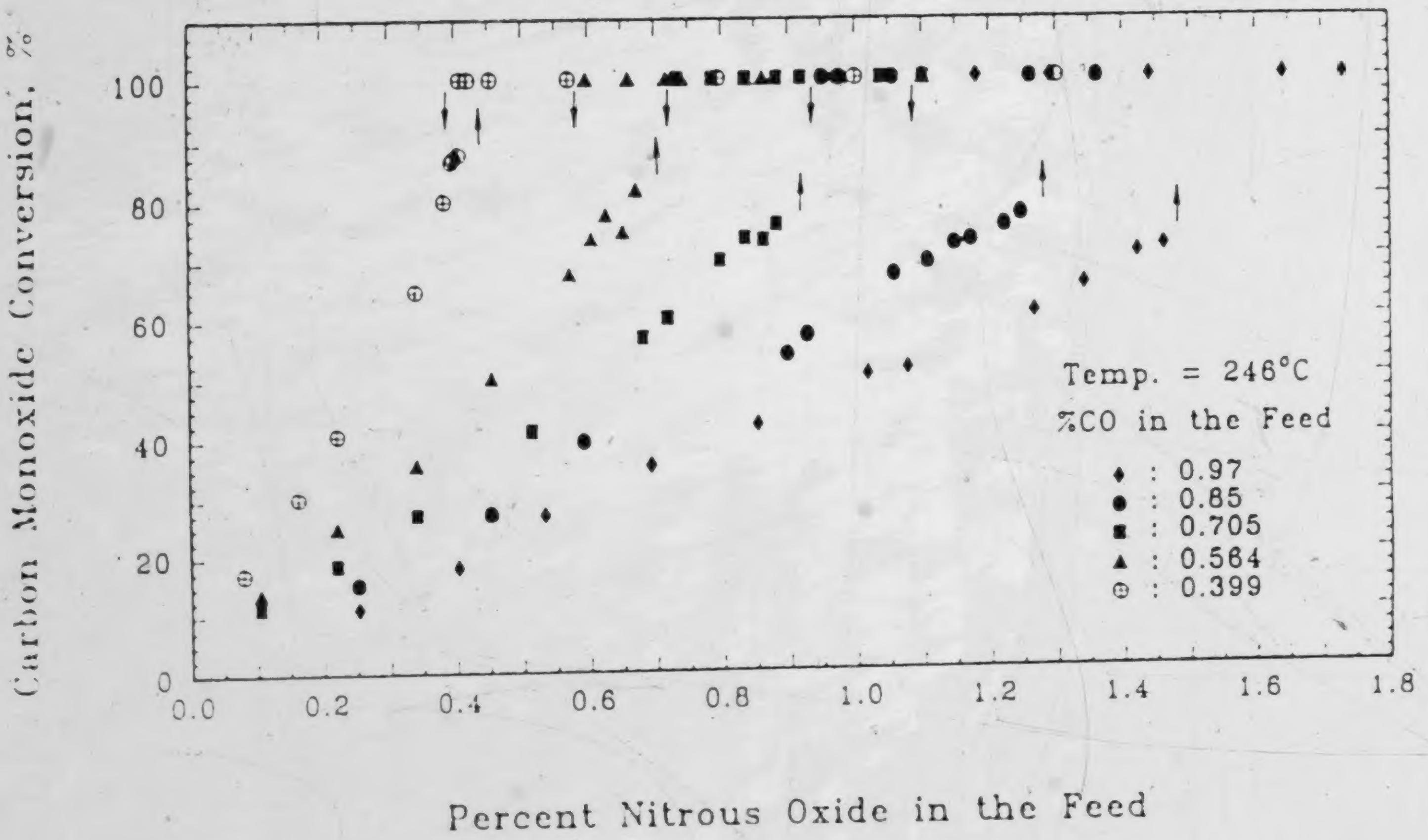

Figure 3.6 CO Conversion for N_2O+CO at 246°C

Figure 3.6 can be quantitatively predicted by using Figure 3.2 or Figure 3.4. For example, traversing Figure 3.4 vertically at %CO=0.4, shows that the CO conversion should increase as the %N_2O in the feed is increased, eventually bifurcating to a conversion of 100% for a sufficiently high value of the %N_2O in the feed. This is exactly what is seen in Figure 3.6. It is further seen in Figure 3.6 that the feed %CO now has the same effect as that displayed by the feed %N_2O in Figures 3.2 and 3.4, i.e. an increase in the %CO value widens the multiplicity region and moves the transition boundaries towards the direction of higher %N_2O in the feed.

3.2.4 Adsorption Inhibition Effects

The preceding results all show that the CO_2 formation rate is very low for high CO feed concentrations. In this region there is a negative order dependence of the rate on the CO concentration. In other words, adsorbed CO can inhibit the reduction of nitrous oxide. A similar negative order dependence of the rate with respect to the N_2O concentration was not observed for the limited range of the feed %N_2O used at 246°C.

To determine if such a dependence does exist for N_2O, a experiment was carried out at a temperature of 210°C, with a constant CO concentration in the feed of 0.3%. The amount of N_2O fed into the reactor was varied from low concentrations to high concentrations, till it reached the maximum feed concentration, which was limited by the mass flow controller. From Figure 3.7 it is seen that at low N_2O concentrations, the CO_2 formation rate increases with increasing the N_2O feed concentration. At high N_2O concentrations, the reaction has a high CO_2 formation rate; in fact, all of the feed CO is oxidized into CO_2 (100% conversion). In the region of the high CO_2 formation rates, the rate does not decline with increasing the $\%N_2O$ in the feed, even though the N_2O concentration is in large excess over the CO feed concentration. Hence, nitrous oxide does not inhibit the reaction over the range of the N_2O concentrations studied. Nitrous oxide reduction by carbon monoxide is only inhibited by one of reactants, namely carbon monoxide. This implies that the existence of adsorbed N_2O is questionable, or at most it is only present on the surface in very small quantities.

3.2.5 Formation of Molecular Oxygen

It is generally agreed that during N_2O reduction by CO, an oxygen surface species is formed through N_2O decomposition. It is possible that an oxygen desorption reaction might also be involved as a process for eliminating surface oxygen. Because the concentration of gas-phase oxygen was not analyzed in this work, the possibility of significant oxygen desorption has to be examined by an oxygen balance on the products.

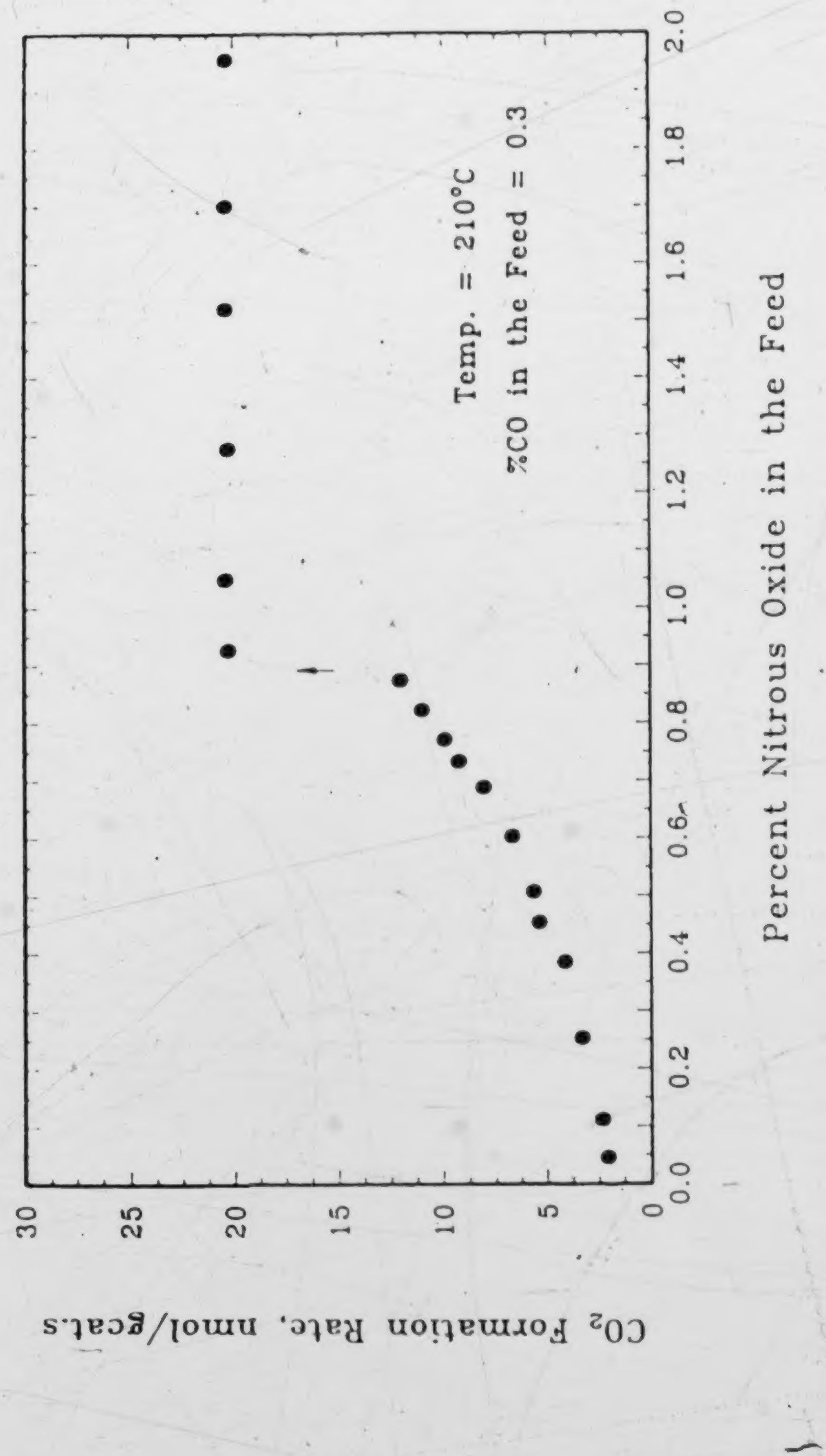

Figure 3.7 Effect of the N$_2$O Concentration on the Reaction Rate

From an atom balance, the potential O_2 concentration can be expressed by the following equation:

$$[O_2]_{EXIT} = ([N_2O]_{FEED} - [N_2O]_{EXIT} - [CO_2]_{EXIT})/2 \qquad (3.1)$$

Since all quantities on the right-hand side of Equation (3.1) are known for each experiment, it is possible to calculate $[O_2]_{EXIT}$. The results of such a calculation are shown in Figure 3.8 for five different sets of experimental data. These results were obtained at three reaction temperatures with various feed compositions. Each type of symbol in Figure 3.8 represents the experimental results obtained at a specific reaction condition. It is seen that the symbols are scattered on both sides of zero. The deviation of data points from zero is in the range of the IR precision. This demonstrates that the oxygen desorption rate is not significant for nitrous oxide reduction by carbon monoxide under the reaction conditions. Therefore, the oxygen desorption step can be neglected in subsequent mechanistic considerations.

3.2.6 Transition Boundary

Summarized in Figure 3.9 are the transition points (both from high to low conversion and from low to high conversion) as functions of the %CO and the %N_2O in the feed at constant reaction temperatures, 170, 190, 210 and 246°C. The pairs of a half-filled symbol and an empty symbol represent

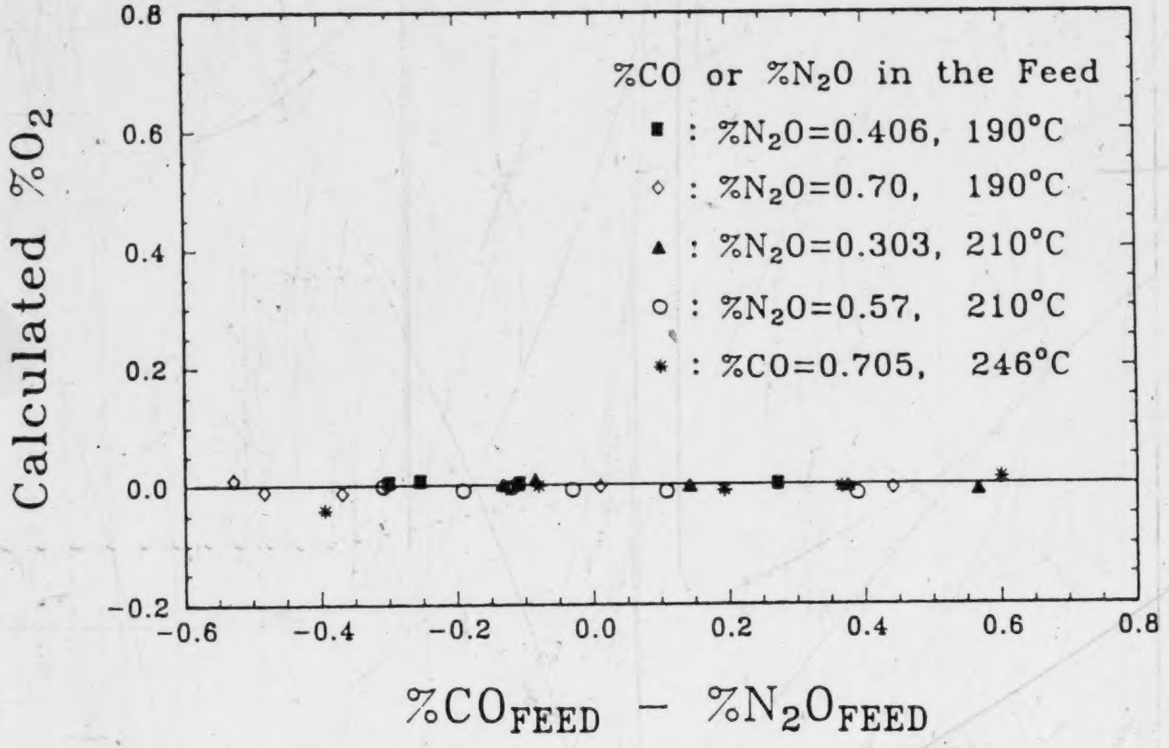

Figure 3.8 Calculated O_2 Concentrations in the Reactor Exit

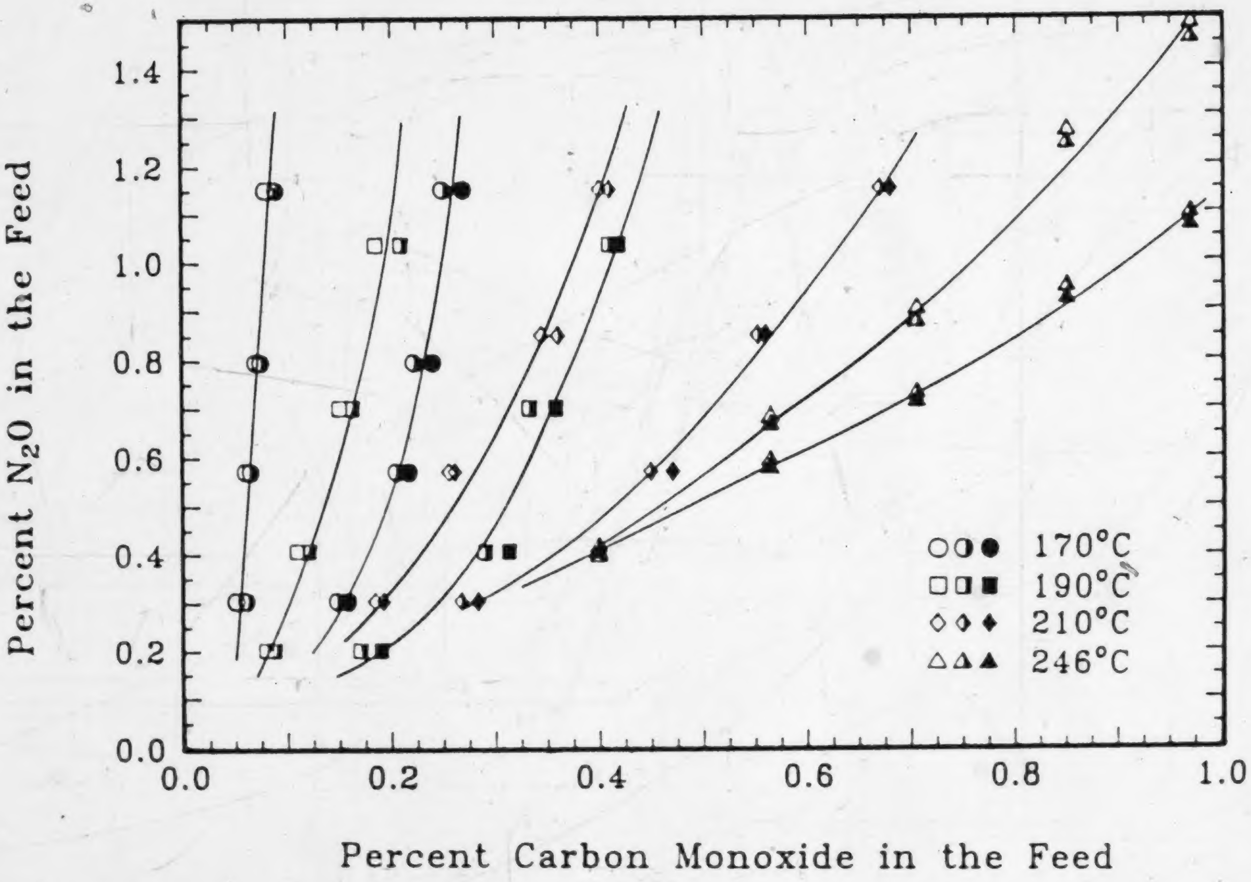

Figure 3.9 Effect of Temperature on the Multiplicity Behavior

the transition boundary from low conversion to high conversion, while the pairs of a half-filled symbol and a filled symbol represent the transition boundary from high conversion to low conversion. Therefore, regions between sets of paris of symbols are the multiplicity regions. The left-most region has unique high conversions, while the right-most region has low conversion steady states at constant temperature.

The locations of the transition boundaries are affected by the reaction temperature. With an increase of the temperature, the transition points of both low and high conversions shift to higher CO concentrations for specified %N_2O in the feed. For constant %CO in the feed, an increase in the reaction temperature moves the multiplicity region to lower N_2O concentrations. Decreasing the temperature makes the boundaries move in the other direction (towards lower %CO, and higher %N_2O).

It should be noted that at the highest temperature examined, there is only a small interval between the low conversion boundary and the high conversion boundary. Since increasing the temperature brings the two boundaries closer to each other, it can be expected that at a certain reaction temperature, the multiplicity region will disappear and the reaction will only have one steady state (100% conversion state). The reverse situation applies in the low temperature region. For a sufficiently low temperature, it is expected that the two boundaries will join together and the reaction will have only one steady state (a low conversion state). The effect of the reaction temperature on the width of the multiplicity region is clearly shown in Figure 3.9. Under the present experimental conditions, the reaction has the widest multiplicity region at a temperature of about 200°C. With either increasing or decreasing temperature, the multiplicity region becomes narrower.

Another factor which affects the transition points is the feed composition to the reactor. At a constant temperature, the location of the multiplicity points can be shifted by simply changing the composition of the reactants (CO or N_2O). Raising the N_2O (or CO) composition in the feed moves the transition points to higher CO (or N_2O) concentrations. The overall effect of the feed composition on the width of the multiplicity region is that increasing either reactant feed composition will enlarge the multiplicity region.

3.3 Inter- and Intraparticle Mass Transfer Effects

Before proceeding to an examination of various mechanisms for the N_2O reduction reaction it is first necessary to determine to what extent, if any, the experimental observations have been affected by internal and external mass transfer limitations. Satterfield (1980) provides several approximate criteria which can be used to determine if the observed kinetics are representative of the intrinsic kinetics.

Intraparticle diffusional effects can be assessed by determining the value of a Thiele modulus of the form:

$$\phi_s = \frac{r_p^2(-r)}{D_{eff}C_s} \tag{3.2}$$

where r_p is the effective radius of the catalyst pellet (cm), (-r) is the observed rate of reaction (mol/s·cm³), D_{eff} is the effective diffusion coefficient (cm²/s), and C_s is the concentration at the outside of the catalyst pellet (mol/cm³). According to Satterfield (1980) intrinsic kinetics are being observed if $\phi_s<6$ for a zeroth-order reaction, or $\phi_s<1$ for a first-order reaction. In addition, Smith et al. (1975) have shown that for a negative-order reaction, $\phi_s<10$ is sufficient for intrinsic kinetics to be measured.

For the data collected in the "low" conversion region, the calculation of ϕ_s shows that intrinsic kinetic behavior has been observed. For example, at 210°C, with $\%N_2O=0.855$ and $\%CO=0.323$ in the feed, a CO conversion of 0.796 was achieved with a $\%CO=0.066$ in the reactor and a reaction rate of 1.76×10^{-8} mol/g·s. The catalyst was an egg-shell type catalyst in which all the platinum was deposited in the outer 10% (or less) of the volume of the pellets. Thus, while the volume of a catalyst pellet is 0.0258 cm³, the "effective" volume of catalyst is only 0.00258 cm³ per pellet. Since there are 454 pellets in 20 g of catalyst, the actual effective volume of catalyst is 1.17 cm³. Thus, (-r) is determined to be $1.76\times10^{-8}(20/1.17) = 3\times10^{-7}$ mol/s·cm³. The value of r_p can be calculated from 3V/S which gives a value of 0.016 cm when the effective volume is used for a single particle combined with an external surface area of 0.048 cm^2 for a pellet. At 210°C, a %CO of 0.066 translates into a concentration of $C_s=1.66\times10^{-8}$ mol/cm^3 and a value of $D_{eff}=0.0192$ cm^2/s for CO in N_2 can be estimated from tabulated values for similar catalysts as described by Satterfield (1980). Thus, using the preceding values it is found that $\phi_s=0.24$ which ensures that intrinsic kinetics were measured. Similar, or lower, values of ϕ_s are found for all other rate measurements in the low rate region (conversions up to 80%). Thus, the measurements on the low conversion rate branch are unaffected by internal diffusional limitations. Unfortunately, the same cannot be conclusively stated for the measurements in the "high" rate region (conversions very close to 100%) because the very low CO concentrations in the reactor could not be accurately determined. Thus, because of the possibility of diffusional effects on the high rate data, in the following only the low rate data will be used for discriminating among mechanisms and for estimating parameters.

In the preceding calculation it was assumed that the surface concentration was equal to the bulk concentration (no interparticle limitations). This can be readily shown to be the case through a calculation of the external fluid-to-particle mass transfer coefficient. For the previously used experimental conditions, the mass transfer coefficient k_c (cm/s) can be found from (Satterfield, 1980):

$$k_c = \frac{Gj_D}{\rho S_c^{0.67}} = \frac{0.357G}{\epsilon\rho} (\frac{\mu}{d_pG})^{0.359} (\frac{\rho D}{\mu})^{0.67} \qquad (3.3)$$

where $\epsilon=0.4$, $d_p=0.32$ cm, and at 210°C, $\mu=2.5\times10^{-4}$ g/cm·s, $\rho=7.04\times10^{-4}$ g/cm³ and D for CO in N_2 is 0.5 cm²/s. The superficial mass velocity, G, must be based on a flow rate of approximately 500 cm³/s (independent of temperature) delivered by the recycle compressor giving G=0.072 g/s·cm². From these values, $k_c=22.6$ cm/s is obtained from Equation 3.3. However, from

$$\text{rate (mol/s)} = A_ek_e(C_b-C_s) \qquad (3.4)$$

it is possible to determine the concentration gradient between the bulk and the interface with the pellets. The total external area of the 454 pellets is 219 cm² which gives that C_b-C_s is 7.1×10^{-11} mol/cm³ which is less than 0.5% of the bulk concentration, i.e. $C_s/C_b > 0.995$ which means that the external gradient is negligible. The absence of any interparticle mass transfer effects was also verified experimentally by varying the flow rate delivered by the recycle compressor. No effect on the reaction rate was observed for a wide range of recycle flow rates.

3.4 Summary

The reduction of nitrous oxide by carbon monoxide, on a supported platinum catalyst, in the temperature range of 170 to 246°C, has been examined. Multiplicity behavior was observed under the reaction conditions. In the multiplicity region, the reaction rate is dependent on the reaction starting conditions. The location of the multiplicity region is influenced by many factors, such as reaction temperature, the CO feed composition and the N_2O feed composition. Increasing the temperature shifts the multiplicity region towards higher CO feed compositions for a constant N_2O feed mole fraction, and towards lower N_2O feed compositions for a constant CO feed mole fraction. At a constant temperature, increasing the feed concentrations shifts the multiplicity region to higher concentrations. To our knowledge this is the first report of multiplicity behavior for the reduction of nitrous oxide by carbon monoxide.

Another important observation is that while CO can inhibit the reaction rate, a similar effect is not found for N_2O. CO_2 and N_2 are the only reaction products since the rate of oxygen desorption was found to be negligible.

4. EXAMINATION OF MECHANISMS FOR THE N_2O+CO REACTION

4.1 Introduction

According to the previously mentioned studies, possible reaction steps involved in the N_2O+CO reaction on a platinum catalyst are as follows:

(1) adsorption/desorption steps

$$CO(g) + M \rightleftharpoons CO\text{-}M \qquad (4.1)$$

$$N_2O(g) + M \rightleftharpoons N_2O\text{-}M \qquad (4.2)$$

$$O_2(g) + 2\,M \rightleftharpoons 2\,O\text{-}M \qquad (4.3)$$

(2) N_2O decomposition steps

$$N_2O(g) + M \longrightarrow N_2(g) + O\text{-}M \qquad (4.4)$$

$$N_2O\text{-}M \longrightarrow N_2(g) + O\text{-}M \qquad (4.5)$$

$$2\,N_2O(g) + M \longrightarrow 2\,N_2(g) + O_2(g) + M \qquad (4.6)$$

(3) surface reaction steps (L-H type)

$$N_2O\text{-}M + CO\text{-}M \longrightarrow N_2(g) + CO_2(g) + 2\,M \qquad (4.7)$$

$$CO\text{-}M + O\text{-}M \longrightarrow CO_2(g) + 2\ M \qquad (4.8)$$

(4) gas-surface reaction steps (E-R type)

$$N_2O(g) + CO\text{-}M \longrightarrow N_2(g) + CO_2(g) + M \qquad (4.9)$$

$$CO(g) + O\text{-}M \longrightarrow CO_2(g) + M \qquad (4.10)$$

However, some of these reaction steps do not occur, or are not important for nitrous oxide reduction by carbon monoxide under the conditions used in this study. Hence, before attempting to describe the kinetics of N_2O reduction by CO, an examination, in light of the experimental data, will be made to determine if some of these steps can be eliminated.

4.1.1 Oxygen Desorption (step 4.3)

As was shown in Chapter 3, the calculated value of $[O_2]_{EXIT}$ scatters about a value of zero for the various experiments. This indicates that the oxygen desorption rate is negligible. Thus, oxygen desorption, step (4.3), can be eliminated in the following consideration of the mechanism of the N_2O+CO reaction system. A further consequence of this is that it is also possible to eliminate step (4.6) from further consideration.

4.1.2 Nitrous Oxide Adsorption (step 4.4)

It was observed from the experiments that, when the reaction occurs in the low N_2O concentration region, the CO_2 formation rate increases with increasing N_2O concentration in the feed, whereas the rate remains constant in the high concentration region (see Figure 3.7). These experiments indicate that excess N_2O does not have an inhibitive effect on CO oxidation rates. Thus, either N_2O does not adsorb on the catalytic surface, or if it does adsorb it immediately decomposes (low surface coverage). Otherwise, increasing the N_2O feed composition would increase the N_2O surface coverage, resulting in less CO adsorbed on the surface. This would cause a decline of the CO oxidation rate.

Thus, the observed reactor behavior can be described by a reaction mechanism, which does not include a N_2O adsorption/desorption step. In the following studies, this process, i.e. step (4.2), is neglected. Since a N_2O surface species does not exist, N_2O-M decomposition, step (4.5), and surface reaction, step (4.7), are also eliminated from consideration.

4.1.3 Remaining Reaction steps

From the experimental data it has been possible to immediately eliminate five of the reaction steps listed at the beginning of this section. This leaves five possible reaction steps. They are:

(1) adsorption/desorption step

$$CO(g) + M \rightleftharpoons CO\text{-}M \qquad (4.1)$$

(2) N_2O decomposition step

$$N_2O(g) + M \longrightarrow N_2(g) + O\text{-}M \qquad (4.4)$$

(3) surface reaction steps (L-H type)

$$CO\text{-}M + O\text{-}M \longrightarrow CO_2(g) + 2\,M \qquad (4.8)$$

(4) gas-surface reaction steps (E-R type)

$$N_2O(g) + CO\text{-}M \longrightarrow N_2(g) + CO_2(g) + M \qquad (4.9)$$

$$CO(g) + O\text{-}M \longrightarrow CO_2(g) + M \qquad (4.10)$$

The remaining part of this chapter is concerned with examining the predictions of various N_2O+CO reaction mechanisms. Mechanisms to be proposed are composed of varying numbers of elementary reactions. Among them, CO adsorption/desorption is considered as a basic step (supported by the experimental data). It will be involved in all of the examined reaction mechanisms. The assumptions of CO adsorption/desorption equilibrium and reaction steady state are made in the model description. Relaxing the equilibrium assumption for CO adsorption/desorption was found to have only a minor effect on the model predictions. Steadt-state balance equations for each of the following mechanisms are summarized in Appendix 5.

4.2 Mechanism 1

According to the observed products of the N_2O+CO reaction, the simplest potential mechanism for this reaction is composed of two reaction steps. They are CO adsorption/-desorption, step (4.1), and an E-R reaction, step (4.9), between gas phase N_2O and adsorbed CO. The overall mechanism is as follows:

$$CO(g) + M \rightleftharpoons CO\text{-}M \qquad (4.1)$$

$$N_2O(g) + CO\text{-}M \longrightarrow N_2(g) + CO_2(g) + M \qquad (4.9)$$

If gas-surface equilibrium is assumed, the CO surface coverage can be expressed by:

$$\theta_{CO} = \frac{K_1\,[CO]}{1 + K_1\,[CO]} \qquad (4.11)$$

Hence, the reaction rate is

$$R_{CO_2} = a\ k_9\ [N_2O]\ [CO\text{-}M]$$

$$= \frac{a\ L\ k_9\ K_1\ [N_2O]\ [CO]}{1 + K_1\ [CO]} \qquad (4.12)$$

It is seen that the reaction rate increases monotonically with increasing reactant concentrations. Thus, this rate expression cannot lead to multiple steady-state behavior. It can be concluded that the process of nitrous oxide reduction by carbon monoxide cannot be described by Mechanism 1. Thus, step (4.9) does not play a role in producing multiple steady states. From this point of view, step (4.9) is not an important step, although it cannot be ruled out of the overall reaction mechanism.

4.3 Mechanism 2

An alternate pathway for producing the products is via the reaction of adsorbed oxygen with adsorbed CO. The adsorbed oxygen is produced through N_2O decomposition, step (4.4). Because both oxygen and carbon monoxide compete for the same empty surface sites, the coverage of these two species varies with the feed composition. It can be expected that at high CO concentrations (low N_2O concentrations), the surface will be highly covered with CO. Alternatively, oxygen will be the main surface species when the N_2O concentration is in large excess over the CO concentration.

Mechanism 2 is assumed to proceed through the following reaction steps:

$$\mathrm{CO(g)} + \mathrm{M} \rightleftharpoons \mathrm{CO\text{-}M} \qquad (4.1)$$

$$N_2O(g) + M \longrightarrow N_2(g) + O\text{-}M \qquad (4.4)$$

$$CO\text{-}M + O\text{-}M \longrightarrow CO_2(g) + 2\ M \qquad (4.8)$$

Based on this mechanism, balance equations can be written for the gas and the surface phases. From these balance equations, the fractional surface coverages can be determined for given reactant concentrations when the kinetic parameters and reactor operating parameters are specified. For example, assuming that adsorption/desorption equilibrium holds for CO and using a steady-state balance equation for the surface oxygen, it gives that:

$$\theta_o = \frac{K_{4/8}\ [N_2O]}{K_1[CO] - K_4[N_2O]} \qquad (4.13)$$

$$\theta_{CO} = \frac{K_1[CO]-(K_4+K_{4/8}[N_2O])}{1+K_1[CO]-K_4[N_2O]} \qquad (4.14)$$

From step (4.8) it is seen that the rate expression will now be given by:

$$R_{CO_2} = a\ k_8\ [CO\text{-}M]\ [O\text{-}M]$$

$$= \frac{K_{LH}[N_2O](K_1[CO]-(K_4+K_{4/8}[N_2O]))}{(1+K_1[CO]-K_4[N_2O])(K_1[CO]-K_4[N_2O])} \qquad (4.15)$$

Because the experimental rates are known as functions of the reactant compositions, it is now possible to estimate the values of the kinetic parameters so as to obtain agreement between the model and the data (assuming that such agreement is possible). Note, this procedure can only be carried out for the experiments in which the conversions of CO and N_2O were not in the neighborhood of 100% because it is not possible to reliably determinate the reactor concentrations in this reactor. Thus, in the first part of the parameter estimation process, the model predictions are forced to match the bifurcation point locations for the transition from the low to the high conversions. Model agreement with the high to low conversion bifurcation point locations is not initially considered. The computer program for calculating the CO conversions is presented in Appendix 7. The values of the kinetic parameters used for the various models are listed in Table 4.1, and the reaction steps included in each mechanism are summarized in Table 4.2. Initial model examination is based on the agreement of the predictions with the experimental observations at 210°C.

Shown in Figure 4.1 are experimental CO conversions and the predictions from Mechanism 2. The experimental results are represented by symbols, and the numerical results are represented by lines. The results indicate that Mechanism 2 can describe the multiplicity behavior of this reaction system. Unfortunately, it is also seen from Figure 4.1 that the CO conversion predictions are not accurate. Except for a few points close to the bifurcation point locations, all of the

Table 4.1 Values of Parameters for Mechanisms

Figure	Values of Kinetic Parameters*
4.1	$K_1=325$, $K_4=0.15$, $K_{4/8}=5$, $K_{LH}=16$
4.2	$K_1=700$, $K_4=0.15$, $K_{4/8}=9$, $K_{LH}=25$, $K_{ERN2O}=0.045$
4.3	$K_1=325$, $K_4=0.2$, $K_{4/8}=10$, $K_{LH}=12$, $K_{ERN2O}=0.08$, $K_{ERCO}=8$
4.4	$K_1=325$, $K_4=0.08$, $K_{4/8}=8$, $K_{LH}=9$, $K_{16}=2$
4.5	$K_1=700$, $K_4=0.15$, $K_{4/8}=9$, $K_{LH}=25$, $K_{17}=0.09$
4.6	$K_1=100$, $K_4=0.01$, $K_{4/8}=5$, $K_{LH}=5.6$, $K_{18}=1.5$
4.7	$K_1=700$, $K_4=1.00$, $K_{4/8}=1.2$, $K_{LH}=16$, $\mu=1.0$
4.8	$K_1=225$, $K_4=0.25$, $K_{4/8}=2.4$, $K_{LH}=8.75$, $N_{CO}=1.03$

* These parameters are used to describe the observations at a temperature of 210°C.

Table 4.2 Reaction Steps Involved in Mechanisms

Mechanism	Reaction Steps
Mech. 1	(4.1), (4.9)
Mech. 2	(4.1), (4.4), (4.8)
Mech. 3	(4.1), (4.4), (4.8), (4.9)
Mech. 4	(4.1), (4.4), (4.8), (4.10)
Mech. 5	(4.1), (4.4), (4.8), (4.9), (4.10)
Mech. 6	(4.1), (4.4), (4.8), (4.16)
Mech. 7	(4.1), (4.4), (4.8), (4.17)
Mech. 8	(4.1), (4.4), (4.8), (4.18)
Mech. 9	(4.1), (4.4), (4.8), with $\mu = 1.0$
Mech. 10	(4.1), (4.4), (4.8), with $N_{CO}>1.0$
Mech. 11	(4.1), (4.4), (4.8), (4.10), with $N_{CO}>1.0$

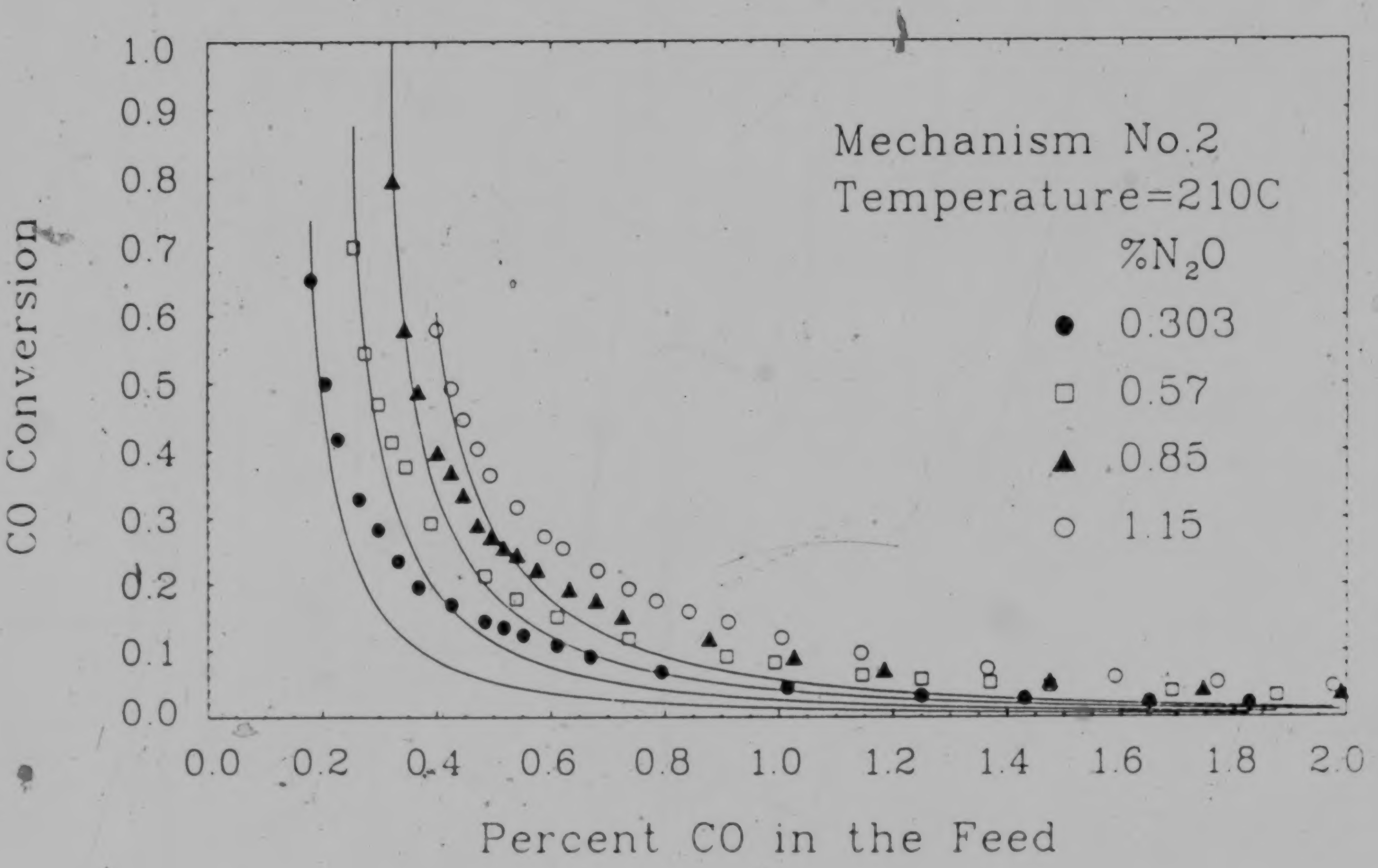

Figure 4.1 CO Conversion Predictions from Mechanism 2

predicted CO conversions are below the experimental observations. It is not possible for any set of parameter values to have complete agreement with the low to high bifurcation points as well as the low conversions. Clearly, this mechanism is unable to describe the experimental observations. However, it can qualitatively describe multiplicity behavior for the N_2O+CO reaction system. This is because N_2O decomposition, step (4.4), combined with the bimolecular surface reaction, step (4.8), produces an overall mechanism which is very similar to the classical Langmuir-Hinshelwood mechanism for the CO+O_2 reaction, a mechanism which is known to give rise to multiplicity behavior.

The numerical predictions show that at high CO concentrations, the catalytic surface is highly covered by CO. Very few empty sites are available for N_2O molecules to decompose on the surface. Because of a lack of surface oxygen, the CO oxidation rate is limited. In other words, the N_2O decomposition rate limits the CO oxidation rate. Hence, in the actual process of nitrous oxide reduction by carbon monoxide, some other step(s) must be involved. Possible reaction steps which could lead to higher CO conversions at high CO concentrations are listed below:

1. other possible CO oxidation pathways, such as steps (4.9) and (4.10);
2. reaction steps which can prevent the catalyst surface from being highly covered by CO, such as:

$$\text{CO-M} + \text{CO-M} \longrightarrow \text{CO(g)} + \text{CO-M} + \text{M} \qquad (4.16)$$

$$\text{CO(g)} + \text{CO-M} \longrightarrow 2\ \text{CO(g)} + \text{M} \qquad (4.17)$$

3. an additional reaction step for producing surface oxygen

$$\text{N}_2\text{O(g)} + \text{CO-M} \longrightarrow \text{N}_2\text{(g)} + \text{CO(g)} + \text{O-M} \qquad (4.18)$$

The mechanisms to be examined in the following contain one or more of these reaction steps, together with the steps in Mechanism 2. The purpose of these modified mechanisms is to obtain improved predictions for the low conversion data.

4.4 Mechanism 3

First of all, the effect of other CO oxidation pathways on the model predictions will be examined. The reaction between gas phase nitrous oxide and adsorbed carbon monoxide (step 4.9) is introduced into Mechanism 2 to create Mechanism 3. The step (4.9) is favored at high CO concentrations and its reaction rate is not affected by a lack of surface oxygen. It can be expected that including this step in the reaction mechanism will increase CO conversions at high CO concentrations. Hence, Mechanism 3 is composed of reaction step (4.10) and the steps in Mechanism 2, giving the overall mechanism:

$$CO(g) + M \rightleftarrows CO\text{-}M \qquad (4.1)$$

$$N_2O(g) + M \longrightarrow N_2(g) + O\text{-}M \qquad (4.4)$$

$$CO\text{-}M + O\text{-}M \longrightarrow CO_2(g) + 2\ M \qquad (4.8)$$

$$N_2O(g) + CO\text{-}M \longrightarrow N_2(g) + CO_2(g) + M \qquad (4.9)$$

The predictions from Mechanism 3 are presented in Figure 4.2. Comparing Figure 4.2 with Figure 4.1, it is seen that Mechanism 3 provides a better description of the experimental observations than does Mechanism 2. At very high CO concentrations the predicted CO conversions are increased as expected. In the intermediate region, Mechanism 3 also provides better predictions. However, the CO conversions still do not totally match the experimental observations. In the range of %CO from 1.4 to 2.0 with $\%N_2O=1.15$, the predicted CO conversions are higher than the observations; while for $\%N_2O=0.303$, the predicted CO conversions are below the experimental points. At intermediate %CO from 0.2 to 1.4 the predicted CO conversions are all below the observed values for $\%N_2O=0.303$ and $\%N_2O=0.57$. For high N_2O feed compositions, the predictions are in good agreement with the data. Mechanism 3 still cannot give completely satisfactory predictions for the low conversion branch. Such discrepancies were found for all values of the rate constants which were examined.

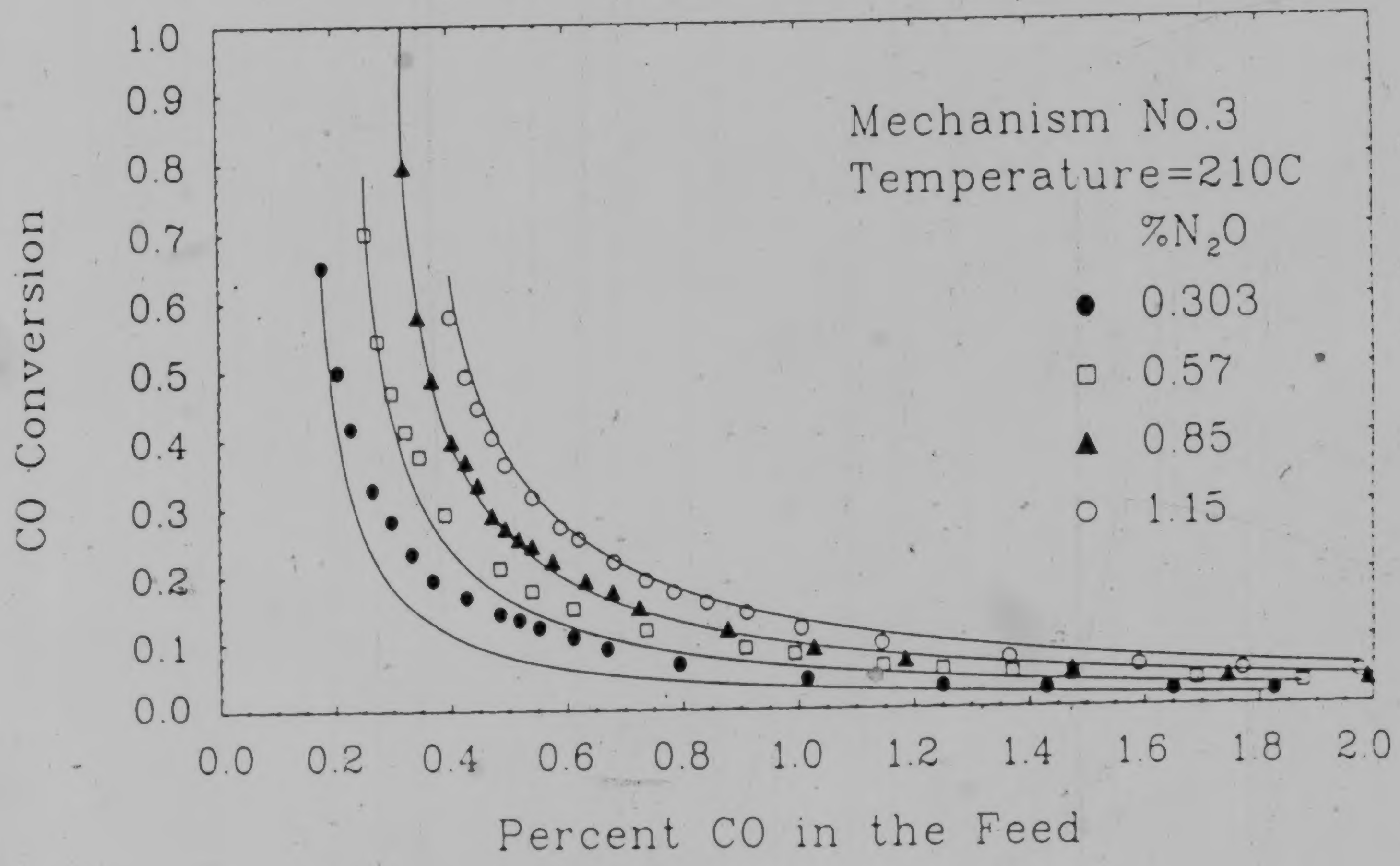

Figure 4.2 CO Conversion Predictions from Mechanism 3

4.5 Mechanism 4

Mechanism 4 is a combination of an Eley-Rideal type CO oxidation step (4.10) with Mechanism 2 (the E-R step in Mechanism 4 uses gas-phase CO whereas that in Mechanism 3 uses gas-phase N_2O). Mechanism 4 consists of the following reaction steps:

$$CO(g) + M \rightleftarrows CO\text{-}M \qquad (4.1)$$

$$N_2O(g) + M \longrightarrow N_2(g) + O\text{-}M \qquad (4.4)$$

$$CO\text{-}M + O\text{-}M \longrightarrow CO_2(g) + 2\ M \qquad (4.8)$$

$$CO(g) + O\text{-}M \longrightarrow CO_2(g) + M \qquad (4.10)$$

During the modelling work, it was found that the predictions from Mechanism 4 are not as good as the predictions from Mechanism 3. The predicted CO conversions are all below the experimental points when the bifurcation locations are matched. By comparing these predictions with the Mechanism 2 results, it is found that the predictions from these two mechanisms are almost identical at high CO concentrations. This is due to the similar CO oxidation processes involved in Mechanisms 2 and 4. In both mechanisms CO oxidation needs surface oxygen, and it is only provided by the N_2O decomposition step. Because Mechanism 4 does not provide extra surface oxygen, the predicted conversions are not increased in the high CO concentration region.

4.6 Mechanism 5

Based on Mechanism 2, reaction steps (4.9) and (4.10) have been employed in the establishment of Mechanisms 3 and 4, respectively. The results have shown that neither Mechanism 3 nor Mechanism 4 provides satisfactory predictions. At very high CO concentrations, the predictions from Mechanism 4 are much too low, while the predictions from Mechanism 3 are somewhat better. In the present mechanism (Mechanism 5), both reaction steps, (4.9) and (4.10) are included as pathways for CO_2 formation.

$$CO(g) + M \rightleftharpoons CO\text{-}M \qquad (4.1)$$

$$N_2O(g) + M \longrightarrow N_2(g) + O\text{-}M \qquad (4.4)$$

$$CO\text{-}M + O\text{-}M \longrightarrow CO_2(g) + 2\ M \qquad (4.8)$$

$$N_2O(g) + CO\text{-}M \longrightarrow N_2(g) + CO_2(g) + M \qquad (4.9)$$

$$CO(g) + O\text{-}M \longrightarrow CO_2(g) + M \qquad (4.10)$$

However, the model predictions indicate that no significant improvement of the predictions occurs through the use of Mechanism 5. The predictions are shown in Figure 4.3. In the very high CO region, the predictions have been improved

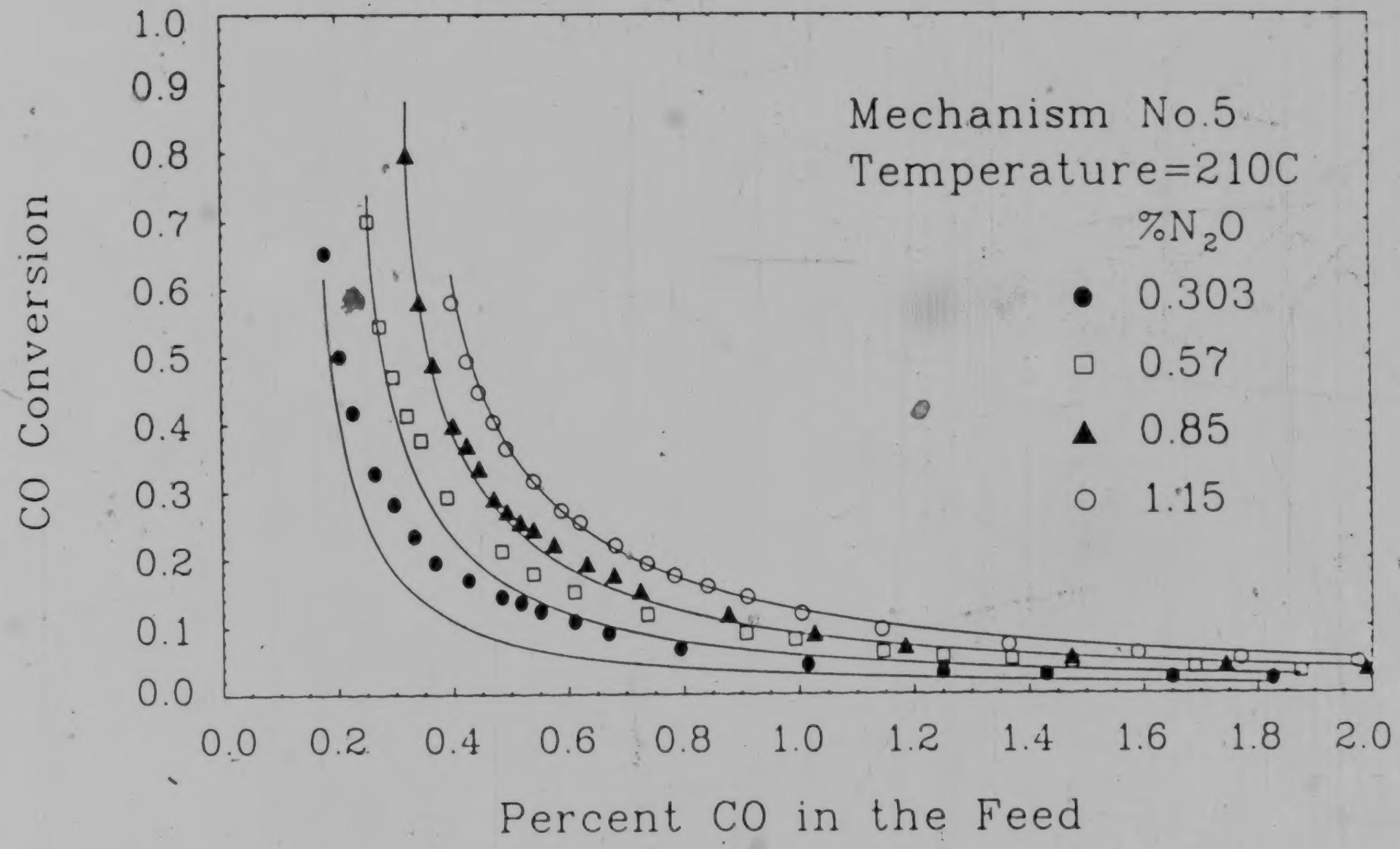

Figure 4.3 CO Conversion Predictions from Mechanism 5

slightly, but, in the intermediate region, the predictions still do not match the experiments for the cases of $\%N_2O=0.303$ and $\%N_2O=0.57$. The predictions from Mechanism 5 are in fact very similar to those from Mechanism 3.

4.7 Mechanism 6

In order to improve (increase the CO conversions) the predictions for the intermediate and high CO regions, additional CO oxidation pathways were introduced into the reaction mechanism. The results show that this method does not work very well. Hence, other kinds of reaction steps will now be examined. For example, any process which limits the maximum CO coverage can potentially result in higher conversions in the high CO region. Such a process is given by step (4.16) in which it proposed that energy transfer from one adsorbed CO molecule to another would possibly provide the second molecule with sufficient energy for desorption to occur. Thus, Mechanism 6 is given by Mechanism 2 plus step (4.16):

$$CO(g) + M \rightleftharpoons CO\text{-}M \qquad (4.1)$$

$$N_2O(g) + M \longrightarrow N_2(g) + O\text{-}M \qquad (4.4)$$

$$CO\text{-}M + O\text{-}M \longrightarrow CO_2(g) + 2\,M \qquad (4.8)$$

$$\text{CO-M} + \text{CO-M} \longrightarrow \text{CO(g)} + \text{CO-M} + \text{M} \tag{4.16}$$

Unfortunately, upon examination it is found that the predictions from this model are intermediate between those from Mechanism 2 and the actual data (see Figure 4.4). The predicted curves all fall below the experimental data points when the CO feed composition is not very close to the corresponding bifurcation point.

4.8 Mechanism 7

In Mechanism 6, the energy necessary for "assisted" CO desorption was proposed to come from other adsorbed CO molecules. This idea can be extended to include energy transfer from gas-phase CO molecule, as in step (4.17). Thus, Mechanism 7 is given by:

$$\text{CO(g)} + \text{M} \rightleftharpoons \text{CO-M} \tag{4.1}$$

$$\text{N}_2\text{O(g)} + \text{M} \longrightarrow \text{N}_2\text{(g)} + \text{O-M} \tag{4.4}$$

$$\text{CO-M} + \text{O-M} \longrightarrow \text{CO}_2\text{(g)} + 2\ \text{M} \tag{4.8}$$

$$\text{CO(g)} + \text{CO-M} \longrightarrow 2\ \text{CO(g)} + \text{M} \tag{4.17}$$

Obviously, reaction step (4.17) is very similar to step (4.16). Both steps result in the removal of surface CO and the production of empty sites. The main difference is that

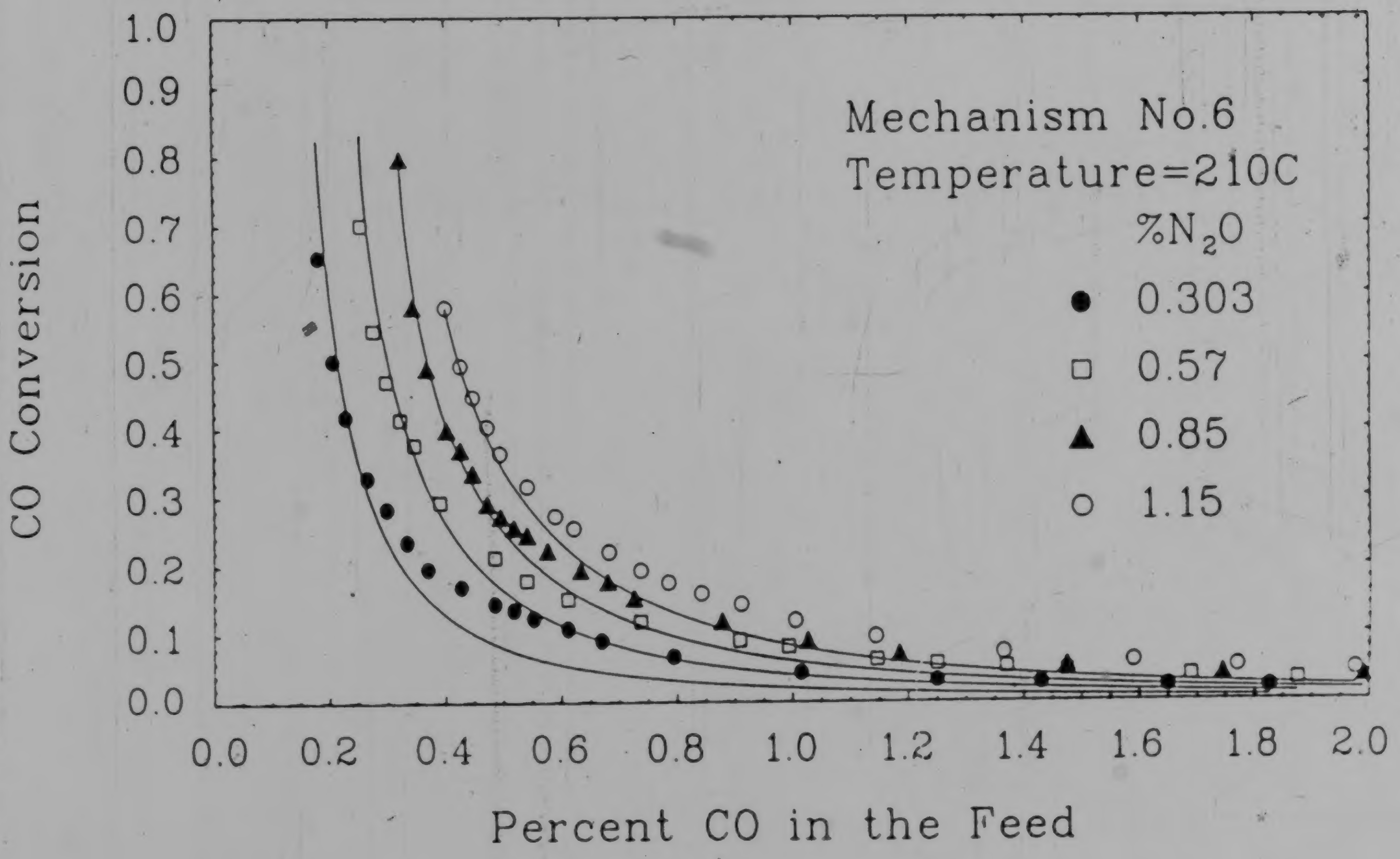

Figure 4.4 CO Conversion Predictions from Mechanism 6

in Mechanism 7 the "assisted" CO desorption rate will be directly proportional to the gas-phase CO concentration, whereas in Mechanism 6 this rate is only indirectly (and weakly) linked to the gas-phase CO concentration via the fractional coverage of CO which becomes relatively constant for high values of the gas-phase CO. From Figure 4.5 it is seen that the predictions have been significantly improved over Mechanism 2 (and even over Mechanism 3). However, certain systematic discrepancies are still apparent.

4.9 Mechanism 8

A further alternate route of displacing adsorbed CO is via N_2O collisions. Such a process, including subsequent N_2O decomposition, is given by step (4.18) which when included in Mechanism 2 produces Mechanism 8:

$$CO(g) + M \rightleftharpoons CO\text{-}M \tag{4.1}$$

$$N_2O(g) + M \longrightarrow N_2(g) + O\text{-}M \tag{4.4}$$

$$CO\text{-}M + O\text{-}M \longrightarrow CO_2(g) + 2M \tag{4.8}$$

$$N_2O(g) + CO\text{-}M \longrightarrow N_2(g) + CO(g) + O\text{-}M \tag{4.18}$$

The predictions from this mechanism are shown in Figure 4.6. It is noticed that curves in Figure 4.6 are identical to the curves in Figure 4.3 (predictions from Mechanism 3).

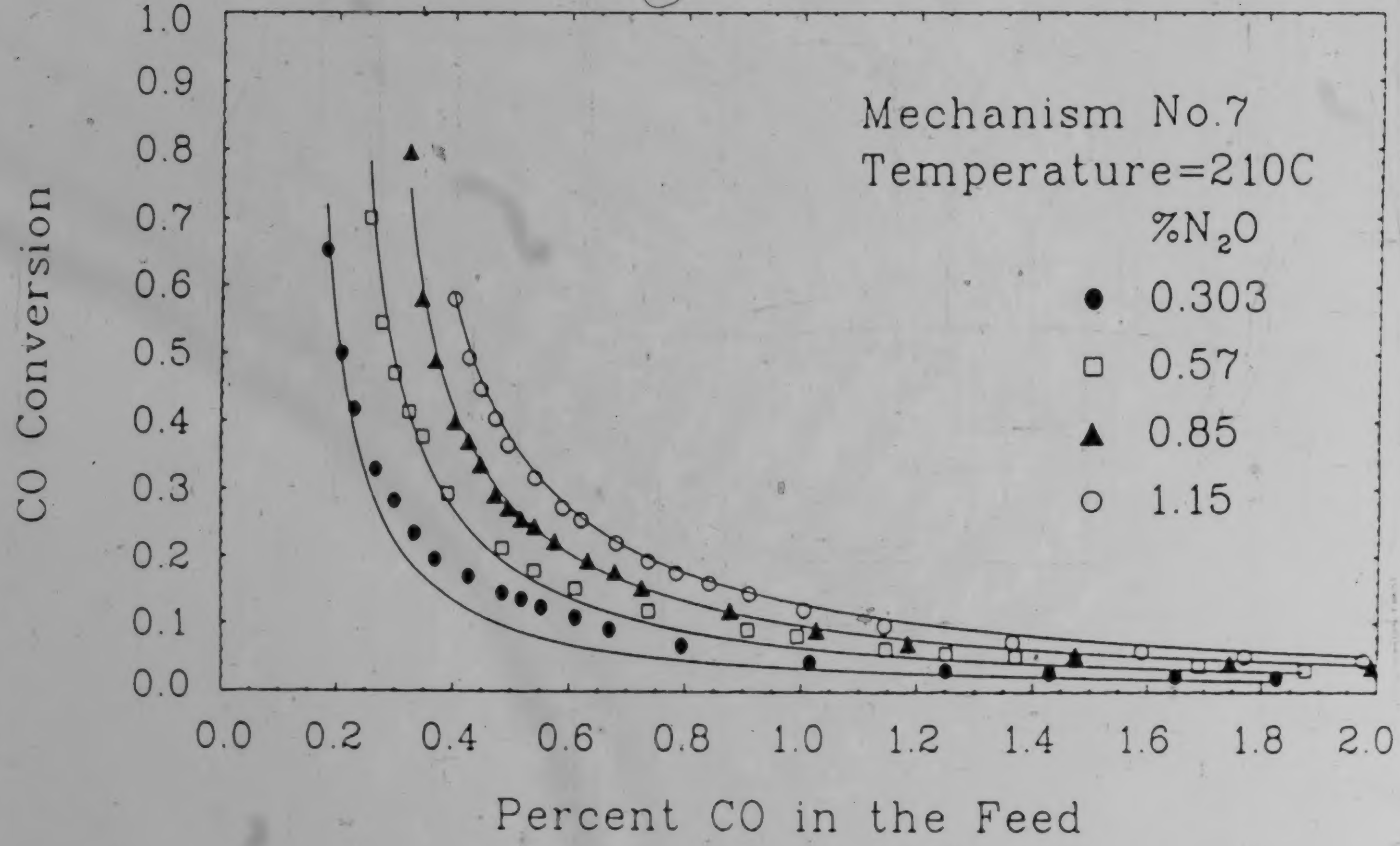

Figure 4.5 CO Conversion Predictions from Mechanism 7

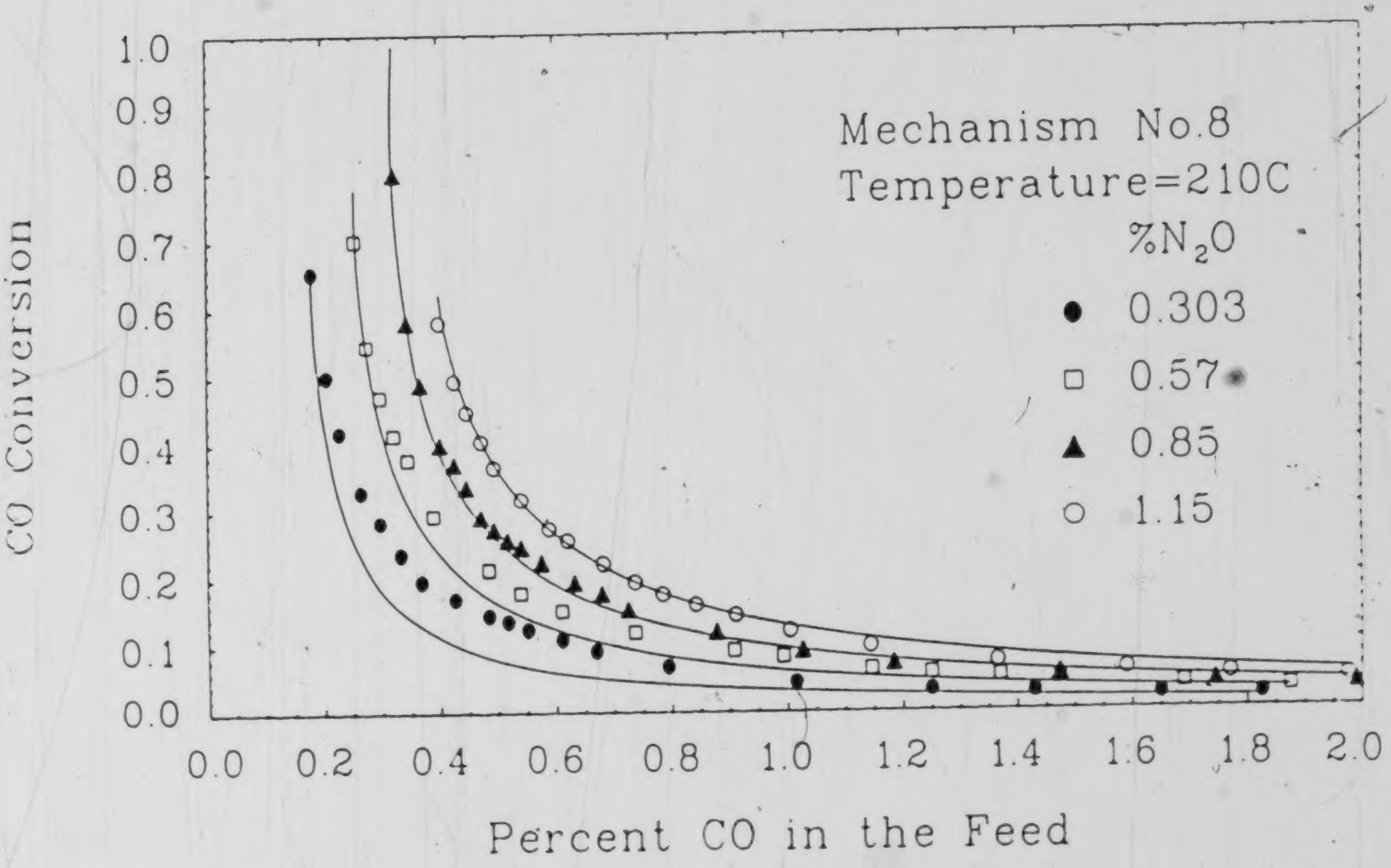

Figure 4.6 CO Conversion Predictions from Mechanism 8

In fact, Mechanism 3 and Mechanism 7 are very similar to each other. In Mechanism 3, the products for N_2O reaction with CO-M are gas phase N_2 and CO_2, while in Mechanism 7 the products for the same reaction step are gas phase N_2 and CO, and surface phase oxygen. When the reaction occurs at high CO concentrations, the surface oxygen reacts with CO immediately, and CO_2 is formed. Hence, in the former mechanism CO oxidation proceeds via one reaction step; in the latter it proceeds via two steps. This slight change does not have much influence on the model predictions.

In all of the preceding mechanisms, an ideal Langmuir surface has always been assumed, i.e. the surface is energetically uniform. However, there are many reports that the CO sticking probability and the heat of adsorption vary with the CO surface coverage. In addition, the saturation CO surface coverage is often found to be less than unity on highly dispersed platinum surfaces. This leads to the possibility that an over simplification of the CO adsorption/desorption process may cause the discrepancies between the model predictions and the data. Hence, in the following mechanisms modifications to the ideal surface assumption will be considered.

4.10 Mechanism 9

It was reported (Ertl et al., 1977) that on a Pt(111) surface the CO adsorption energy (ΔH_{ads}) decreases linearly from 136 kJ/mol at θ_{CO}=0.0 to 112 kJ/mol at θ_{CO}=0.45. At θ_{CO}=0.45, ΔH_{ads} makes a sudden drop by 12 kJ/mol and after θ_{CO}=0.6, ΔH_{ads} decreases rapidly to zero. One means by which these observations can be incorporated into a model is by assuming that the CO desorption activation energy is a function of the surface coverage. In Mechanism 9 the same reaction steps as Mechanism 2 are used, but it is assumed that CO desorption energy is exponentially dependent on the CO coverage. Thus, the CO desorption rate constant can be expressed as follows:

$$k_{CO,des} = k^{\circ}_{CO,des} \, EXP(-E_{des}/RT) \, EXP(\mu\theta_{CO}) \qquad (4.19)$$

where μ is a constant. If μ=0.0, the desorption process is not affected by the CO coverage. For positive values of μ, the CO desorption rate constant increases with the CO coverage which is in accord with reported observations.

Model predictions from Mechanism 9 using μ=1.0 are shown in Figure 4.7. It is seen from Figure 4.7 that the predictions from Mechanism 9 are a little better than the predictions from Mechanism 2, but, when the low bifurcation points are forced to match, the predicted CO conversions are still lower than the experimental data. This discrepancy persists for other values of μ. Therefore, it can be said that the variation of the CO heat of adsorption with CO coverage is not the main factor which affects the CO conversions in the high CO region.

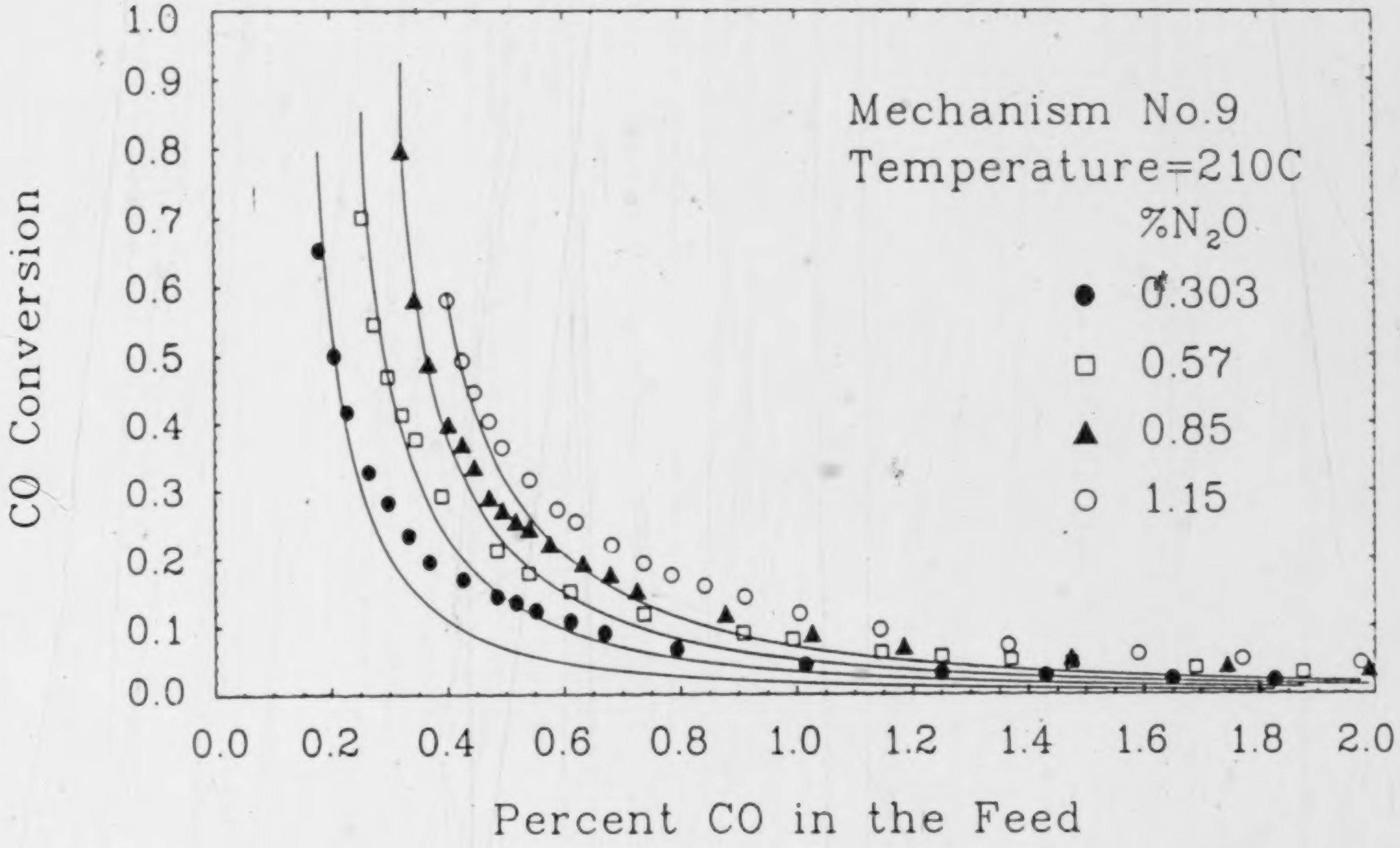

Figure 4.7 CO Conversion Predictions from Mechanism 9

4.11 Mechanism 10

Mechanism 10 has the same reaction steps as Mechanism 2, but, in Mechanism 10, a CO self-exclusion effect is used in the mathematical model, in order to account for the reported observations (Dorling and Moss, 1967; Freel, 1972) that the adsorption stoichiometry for CO on Pt can be somewhat less than one CO molecule for each exposed Pt atom. One way of expressing the net CO adsorption rate to account for this is given by:

$$R_{CO,ads} = k_1 \, [CO] \, (1-\theta_o-\theta_{CO}) \, \frac{(1-N_{CO}\theta_{CO})}{(1-\theta_{CO})} - k_{-1} \, \theta_{CO} \qquad (4.20)$$

When $N_{CO}=1.0$ in Equation (4.20) the rate of adsorption reverts to the standard Langmuir form, however values of N_{CO} greater than unity correspond to adsorption stoichiometries of less than unity (N_{CO}^{-1}). Thus to be consistent with the experimental observations that the CO adsorption stoichiometry is in the range 0.8 to 1.0, it is necessary to restrict N_{CO} to the range 1.0 to 1.25. Using the above CO adsorption rate expression in the balance equations for Mechanism 10, the CO conversions can be calculated, and typical results are shown in Figure 4.8 for a value of $N_{CO}=1.03$. This value of the self-exclusion factor was estimated by minimizing the sum of the squared errors between the calculated and the experimental CO conversions. It is seen from Figure 4.8 that the predictions from Mechanism 10 match the experimental data very well in the high CO region. The calculated CO

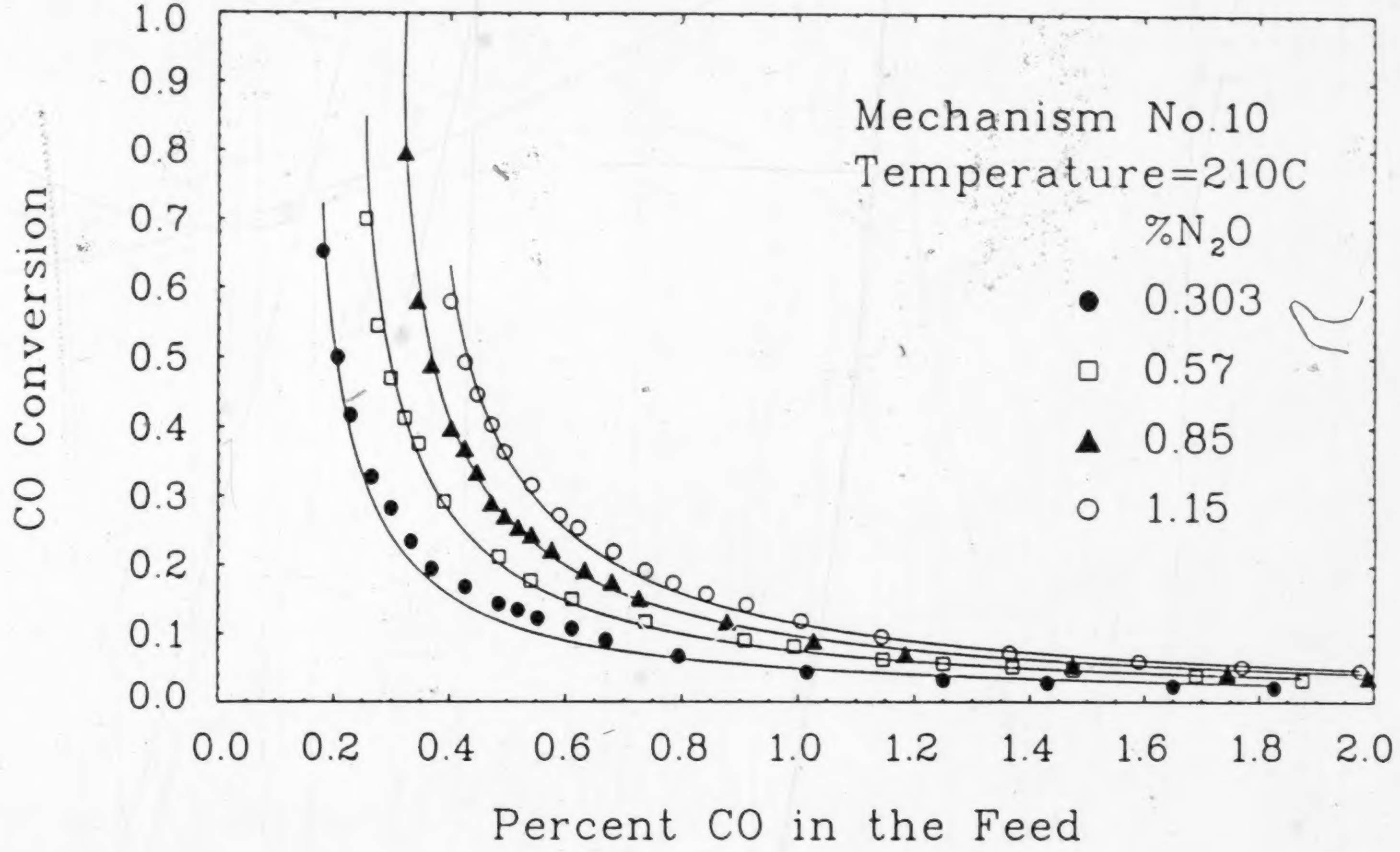

Figure 4.8 CO Conversion Predictions from Mechanism 10 at 210°C

conversion curves pass through most of the experimental data points. In the intermediate CO region, the predictions are also very much improved. In the previous models, the predictions poorly fit the data for the cases of $\%N_2O=0.303$ and 0.57, but it is seen that Mechanism 10 can give satisfactory predictions. It can be concluded that among the various mechanisms, Mechanism 10 provides the best model predictions for the low conversion branch.

In addition, with the self-exclusion factor held constant of 1.03, this mechanism is able to describe the reactor behavior over a wide temperature range (see Figures 4.9 and 4.10). In Figure 4.9 it is seen that good agreement of the model predictions with the experimental data at a temperature of 190°C is obtained (of course, new values of the rate constants were used). The accuracy of the predictions for this temperature is as high as for the experiments at 210°C. While the predictions for 246°C show somewhat more deviation than those for the 190°C and the 210°C experiments (see Figure 4.10), the predictions nevertheless are within the experimental errors associated with the data. Overall, Mechanism 10 can provide relatively accurate predictions for all of the experimental observations.

Using the parameter values obtained for the three temperatures, the activation energies for each reaction step were obtained from an Arrhenius plot of ln(k) versus 1/T, shown in Figure 4.11. The slope of each curve is the apparent activation energy for a particular reaction step. The

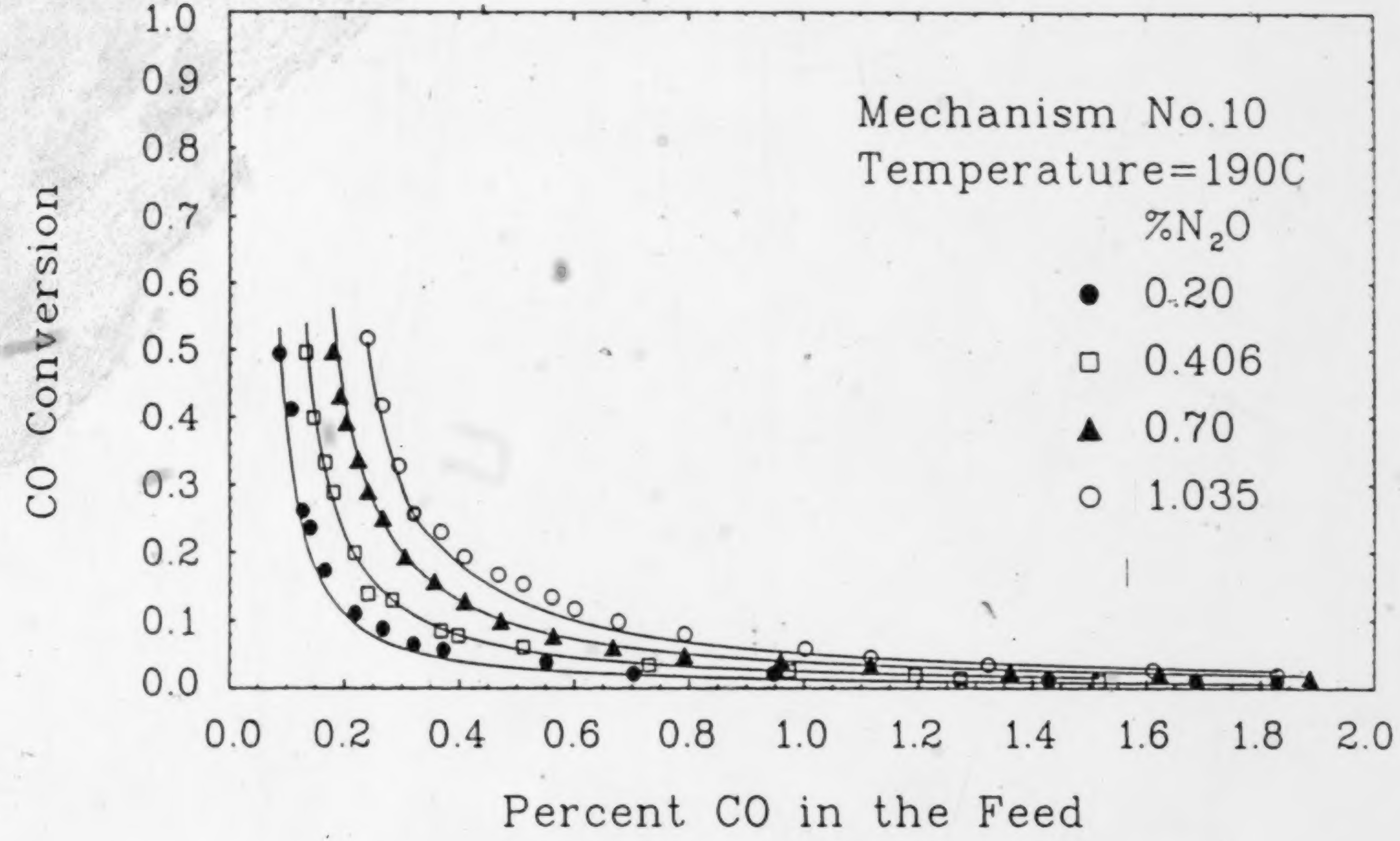

Figure 4.9 CO Conversion Predictions from Mechanism 10 at 190°C

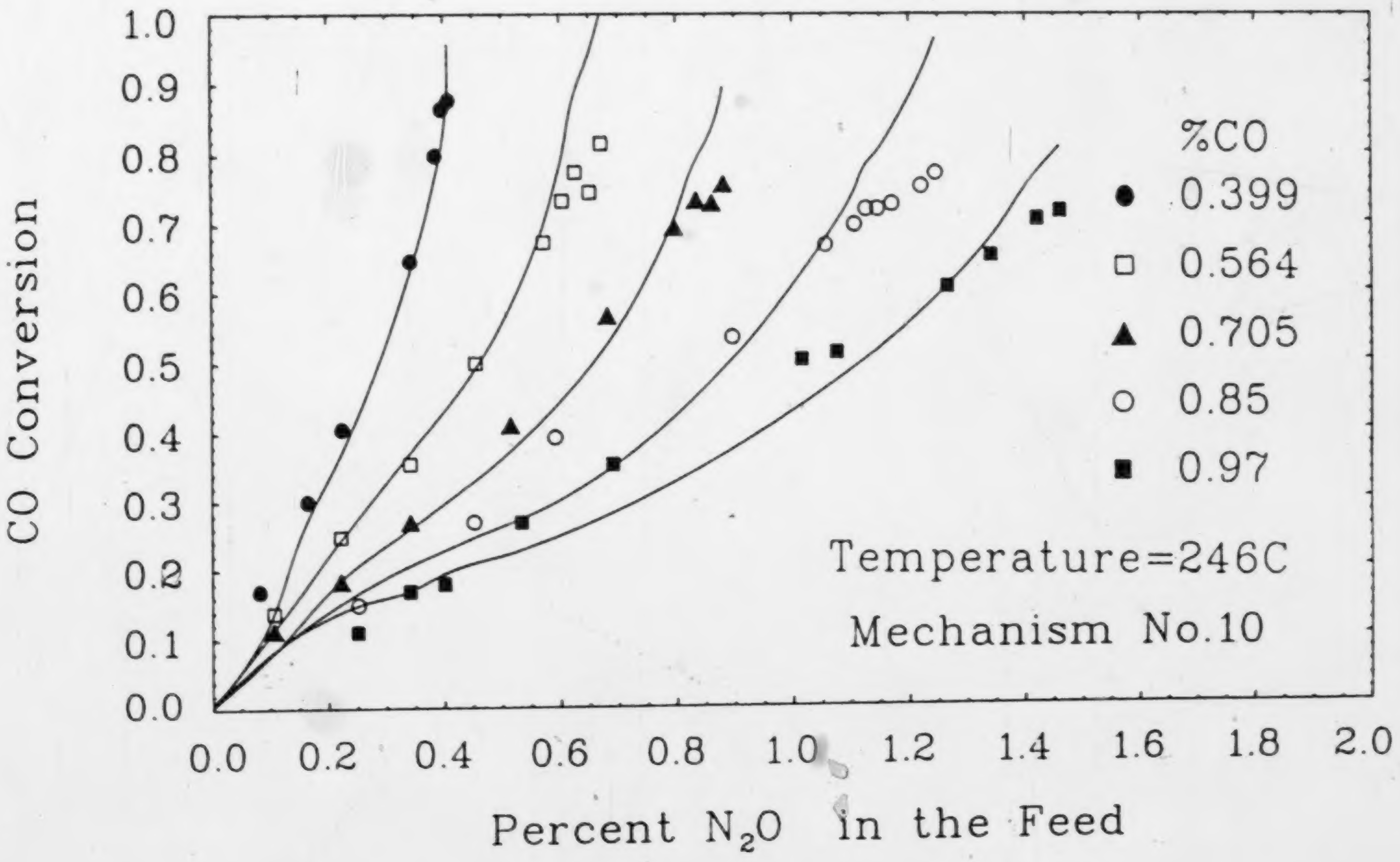

Figure 4.10 CO Conversion Predictions from Mechanism 10 at 246°C

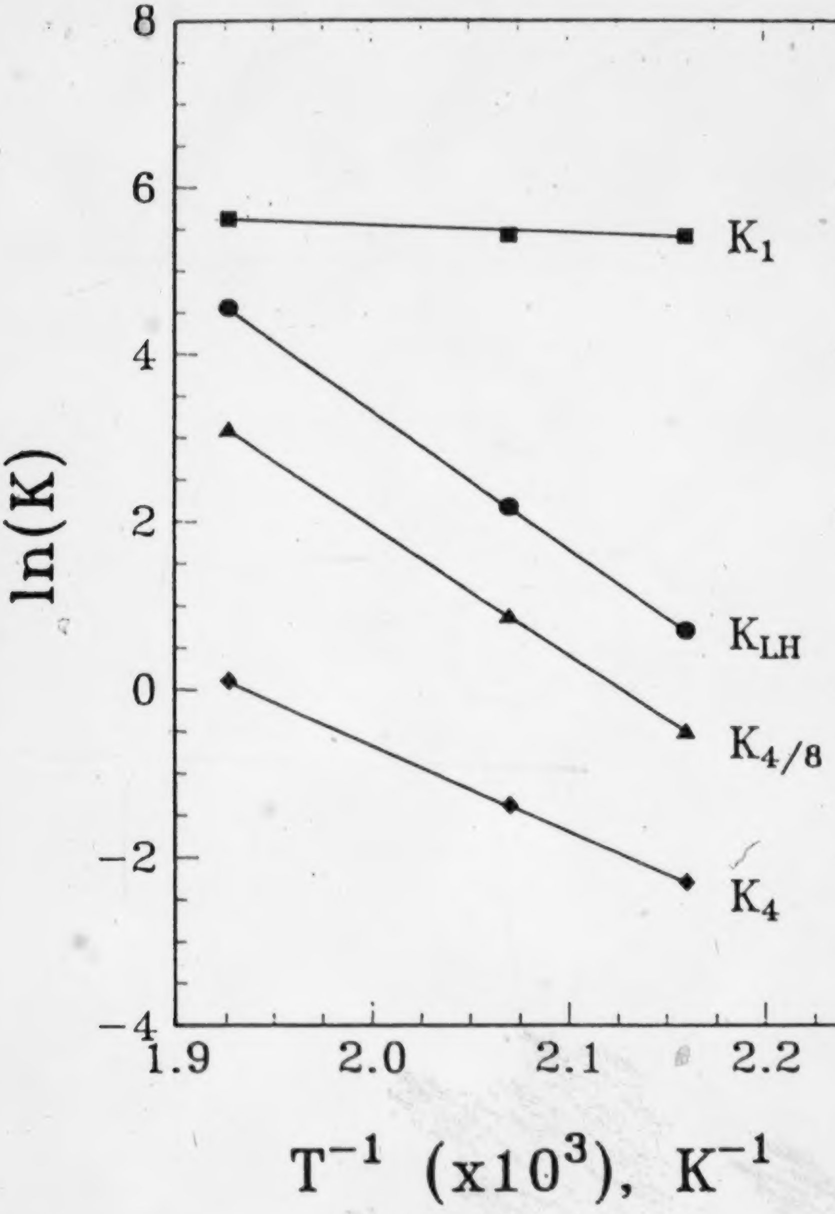

Figure 4.11 Arrhenius Analysis for Activation Energies

values of all model parameters and activation energies used for the predictions from Mechanism 10 shown in Figures 4.8 to 4.10 are listed in Table 4.3. It is seen that the CO desorption activation energy is estimated to be E_{-1}/R = 1000 from fitting the low CO conversion branch (surface saturated with CO). Ertl et al. (1977) reported that at $\theta_{CO}=0.0$, the CO heat of adsorption is 136 kJ/mol ($\Delta H_{ads}/R=17100$ K) whereas at $\theta_{CO}=0.7$ the CO heat of adsorption dropped almost to zero. Because our estimation is based on the high CO coverage region, the apparent activation energy should be much less than $\Delta H_{ads}/R=17100$ K, in fact, the value of E_{-1} resulting from Mechanism 10 is very close to zero.

It needs to be emphasized that the preceding model predictions have been made without concern about how the predictions would match the high conversion branch. Since a suitable mechanism must be able to describe the reaction behavior for both low and high conversions as well as the bifurcation point locations, the next step is to examine the predictions for the high conversion branch.

Shown in Figure 4.12 are predictions from Mechanism 10 for both low and high conversions. The computer program is attached in Appendix 7. Because agreement with all of the experimental data is desired, certain compromises have been made in terms of the parameter values. Thus, the predictions for the low branch do not totally agree with the experiments, and while the upper bifurcation points have been matched, the predictions for the high CO conversions are

Table 4.3 Values of Kinetic Parameters for Predictions in Figure 4.8 to Figure 4.10

Parameters	T=190°C	T=210°C	T=246°C	E/R
K_1	200	225	275	1000
K_4	0.1	0.25	1.1	10000
$K_{4/8}$	0.606	2.4	22.1	
K_{LH}	2.0	8.75	94.5	16500
N_{CO}	1.03	1.03	1.03	

incorrect. The disagreement between the model predictions and the experiments is clearly shown in Figure 4.12. The experiments indicate that high conversions do not decline with decreasing CO feed composition. The predictions for a temperature of 246°C also demonstrate the disagreement (see Figure 4.13). The model predicts that for the high CO conversion branch, the CO conversion should decrease with increasing N_2O mole fraction in the feed when the CO feed composition is kept constant. However, it was experimentally observed that CO is always completely converted into CO_2 (see Figure 3.7) when the reaction occurs in the high conversion region.

The failure of the model predictions can be understood by examining the elementary steps in Mechanism 10. According to the mechanism, the formation rate of surface oxygen is dependent upon the nitrous oxide concentration and the concentration of empty sites. When the N_2O feed composition is increased, or the CO feed composition is decreased, the oxygen surface coverage increases. When the oxygen surface

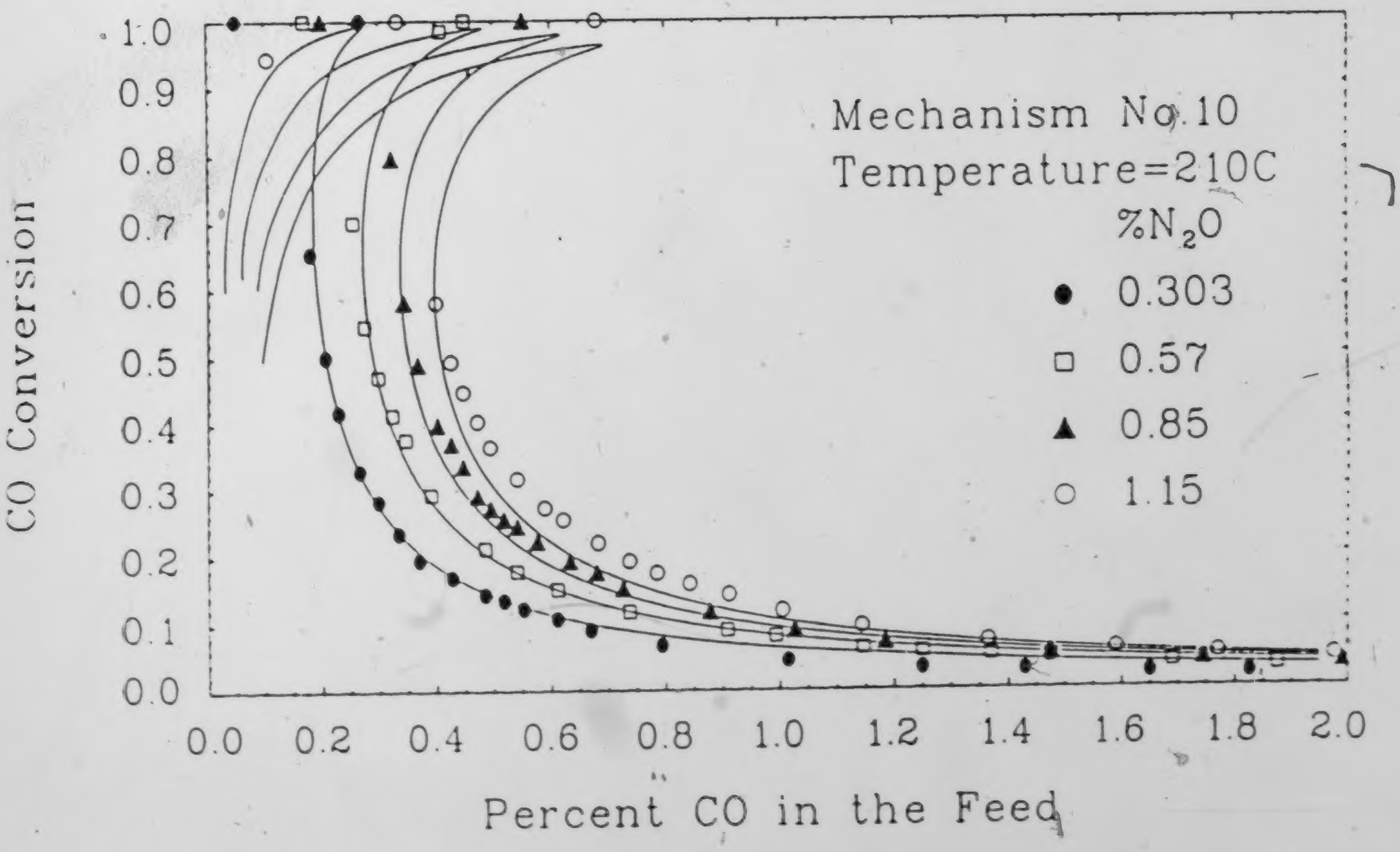

Figure 4.12 Overall Predictions from Mechanism 10 at 210°C

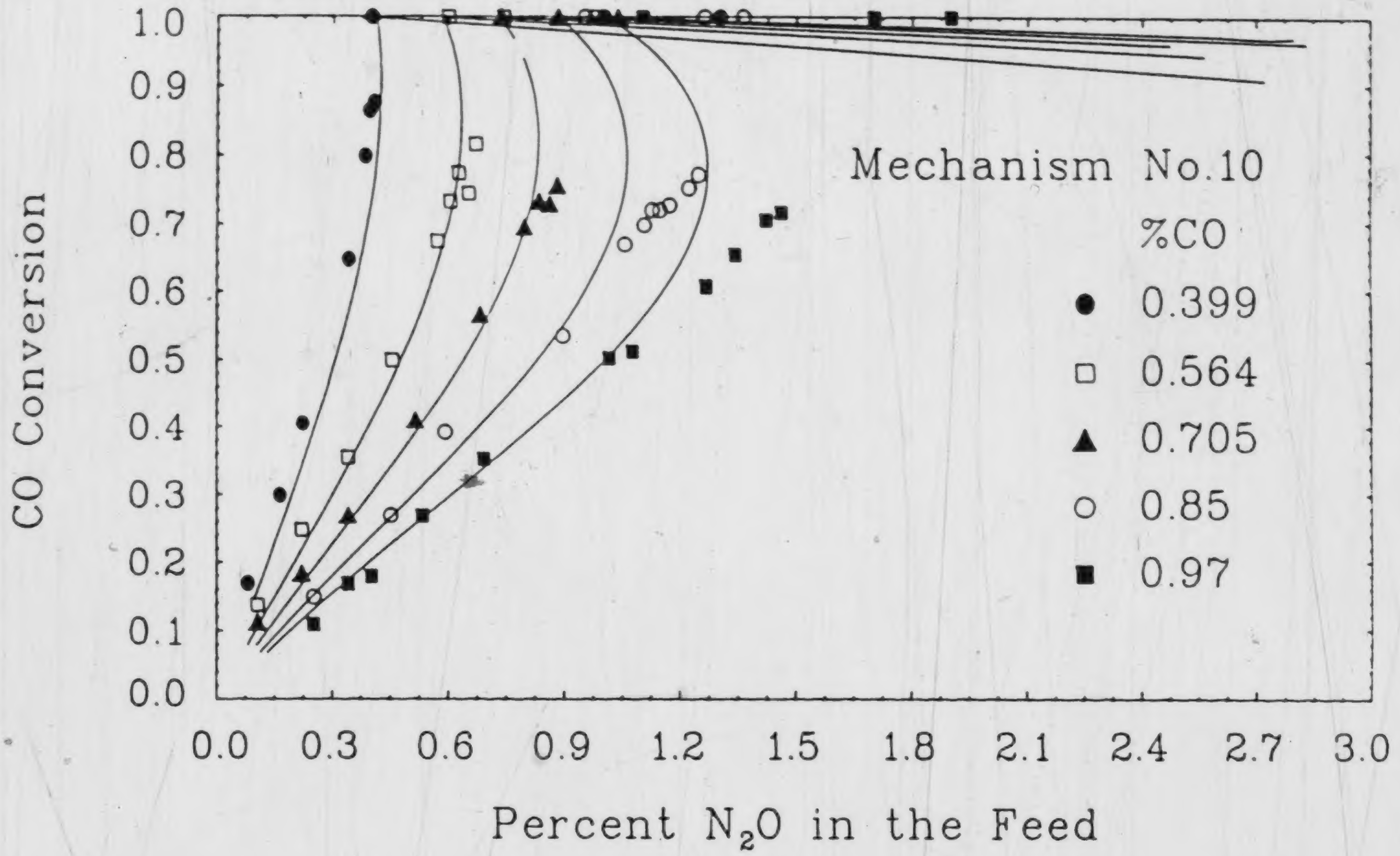

Figure 4.13 Overall Predictions from Mechanism 10 at 246°C

coverage becomes very high (close to unity) it interferes with the adsorption of CO. Since CO_2 can only be formed by the bimolecular surface reaction, decreased CO adsorption leads to decreased rates of CO_2 formation (and decreased CO conversions).

4.12 Mechanism 11

There are many possible modifications to Mechanism 10 which could potentially circumvent the problems caused by the very high surface coverages of oxygen. One route would be to postulate that an Eley-Rideal type reaction, step (4.10), also contributes to the overall conversion of CO. Thus, the overall mechanism would be given by:

$$CO(g) + M \rightleftarrows CO\text{-}M \qquad (4.1)$$

$$N_2O(g) + M \longrightarrow N_2(g) + O\text{-}M \qquad (4.4)$$

$$CO\text{-}M + O\text{-}M \longrightarrow CO_2(g) + 2M \qquad (4.8)$$

$$CO(g) + O\text{-}M \longrightarrow CO_2(g) + M \qquad (4.10)$$

When the reaction occurs with a large feed ratio of [CO] to [N_2O], CO_2 is mainly formed through the L-H reaction, step (4.8). However, when the CO feed composition is very much lower than the N_2O composition, the E-R reaction, step (4.10), plays an important role in the formation of CO_2.

Shown in Figures 4.14 to 4.16 are the predictions from Mechanism 11. In the modelling process, the predictions are forced to match not only the low and high CO conversions, but also the bifurcation point locations. As expected, Mechanism 11 provides better predictions at low CO concentrations than Mechanism 10. At very low CO concentrations (see Figures 4.14 and 4.15), CO conversions remain over 98 percent. At a temperature of 210°C, the predictions agree very well with the bifurcation point locations and the high CO conversions, but, in the high CO region the predicted CO conversions are higher than the experimental observations. Similar, but smaller, disagreements are found between the predictions and the observations at 190°C.

The predictions for the 246°C observations are not as accurate as for other two cases (see Figure 4.16). At CO feed compositions, 0.399%, 0.564% and 0.705%, the predictions for low CO conversions fall consistently under the experimental results. However, the predicted bifurcation point locations are in good agreement with the observations. For high CO feed compositions, the situation is opposite. The predicted bifurcation locations are not quite correct, but, the mechanism can accurately describe the CO conversions for both high and low N_2O feed compositions.

The parameters used in Mechanism 11 are listed in Table 4.4. Due to the E-R reaction step in Mechanism 11, the value of the CO self-exclusion factor is less than the value of 1.03 used with Mechanism 10. In Mechanism 11, N_{CO} was

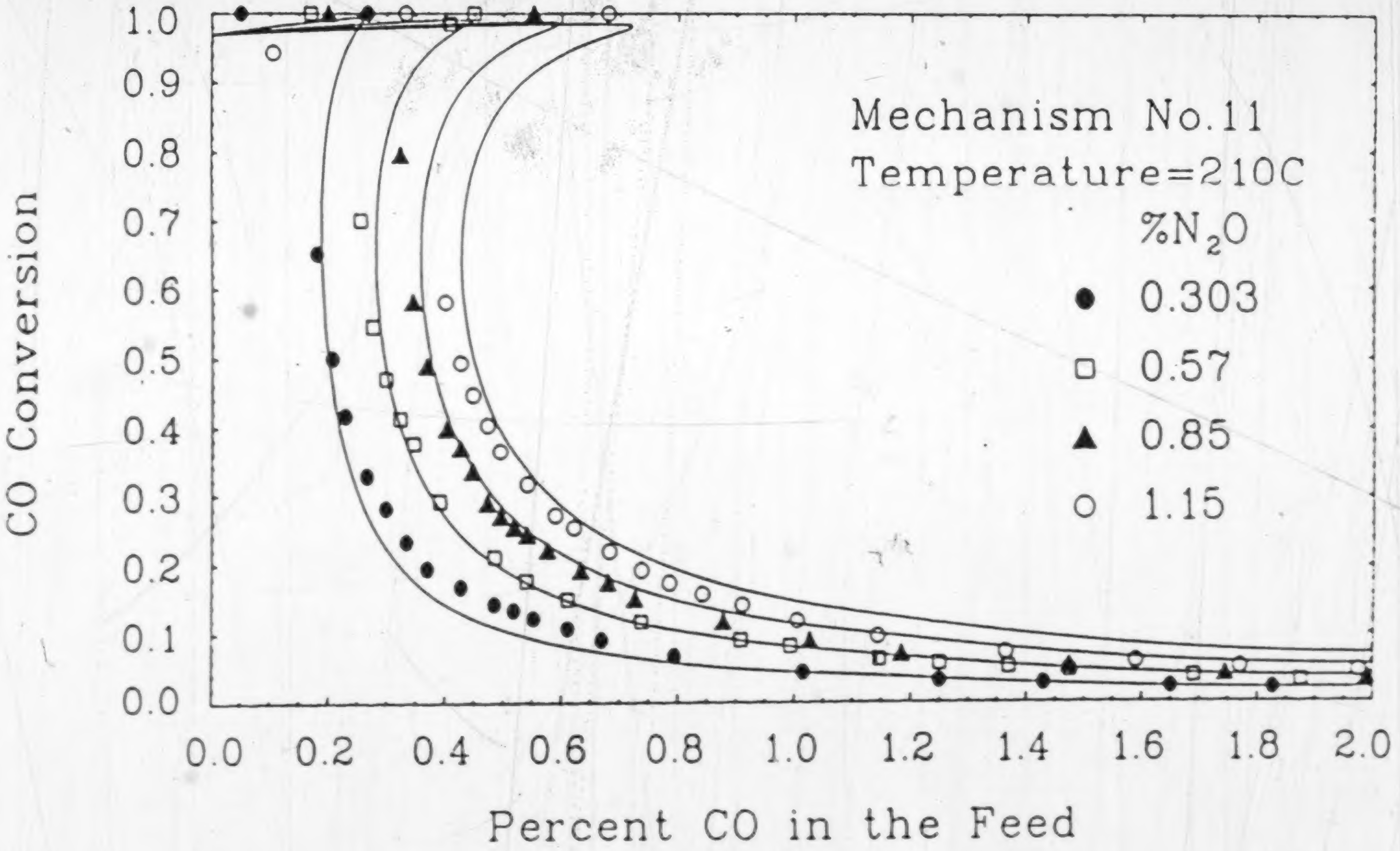

Figure 4.14 CO Conversion Predictions from Mechanism 11 at 210°C

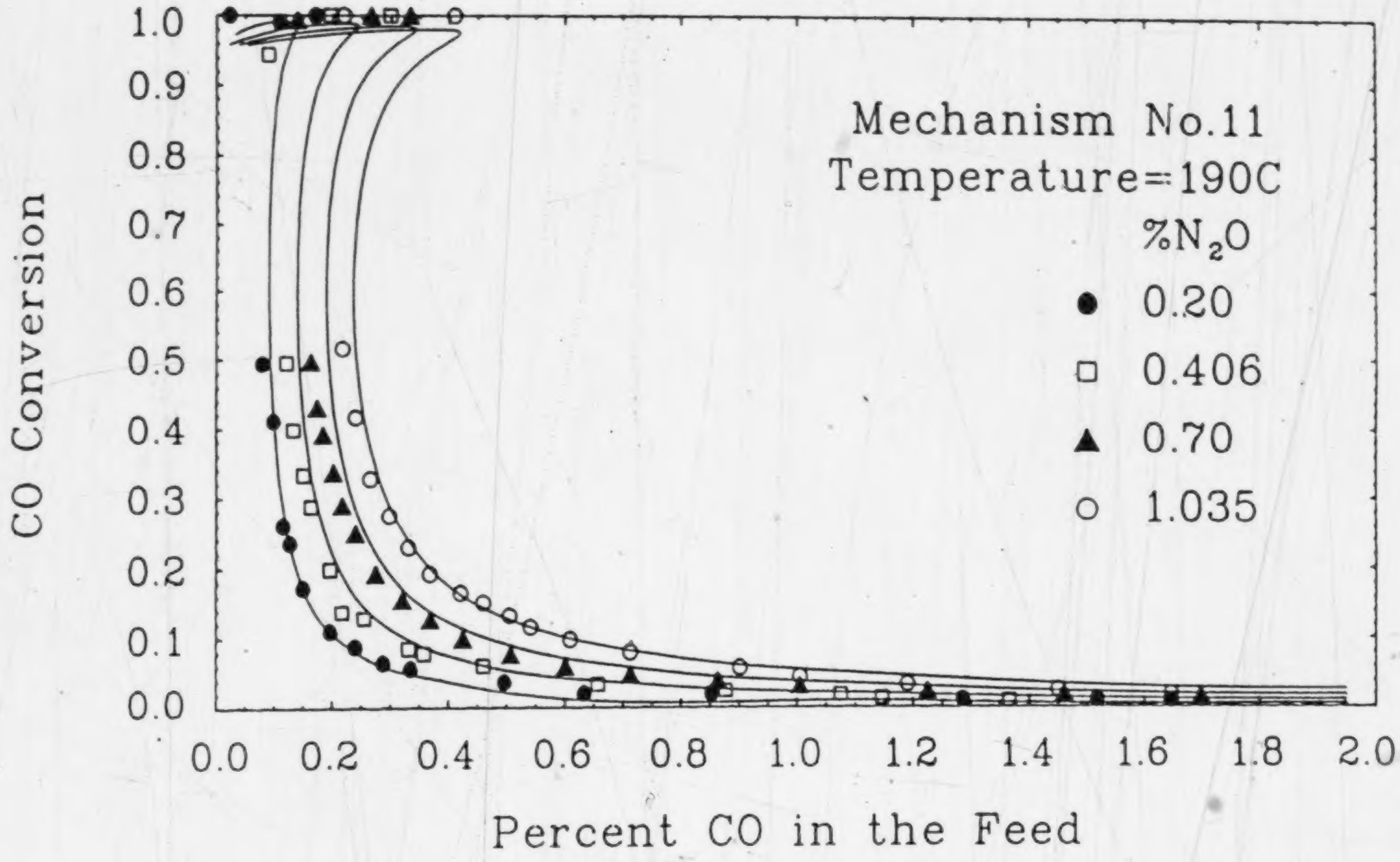

Figure 4.15 CO Conversion Predictions from Mechanism 11 at 190°C

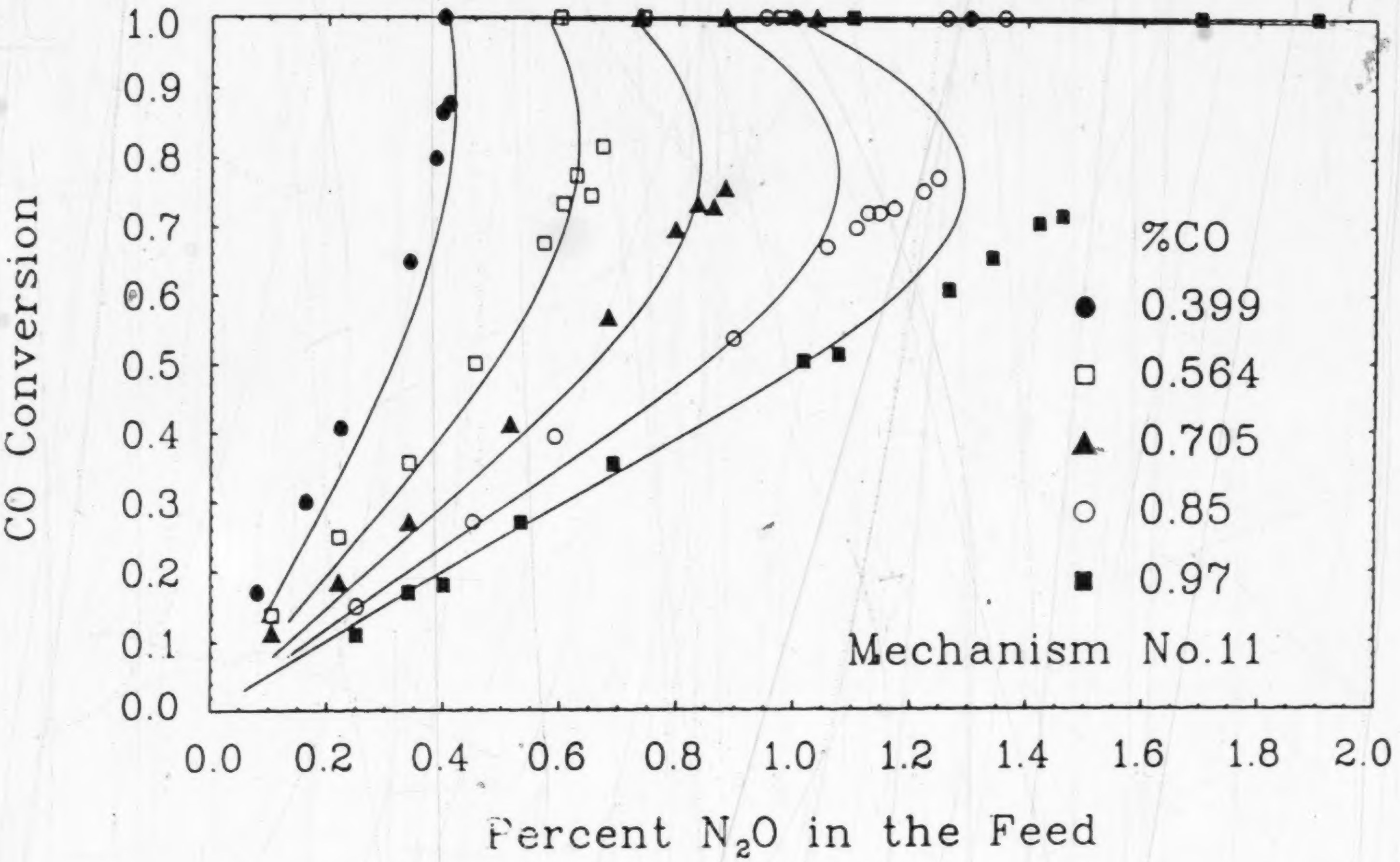

Figure 4.16 CO Conversion Predictions from Mechanism 11 at 246°C

estimated to be 1.011 (independent of temperature). The activation energies found from an Arrhenius type analysis are also listed in Table 4.4 (see Figure 4.17).

Table 4.4 Values of Kinetic Parameters for Mechanism 11

k	T=190°C	T=210°C	T=246°C	E/R
k_{-1}	0.046	0.050	0.058	987
k_4	0.14	0.40	2.2	12200
k_8	650	1000	2000	4760
k_{12}	0.5	0.9	2.3	6250

$N_{CO} = 1.011$, CO sticking probability = 0.85×10^{-5}

It is seen that the inclusion of the step (4.10) results in overall good, but not perfect, agreement between the model predictions and the experimental observations. Instead of using step (4.10), it is possible that alternative hypotheses would lead to similar, or better, agreement. For example, an oxygen exclusion parameter, similar to that for CO, would have the effect of producing high conversions in the low CO region by preventing saturation oxygen coverage from occurring. Alternatively, a decrease in the oxygen sticking probability due to a reconstruction of the platinum surface would also possibly result in better agreement. These alternatives should be considered in any further modelling of the kinetic behavior of this reaction system.

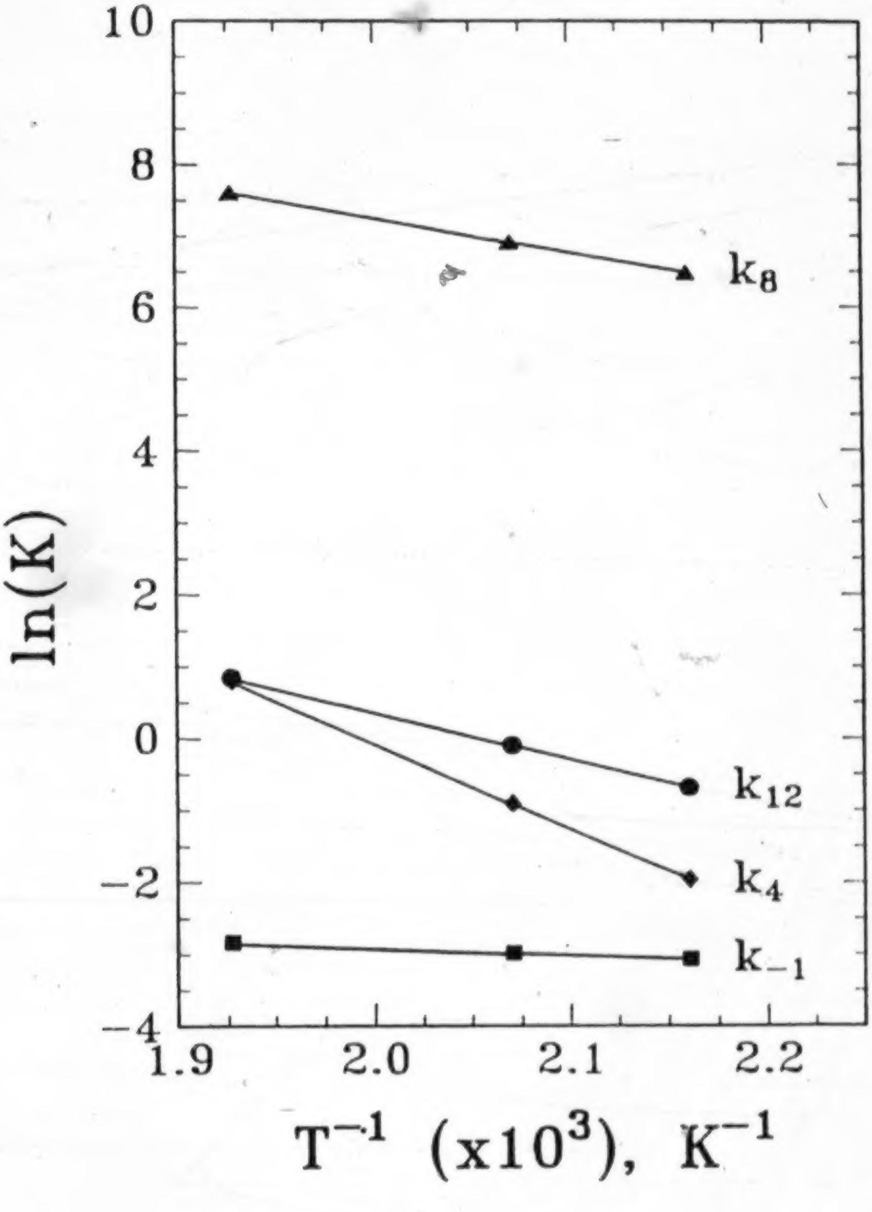

Figure 4.17 Arrhenius Analysis for Mechanism 11 Parameters

4.13 Summary

Eleven mechanisms for nitrous oxide reduction by carbon monoxide on a supported platinum catalyst have been examined. By comparing the predictions from the various mechanisms, it can be concluded that Mechanism 11 provides the best predictions for the N_2O+CO system.

4.14 Nomenclature

a : catalyst surface area, m^2

CO-M : adsorbed CO surface species

k_i : adsorption, or reaction, rate constant (value of i refers to the number of the corresponding step in the mechanism)

k_{-i} : desorption rate constant (value of i refers to the number of the corresponding step in the mechanism)

K_1 : k_1/k_{-1}

K_4 : k_4/k_{-1}

K_8 : $k_8\ L/k_{-1}$

K_{16} : $k_{16}\ L/k_{-1}$

K_{17} : k_{17}/k_{-1}

K_{18} : k_{18}/k_{-1}

$K_{4/8}$: K_4/K_8

K_{ERCO} : $a\ k_{10}\ L/Q$

K_{ERN2O} : $a\ k_9\ L/Q$

K_{LH} : $a\ k_8\ L/Q$

L : number of active sites per square meter

M : active site on catalyst surface

N_2O-M : adsorbed N_2O surface species

N_{CO} : a CO self-exclusion factor

O-M : adsorbed oxygen surface species

R : reaction rate

θ : fractional coverage

μ : parameter used in Mechanism 9

5. EXPERIMENTAL OBSERVATIONS FOR THE NO+CO REACTION

The experimental observations of nitrous oxide reduction by carbon monoxide on a supported platinum catalyst have been presented in Chapter 3, and several possible mechanisms have been examined in Chapter 4. These observations and calculations will now be used as a guide in an examination of a related reaction system, namely the reduction of nitric oxide by carbon monoxide. In the present chapter, experimental observations for this reaction are presented, and in the next chapter attention will be focussed on the mechanism of the NO+CO reaction on a supported platinum catalyst.

5.1 Preliminary

As with the N_2O+CO system, the experimental work for the NO+CO reaction was also concerned with finding multiplicity behavior. It was desired to examine the effects of reactant flow rate, feed composition, and reaction temperature on the reactor behavior. Experiments were carried out at three different temperatures: 150°C, 170°C and 190°C, with a constant total flow rate to the reactor of 200 SCCM. These observations are presented in Section 5.2. The influence of total flow rate on the reactor behavior was determined using total flow rates of 100, 200 and 400 SCCM, respectively, at a temperature of 170°C. These observations are shown in Section 5.3. All the experimental data contained in the current chapter are listed in Appendix 4. From preliminary studies at these reaction conditions, it was found that two main reactions occurred, the overall stoichiometry being:

$$2\ NO + CO \longrightarrow N_2O + CO_2 \qquad (5.1)$$

$$2\ NO + 2\ CO \longrightarrow N_2 + 2\ CO_2 \qquad (5.2)$$

The reaction products CO_2 and N_2O were analyzed by IR under steady-state condition. The NO and CO concentrations were not monitored because IR is not very sensitive for these compounds. The amount of molecular nitrogen formed during the reaction was always calculated, based on the reaction stoichiometry, according to:

$$[N_2]_{EXIT} = ([CO_2]_{EXIT} - [N_2O]_{EXIT})/2 \qquad (5.3)$$

Nitric oxide was determined through a nitrogen atom balance equation:

$$[NO]_{EXIT} = [NO]_{FEED} - 2\ ([N_2]_{EXIT} + [N_2O]_{EXIT}) \qquad (5.4)$$

In this system, since NO molecule can be completely reduced to molecular N_2, or partially reduced to N_2O during the reaction, it is necessary to determine both the conversion of NO as well as the selectivity, where, in this work, selectivity is defined as the ratio of the N_2O formation rate to the N_2 formation rate (Selectivity = $[N_2O]/[N_2]$).

In contrast to the N_2O+CO system, there are many previous reports that nitric oxide reduction by carbon monoxide can have multiple steady states. In order to observe the multiplicity behavior, if any, the experiments described herein were carried out at constant reaction temperature and with constant NO feed composition, with the CO feed composition varied systematically. Before starting each experiment, the reactor was purged with the NO/N_2 gas mixture, or with the CO/N_2 gas mixture.

5.2 Effect of Reaction Temperature on the Reactor Behavior

5.2.1 CO Conversion

Shown in Figure 5.1 are the CO conversions at a temperature of 150°C, with a total flow rate of 200 SCCM for various values of the CO feed composition. It is seen from Figure 5.1 that the reaction system displays multiplicity behavior very similar to that seen for the N_2O+CO system. When the reaction occurs at low CO feed compositions, high conversions are obtained. While there is considerable scatter, the high conversions do not systematically vary with either increasing CO feed composition, or with changing NO feed composition. When the %CO in the feed reaches certain critical values, the CO conversion drops to a very low value. The location of the transition point from high conversion to low conversion depends on the %NO in the feed. Increasing the %NO in the feed shifts the transition point

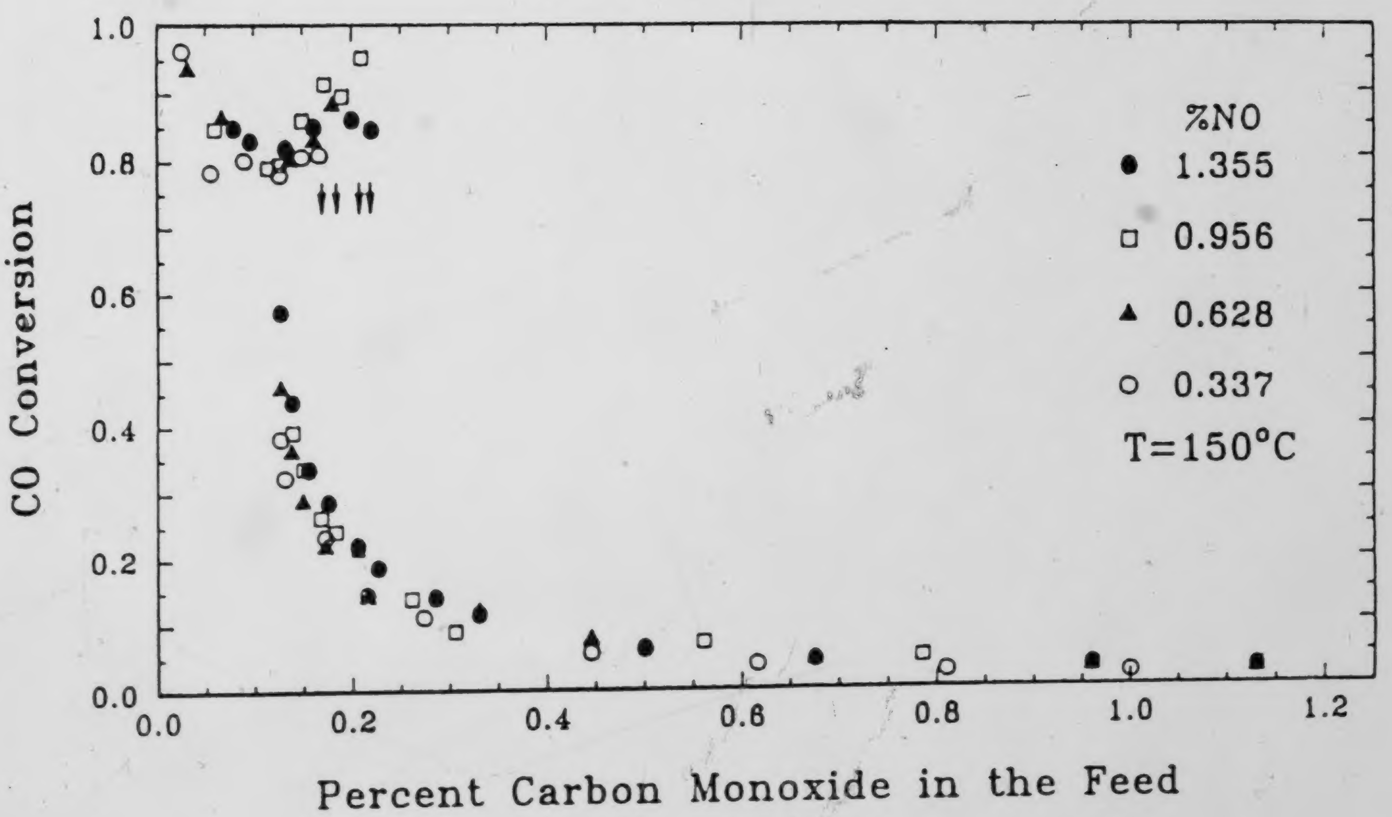

Figure 5.1 CO Conversion for NO+CO at 150°C, 200 SCCM

towards higher CO concentrations.

When the reaction is carried out at high CO concentrations, low conversions are obtained. Unlike the high conversion branch, the CO conversions are affected by both the %CO and the %NO values in the feed. At very high CO concentrations, decreasing the CO feed composition results in only a slight increasing of the CO conversion (zeroth order reaction with respect to CO). When the CO feed composition is close to the transition point, the conversion increases rapidly as the %CO in the feed is reduced (approximately negative first order with respect to CO). The location of the lower transition point is also influenced by the %NO in the feed. With increasing NO feed composition, the transition boundary shifts to higher CO concentrations. For intermediate CO concentrations two steady states exist, a high conversion state and a low CO conversion state. In this region, the reaction state is dependent upon the initial reaction conditions.

Similar results were obtained at temperatures of 170 and 190°C with a total flow rate of 200 SCCM. The results are shown in Figures 5.2 and 5.3, respectively. In contrast with the N_2O+CO system where the high conversions remained near 100% for the entire temperature range studied, it is seen that for the NO+CO system the reaction temperature has an influence on the high CO conversions. These figures also indicate that the reaction temperature affects the location of the transition boundaries. With increasing reaction

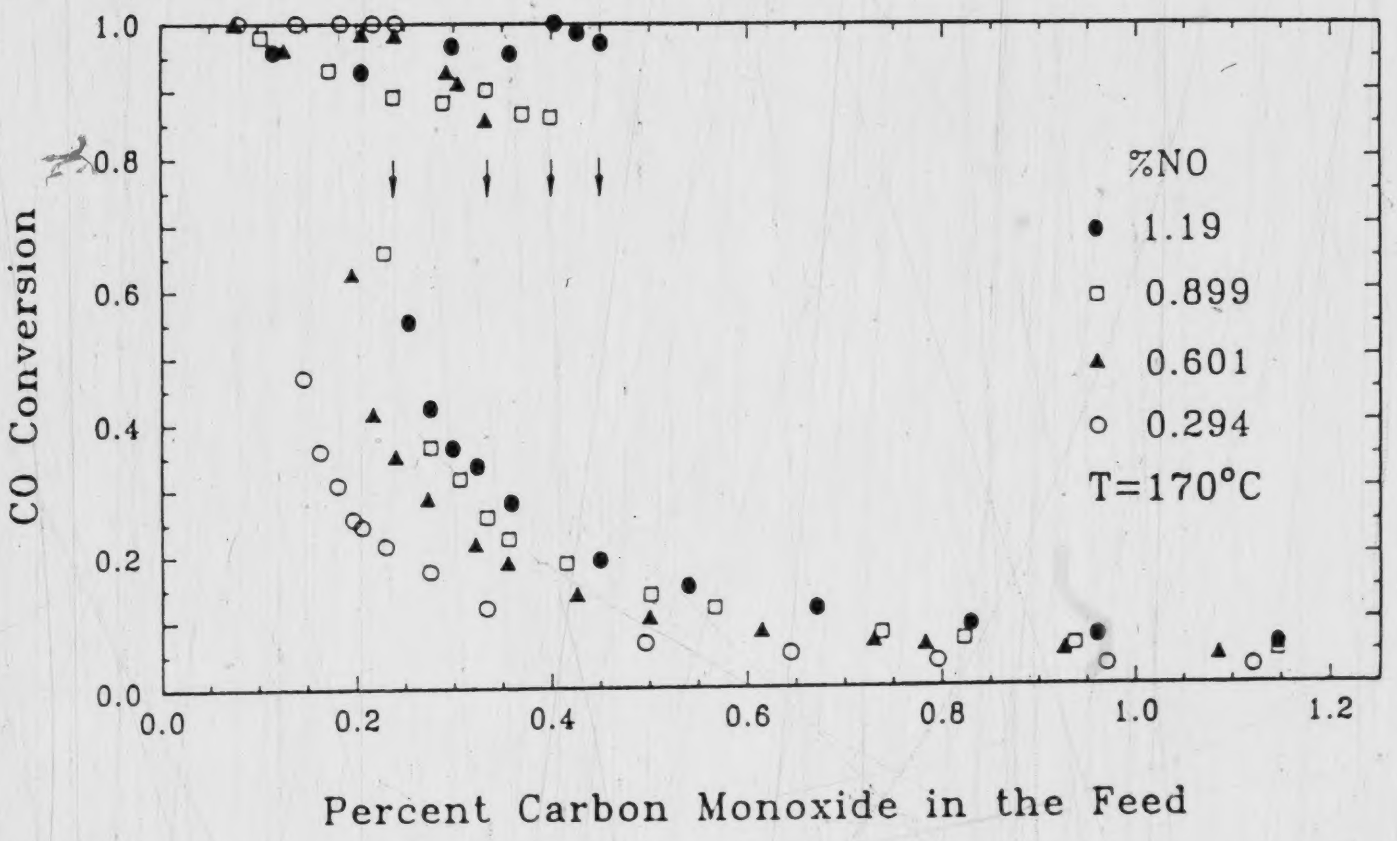

Figure 5.2 CO Conversion for NO+CO at 170°C, 200 SCCM

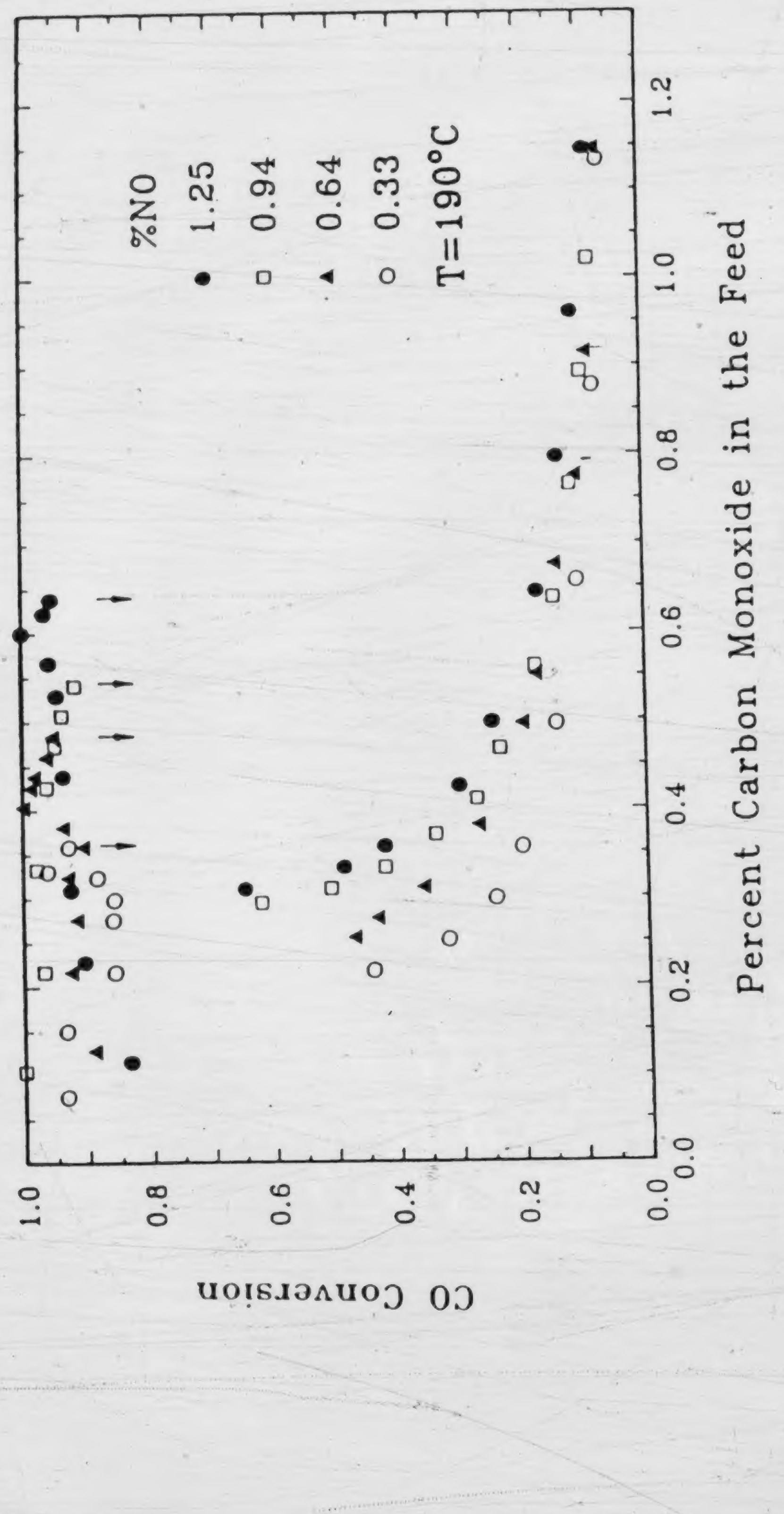

Figure 5.3 CO Conversion for NO+CO at 190°C, 200 SCCM

temperature, the bifurcation locations are shifted towards higher CO concentrations.

Temperature also strongly affects the width of the multiple-steady-state region. The multiplicity region at a temperature of 150°C is much narrower than that at a temperature of 190°C. The influence of the %NO in the feed on the multiplicity region varies with reaction temperature. At higher temperature, the NO feed composition has a stronger effect on the location of the transition boundary. It is seen in Figure 5.1 that at a temperature of 150°C, the high transition boundaries are in a range of 0.15 to 0.25 %CO, whereas at a temperature of 190°C, the high transition boundaries are located between 0.3 and 0.7 %CO. The low transition boundaries also display this feature.

5.2.2 NO Conversion

For reaction temperatures of 150, 170 and 190°C, shown in Figures 5.4 to 5.6, respectively, are the calculated NO conversions as a function of feed %CO. It is seen that, for the high conversion curves, the NO conversion strongly depends on the CO and NO feed compositions. In fact, the NO conversion varies almost linearly with changing CO concentrations. Conversely, increasing the NO feed concentration decreases the NO conversion. For example, at 170°C with %NO=0.294, NO conversion is 100% at the high transition boundary, whereas with %NO=1.19, the highest NO conversion is about 65 percent. In comparison with the CO conversions

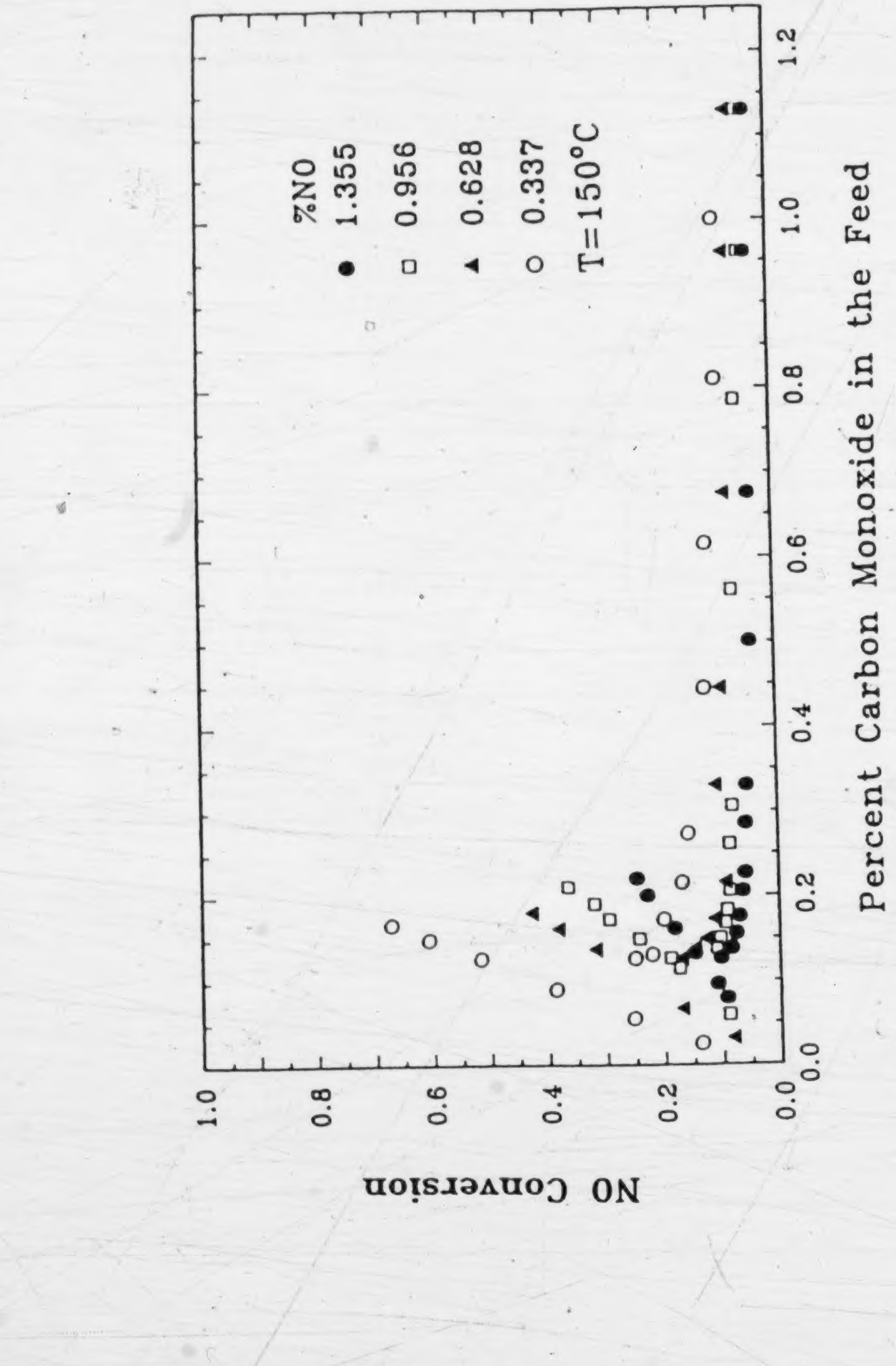

Figure 5.4 NO Conversion for NO+CO at 150°C, 200 SCCM

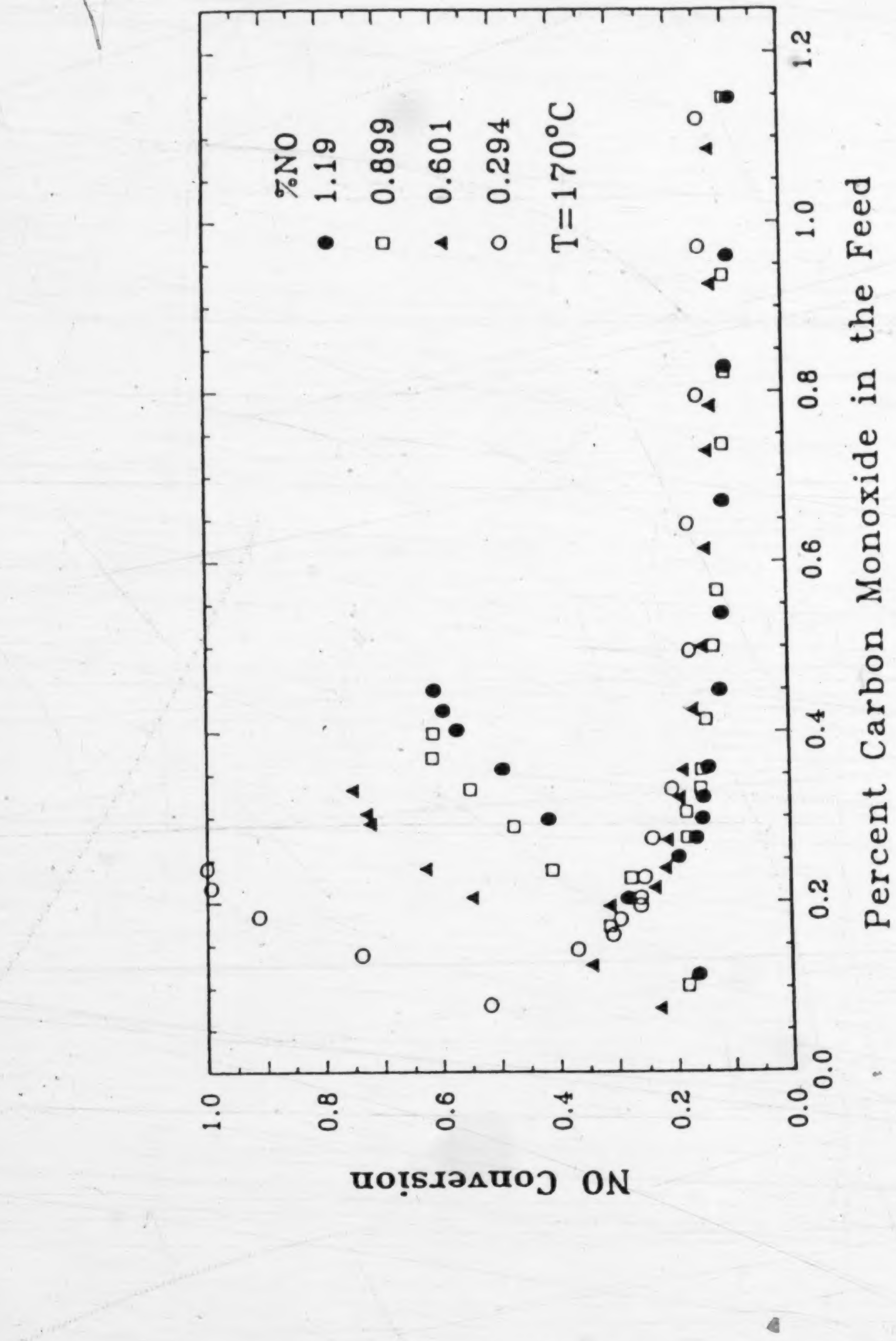

Figure 5.5 NO Conversion for NO+CO at 170°C, 200 SCCM

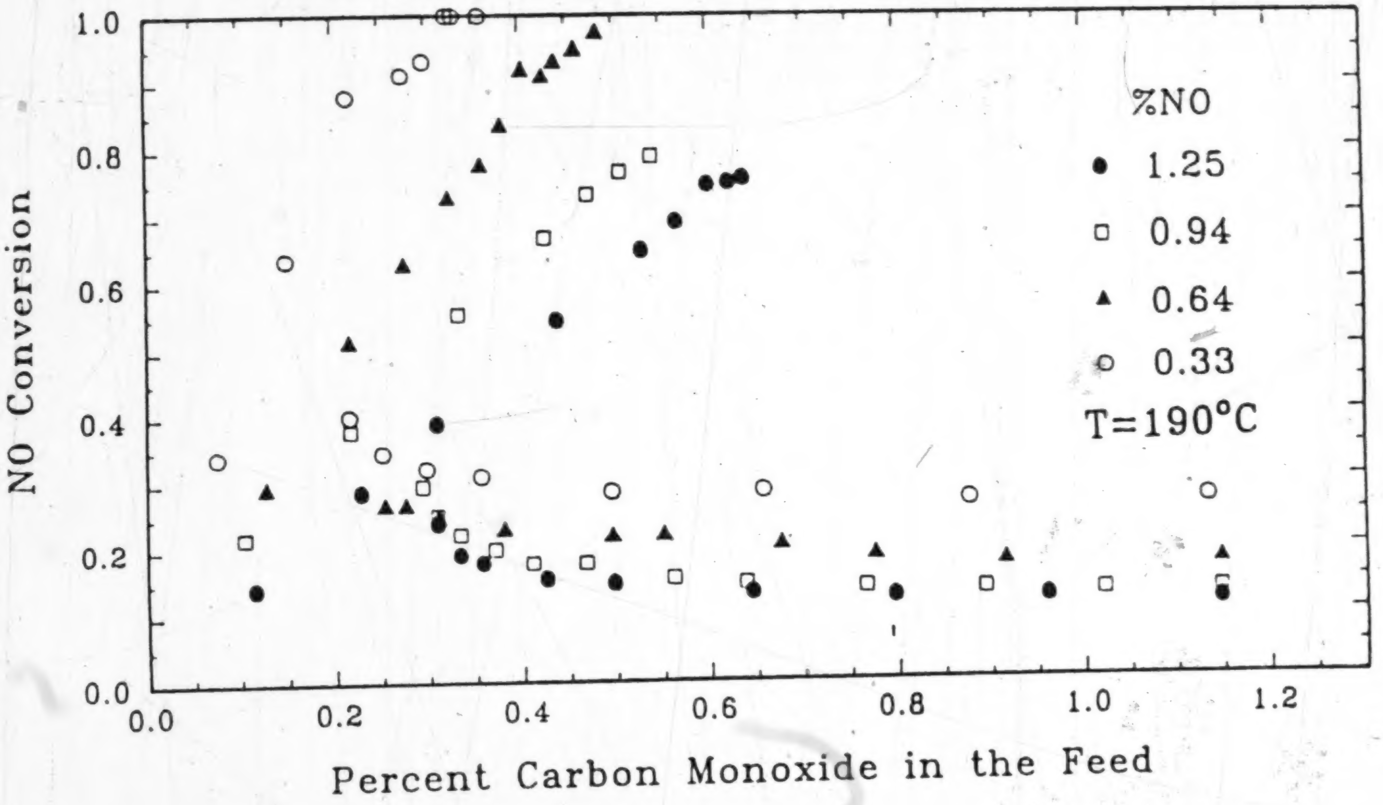

Figure 5.6 NO Conversion for NO+CO at 190°C, 200 SCCM

in the high conversion region, the NO conversions are generally much lower.

For the low NO conversion branch it is seen that neither the CO nor the NO concentration has much influence on the NO conversion. At very high CO concentrations, the NO conversion increases very slightly with decreasing CO feed composition, and near the transition points, the NO conversion increases more noticeably. NO feed concentration has the same effect on the NO conversion in both the low and the high conversion regions, however, the effect is much weaker in the low NO conversion region than in the high CO conversion region.

Unlike the CO conversion, the NO conversion is strongly affected by the reaction temperature. Compared with the 170°C results, the NO conversions at 190°C in both branches are significantly increased at corresponding feed compositions, while the NO conversions at 150°C are reduced.

5.2.3 CO_2 Formation Rate

Carbon dioxide formation rates as functions of CO feed composition are presented in Figures 5.7 to 5.9, respectively, for reactor temperatures of 150, 170 and 190°C. It is seen that on the high rate branch, CO_2 formation rate varies linearly with CO concentration and all of the point fall approximately on one line. When the %CO reaches the transition point, the CO_2 formation rate drops to the low rate branch. On the low branch, the CO_2 formation rate remains

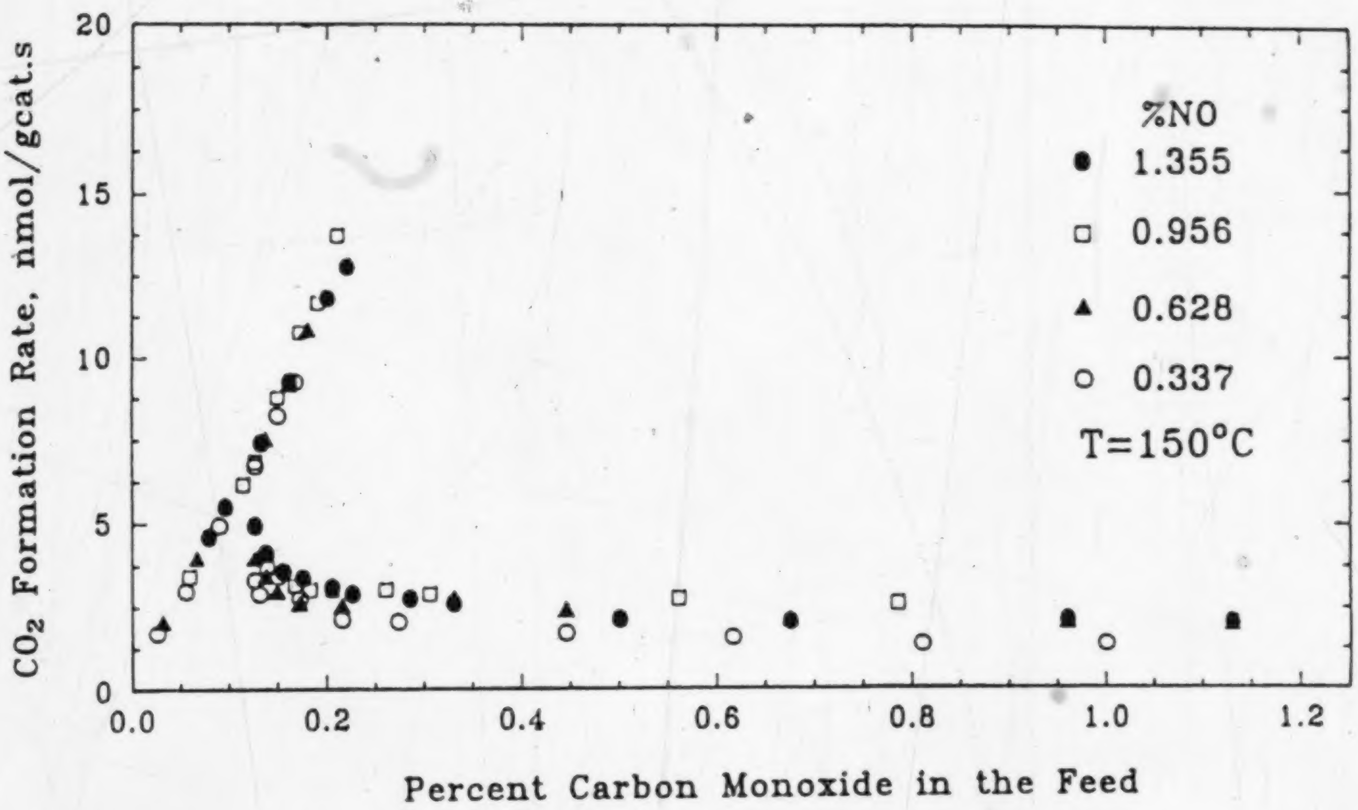

Figure 5.7 CO$_2$ Formation Rate for NO+CO at 150°C, 200 SCCM

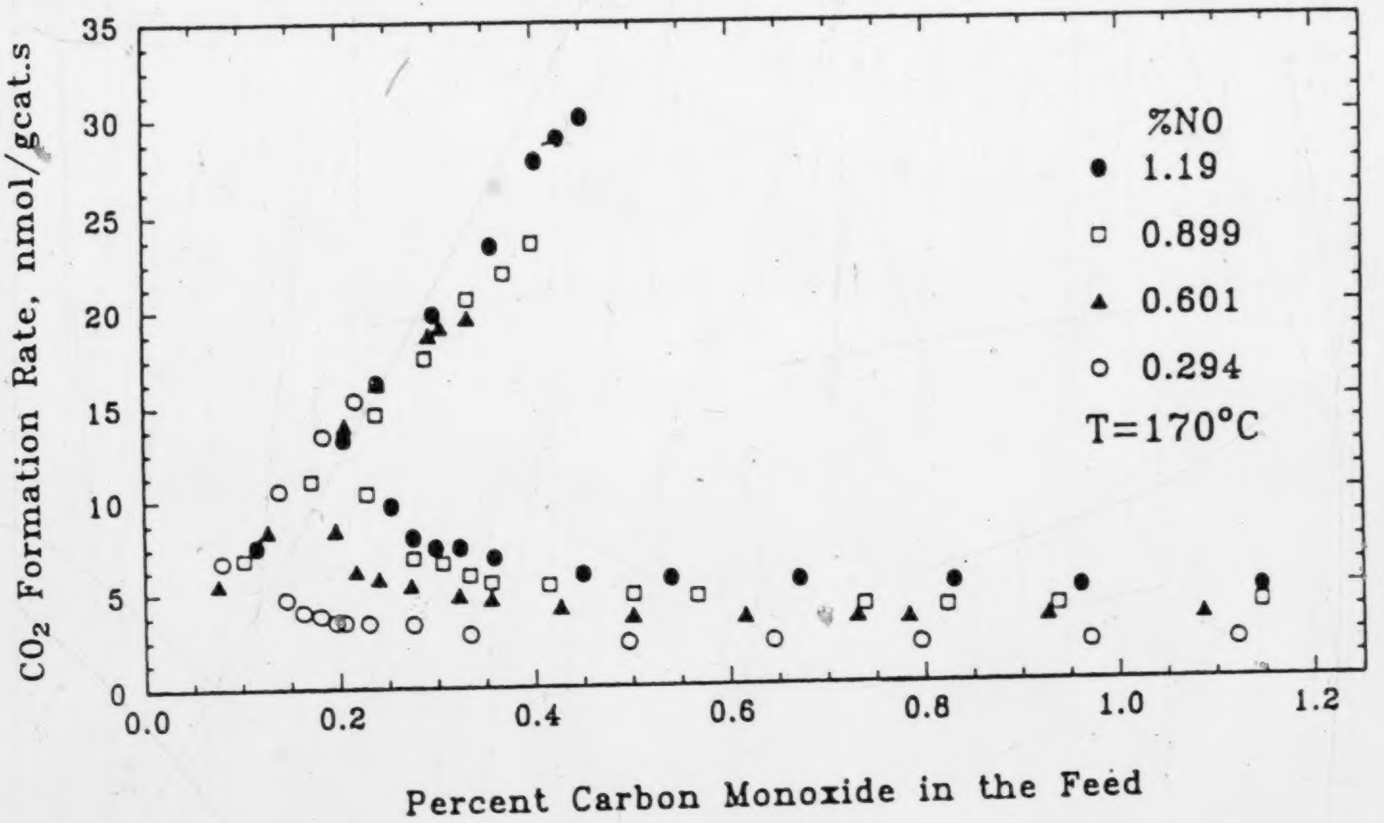

Figure 5.8 CO_2 Formation Rate for NO+CO at 170°C, 200 SCCM

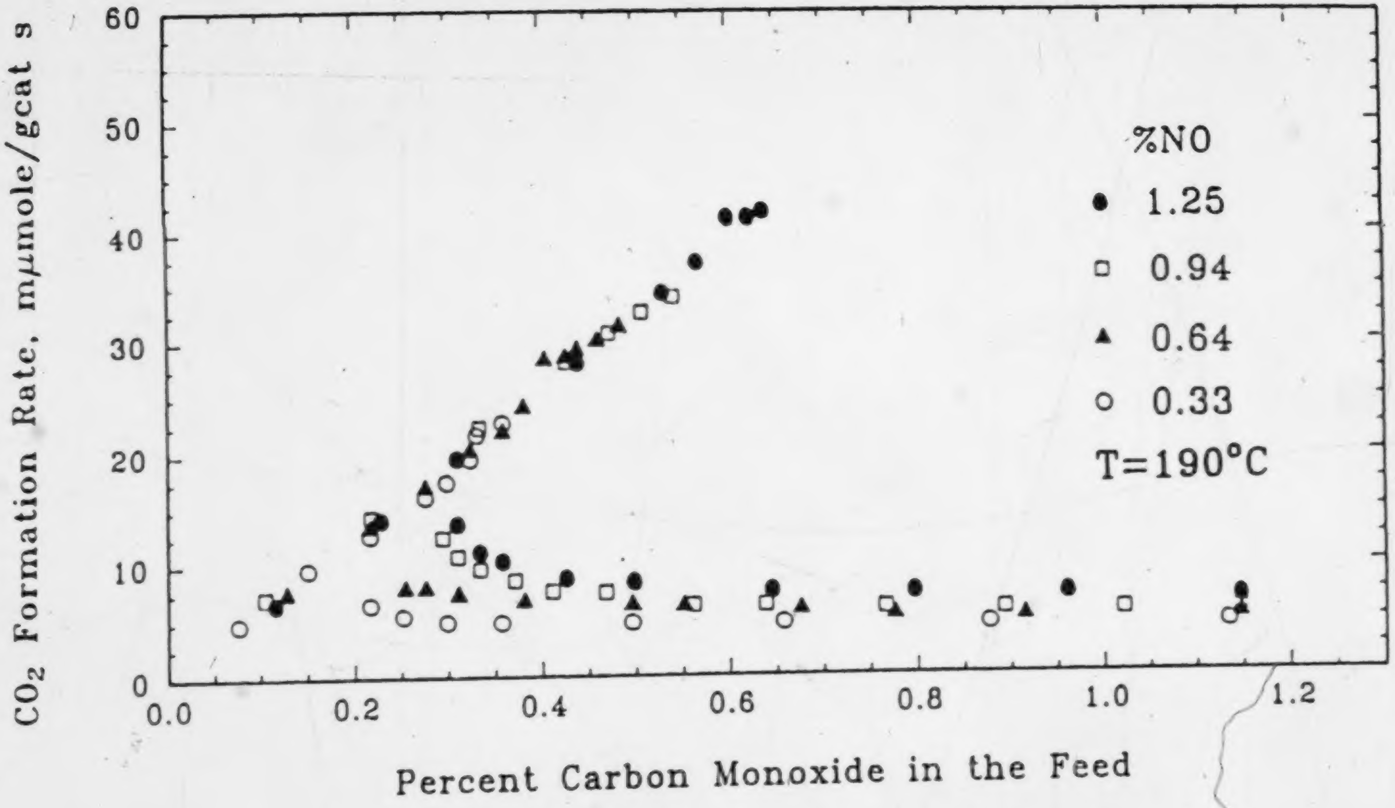

Figure 5.9 CO$_2$ Formation Rate for NO+CO at 190°C, 200 SCCM

essentially constant at high CO concentrations. Near the transition region, the rate increases with decreasing %CO in the feed. Reaction temperature does not have much effect on the high rate branch, as the slopes of all of the high rate curves in Figures 5.7 to 5.9 are almost identical. However, for the low rate branch, increasing the temperature results in an increase of the CO_2 formation rate.

5.2.4 Nitrous Oxide in the Reactor

Unlike the case of N_2O+CO which only produces a single product (CO_2), the reduction of NO by CO can result in the production of N_2 and/or N_2O. The observed nitrous oxide concentrations in the reactor as a function of the CO feed composition are presented in Figures 5.10 to 5.12. It is seen that the N_2O composition in the reactor mirrors the reaction rate and multiplicity behavior. When the CO feed concentration is low, the %N_2O in the reactor increases with increasing CO concentration (in the region where the rate increases with increasing CO). The N_2O formation rate also increases with increasing NO feed concentrations in both the high and the low rate regions.

5.3 Effect of Total Flow Rate on the Reactor Behavior

The preceding experimental observations were made using a constant flow rate to the reactor of 200 SCCM. For a reactor temperature of 170°C, the effect of using feed flow rates of 100 SCCM and 400 SCCM was examined, and the

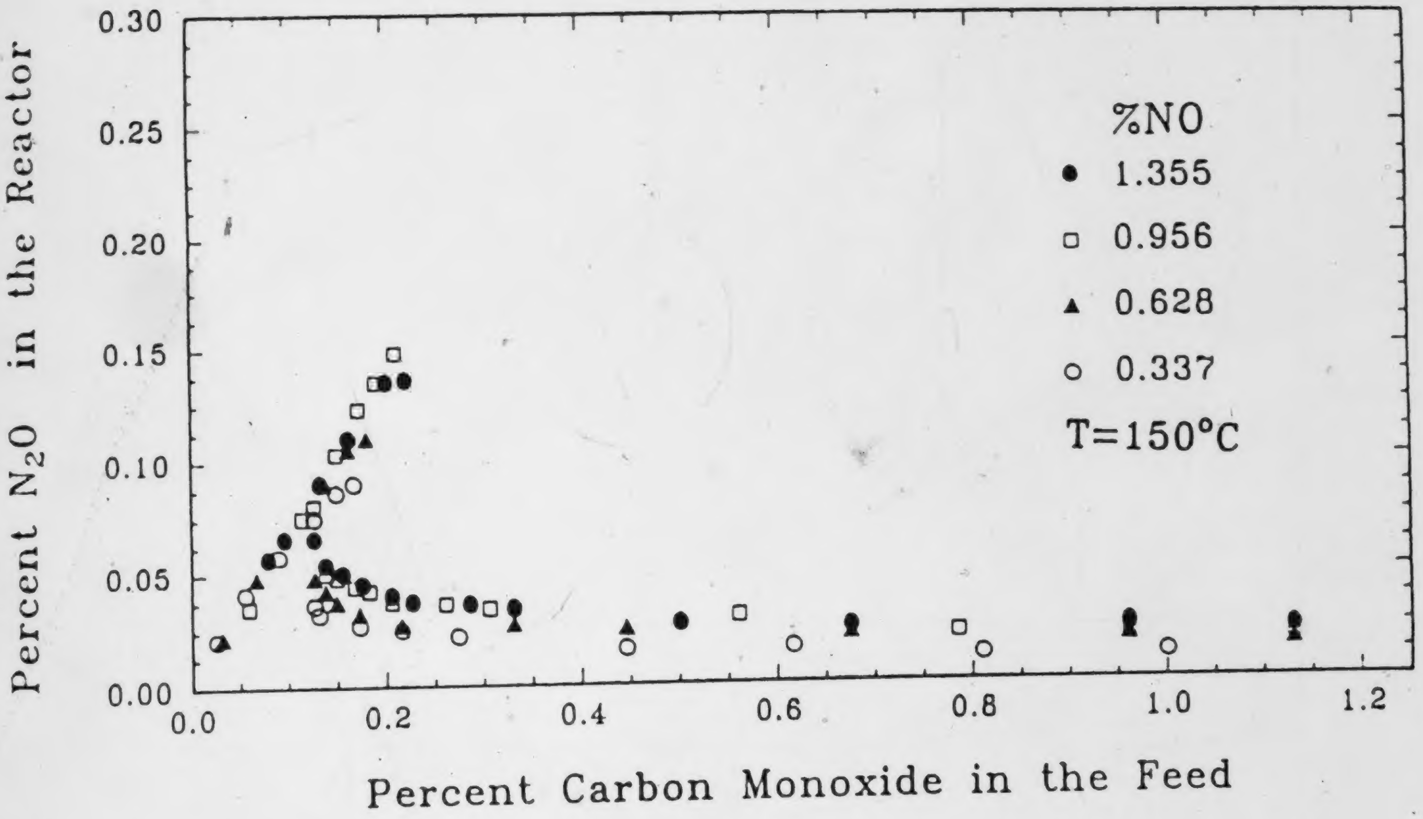

Figure 5.10 N_2O Formation Rate for NO+CO at 150°C, 200 SCCM

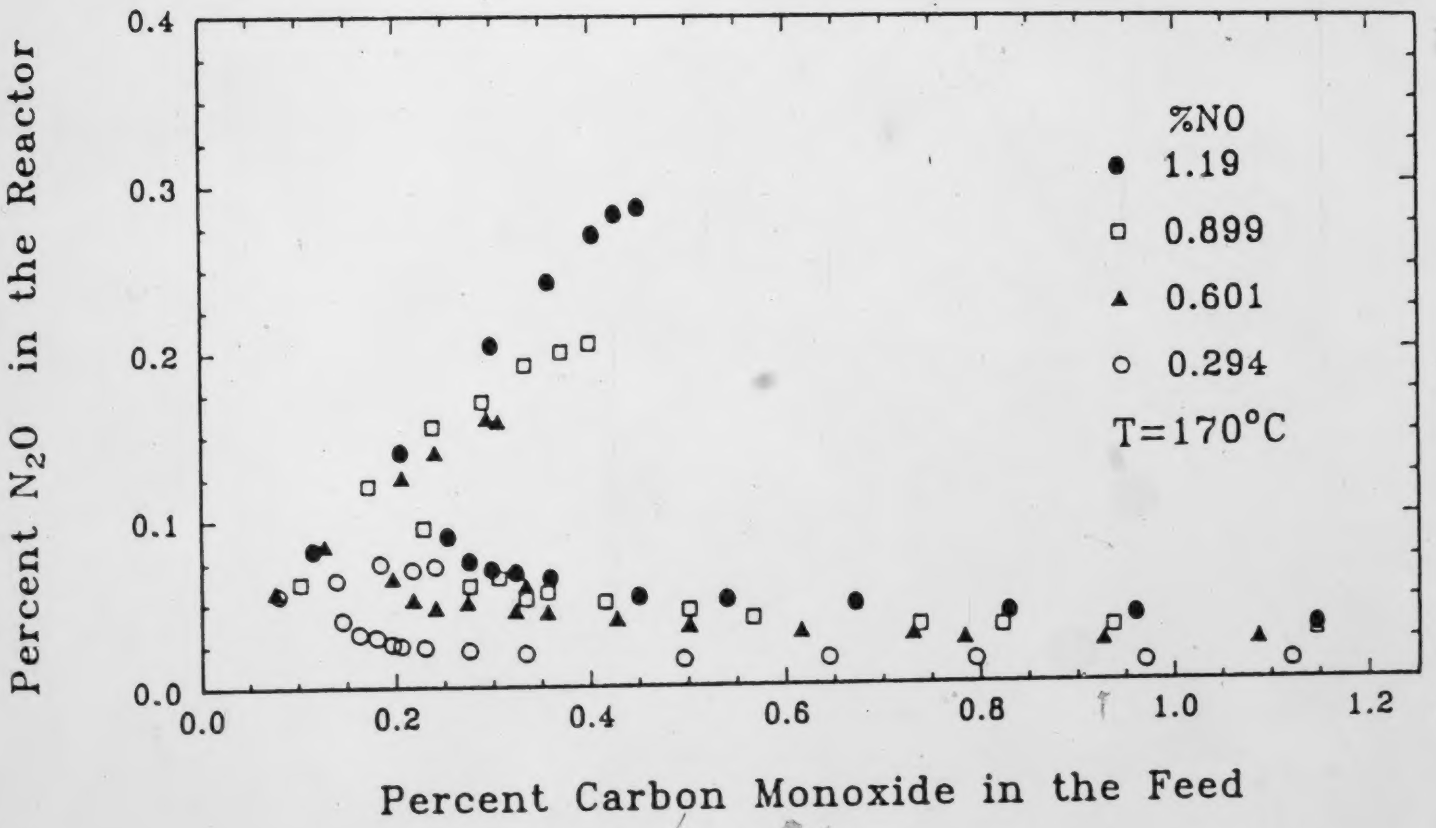

Figure 5.11 N_2O Formation Rate for NO+CO at 170°C, 200 SCCM

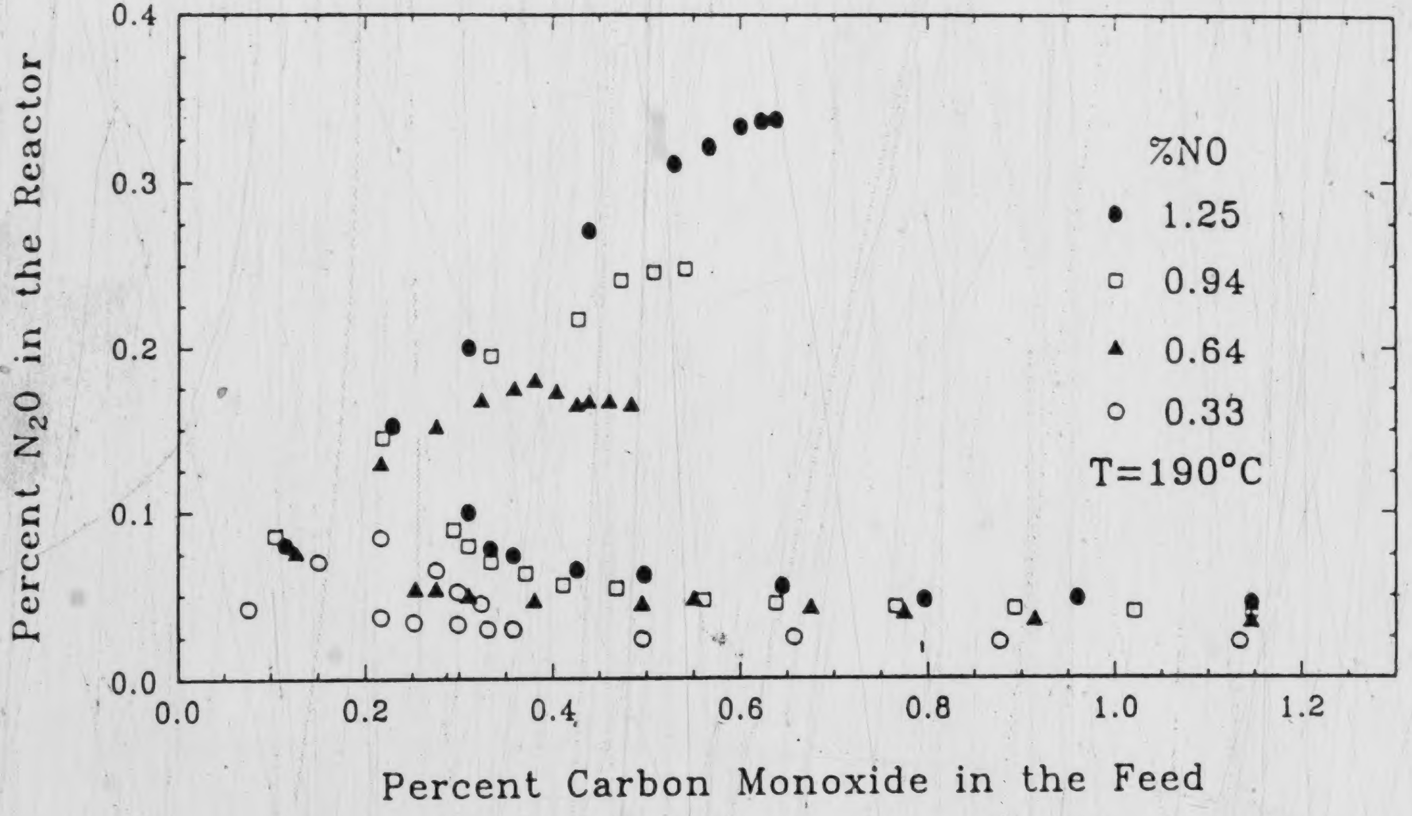

Figure 5.12 N_2O Formation Rate for NO+CO at 190°C, 200 SCCM

experimental observations (CO conversion, NO conversion, rates of CO_2 formation and concentration of N_2O in the reactor) are summarized in Figures 5.13 to 5.20. By comparing these figures with the previously presented figures, it is seen that while the total flow rate has an influence on the reaction behavior, it does not qualitatively change the observations.

A close examination reveals that, in general, decreasing the feed flow rate is qualitatively similar to increasing the reaction temperature, and vice versa. This holds for the CO and NO conversion and $\%N_2O$ in the reactor observations, as well as for the bifurcation point location movements. The only apparent exception concerns the absolute rates of CO_2 formation and even for this case the pattern holds if the CO_2 production rates are normalized by the feed flow rate.

5.4 Selectivity

The selectivity has been defined to be the ratio of the formation rates of N_2O to N_2. This quantity is a measure of the product distribution. A value of the selectivity greater than unity means that N_2O is favoured over N_2O as a reaction product. Shown in Figures 5.21 and 5.22 are N_2O selectivities at 170 and 190°C, respectively. It is seen from the figures that in the high conversion region (low CO concentrations), reaction selectivity decreases significantly with increasing CO feed composition for a specified NO

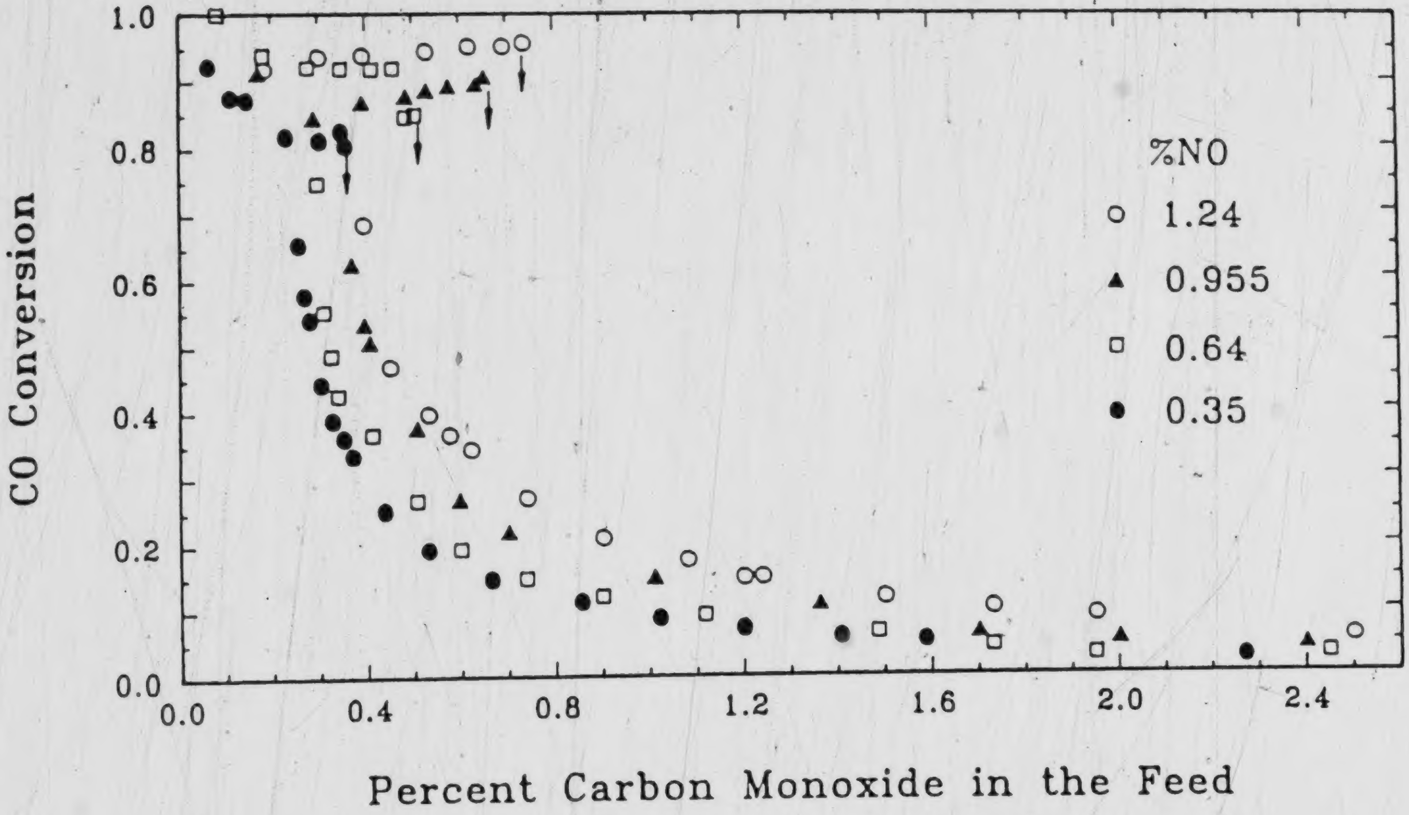

Figure 5.13 CO Conversion for NO+CO at 170°C, 100 SCCM

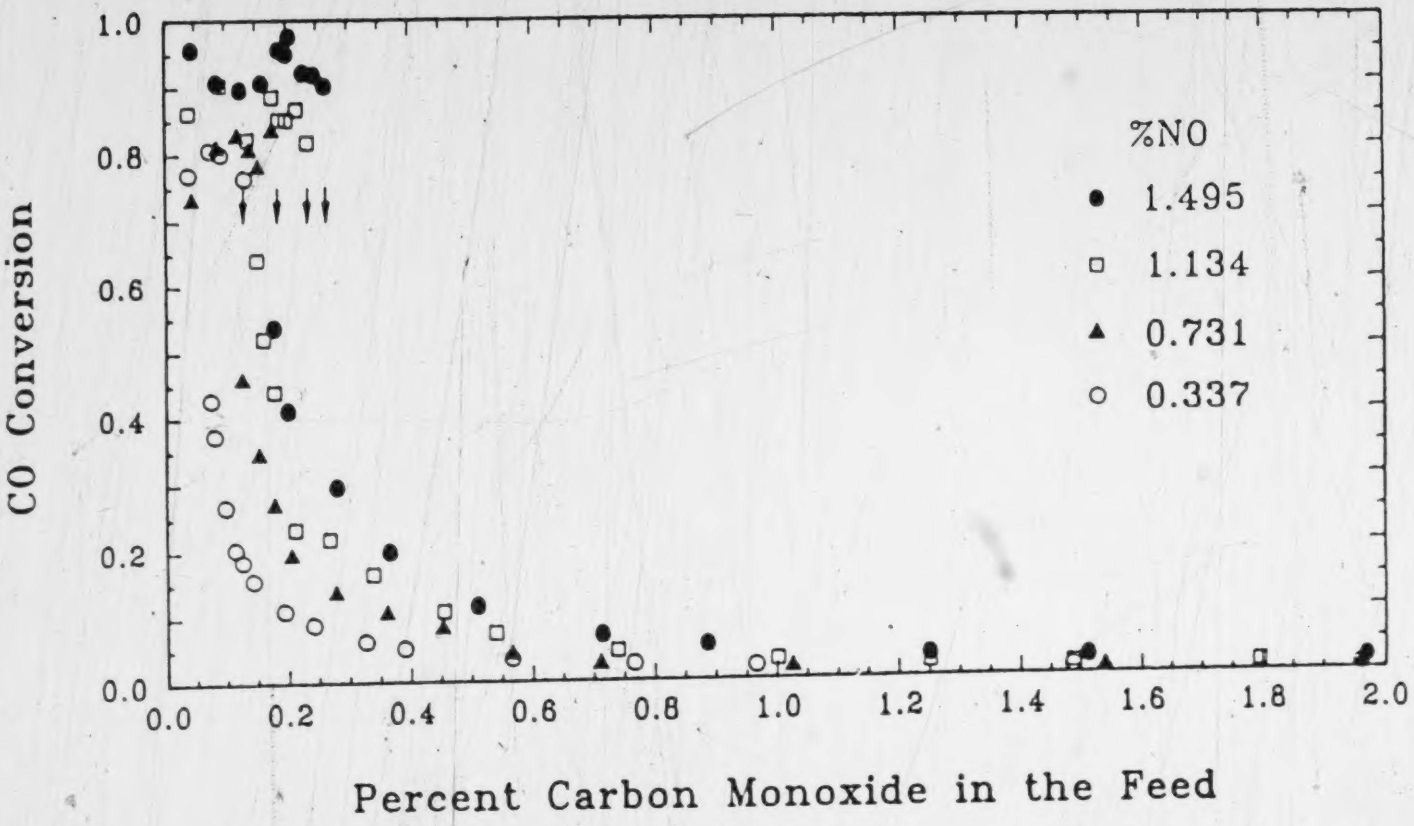

Figure 5.14 CO Conversion for NO+CO at 170°C, 400 SCCM

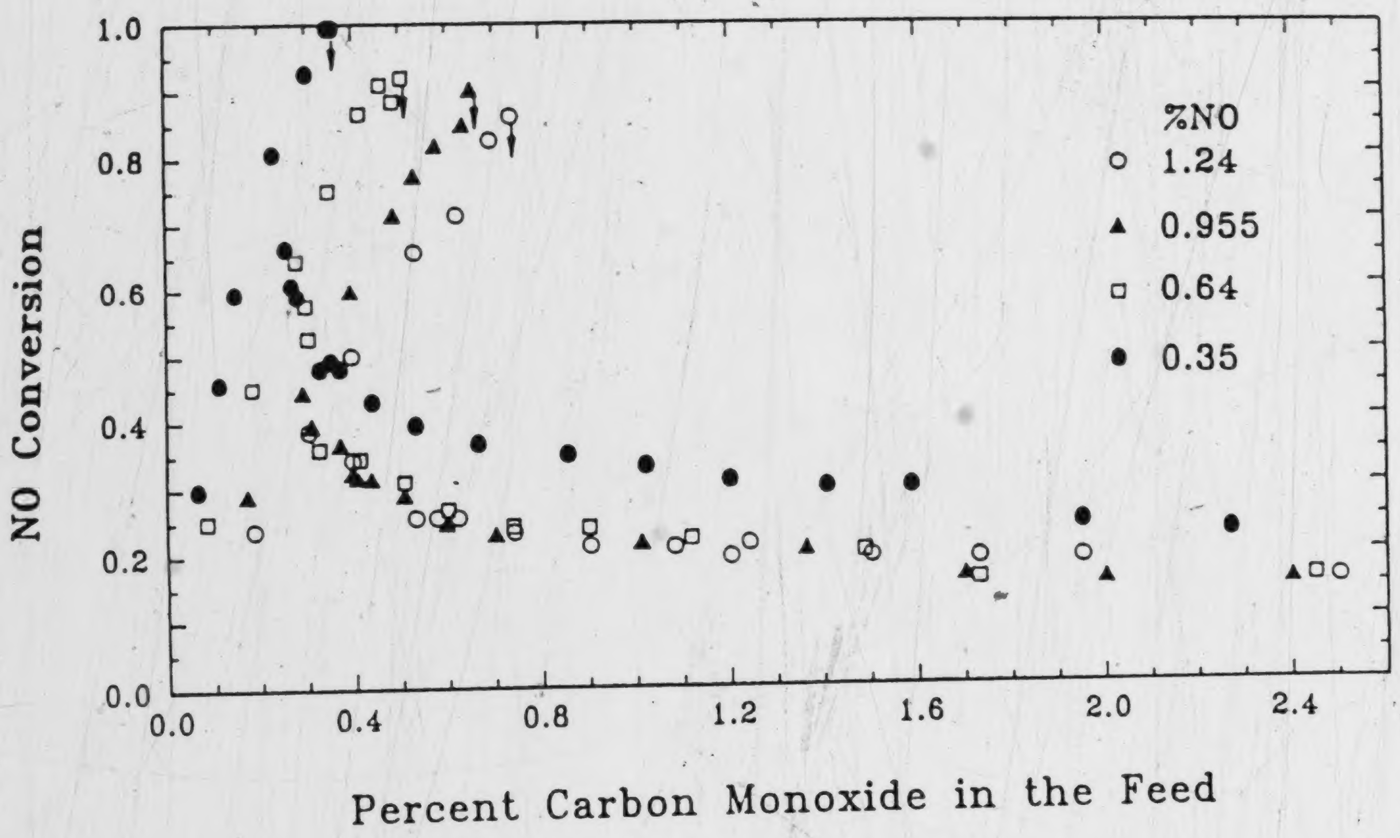

Figure 5.15 NO Conversion for NO+CO at 170°C, 100 SCCM

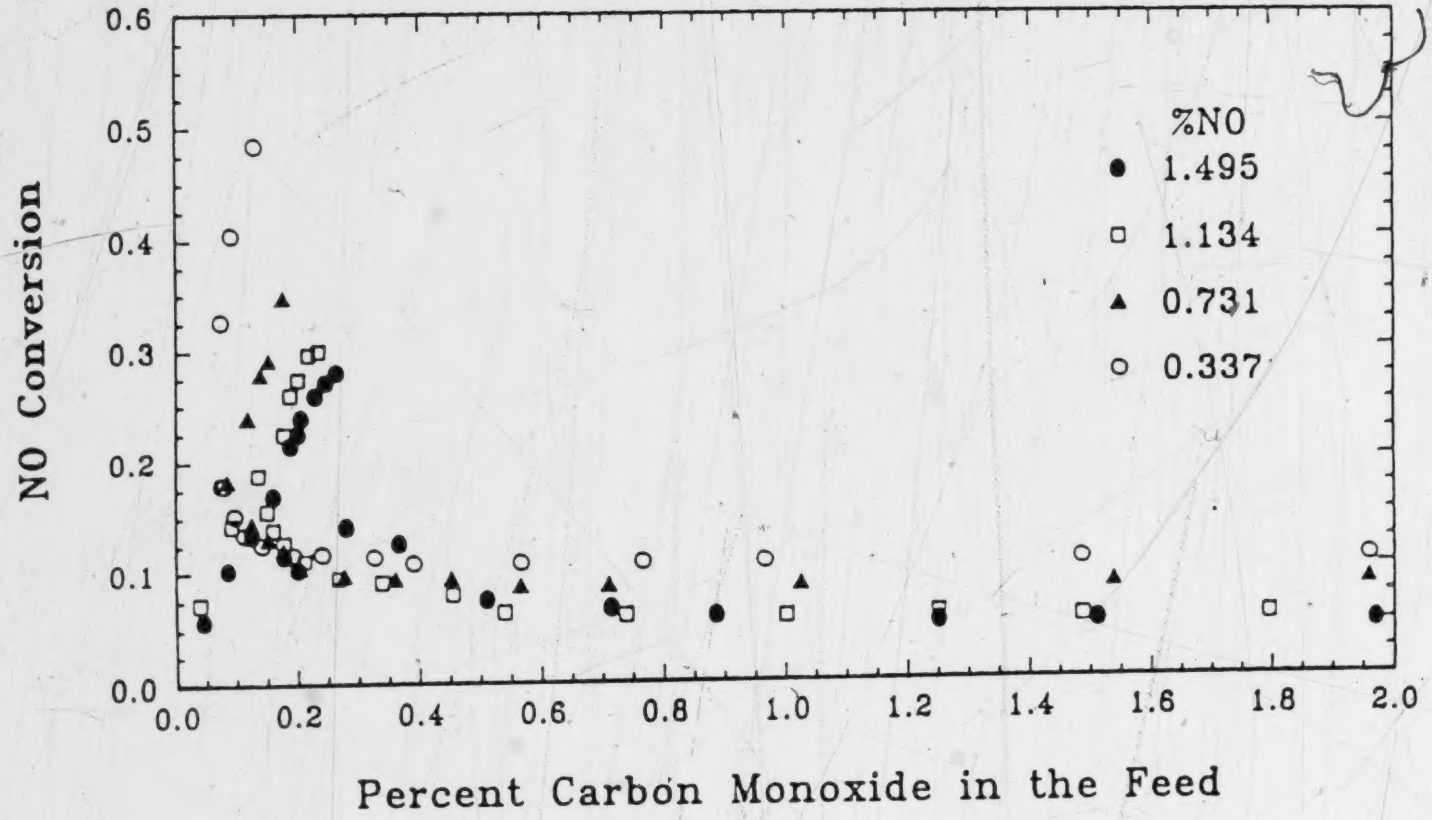

Figure 5.16 NO Conversion for NO+CO at 170°C, 400 SCCM

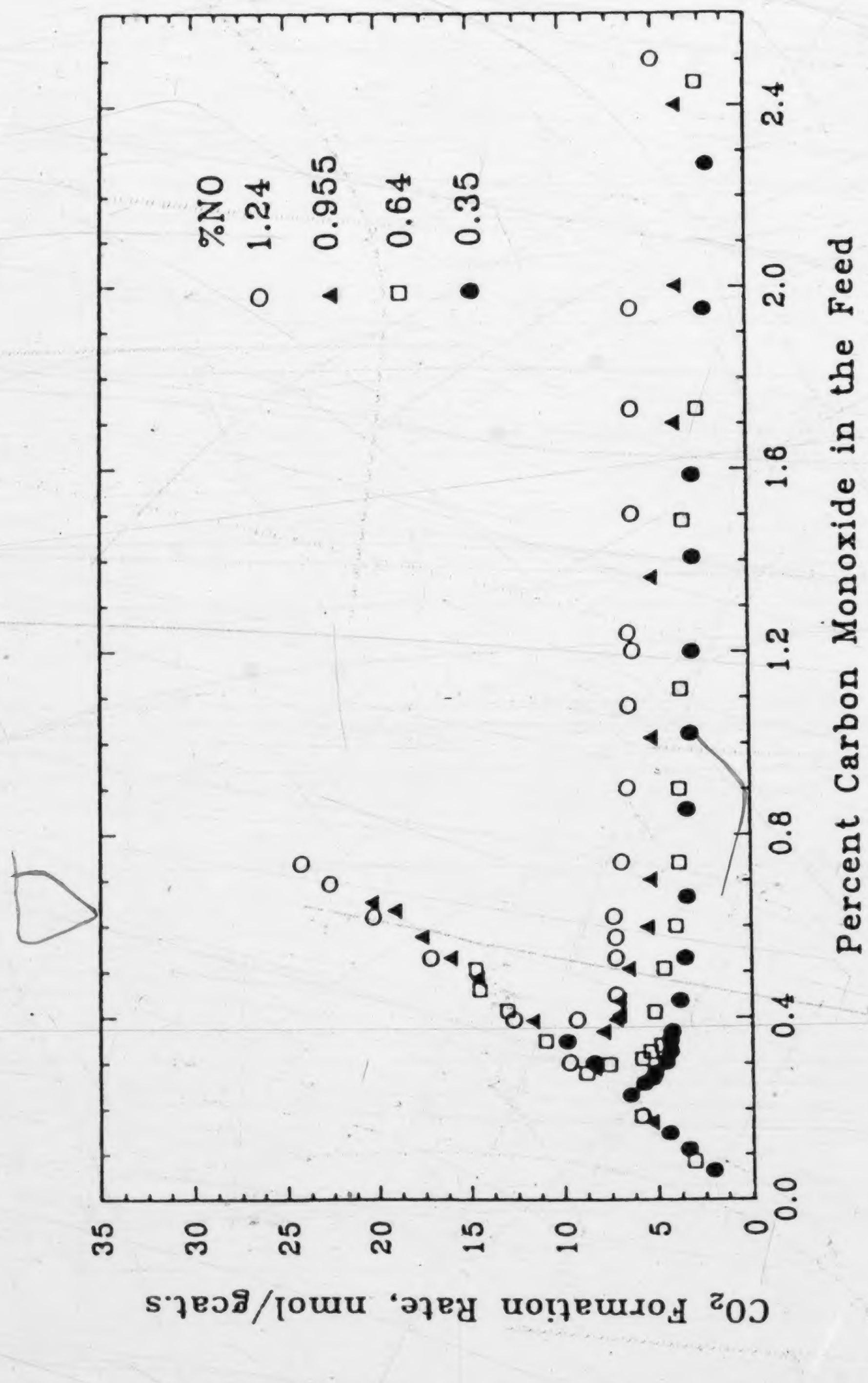

Figure 5.17 CO$_2$ Formation Rate at 170°C, 100 SCCM

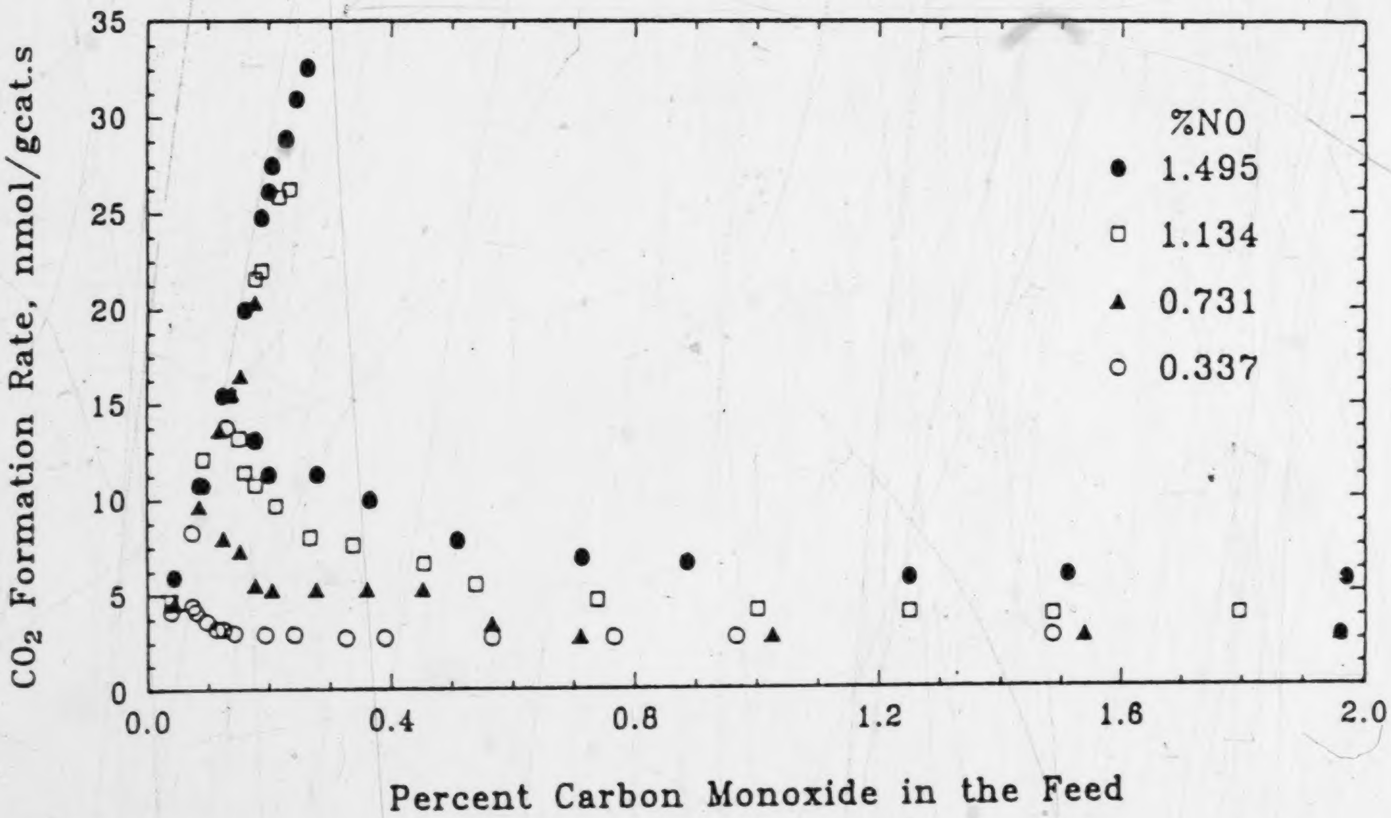

Figure 5.18 CO_2 Formation Rate at 170°C, 400 SCCM

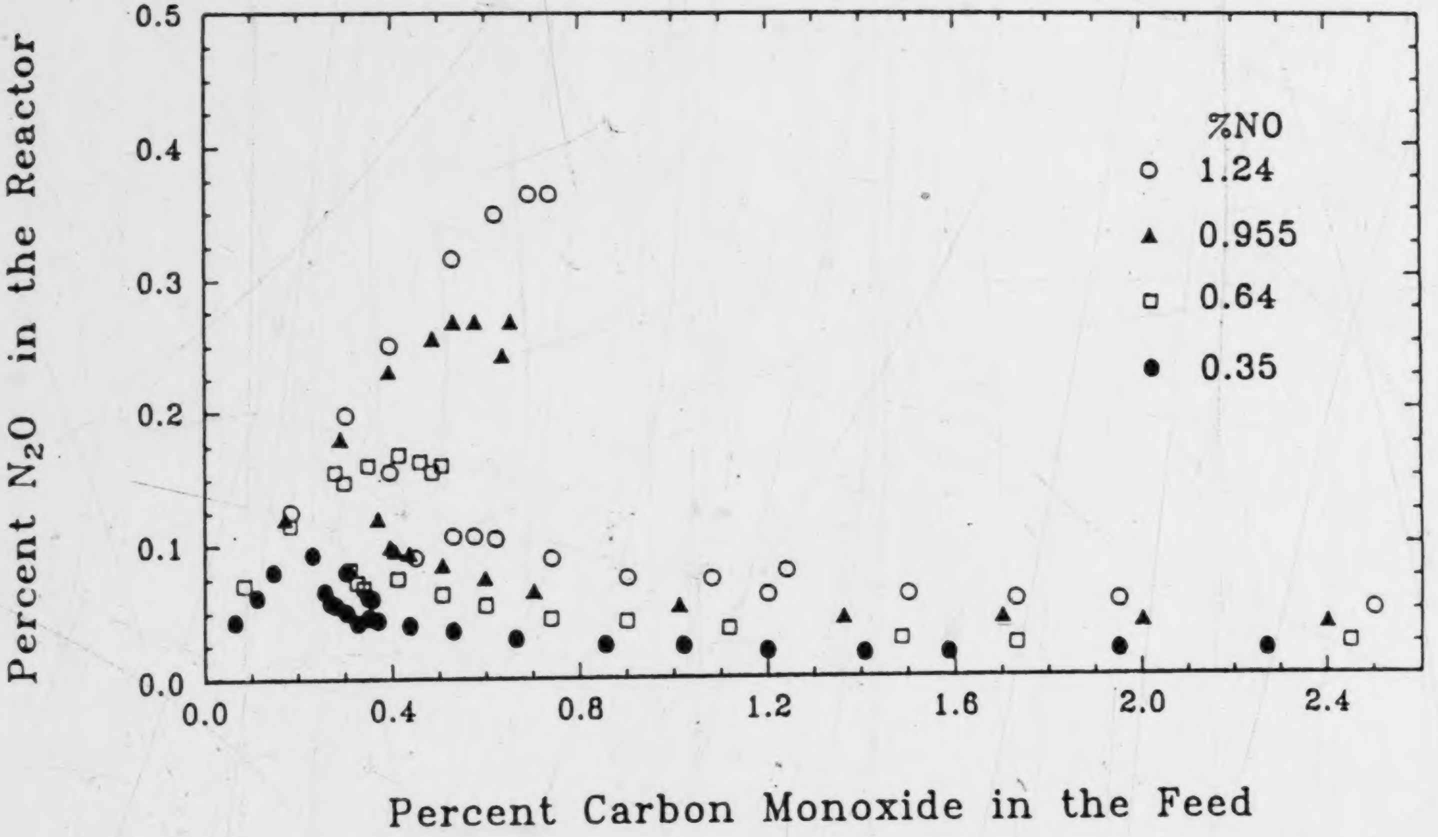

Figure 5.19 N_2O Formation Rate at 170°C, 100 SCCM

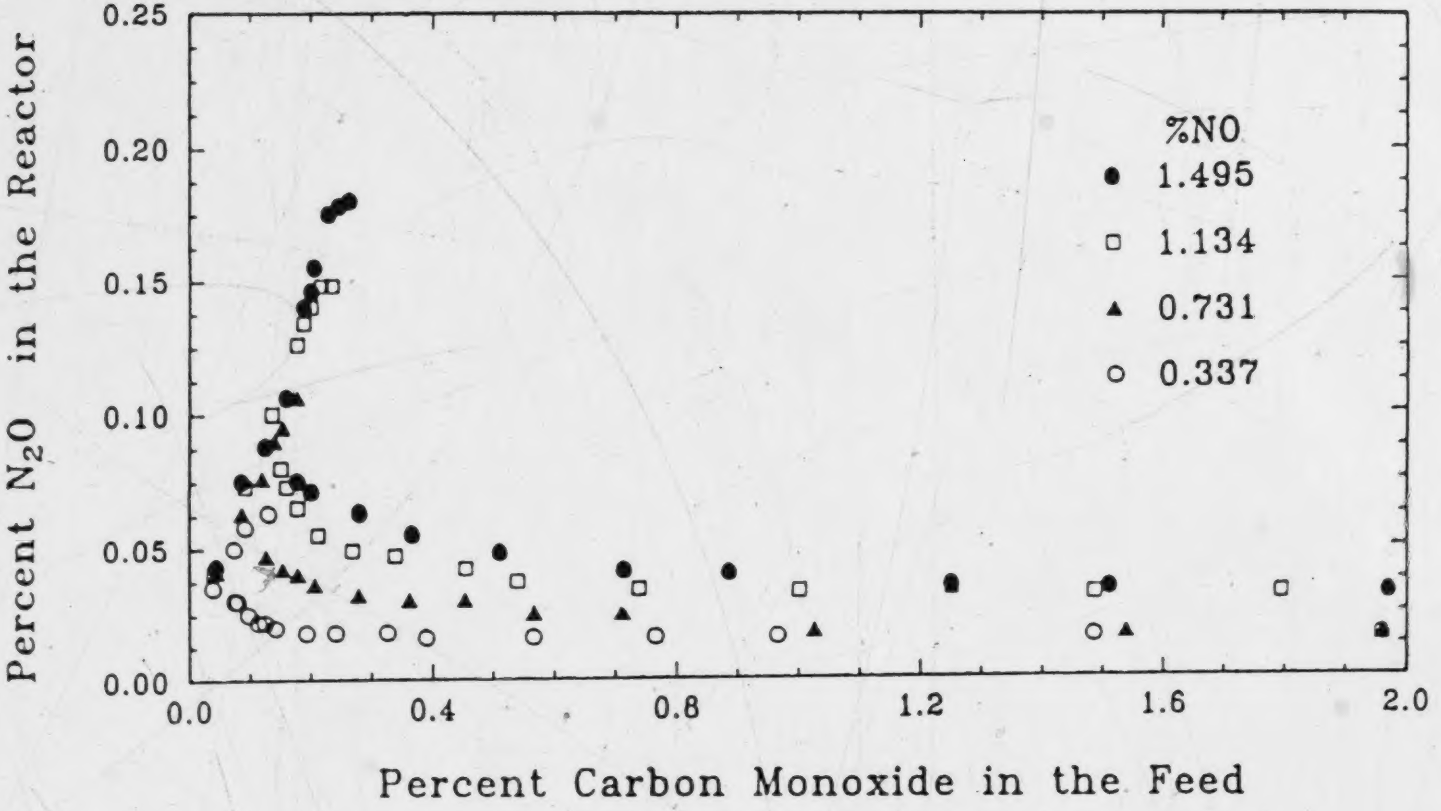

Figure 5.20 N_2O Formation Rate at 170°C, 400 SCCM

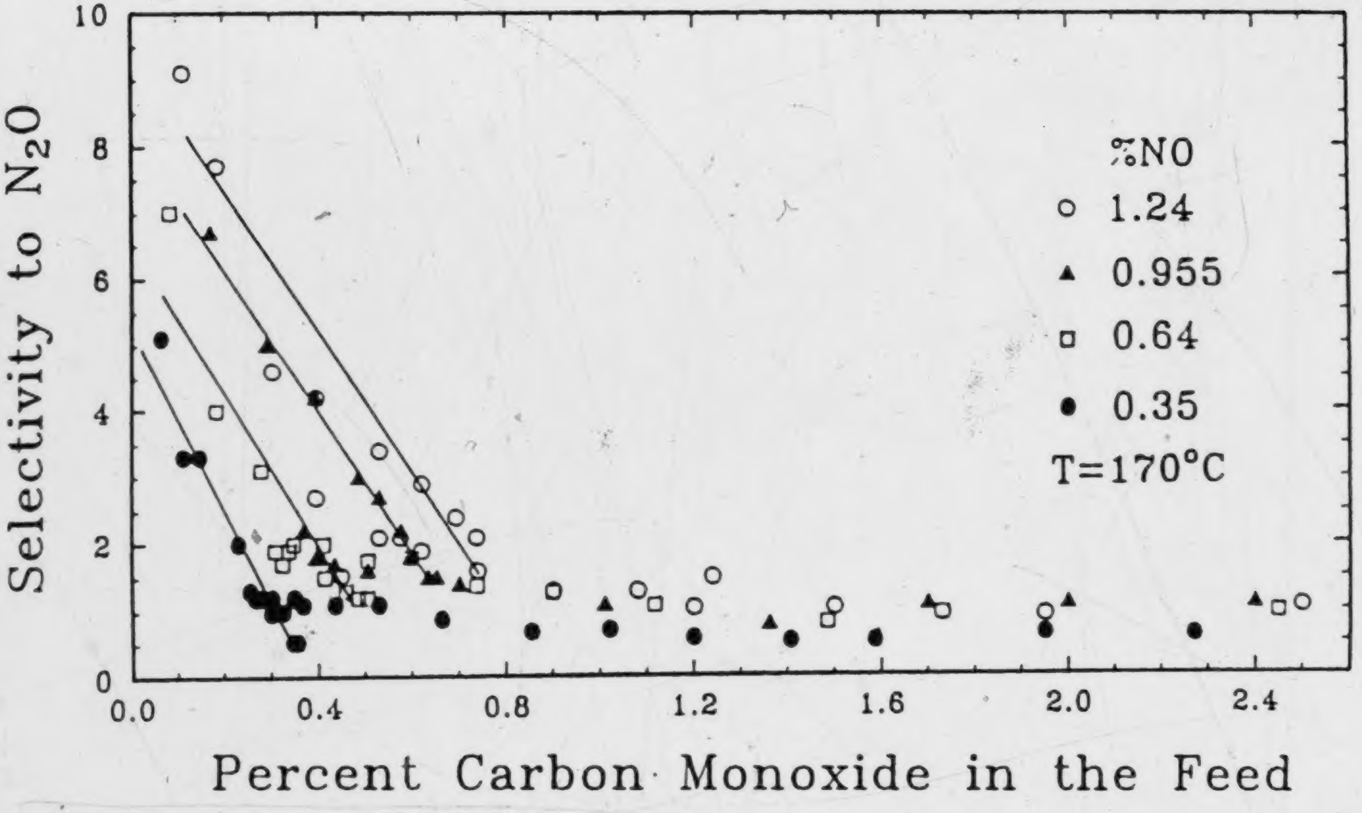

Figure 5.21 Selectivity for NO+CO at 170°C, 100 SCCM

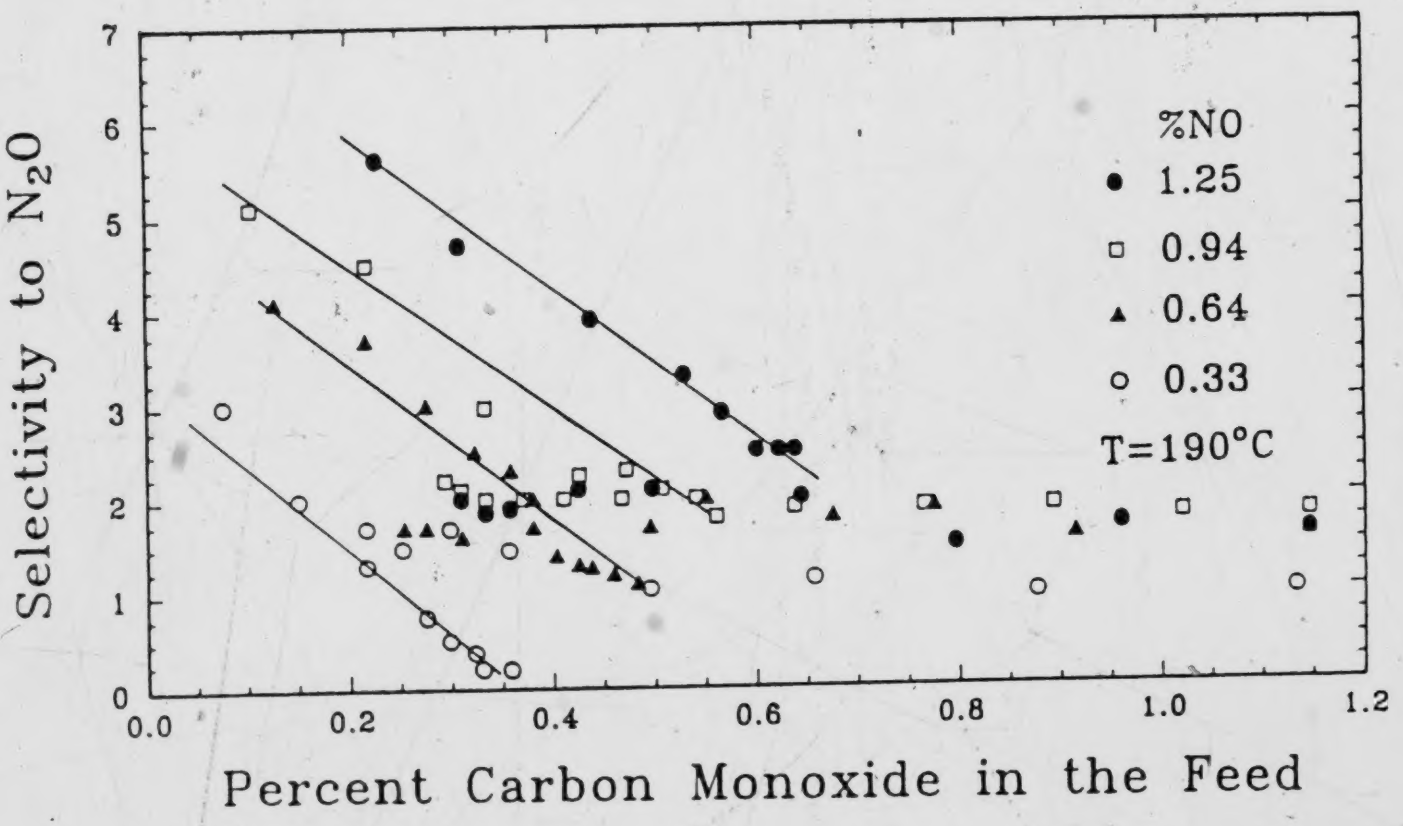

Figure 5.22 Selectivity for NO+CO at 190°C, 200 SCCM

feed composition. In addition, the NO concentration has a large influence on the selectivity. For a specified CO concentration, the higher the NO feed composition, the higher the reaction selectivity. In the low conversion region (high CO concentrations), the selectivity is approximately independent of the CO concentration. The scatter in the selectivity data is due to the combination of the experimental error with the necessity of subtracting one small number from another (see Equation 5.3), the result of which is then used as the denominator in the selectivity calculation. In particular, when the reaction occurs in the low conversion region, the value of the reaction selectivity is strongly affected by the analysis accuracy.

5.5 Summary

Nitric oxide reduction by carbon monoxide was carried out on a supported platinum catalyst, in a temperature range of 150 to 190°C, with total flow rates to the reactor of 100, 200 and 400 SCCM, respectively. It was observed that this system can display multiple-steady-state behavior. The actual reaction state in the multiplicity region is totally dependent on the starting conditions. The locations of the bifurcation points are strongly affected by the reactor operating parameters such as reaction temperature, flow rate to the reactor and NO feed composition. Increasing temperature causes the multiplicity region to shift to higher CO concentrations. The same effect can be achieved by reducing the total flow rate to the reactor or by increasing the NO feed composition.

The observed products are CO_2 and N_2O, and the presence of N_2 can be found from a component balance. The ratio of N_2O to N_2 (the selectivity) remains constant in the low conversion region, while in the high conversion region the ratio decreases with increasing CO feed concentration. The selectivity is also affected by the reaction temperature and the flow rate to the reactor. Increasing the temperature, or decreasing the flow rate, results in a decrease of the ratio of N_2O to N_2.

NO conversions are very dependent on the NO feed concentration. Generally, higher NO conversions can be achieved for low NO feed concentrations. In the high conversion region, the NO conversion increases with increasing CO feed concentration, and in the low conversion region, the NO conversion remains almost constant.

6. EXAMINATION OF MECHANISMS FOR THE NO+CO REACTION

6.1 Introduction

From the introductory literature review, it is seen that the reduction of NO by CO has been extensively studied on both supported and unsupported noble metal catalysts. Over ten possible reaction steps have been proposed for the NO+CO reaction process. However, it is still not certain whether all of these steps are involved in the reaction process. Among them, either the decomposition of adsorbed NO, or the reaction between adsorbed NO and adsorbed CO, is commonly taken as the rate-limiting step in proposed reaction mechanisms (Chin and Bell, 1983; Hecker and Bell, 1983; Klein et al., 1985). In many reports, nitrous oxide formation was assumed to occur via the reaction of adsorbed NO with adsorbed N atoms. (Lambert and Comrie, 1974; Pirug and Bonzel, 1977). As well, it has been claimed that N_2O might be formed via the reaction between two adsorbed NO (Hendershot and Hansen,1986), or the reaction between adsorbed NO and gas-phase NO (Lim et al., 1986). No consensus on a detailed reaction mechanism has emerged. In the current chapter, several reaction mechanisms for the NO+CO reaction, based on the experimental observations of this work and previous investigations, will be examined.

6.2 Reaction Steps

During the experiments, it was observed that nitrous oxide is one of the main products of the NO+CO reaction. Because N_2O can react with CO under the reaction conditions (see Chapter 3), a NO+CO reaction mechanism must include a N_2O+CO reaction mechanism. It was shown in Chapter 4 that a satisfactory description of the N_2O+CO reaction is given by Mechanism 11:

$$CO(g) + M \rightleftharpoons CO\text{-}M \tag{6.1}$$

$$N_2O(g) + M \longrightarrow N_2(g) + O\text{-}M \tag{6.2}$$

$$CO\text{-}M + O\text{-}M \longrightarrow CO_2(g) + 2\,M \tag{6.3}$$

$$CO(g) + O\text{-}M \longrightarrow CO_2(g) + M \tag{6.4}$$

Hence, steps (6.1) to (6.4) with the previously estimated kinetic parameters will be included in all of the NO+CO mechanisms. According to the previous investigations, the other reaction steps which are possibly involved in the NO+CO reaction are: NO adsorption/desorption steps, a N_2O formation step, a NO decomposition step and a desorption step for nitrogen gas. Several of these steps will be examined in the current work. These reactions are classified as follows:

(1) NO adsorption/desorption

$$NO(g) + M \rightleftharpoons NO\text{-}M \tag{6.5}$$

(2) N_2O formation

$$NO(g) + NO\text{-}M \longrightarrow N_2O(g) + O\text{-}M \tag{6.6}$$

$$2\ NO\text{-}M \longrightarrow N_2O(g) + O\text{-}M + M \tag{6.7}$$

$$NO\text{-}M + N\text{-}M \longrightarrow N_2O(g) + 2\ M \tag{6.8}$$

(3) NO decomposition

$$NO\text{-}M + M \rightleftharpoons N\text{-}M + O\text{-}M \tag{6.9}$$

$$NO\text{-}M + CO\text{-}M \longrightarrow CO_2(g) + N\text{-}M + M \tag{6.10}$$

(4) nitrogen desorption

$$2\ N\text{-}M \longrightarrow N_2(g) + 2\ M \tag{6.11}$$

Using the above reaction steps, four reaction mechanisms will be proposed in the following sections. Each reaction mechanism will have one N_2O formation step. The initial examination will be based on how the predictions match the experimental observations at 190°C because at this temperature, experimental observations are available for both the N_2O+CO and NO+CO reactions. In particular, the model predictions for the NO+CO reaction system are forced to match as closely as possible the experimental observations of CO conversion, NO conversion and bifurcation point locations. The same mathematical method is used here as in Chapter 4 to determine the N_2O+CO reaction behavior. The computer program can predict the variation of CO conversion, NO conversion, N_2O concentration and reaction selectivity with respect to CO feed composition.

6.3 Mechanism 1

In mechanism 1, it is assumed that N_2O is produced via a gas-surface reaction, step (6.6), between adsorbed NO and gas phase NO where adsorbed NO is formed through reaction step (6.5). These two steps together with Mechanism 4.11 comprise the simplest mechanism for the NO+CO reaction. The overall reaction is thus given by:

$$CO(g) + M \rightleftarrows CO\text{-}M \tag{6.1}$$

$$N_2O(g) + M \longrightarrow N_2(g) + O\text{-}M \tag{6.2}$$

$$CO\text{-}M + O\text{-}M \longrightarrow CO_2(g) + 2\,M \tag{6.3}$$

$$CO(g) + O\text{-}M \longrightarrow CO_2(g) + M \tag{6.4}$$

$$NO(g) + M \rightleftharpoons NO\text{-}M \qquad (6.5)$$

$$NO(g) + NO\text{-}M \longrightarrow N_2O(g) + O\text{-}M \qquad (6.6)$$

To describe the reaction behavior with this mechanism, three gas-phase and three surface-phase balance equations are needed, with three unknown kinetic parameters (kinetic parameters for reaction steps (6.5) and (6.6)). Through solving the algebraic balance equations, the unknown kinetic parameters are evaluated by minimizing the deviation from the experimental observations.

From the model predictions, typical behavior of which is shown in Figure 6.1, it is found that Mechanism 1 can describe multiplicity behavior. However, when the predictions are forced to match the bifurcation point locations it is found that the CO and NO conversions and the predicted N_2O concentrations are much higher than that seen experimentally. In addition, very little molecular nitrogen is formed during the reaction. This results in the predicted selectivities being over ten times higher than the observations. The disagreement between the predicted and observed selectivities is mainly caused by the lack of an alternate pathway for molecular nitrogen formation in the reaction mechanism. The selectivity is completely controlled by the N_2O decomposition step. When the predicted CO and NO conversions are in agreement with that found experimentally, then the predicted selectivities do not accord with the observations. Hence,

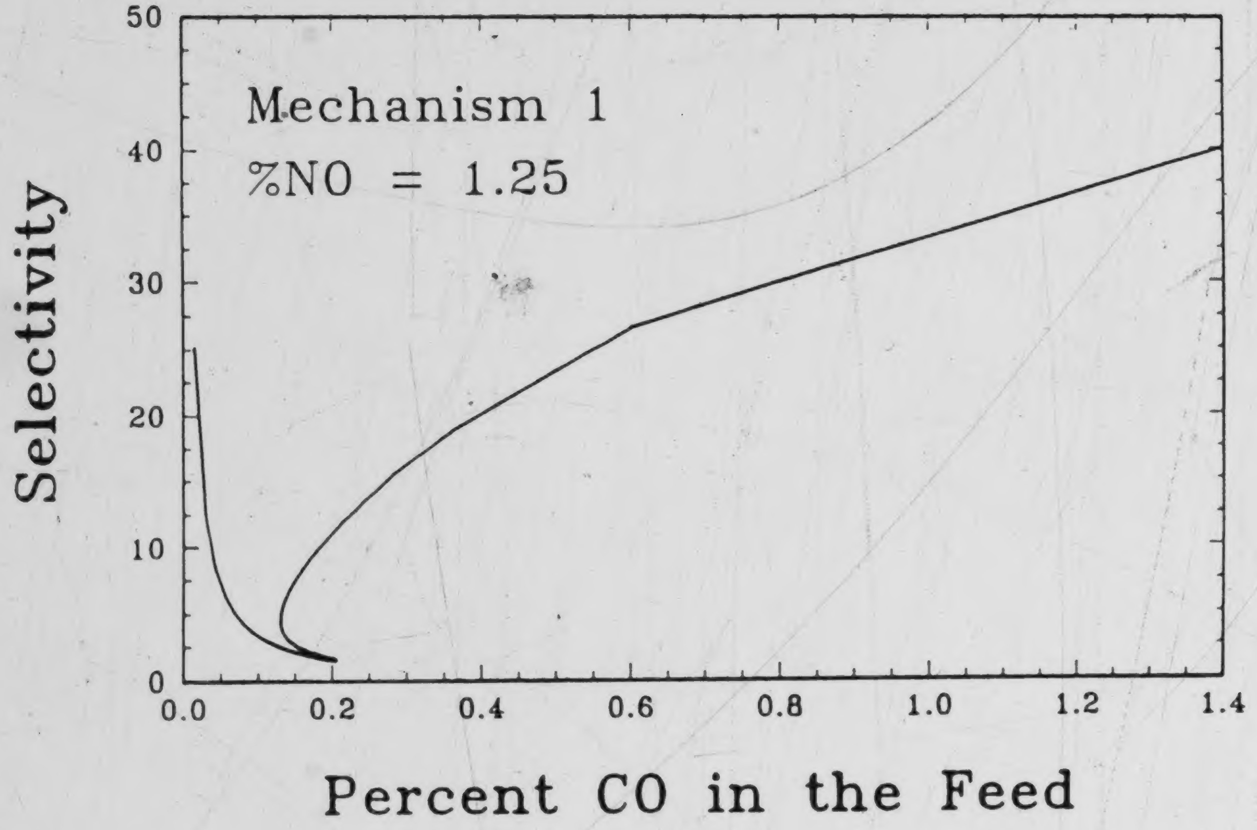

Figure 6.1 Selectivity Predictions from Mechanism 1

this mechanism cannot provide satisfactory predictions for nitric oxide reduction by carbon monoxide. The values of the kinetic parameters used for the various models are listed in Table 6.1.

6.4 Mechanism 2

In contrast to Mechanism 1, in Mechanism 2 it is assumed that N_2O is produced by a reaction between two adsorbed NO molecules, thus step (6.6) is replaced by step (6.7) giving the overall mechanism:

$$CO(g) + M \rightleftharpoons CO\text{-}M \tag{6.1}$$

$$N_2O(g) + M \longrightarrow N_2(g) + O\text{-}M \tag{6.2}$$

$$CO\text{-}M + O\text{-}M \longrightarrow CO_2(g) + 2\ M \tag{6.3}$$

$$CO(g) + O\text{-}M \longrightarrow CO_2(g) + M \tag{6.4}$$

$$NO(g) + M \rightleftharpoons NO\text{-}M \tag{6.5}$$

$$2\ NO\text{-}M \longrightarrow N_2O(g) + O\text{-}M + M \tag{6.7}$$

Because both Mechanism 1 and Mechanism 2 have similar N_2 formation processes, Mechanism 2 has the same problem in predicting N_2O concentrations and selectivity. The predicted selectivities, typical results of which are shown in Figure

Table 6.1 Values of Parameters for Mechanisms

Parameter	Mech. 1	Mech. 2	Mech. 3	Mech. 4
k_{-1}	0.046	0.046	0.046	0.046
k_2	0.14	0.14	0.14	0.14
k_3	650	650	650	650
k_4	0.5	0.5	0.5	0.5
k_{-5}	0.07	0.3	0.5	0.2
k_6	0.016			
k_7		90000		
k_8			20000	40000
k_9				95000
k_{-9}				50
k_{10}			2900	
k_{11}			8000	40000
S_{CO}	8.6×10^{-6}	8.6×10^{-6}	8.6×10^{-6}	8.6×10^{-6}
S_{NO}	8.0×10^{-8}	7.0×10^{-7}	3.3×10^{-7}	3.3×10^{-7}

6.2, are always much higher than the experimental observations; in other words, the formation rate of nitrogen is much to low.

The calculations from Mechanisms 1 and 2 have shown that if N_2O decomposition is the sole pathway for molecular nitrogen formation, then the predicted selectivity deviates markedly from the observations. This implies that in the actual reaction process, molecular nitrogen is possibly produced by more than one reaction step. Hence, in the following mechanisms, it is assumed that there are two formation pathways for molecular nitrogen. One is through a nitrous oxide decomposition step; the other is via atomic nitrogen recombination and desorption. The surface nitrogen atoms are produced by NO decomposition steps, (6.9) or (6.10). The surface nitrogen can possibly also react with surface NO and produce nitrous oxide.

6.5 Mechanism 3

In mechanism 3, atomic nitrogen is formed during the bimolecular surface reaction between adsorbed NO and CO, and the reaction process can be described by the following steps:

$$CO(g) + M \rightleftharpoons CO\text{-}M \tag{6.1}$$

$$N_2O(g) + M \longrightarrow N_2(g) + O\text{-}M \tag{6.2}$$

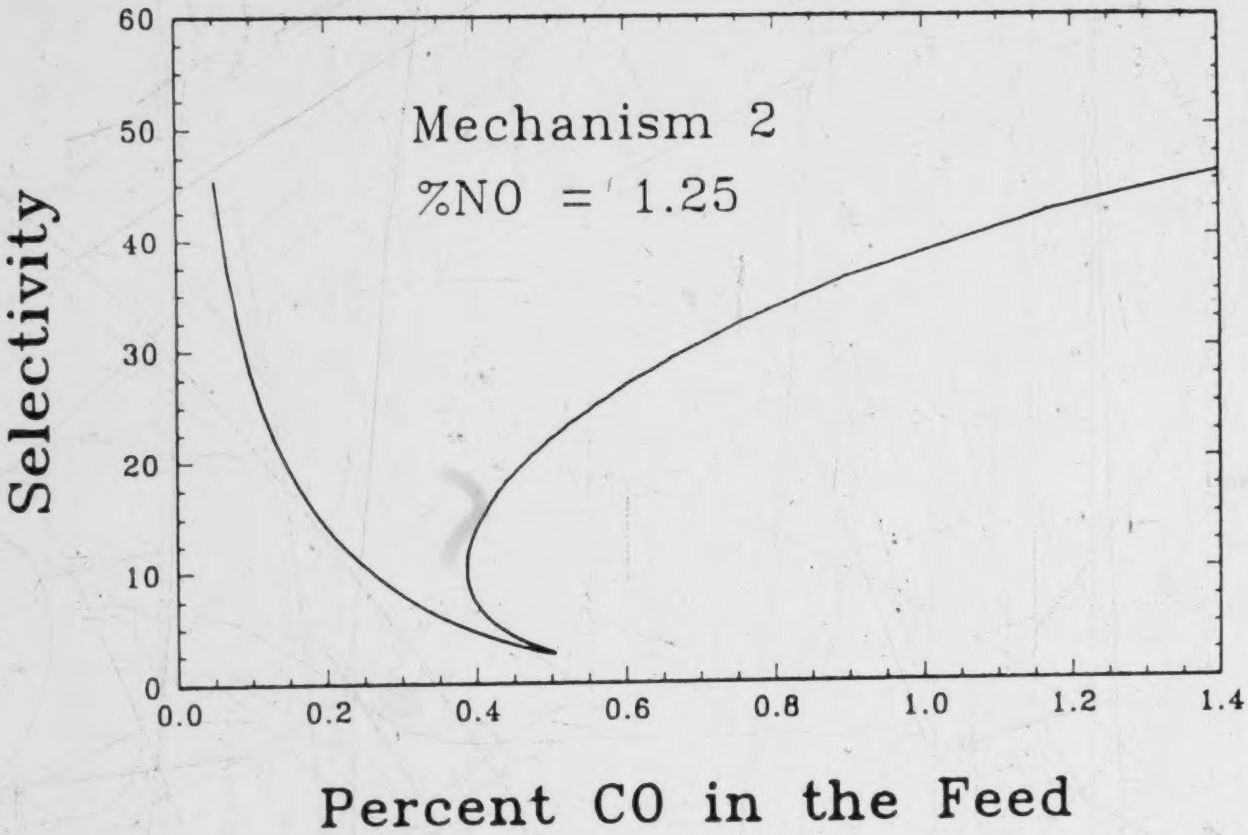

Figure 6.2 Selectivity Predictions from Mechanism 2

$$\text{CO-M} + \text{O-M} \longrightarrow \text{CO}_2(g) + 2\ \text{M} \qquad (6.3)$$

$$\text{CO}(g) + \text{O-M} \longrightarrow \text{CO}_2(g) + \text{M} \qquad (6.4)$$

$$\text{NO}(g) + \text{M} \rightleftharpoons \text{NO-M} \qquad (6.5)$$

$$\text{NO-M} + \text{N-M} \longrightarrow \text{N}_2\text{O}(g) + 2\ \text{M} \qquad (6.8)$$

$$\text{NO-M} + \text{CO-M} \longrightarrow \text{CO}_2(g) + \text{N-M} + \text{M} \qquad (6.10)$$

$$2\ \text{N-M} \longrightarrow \text{N}_2(g) + 2\ \text{M} \qquad (6.11)$$

Typical selectivity predictions for this mechanism are shown in Figure 6.3. It is seen that, from the inclusion of the additional N_2 formation pathway, step (6.11), the predicted selectivities have been improved, compared to Mechanisms 1 and 2. The selectivities are in the same order of magnitude as the observed selectivities. The agreement is especially good in the low conversion region. In addition, in this region the NO and CO conversion predictions closely match the observations

Unfortunately, the predicted selectivities in the high conversion region still do not agree with the experiments. In Chapter 5, the experimental results indicate that the selectivity increases strongly with decreasing CO feed composition in the high conversion region. However, the predictions from the present mechanism show that the

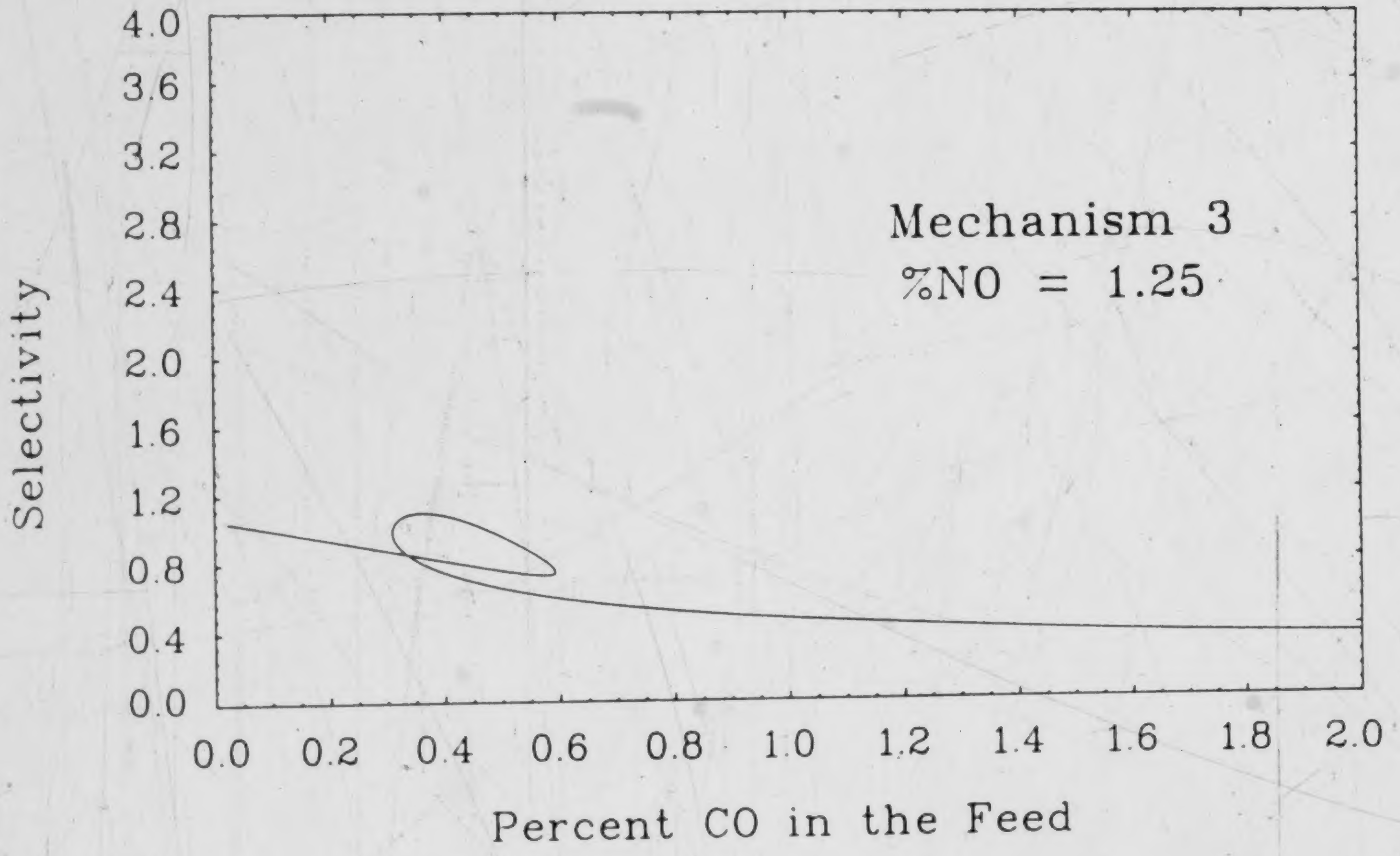

Figure 6.3 Selectivity Predictions from Mechanism 3

variation of the selectivity in the high conversion region is slight. Hence, this mechanism still cannot describe the NO+CO reactor behavior.

6.6 Mechanism 4

Substituting step (6.9) for (6.10) in Mechanism 3 gives Mechanism 4 in which adsorbed nitrogen is formed as a result of the dissociation of adsorbed NO:

$$CO(g) + M \rightleftharpoons CO\text{-}M \qquad (6.1)$$

$$N_2O(g) + M \longrightarrow N_2(g) + O\text{-}M \qquad (6.2)$$

$$CO\text{-}M + O\text{-}M \longrightarrow CO_2(g) + 2\,M \qquad (6.3)$$

$$CO(g) + O\text{-}M \longrightarrow CO_2(g) + M \qquad (6.4)$$

$$NO(g) + M \rightleftharpoons NO\text{-}M \qquad (6.5)$$

$$NO\text{-}M + N\text{-}M \longrightarrow N_2O(g) + O\text{-}M \qquad (6.8)$$

$$NO\text{-}M + M \rightleftharpoons N\text{-}M + O\text{-}M \qquad (6.9)$$

$$2\,N\text{-}M \longrightarrow N_2(g) + 2\,M \qquad (6.11)$$

The selectivity predictions from Mechanism 4 are shown in Figure 6.4.

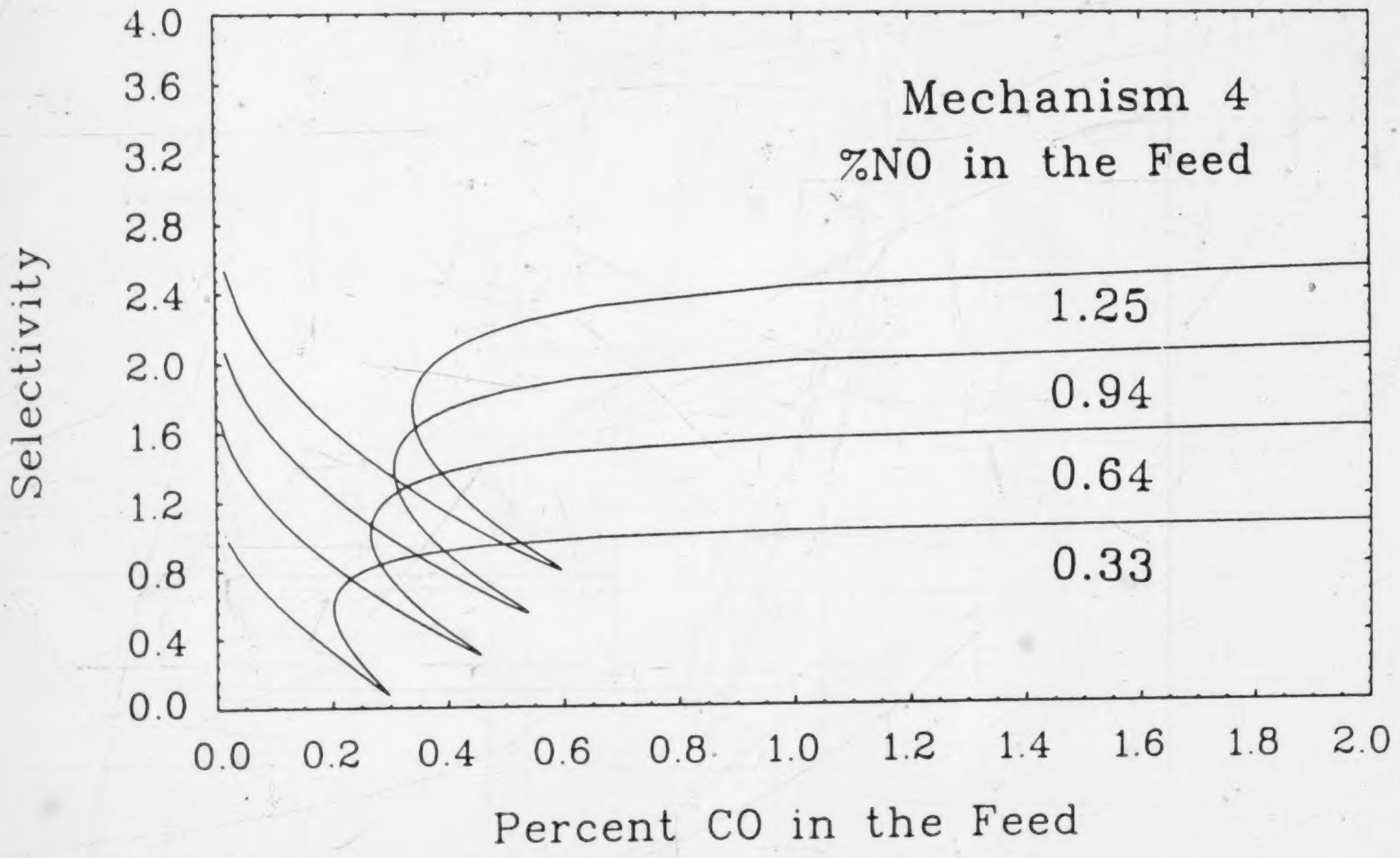

Figure 6.4 Selectivity Predictions from Mechanism 4

It is seen that the predicted selectivities are in qualitative agreement with that found experimentally (compare Figure 6.4 to Figure 5.22). This qualitative agreement also extends to the predictions for the CO and NO conversions, as well as the %N_2O in the reactor (compare Figures 6.5, 6.6 and 6.7 to Figures 5.3, 5.6 and 5.12, respectively). Thus, Mechanism 4 is a promising candidate for future examination as a description of the NO+CO reaction on supported platinum.

6.7 Summary

From a comparison of the model predictions, is seen that only Mechanism 4 can describe the observed trends for the NO+CO reaction. Although this mechanism does not give a perfect description for the NO+CO reaction, it nevertheless indicates that N_2O is an intermediate during the reduction of NO by CO, and also that N_2O is formed by a reaction between adsorbed NO and adsorbed N atoms. This conclusion is in accordance with the observations made by Halpern et al. (1981) who found that N_2O was the only product observed when nitrogen atoms were reacted with chemisorbed oxygen on platinum, even though it was initially expected that the simple molecule NO would be the main product. It has also been suggested that N_2O might be formed by the reaction between adsorbed NO and N atoms. The experimental observations made by Shelef, et al. (1968) also support this view. They claimed that when the reaction temperature is below 300°C, N_2O is

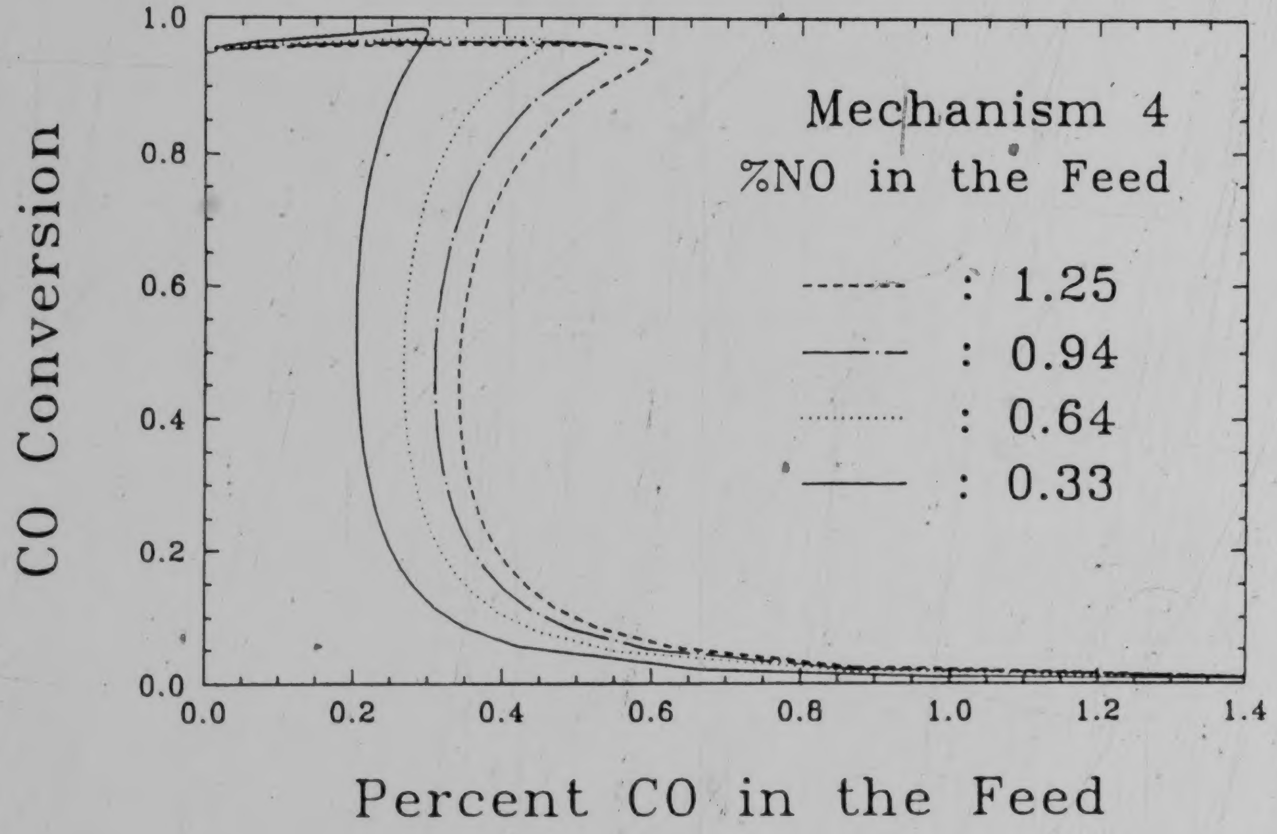

Figure 6.5 CO Conversion Predictions from Mechanism 4

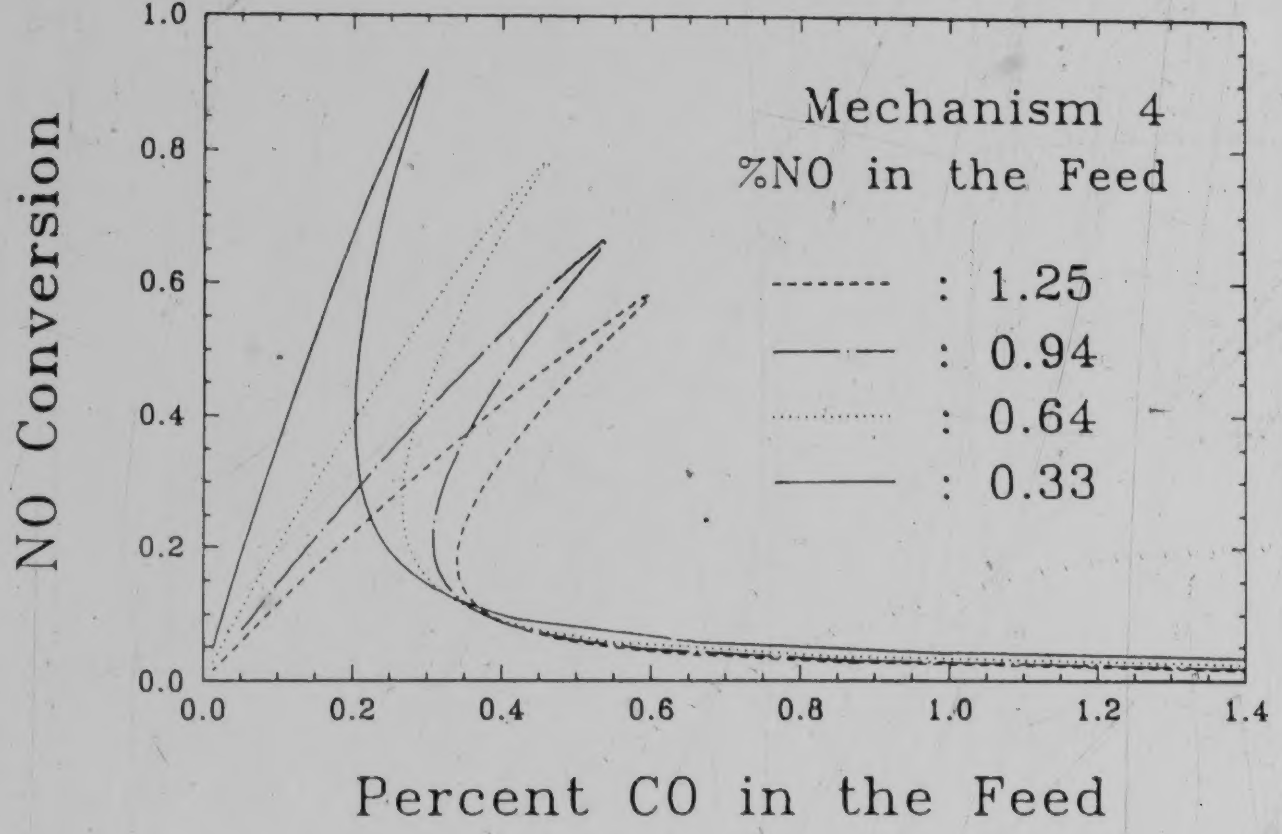

Figure 6.6 NO Conversion Predictions from Mechanism 4

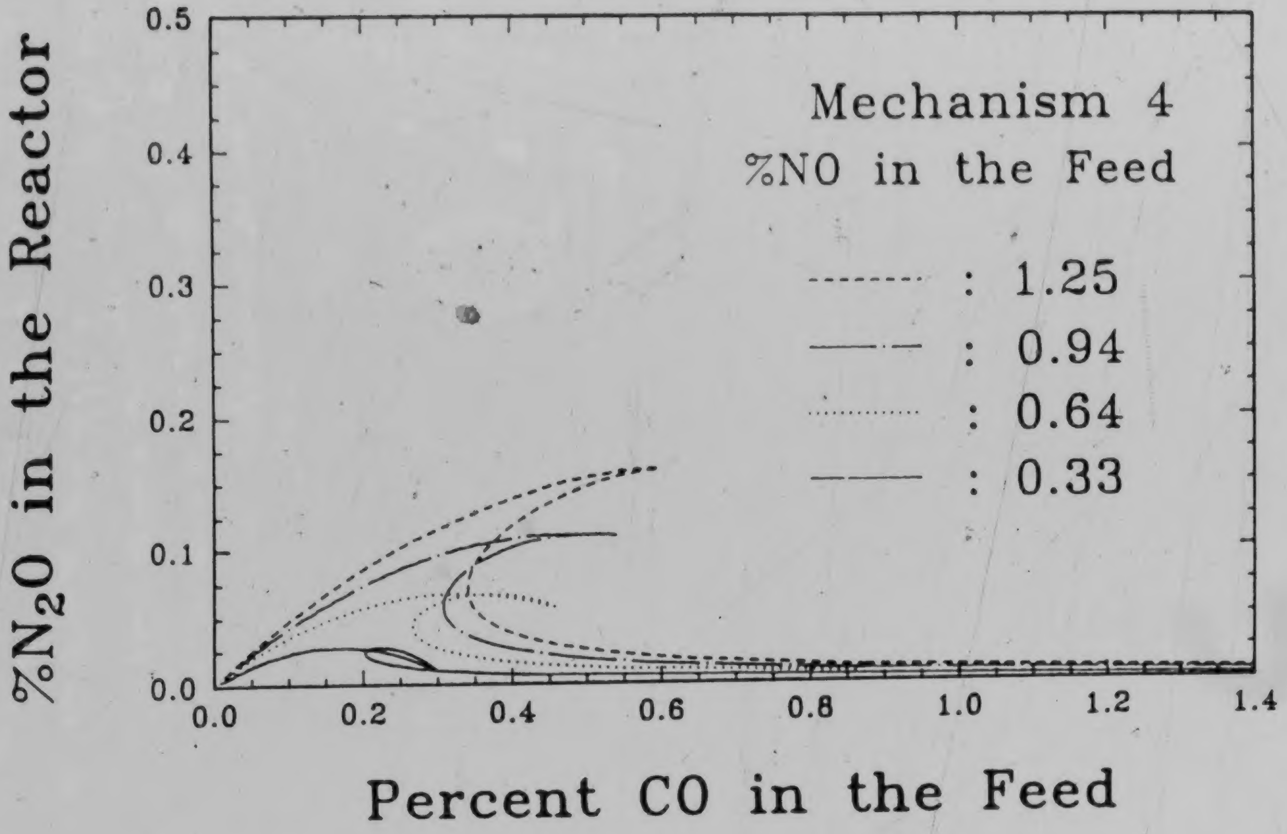

Figure 6.7 N_2O Concentration Predictions from Mechanism 4

the major nitrogen containing product.

It should be mentioned that during the development of the reaction models in this work, no account was taken of the formation and destruction of a NCO isocyanate complex. In the last few years there has been much discussion regarding the formation of isocyanate species (NCO) during the reaction of NO and CO over transition metal catalysts. Some reports maintain that the isocyanate species is bound to the metal (M-NCO), while other studies show that the interaction of NO and CO on supported catalysts occurs on the support and not on the metal. The isocyanate structure, if it exists at all, is still unclear. Thus, in the present work the presence of a NCO species on the surface and its effect on the reaction were ignored.

6.8 Nomenclature

CO-M	: adsorbed CO surface species
k_i	: adsorption, or reaction, rate constant (value of i refers to the number of the corresponding step in the mechanism)
k_{-i}	: desorption rate constant (value of i refers to the number of the corresponding step in the mechanism)
M	: active site on catalyst surface
N-M	: adsorbed nitrogen surface species
NO-M	: adsorbed NO surface species
N_{CO}	: a CO self-exclusion factor

O-M : adsorbed oxygen surface species

S_{CO} : CO sticking probability

S_{NO} : NO sticking probability

7. CONCLUSIONS

1. The reduction of N_2O by CO on Pt/γ-Al_2O_3 displays multiplicity behavior over a temperature range of 170 to 246°C. The width of the multiplicity region is strongly affected by reaction temperature and feed concentration.
2. The multiplicity behavior of the N_2O+CO reaction system can be described by a mechanism consisting of a combination of Langmuir-Hinshelwood and Eley-Rideal reaction steps, with a CO self-exclusion effect playing a key role.
3. The reduction of NO by CO on a Pt/γ-Al_2O_3 catalyst also exhibits multiplicity behavior. The influence of flow rate, reaction temperature and feed concentration on the reaction behavior was examined.
4. The experiments and the modelling indicate that N_2O is an intermediate for the formation of N_2. However, it cannot be ruled out that part of the N_2 was formed directly from NO decomposition.
5. From the examination of several reaction mechanisms, it appears that a surface nitrogen species is formed during the reduction of NO by CO.

BIBLIOGRAPHY

Adlhoch, W., R. Kohler and H.-G. Lintz, "Die Kinetik der Reaktion Zwischen N_2O und CO an Polykristallinem Platin bei Niedrigen Drucken", Z. Physik. Chem. Neue Folge **120**, 111-118 (1980).

Adlhoch, W. and H.-G. Lintz, "Instabilität und Oszillation der Reaktionsgeschwindigkeit bei der Reaktion von CO mit NO an Platin im Knudsen-Gebiet", Z. Physik. Chem. Neue Floge **103**, 207-211 (1976).

Adlhoch, W. and H.-G. Lintz, "Die Kinetik der Reaktion Zwischen NO und CO an Polykristallinem Platin bei Niedrigen Drucken I. Messmethode und Experimenteller Befund", Surf. Sci. **78**, 58-68 (1978).

Adlhoch, W. and H.-G. Lintz, "Die Kinetik der Reaktion Zwischen NO und CO an Polykristallinem Platin Bei Niedrigen Drucken II. Deutung und Aufstellung einer Elementarreaktionensequenz", Surf. Sci. **78**, 69-78 (1978).

Adlhoch, W., H.-G. Lintz and T. Weisker, "Oszillationen der Reaktionsgeschwindigkeit bei der Reaktion von NO mit CO an Platin im Knudsengebiet" Surf. Sci. **103**, 576-585 (1981).

Alnot, M., A. Cassuto, J. Fusy and A. Pentenero, "Comparative Adsorption of O_2 and N_2O on Platinum Recrystallized Ribbons", Jpn. J. Appl. Phys., Suppl. 2, part 2, 79-84 (1974).

Amirnazmi, A. and M. Boudart, "Decomposition of Nitric Oxide on Platinum", J. Catal. **39**, 383-394 (1975).

Avery, N. R., "An EELS Study of N_2O Adsorption on Pt(111)", Surf. Sci. **131**, 501-510 (1983).

Bolten, H., T. Hahn, J. Leroux and H.-G. Lintz, "Bistability of the Reaction Rate in the Oxidation of Carbon Monoxide by Nitrogen Monoxide on Polycrystalline Platinum", Surf. Sci. **160**, L529-L532 (1985).

Bonzel, H. P. and R. Ku, "Adsorbate Interactions on a Pt(110) Surface I. Sulfur and Carbon Monoxide", J. Chem. Phys. **58**, 4617-4624 (1973).

Brown, M. F. and R. D. Gonzalez, "An Infrared Study of the Interaction between Adsorbed CO and Adsorbed NO on Supported Ru and Supported Pt", J. Catal. **44**, 477-487 (1976).

Chin, A. A. and A. T. Bell, "Kinetics of NO Decomposition on

Silica-Supported Rhodium", J. Phys. Chem. 87, 3700-3706 (1983).

Conrad, H., G. Ertl and J. Küppers, "Interactions Between Oxygen and Carbon Monoxide on a Pd(111) Surface", Surf. Sci. 76, 323-342 (1978).

Diamantis, A. A. and G. J. Sparrow, "Model of Attachment of Adsorbed Nitrous Oxide", J. Colloid. Interface Sci. 47, 455-458 (1974).

Dorling, T. A. and R. L. Moss, "The Structure and Activity of Supported Metal Catalysts II. Crystallite Size and CO Chemisorption on Platinum/Silica Catalysts", J. Catal. 7, 378-385 (1967).

Engel, T., "A Molecular Beam Interaction of He, CO and O_2 Scattering from Pd(111)", J. Chem. Phys. 69, 373-385 (1978).

Engel, T. and G. Ertl, "Elementary Steps in the Catalytic Oxidation of Carbon Monoxide on Platinum Metals", Adv. in Catal. 28, 1-78 (1979).

Ertl, G., M. Neumann and K. M. Streit, "Chemisorption of CO on the Pt(111) Surface", Surf. Sci. 64, 393-410 (1977).

Freel, J., "Chemisorption on Supported Platinum. II: Stoichiometry for Hydrogen, Oxygen and Carbon Monoxide", J. Catal. 25, 149-160 (1972).

Fu, C. M., V. N. Korchak and W. K. Hall, "Decomposition of Nitrous Oxide on FeY Zeolite", J. Catal. 68, 166-171 (1981).

Gasser, R. P. H. and C. J. Marsay, "The Chemisorption of Nitrous Oxide at Low Pressures by Rhenium", Surf. Sci. 20, 116-122 (1970).

Gland, J. L. and B. A. Sexton, "Nitric Oxide Adsorption on the Pt(111) Surface", Surf. Sci. 94, 355-368 (1980).

Gorte, R. J., L. D. Schmidt and J. L. Gland, "Binding States and Decomposition of NO on Single Crystal Planes of Pt", Surf. Sci. 109, 367-380 (1981).

Graham, W. R. C. and D. T. Lynch, "CO Oxidation on Pt: Model Discrimination Using Experimental Bifurcation Behavior", AIChE J. 33, 792-800 (1987).

Habraken, F. H. P. M. and G. A. Bootsma, "The Kinetics of the Interactions of O_2 and N_2O with a Cu(110) Surface and of the Reaction of CO with Adsorbed Oxygen Studied by Means of Ellipsometry, AES and LEED", Surf. Sci. 87, 333-347 (1979).

Halpern, B. L., E. J. Murphy and J. B. Fenn, "Surface-Catalyzed Production of Nitrous Oxide from the Reaction of N Atoms and O_2 on Platinum", J. Catal. **71**, 434-438 (1981).

Hardee, J. R. and J. W. Hightower, "Nitric Oxide Reduction by Methane over Rh/Al_2O_3 Catalysts", J. Catal. **86**, 137-146 (1984).

Hecker, W. C. and A. T. Bell, "Reduction of NO by CO over Silica-Supported Rhodium: Infrared and Kinetic Studies", J. Catal. **84**, 200-215 (1983).

Hecker, W. C. and A. T. Bell, "Infrared Observations of Rh-NCO and Si-NCO Species Formed During the Reaction of NO by CO Over Silica Supported Rhodium", J. Catal. **85**, 389-397 (1984).

Hendershot, R. E. and R. S. Hansen, "Reduction of Nitric Oxide with Carbon Monoxide on the Rh(100) Single-Crystal Surface", J. Catal. **98**, 150-165 (1986).

Herz, R. K. and S. P. Marin, "Surface Chemistry Models of Carbon Monoxide Oxidation on Supported Platinum Catalysts", J. Catal. **65**, 281-296 (1980).

Hinshelwood, C. N. and C. R. Prichard, "A Comparison Between the Homogeneous Thermal Decomposition of Nitrous Oxide and its Heterogeneous Catalytic Decomposition on the Surface of Platinum", J. Chem. Soc. **127**, 327-336 (1925).

Hu, Y-H. and J. W. Hightower, "Nitric Oxide Reduction by Methane over a Platinum Catalyst", ACS Symposium on Emission Control Catalysts, San Francisco Meeting, August 29-September 3, 841-850 (1976).

Klein, R. L., S. Schwartz and L. D. Schmidt, "Kinetics of the NO+CO Reaction on Clean Pt: Steady-State Rates", J. Phys. Chem. **89**, 4908-4914 (1985).

Lambert, R. M. and C. M. Comrie, "The Oxidation of CO by NO on Pt(111) and Pt(110)", Surf. Sci. **46**, 60-81 (1974).

Lesley, M. W. and L. D. Schmidt, "Chemical Autocatalysis in the NO+CO Reaction on Pt(100)", Chem. Phys. Lett. **102**, 459-463 (1983).

Lesley, M. W. and L. D. Schmidt, "The NO+CO Reaction on Pt(100)", Surf. Sci. **155**, 215-240 (1985).

Lim, K. J., D. G. Löffler and M. Boudart, "Nitrogen Desorption in the Reaction of Nitric Oxide on Carbon-Supported

Platinum Catalysts", J. Catal. 100, 158-166 (1986).

Lintz, H.-G., "The Oxidation of CO by O_2, NO and N_2O on Polycrystalline Platinum under Knudsen Conditions: A Comparison", Surf. Sci. 108, L486-L489 (1981).

Lintz, H.-G. and L. Riekert, "The Decomposition of Nitrous Oxide on Polycrystalline Platinum", J. Catal. 88, 244-245 (1984).

Loirat, H., F. Caralp and M. Destriau, "Rate Constant and Activation Energy of the Exchange Reaction $CO + N_2O \rightarrow CO_2 + N_2$ in the Temperature Range 1060-1220 K. Application of the Thermal Explosion Theory to a System with Two Parallel Reactions", J. Phys. Chem. 87, 2455-2457 (1983).

Lorimer, D. and A. T. Bell, "Reduction of NO by CO over a Silica-Supported Platinum Catalyst: Infrared and Kinetic Studies", J. Catal. 59, 223-238 (1979).

Lynch, D. T., Ph. D. thesis, Department of Chemical Engineering, "Oscillatory Behavior in Catalytic Reactions: A Mathematical and Experimental Investigation", University of Alberta, Edmonton (1981).

Lynch, D. T., "Use of Elementary Step Mechanisms to Explain Resonant Behavior for CO oxidation on Platinum", Can. J. Chem. Eng. 62, 691-698 (1984).

Lynch, D. T., G. Emig and S. E. Wanke, "Oscillations During CO Oxidation Over Supported Metal Catalysts III. Mathematical Modeling of the Observed Phenomena", J. Catal. 97, 456-468 (1986).

Madey, T. E., N. R. Avery, A. B. Anton, B. H. Toby and W. H. Weinberg, "Summary Abstract: The Adsorption and Decomposition of N_2O on Ru(001)", J. Vac. Sci. Technol. A 1, 1220-1221 (1983).

Milks, D. and R. A. Matula, "A Single-Pulse Shock-Tube Study of the Reaction Between Nitrous Oxide and Carbon Monoxide", Proc. 14th Int. Symp. Combust., 83-96 (1972).

Morrow, B. A., J. P. Chevrier and L. E. Moran, "An Infrared Study of the Adsorption of NO on Silica-Supported Platinum over a Wide Temperature Range", J. Catal. 91, 208-215 (1985).

Mummey, M. J. and L. D. Schmidt, "Decomposition of NO on Clean Pt near Atmospheric Pressures I. Steady State Kinetics", Surf. Sci. 109, 29-42 (1981).

Pirug, G. and H. P. Bonzel, "A Low-Pressure Study of the

Reduction of NO by H_2 on Polycrystalline Platinum", J. Catal. **50**, 64-76 (1977).

Redmond, J. P., "Kinetics of the Low Pressure Nitrous Oxide Decomposition on a Platinum Filament", J. Phys. Chem. **67**, 788-793 (1963).

Satterfield, C. N., "Heterogeneous Catalysis in Particle", McGraw-Hill, New York, (1980).

Schmidt, L. D., D. Hasenberg, S. Schwartz and G. A. Papapolymerou, "Surface Reactions on Clean Platinum and Rhodium at Low and High Pressures", ACS Symposium Series, Catalyst Characterization Science, **288**, 177-184 (1985).

Schwartz, S. B. and L. D. Schmidt, "Is There a Single Mechanism of Catalytic Rate Oscillation on Pt?", Surf. Sci. **183**, L269-L278 (1987).

Shelef, M., K. Otto and H. Gandhi, "The Oxidation of CO by O_2 and by NO on Supported Chromium Oxide and Other Metal Oxide Catalysts", J. Catal. **12**, 361-375 (1968).

Smith, T. G., J. Zahradnik and J. J. Carberry, "Non-isothermal Inter-intraphase Effectiveness Factors for Negative Order Kinetics - CO Oxidation Over Pt", Chem. Eng. Sci. **30**, 763-767 (1975).

Soler, J. M. and N. Garcia, "How Much Quantitative Information May be Expected from Programmed Desorption Experiments?", Surf. Sci. **124**, 563-570 (1983).

Solymosi, F., L. Völgyesi and J. Sárkáry, "The Effect of the Support on the Formation and Stability of Surface Isocyanate on Platinum", J. Catal. **54**, 336-344 (1978).

Steacie, E. W. R. and J. W. McCubbine, "The Decomposition of Nitrous Oxide on the Surface of Platinum I. The Retarding Effect of Oxygen", J. Chem. Phys. **2**, 585-589 (1934).

Summers, J. C. and L. L. Hegedus, "Modes of Catalyst Deactivation in Stoichiometric Automobile Exhaust", Ind. Eng. Chem. Prod. Res. Dev. **18**, 318-324 (1979).

Takoudis, C. G. and L. D. Schmidt, "Kinetics of N_2O Decomposition on Polycrystalline Platinum", J. Catal. **80**, 274-279 (1983).

Tan, S. A., R. B. Grant and R. M. Lambert, "The Silver-Catalysed Decomposition of N_2O and the Catalytic Oxidation of Ethylene by N_2O over Ag(111) and Ag/α-Al_2O_3", J. Catal. **104**, 156-163 (1987).

Umbach, E. and D. Menzel, "Horizontal and Vertical

Configurations of Molecular N_2O on W(110) and Ru(001)", Chem. Phys. Lett. **84**, 491-496 (1981).

Weinberg, W. H, "A Model Description of the Adsorption and Decomposition of Nitrous Oxide on Clean and Carbon Covered Platinum Surfaces", J. Catal. **28**, 459-470 (1973).

Weinberg, W. H. and R. P. Merrill, "Crystal Field Surface Orbital-Bond Energy Bond Order Calculations for Surface Reactions I. The Reactions $CO+O_2$, NO+CO and H_2+O_2 on a Pt(111) Surface", J. Catal. **40**, 268-280 (1975).

Winter, E. R. S., "The Decomposition of Nitrous Oxide on the Rare-Earth Sesquioxides and Related Oxides", J. Catal. **15**, 144-152 (1969).

Yao, H. C., M. Sieg and H. K. Plummer, Jr., "Surface Interactions in the $Pt/\gamma-Al_2O_3$ System", J. Catal. **59**, 365-374 (1979).

APPENDIX 1. CALIBRATION CURVES

Presented in this appendix are the calibration curves for the infrared spectrophotometer and the mass flow meters.

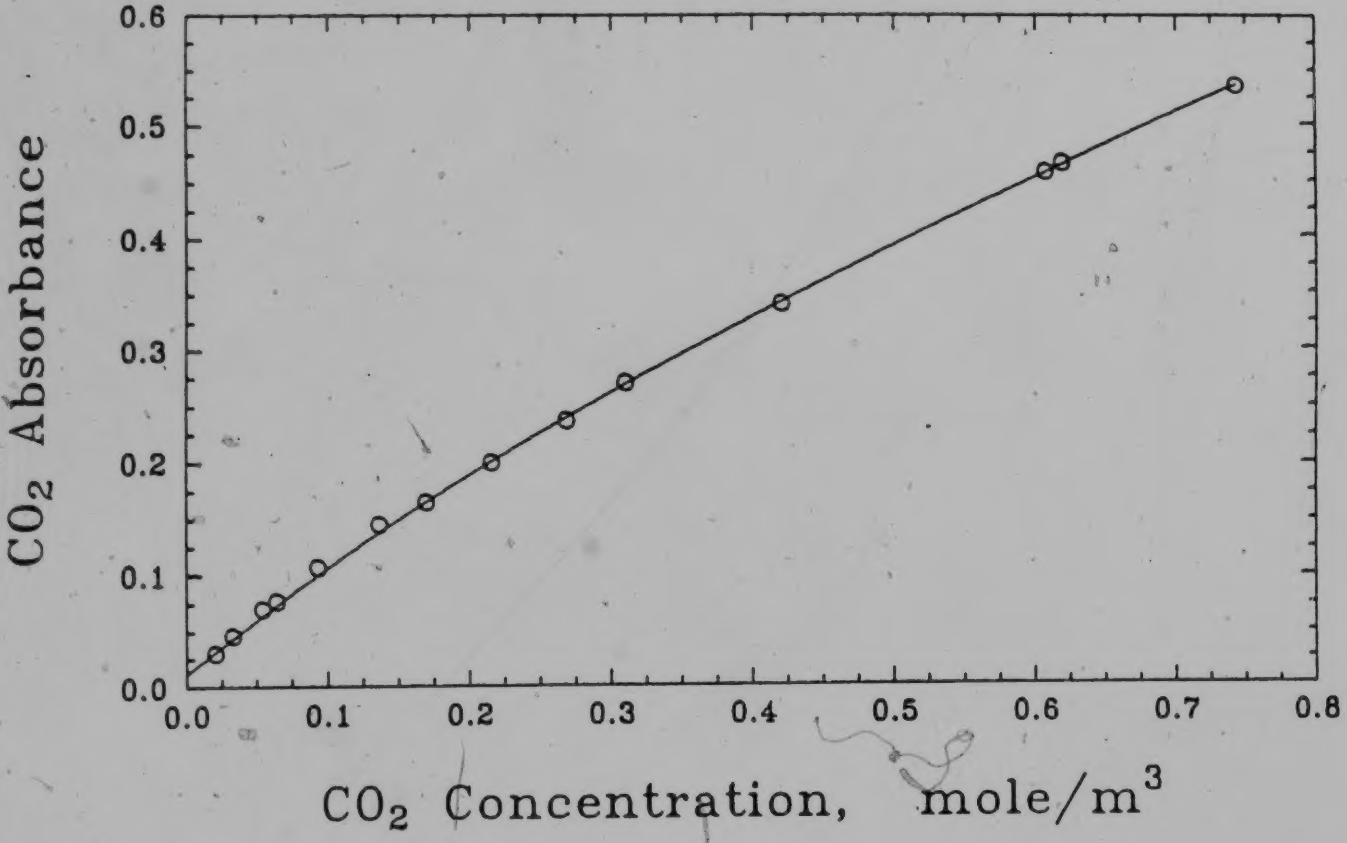

CO_2 Concentration Calibration Curve

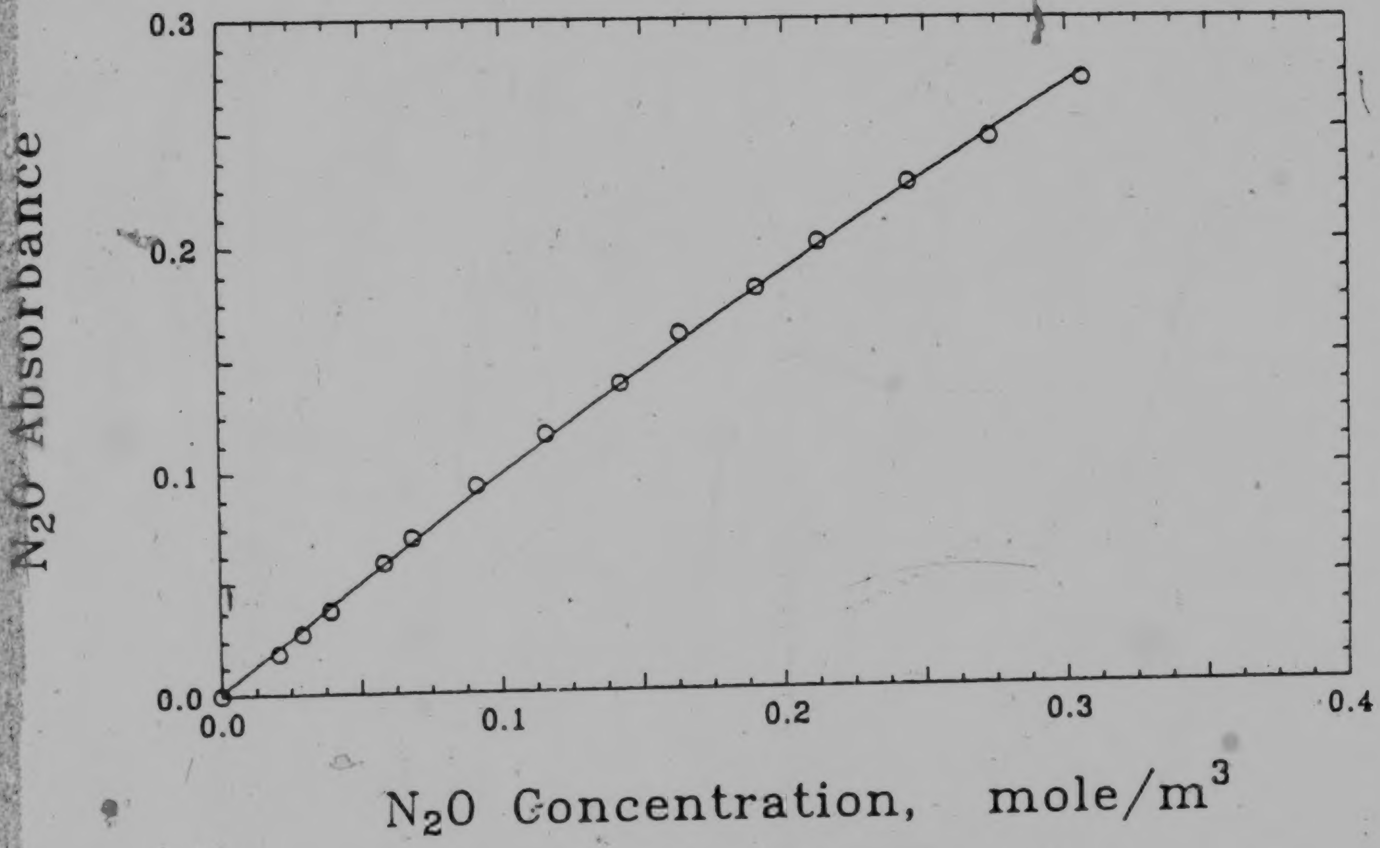

N_2O Concentration Calibration Curve

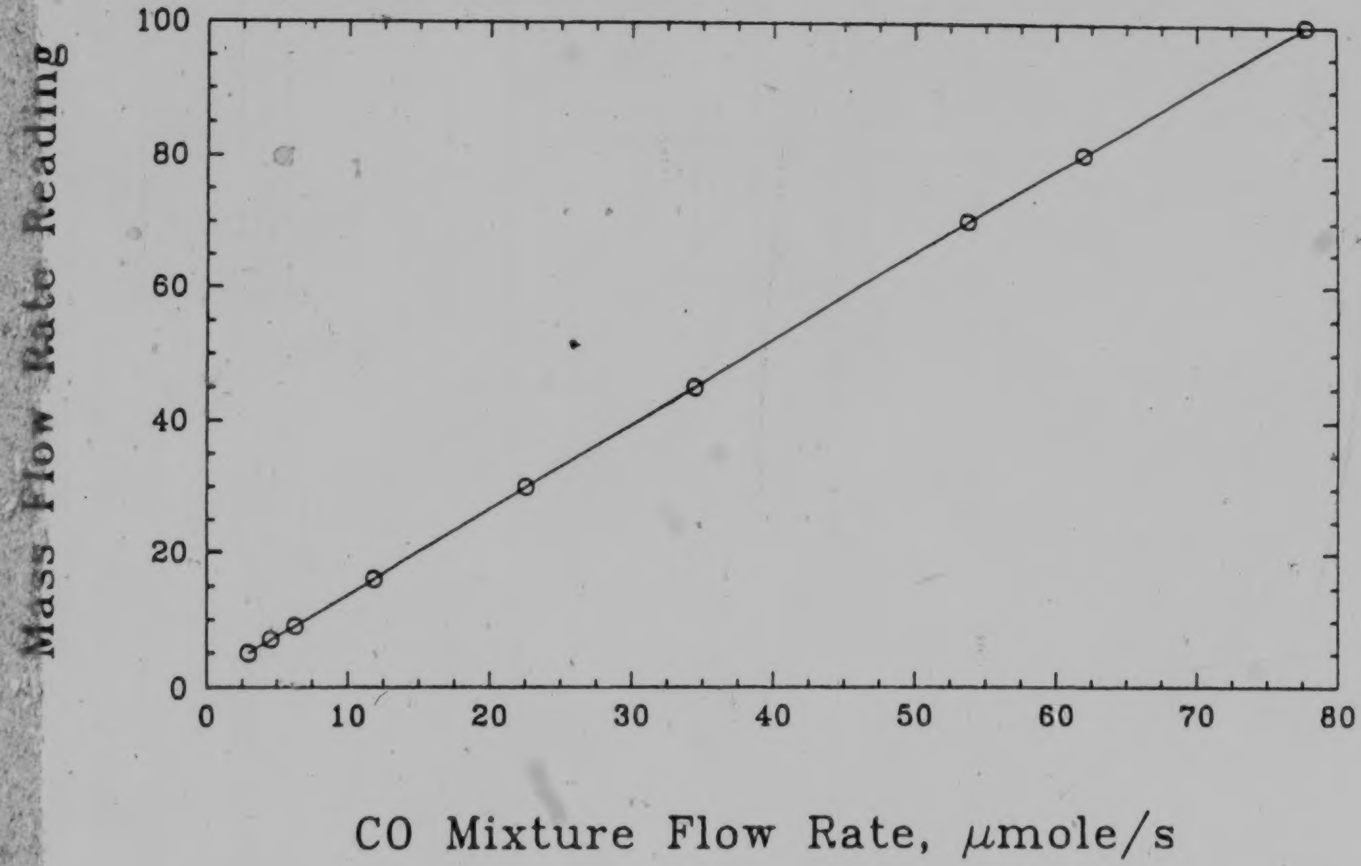

Mass Flow Rate Calibration Curve for CO Mixture

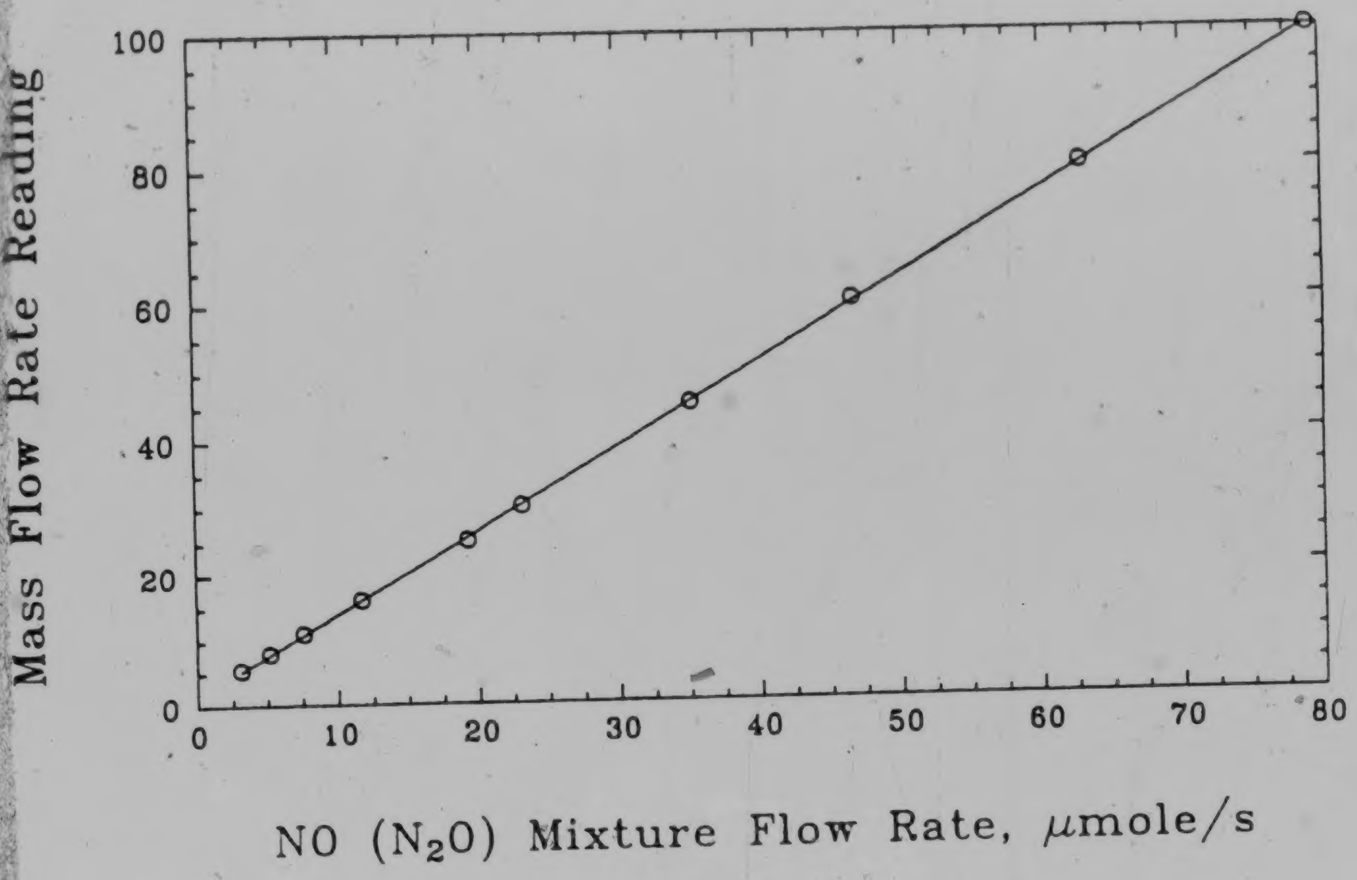

Mass Flow Rate Calibration Curve for NO (or N_2O) Mixture

APPENDIX 2. EXPERIMENTAL DATA FOR N_2O+CO

This appendix contains the experimental data for the N_2O+CO reaction. The data are classified according to the reaction temperature. Each table in this appendix presents the results obtained with a specified concentration of one reactant (CO or N_2O). These experimental results have been presented in Chapter 3.

Table A2.1 Experimental Data for the N_2O+CO Reaction at a Temperature of 190°C, Total Flow Rate of 138 μmol/s

Table A2.1.1 N_2O Feed Composition: 0.20% vol.

[CO] vol%	Conv. of CO, %	$[CO_2]$ vol%	$R \times 10^{-9}$ mol/g·s	$[CO]_r$ vol%	$[N_2O]_r$ vol%
1.646	0.97	0.016	1.10	1.63	0.184
1.518	1.1	0.016	1.10	1.502	0.184
1.286	1.2	0.016	1.10	1.27	0.184
1.032	1.6	0.016	1.10	1.016	0.184
0.853	2.1	0.018	1.24	0.835	0.182
0.633	2.1	0.018	1.24	0.615	0.182
0.496	3.8	0.019	1.30	0.477	0.181
0.335	5.7	0.019	1.30	0.316	0.181
0.288	6.6	0.019	1.30	0.269	0.181
0.240	8.8	0.021	1.44	0.219	0.179
0.197	11.1	0.022	1.51	0.175	0.178
0.150	17.3	0.026	1.79	0.124	0.174
0.127	23.6	0.030	2.06	0.097	0.170
0.115	26.1	0.030	2.06	0.085	0.170
0.0987	31.4	0.031	2.13	0.0677	0.169
0.087	41.1	0.036	2.47	0.051	0.164
0.079	49.4	0.039	2.68	0.040	0.161
-	-	-	-	-	-
0.0255	100	0.0255	1.75	0.000	0.175
0.0434	91.9	0.0399	2.74	0.0035	0.160
0.0854	94.2	0.080	5.49	0.0054	0.12
0.109	99.1	0.108	7.41	0.001	0.092
0.133	100	0.133	9.13	0.000	0.067
0.163	100	0.163	11.19	0.000	0.037
0.170	100	0.185	12.70	0.000	0.015

[CO] - percent CO in the feed.

$[N_2O]$ - percent N_2O in the feed.

R - CO_2 formation rate, mol/gcat·sec.

$[CO_2]$ - percent CO_2 in the reactor.

$[CO]_r$ - percent CO in the reactor.

$[N_2O]_r$ - percent N_2O in the reactor.

Table A2.1.2 N_2O Feed Composition: 0.406% vol.

[CO] vol%	Conv. of CO, %	$[CO_2]$ vol%	Rx10^{-9} mol/g·s	$[CO]_r$ vol%	$[N_2O]_r$ vol%
1.365	1.0	0.014	0.96	1.351	0.392
1.075	1.5	0.016	1.10	1.059	0.390
1.146	1.7	0.020	1.37	1.126	0.386
0.877	2.5	0.022	1.51	0.855	0.384
0.657	3.4	0.022	1.51	0.635	0.382
0.46	6.1	0.028	1.92	0.432	0.378
0.358	7.8	0.028	1.92	0.33	0.378
0.331	8.5	0.028	1.92	0.303	0.378
0.255	12.9	0.033	2.27	0.222	0.373
0.217	13.8	0.030	2.06	0.187	0.376
0.196	19.9	0.039	2.68	0.157	0.367
0.163	28.8	0.047	3.23	0.116	0.359
0.15	33.3	0.050	3.43	0.10	0.356
0.133	39.8	0.053	3.64	0.08	0.353
0.121	49.5	0.060	4.12	0.061	0.346
0.109	100	0.109	7.49	0.00	0.297
-	-	-	-	-	-
0.0323	99.1	0.032	2.20	0.0001	0.374
0.089	94.4	0.084	5.77	0.005	0.322
0.115	95.7	0.11	7.55	0.005	0.296
0.15	100	0.15	10.30	0.000	0.256
0.196	100	0.196	13.46	0.000	0.21
0.253	100	0.254	17.44	0.000	0.152
0.277	100	0.28	19.02	0.000	0.126
0.299	100	0.30	20.53	0.000	0.106

Table A2.1.3 N_2O Feed Composition: 0.70% vol.

[CO] vol%	Conv. of CO, %	$[CO_2]$ vol%	$Rx10^{-9}$ mol/g·s	$[CO]_r$ vol%	$[N_2O]_r$ vol%
1.698	1.6	0.027	1.85	1.671	0.673
1.461	2.0	0.029	1.99	1.432	0.671
1.225	2.4	0.029	1.99	1.196	0.671
1.005	3.2	0.032	2.20	0.973	0.668
0.864	3.9	0.034	2.33	0.83	0.666
0.713	4.8	0.034	2.33	0.679	0.666
0.601	6.0	0.036	2.47	0.565	0.664
0.507	7.7	0.039	2.68	0.468	0.661
0.425	9.9	0.042	2.88	0.383	0.658
0.369	12.7	0.047	3.23	0.322	0.653
0.321	15.6	0.050	3.43	0.271	0.65
0.275	19.3	0.053	3.64	0.222	0.647
0.24	25.0	0.060	4.12	0.18	0.64
0.217	29.0	0.063	4.33	0.154	0.637
0.202	33.7	0.068	4.67	0.134	0.633
0.184	39.1	0.072	4.94	0.112	0.628
0.174	43.1	0.075	5.15	0.099	0.625
0.163	49.7	0.081	5.56	0.082	0.619
-	-	-	-	-	-
0.0389	100	0.039	2.68	0.000	0.661
0.0975	97.4	0.095	6.52	0.0025	0.605
0.139	99.3	0.138	9.47	0.001	0.562
0.207	100	0.207	14.42	0.000	0.49
0.266	100	0.27	18.54	0.000	0.43
0.299	100	0.30	21.97	0.000	0.38
0.333	100	0.33	22.86	0.000	0.36

Table A2.1.4 N_2O Feed Composition: 1.035% vol.

[CO] vol%	Conv. of CO, %	$[CO_2]$ vol%	$Rx10^{-9}$ mol/g·s	$[CO]_r$ vol%	$[N_2O]_r$ vol%
1.646	1.9	0.031	2.20	1.615	1.003
1.45	2.6	0.037	2.54	1.413	0.998
1.19	3.4	0.040	2.75	1.15	0.995
1.005	4.5	0.045	3.09	0.96	0.990
0.902	5.8	0.052	3.57	0.85	0.983
0.713	8.0	0.057	3.91	0.656	0.977
0.609	9.8	0.060	4.12	0.549	0.975
0.541	11.6	0.063	4.33	0.478	0.972
0.505	13.3	0.067	4.60	0.438	0.968
0.46	15.2	0.070	4.81	0.39	0.965
0.421	16.6	0.070	4.81	0.351	0.965
0.368	19.3	0.071	4.81	0.297	0.964
0.331	23.0	0.076	5.22	0.255	0.959
0.298	27.5	0.082	5.63	0.216	0.952
0.265	32.8	0.087	5.97	0.178	0.948
0.24	41.7	0.10	6.87	0.14	0.935
0.217	51.6	0.112	7.69	0.105	0.923
-	-	-	-	-	-
0.065	100	0.065	4.46	0.000	0.97
0.219	100	0.219	15.4	0.000	0.816
0.272	100	0.272	18.67	0.000	0.763
0.318	100	0.318	21.83	0.000	0.717
0.35	100	0.35	24.03	0.000	0.685
0.364	100	0.364	24.99	0.000	0.671
0.41	100	0.41	28.15	0.000	0.625

Table A2.2 Experimental Data for the N_2O+CO Reaction at a Temperature of 210°C, Total Flow Rate of 138 μmol/s

Table A2.2.1 N_2O Feed Composition: 0.303% vol.

[CO] vol%	Conv. of CO, %	[CO_2] vol%	Rx10^{-9} mol/g·s	$[CO]_r$ vol%	$[N_2O]_r$ vol%
1.826	2.1	0.038	2.63	1.788	0.265
1.65	2.3	0.038	2.61	1.612	0.265
1.43	2.8	0.038	2.75	1.392	0.265
1.25	3.2	0.040	2.75	1.21	0.263
1.015	4.4	0.045	3.07	0.97	0.258
0.794	6.8	0.054	3.71	0.74	0.249
0.6696	9.1	0.061	4.18	0.609	0.242
0.611	10.8	0.066	4.53	0.545	0.237
0.552	12.3	0.068	4.66	0.484	0.235
0.518	13.5	0.070	4.80	0.448	0.233
0.485	14.4	0.070	4.79	0.415	0.233
0.427	16.9	0.072	4.95	0.355	0.231
0.369	19.5	0.072	4.94	0.297	0.231
0.333	23.4	0.078	5.35	0.255	0.225
0.298	28.2	0.084	5.77	0.214	0.219
0.265	32.8	0.085	5.97	0.18	0.218
0.228	41.7	0.095	6.53	0.133	0.208
0.206	50.0	0.103	7.07	0.103	0.20
0.184	65.2	0.12	8.24	0.064	0.183
-	-	-	-	-	-
0.05	100	0.05	3.43	0.000	0.253
0.192	93.8	0.180	12.36	0.012	0.123
0.228	96.5	0.220	15.10	0.008	0.083
0.250	98.0	0.245	16.82	0.005	0.058
0.267	100	0.267	18.33	0.000	0.036
0.283	32.0	0.090	6.18	0.193	0.213

Table A2.2.2 N_2O Feed Composition: 0.57% vol.

[CO] vol%	Conv. of CO, %	[CO_2] vol%	Rx10^{-9} mol/g·s	[CO]$_r$ vol%	[N_2O]$_r$ vol%
1.875	3.2	0.06	4.12	1.815	0.51
1.69	3.9	0.066	4.53	1.624	0.504
1.475	4.7	0.070	4.76	1.405	0.50
1.37	5.2	0.071	4.89	1.299	0.499
1.25	5.7	0.071	4.89	1.179	0.499
1.146	6.3	0.072	4.96	1.074	0.498
0.993	8.2	0.081	5.59	0.912	0.489
0.737	11.8	0.087	5.89	0.65	0.483
0.611	15.1	0.092	6.33	0.519	0.478
0.485	21.2	0.103	7.06	0.383	0.467
0.390	29.2	0.114	7.82	0.276	0.456
0.346	37.6	0.13	8.93	0.216	0.44
0.322	41.3	0.133	9.13	0.189	0.437
0.298	46.9	0.14	9.60	0.158	0.43
0.275	54.5	0.14	10.29	0.135	0.43
0.255	70	0.179	12.30	0.076	0.391
–	–	–	–	–	–
0.17	100	0.17	11.67	0.000	0.40
0.24	98.0	0.235	16.13	0.005	0.335
0.379	100	0.379	26.02	0.000	0.191
0.392	99.4	0.390	26.78	0.002	0.18
0.408	98.5	0.402	27.60	0.006	0.168
0.424	97.2	0.412	28.29	0.012	0.158
0.45	100	0.45	30.90	0.000	0.12
0.472	20.5	0.097	6.66	0.375	0.473

Table A2.2.3 N_2O Feed Composition: 0.855% vol.

[CO] vol%	Conv. of CO, %	$[CO_2]$ vol%	$Rx10^{-9}$ mol/g·s	$[CO]_r$ vol%	$[N_2O]_r$ vol%
2.335	3.1	0.072	4.94	2.263	0.783
1.99	3.6	0.072	4.94	1.918	0.783
1.745	4.2	0.074	5.08	1.671	0.781
1.475	5.4	0.079	5.42	1.396	0.776
1.185	7.1	0.084	5.77	1.101	0.771
1.027	9.0	0.092	6.32	0.935	0.763
0.878	11.8	0.104	7.14	0.774	0.751
0.726	15.2	0.11	7.55	0.616	0.745
0.68	17.6	0.12	8.24	0.56	0.735
0.633	19.3	0.122	8.38	0.511	0.733
0.576	22.2	0.128	8.79	0.448	0.727
0.541	24.4	0.132	9.06	0.409	0.723
0.518	25.5	0.132	9.06	0.386	0.71
0.495	27.1	0.134	9.20	0.361	0.721
0.472	29.0	0.137	9.41	0.335	0.718
0.447	33.5	0.15	10.30	0.297	0.705
0.426	36.9	0.15	10.30	0.276	0.705
0.402	39.8	0.157	10.78	0.245	0.698
0.368	48.9	0.18	12.36	0.188	0.675
0.344	58.1	0.20	13.73	0.144	0.655
0.323	79.6	0.257	17.64	0.066	0.598
-	-	-	-	-	-
0.12	99.0	0.119	8.17	0.001	0.736
0.20	100	0.20	13.73	0.000	0.655
0.32	98.0	0.314	21.56	0.006	0.541
0.466	95.0	0.443	30.41	0.003	0.412
0.50	100	0.50	34.33	0.000	0.355
0.51	100	0.51	35.01	0.000	0.345
0.535	99.4	0.532	36.53	0.003	0.323
0.552	100	0.552	37.90	0.000	0.303
0.56	20.3	0.114	7.83	0.446	0.741

Table A2.2.4 N_2O Feed Composition: 1.15% vol.

[CO] vol%	Conv. of CO, %	$[CO_2]$ vol%	$Rx10^{-9}$ mol/g·s	$[CO]_r$ vol%	$[N_2O]_r$ vol%
2.225	3.8	0.085	5.84	2.14	1.065
1.975	4.6	0.09	6.18	1.885	1.06
1.77	5.2	0.092	6.32	1.678	0.058
1.59	6.0	0.096	6.59	1.494	1.054
1.365	7.3	0.10	6.87	1.265	1.05
1.144	9.6	0.11	7.55	1.034	1.04
1.005	11.9	0.12	8.24	0.885	1.03
0.911	14.3	0.13	8.93	0.861	1.02
0.842	15.9	0.134	9.20	0.708	1.016
0.785	17.5	0.137	9.41	0.648	1.013
0.737	19.3	0.142	9.75	0.595	1.008
0.682	22.0	0.15	10.30	0.532	1.00
0.621	25.4	0.158	10.85	0.463	0.992
0.589	27.2	0.16	10.99	0.429	0.99
0.541	31.6	0.171	11.74	0.37	0.979
0.494	36.4	0.18	12.36	0.314	0.97
0.472	41.3	0.19	13.04	0.282	0.96
0.447	44.7	0.20	13.73	0.247	0.95
0.426	49.3	0.21	14.42	0.216	0.94
0.40	58.0	0.232	15.93	0.168	0.918
-	-	-	-	-	-
0.08	100	0.08	5.49	0.000	1.07
0.106	94.3	0.10	6.87	0.006	1.05
0.218	100	0.218	14.97	0.000	0.932
0.333	100	0.333	22.86	0.000	0.82
0.449	100	0.449	30.83	0.000	0.701
0.595	93.4	0.556	38.17	0.039	0.594
0.64	100	0.64	43.94	0.000	0.51
0.668	99.9	0.667	45.79	0.001	0.483
0.68	100	0.68	46.69	0.000	0.47
0.691	21.5	0.149	10.23	0.542	1.001

Table A2.3 Experimental Data for the N_2O+CO Reaction at a Temperature of 246°C, Total Flow Rate of 138 μmol/s

Table A2.3.1 CO Feed Composition: 0.399% vol.

$[N_2O]$ vol%	Conv. of CO, %	$[CO_2]$ vol%	$Rx10^{-9}$ mol/g·s	$[CO]_r$ vol%	$[N_2O]_r$ vol%
1.30	100	0.399	27.42	0.000	0.901
1.00	100	0.399	27.42	0.000	0.601
0.795	100	0.399	27.42	0.000	0.396
0.57	100	0.399	27.42	0.000	0.171
0.453	100	0.399	27.42	0.000	0.054
0.407	100	0.399	27.42	0.000	0.008
0.399	87.0	0.347	23.86	0.052	0.052
-	-	-	-	-	-
0.08	17.0	0.068	4.67	0.331	0.012
0.163	30.0	0.12	8.25	0.279	0.043
0.222	40.6	0.162	11.13	0.237	0.060
0.34	64.7	0.258	17.73	0.141	0.082
0.384	79.9	0.318	21.86	0.081	0.066
0.395	86.5	0.345	23.71	0.054	0.066
0.407	87.7	0.35	24.05	0.049	0.056
0.42	100	0.399	27.42	0.000	0.021

Table A2.3.2 CO Feed Composition: 0.564% vol.

$[N_2O]$ vol%	Conv. of CO, %	$[CO_2]$ vol%	$R \times 10^{-9}$ mol/g·s	$[CO]_r$ vol%	$[N_2O]_r$ vol%
1.10	100	0.564	38.76	0.536	0.536
0.976	100	0.564	38.76	0.412	0.412
0.86	100	0.564	38.76	0.296	0.296
0.74	100	0.564	38.76	0.176	0.176
0.716	100	0.564	38.76	0.152	0.152
0.66	100	0.564	38.76	0.096	0.096
0.597	100	0.564	38.76	0.033	0.033
0.58	72	0.406	27.90	0.174	0.174
-	-	-	-	-	-
0.105	13.8	0.078	5.36	0.486	0.027
0.22	24.8	0.14	9.62	0.424	0.08
0.34	35.5	0.20	13.75	0.364	0.14
0.453	50.0	0.282	19.38	0.282	0.171
0.57	67.4	0.38	26.12	0.184	0.19
0.603	73.3	0.413	28.38	0.151	0.19
0.625	77.4	0.436	29.97	0.128	0.189
0.65	74.5	0.42	28.87	0.144	0.23
0.67	81.6	0.46	31.61	0.008	0.21
0.685	100	0.564	38.76	0.000	0.121

Table A2.3.3 CO Feed Composition: 0.705% vol.

$[N_2O]$ vol%	Conv. of CO, %	$[CO_2]$ vol%	$Rx10^{-9}$ mol/g·s	$[CO]_r$ vol%	$[N_2O]_r$ vol%
1.1	100	0.705	48.45	0.000	0.395
1.036	100	0.705	48.45	0.000	0.601
0.917	100	0.705	48.45	0.000	0.212
0.881	100	0.705	48.45	0.000	0.176
0.834	100	0.705	48.45	0.000	0.129
0.785	100	0.705	48.45	0.000	0.08
0.733	100	0.705	48.45	0.000	0.028
0.716	60	0.423	29.07	0.282	0.293
-	-	-	-	-	-
0.105	11.3	0.08	5.50	0.625	0.025
0.22	18.4	0.13	8.93	0.575	0.09
0.34	27.0	0.19	13.06	0.515	0.15
0.513	41.1	0.29	19.93	0.415	0.223
0.68	56.7	0.40	27.49	0.305	0.28
0.795	69.5	0.49	33.68	0.215	0.305
0.833	73.3	0.517	35.53	0.188	0.316
0.86	72.9	0.510	35.05	0.195	0.35
0.88	75.6	0.533	36.63	0.172	0.347
0.905	100	0.705	48.45	0.000	0.20

Table A2.3.4 CO Feed Composition: 0.85% vol.

$[N_2O]$ vol%	Conv. of CO, %	$[CO_2]$ vol%	$Rx10^{-9}$ mol/g·s	$[CO]_r$ vol%	$[N_2O]_r$ vol%
1.36	100	0.85	58.42	0.000	0.51
1.26	100	0.85	58.42	0.000	0.41
1.055	100	0.85	58.42	0.000	0.025
0.975	100	0.85	58.42	0.000	0.125
0.95	100	0.85	58.42	0.000	0.10
0.925	57	0.485	33.30	0.365	0.075
-	-	-	-	-	-
0.25	15.0	0.10	6.87	0.75	0.143
0.45	27.0	0.23	15.81	0.62	0.25
0.59	39.3	0.334	23.02	0.516	0.356
0.895	53.6	0.45	30.93	0.40	0.445
1.055	66.9	0.562	36.84	0.314	0.493
1.105	69.0	0.580	39.86	0.27	0.525
1.125	72.0	0.605	41.58	0.245	0.520
1.145	72.0	0.605	41.58	0.245	0.54
1.17	72.7	0.611	41.99	0.239	0.548
1.22	75.2	0.632	43.44	0.218	0.559
1.245	77.1	0.648	44.54	0.202	0.597
1.27	100	0.85	58.42	0.000	0.42

Table A3.3.5 CO Feed Composition: 0.97% vol.

$[N_2O]$ vol%	Conv. of CO, %	$[CO_2]$ vol%	$R \times 10^{-9}$ mol/g·s	$[CO]_r$ vol%	$[N_2O]_r$ vol%
1.9	100	0.97	66.67	0.000	0.93
1.73	100	0.97	66.67	0.000	0.76
1.64	100	0.97	66.67	0.000	0.67
1.44	100	0.97	66.67	0.000	0.47
1.29	100	0.97	66.67	0.000	0.32
1.18	100	0.97	66.67	0.000	0.21
1.10	100	0.97	66.67	0.000	0.13
1.075	52	0.504	34.64	0.466	0.571
-	-	-	-	-	-
0.25	11.0	0.138	9.48	0.832	0.112
0.34	16.9	0.163	11.20	0.807	0.177
0.40	18.0	0.190	13.06	0.78	0.21
0.532	26.9	0.26	17.87	0.71	0.272
0.69	35.3	0.34	23.37	0.63	0.35
0.854	42.1	0.406	27.90	0.564	0.448
1.015	50.3	0.485	33.33	0.485	0.53
1.075	51.3	0.495	34.02	0.475	0.58
1.265	60.7	0.585	40.21	0.385	0.68
1.34	65.3	0.63	43.30	0.34	0.71
1.42	70.5	0.68	46.74	0.29	0.74
1.46	71.6	0.69	47.42	0.28	0.77
1.49	100	0.97	66.67	0.000	0.52

APPENDIX 3. CALCULATIONS FOR THE N_2O+CO REACTION

Presented herein are the calculated values for the N_2O+CO reaction. The order of the tables is based on the order of the figures in Chapter 4. The experimental data are also presented for comparison with the calculated values.

Table A3.1 Numerical values for Figure 4.1 from Mechanism 2
$K_1=325$, $K_4=0.15$, $K_{4/8}=5$, $K_{LH}=16$, $T=210°C$

$\%N_2O=0.303$			$\%N_2O=0.57$			$\%N_2O=0.85$			$\%N_2O=1.15$		
%CO	X_e	X_c	%CO	X_e	X_c	%CO	X_e	X_c	%CO	X_e	X_c
1.83	0.021	0.004	1.88	0.032	0.007	1.99	0.036	0.010	1.98	0.046	0.014
1.65	0.023	0.005	1.69	0.039	0.009	1.74	0.042	0.013	1.77	0.052	0.017
1.43	0.028	0.006	1.48	0.047	0.012	1.48	0.054	0.018	1.59	0.060	0.022
1.25	0.032	0.009	1.37	0.052	0.014	1.19	0.071	0.029	1.36	0.073	0.029
1.02	0.044	0.013	1.25	0.057	0.017	1.03	0.090	0.038	1.14	0.096	0.043
0.79	0.068	0.021	1.15	0.063	0.020	0.88	0.118	0.053	1.01	0.119	0.056
0.67	0.091	0.029	0.99	0.082	0.026	0.73	0.152	0.080	0.91	0.143	0.069
0.61	0.108	0.035	0.91	0.091	0.032	0.68	0.176	0.092	0.84	0.159	0.082
0.55	0.123	0.043	0.74	0.118	0.049	0.63	0.193	0.108	0.79	0.175	0.095
0.52	0.135	0.049	0.61	0.151	0.073	0.58	0.222	0.133	0.74	0.193	0.110
0.49	0.144	0.056	0.54	0.178	0.095	0.54	0.244	0.154	0.68	0.220	0.131
0.43	0.169	0.074	0.49	0.212	0.121	0.52	0.255	0.171	0.62	0.254	0.163
0.37	0.195	0.102	0.39	0.292	0.201	0.50	0.271	0.190	0.59	0.272	0.185
0.33	0.234	0.127	0.35	0.376	0.277	0.47	0.290	0.213	0.54	0.316	0.229
0.30	0.282	0.164	0.32	0.413	0.336	0.45	0.335	0.248	0.49	0.364	0.291
0.26	0.328	0.218	0.30	0.470	0.423	0.43	0.369	0.283	0.47	0.403	0.334
0.23	0.417	0.322	0.27	0.545	0.557	0.40	0.398	0.330	0.45	0.447	0.394
0.21	0.500	0.437	0.25	0.700	0.877	0.37	0.489	0.444	0.43	0.493	0.464
0.18	0.652	0.738	0.25	0.700	0.877	0.34	0.581	0.589	0.40	0.580	0.606
0.18	0.652	0.738	0.25	0.700	0.877	0.32	0.796	1.000	0.40	0.580	0.606

Total Error = 0.45

%CO - percent CO in the feed.

X_e - CO conversion obtained from the experiments.

X_c - calculated CO conversion.

Table A3.2 Numerical values for Figure 4.2 from Mechanism 3
$K_1=700$, $K_4=0.15$, $K_{4/8}=9$, $K_{LH}=25$, $K_{ERN2O}=0.045$, T=210°C

$\%N_2O=0.303$			$\%N_2O=0.57$			$\%N_2O=0.85$			$\%N_2O=1.15$		
%CO	X_e	X_c	%CO	X_e	X_c	%CO	X_e	X_c	%CO	X_e	X_c
1.83	0.021	0.016	1.88	0.032	0.030	1.99	0.036	0.042	1.98	0.046	0.058
1.65	0.023	0.018	1.69	0.039	0.033	1.74	0.042	0.049	1.77	0.052	0.066
1.43	0.028	0.021	1.48	0.047	0.039	1.48	0.054	0.060	1.59	0.060	0.075
1.25	0.032	0.025	1.37	0.052	0.043	1.19	0.071	0.078	1.36	0.073	0.090
1.02	0.044	0.032	1.25	0.057	0.048	1.03	0.090	0.093	1.14	0.096	0.112
0.79	0.068	0.043	1.15	0.063	0.053	0.88	0.118	0.114	1.01	0.119	0.131
0.67	0.091	0.053	0.99	0.082	0.063	0.73	0.152	0.148	0.91	0.143	0.149
0.61	0.108	0.060	0.91	0.091	0.071	0.68	0.176	0.162	0.84	0.159	0.166
0.55	0.123	0.069	0.74	0.118	0.094	0.63	0.193	0.180	0.79	0.175	0.183
0.52	0.135	0.076	0.61	0.151	0.122	0.58	0.222	0.208	0.74	0.193	0.200
0.49	0.144	0.084	0.54	0.178	0.147	0.54	0.244	0.229	0.68	0.220	0.224
0.43	0.169	0.102	0.49	0.212	0.173	0.52	0.255	0.246	0.62	0.254	0.259
0.37	0.195	0.130	0.39	0.292	0.250	0.50	0.271	0.265	0.59	0.272	0.282
0.33	0.234	0.153	0.35	0.376	0.314	0.47	0.290	0.288	0.54	0.316	0.325
0.30	0.282	0.185	0.32	0.413	0.365	0.45	0.335	0.318	0.49	0.364	0.383
0.26	0.328	0.231	0.30	0.470	0.436	0.43	0.369	0.349	0.47	0.403	0.420
0.23	0.417	0.317	0.27	0.545	0.543	0.40	0.398	0.391	0.45	0.447	0.471
0.21	0.500	0.408	0.25	0.700	0.785	0.37	0.489	0.483	0.43	0.493	0.529
0.18	0.652	0.641	0.25	0.700	0.785	0.34	0.581	0.596	0.40	0.580	0.641
0.18	0.652	0.641	0.25	0.700	0.785	0.32	0.796	1.000	0.40	0.580	0.641

Total Error = 0.117

Table A3.3 Numerical values for Figure 4.3 from Mechanism 5

$K_1=325$, $K_a=0.2$, $K_{4/8}=10$, $K_{LH}=12$, $K_{ERN2O}=0.08$, $K_{ERCO}=8$, T=210°C

$\%N_2O=0.303$			$\%N_2O=0.57$			$\%N_2O=0.85$			$\%N_2O=1.15$		
%CO	X_e	X_c	%CO	X_e	X_c	%CO	X_e	X_c	%CO	X_e	X_c
1.83	0.021	0.015	1.88	0.032	0.027	1.99	0.036	0.039	1.98	0.046	0.053
1.65	0.023	0.016	1.69	0.039	0.031	1.74	0.042	0.045	1.77	0.052	0.061
1.43	0.028	0.020	1.48	0.047	0.036	1.48	0.054	0.055	1.59	0.060	0.069
1.25	0.032	0.023	1.37	0.052	0.039	1.19	0.071	0.073	1.36	0.073	0.084
1.02	0.044	0.030	1.25	0.057	0.044	1.03	0.090	0.088	1.14	0.096	0.105
0.79	0.068	0.041	1.15	0.063	0.049	0.88	0.118	0.108	1.01	0.119	0.124
0.67	0.091	0.050	0.99	0.082	0.059	0.73	0.152	0.141	0.91	0.143	0.141
0.61	0.108	0.057	0.91	0.091	0.067	0.68	0.176	0.155	0.84	0.159	0.158
0.55	0.123	0.066	0.74	0.118	0.089	0.63	0.193	0.172	0.79	0.175	0.174
0.52	0.135	0.072	0.61	0.151	0.117	0.58	0.222	0.200	0.74	0.193	0.191
0.49	0.144	0.080	0.54	0.178	0.141	0.54	0.244	0.221	0.68	0.220	0.215
0.43	0.169	0.098	0.49	0.212	0.167	0.52	0.255	0.238	0.62	0.254	0.250
0.37	0.195	0.126	0.39	0.292	0.243	0.50	0.271	0.257	0.59	0.272	0.272
0.33	0.234	0.149	0.35	0.376	0.307	0.47	0.290	0.279	0.54	0.316	0.315
0.30	0.282	0.181	0.32	0.413	0.356	0.45	0.335	0.309	0.49	0.364	0.373
0.26	0.328	0.226	0.30	0.470	0.426	0.43	0.369	0.340	0.47	0.403	0.409
0.23	0.417	0.311	0.27	0.545	0.528	0.40	0.398	0.381	0.45	0.447	0.460
0.21	0.500	0.399	0.25	0.700	0.740	0.37	0.489	0.471	0.43	0.493	0.516
0.18	0.652	0.615	0.25	0.700	0.740	0.34	0.581	0.578	0.40	0.580	0.621
0.18	0.652	0.615	0.25	0.700	0.740	0.32	0.796	0.874	0.40	0.580	0.621

Total Error =0.12

Table A3.4 Numerical values for Figure 4.4 from Mechanism 6

$K_1=325$, $K_4=0.08$, $K_{4/8}=8$, $K_{LH}=9$, $K_{16}=2.0$, T=210°C

$\%N_2O=0.303$			$\%N_2O=0.57$			$\%N_2O=0.85$			$\%N_2O=1.15$		
%CO	X_e	X_c	%CO	X_e	X_c	%CO	X_e	X_c	%CO	X_e	X_c
1.83	0.021	0.007	1.88	0.032	0.012	1.99	0.036	0.016	1.98	0.046	0.022
1.65	0.023	0.008	1.69	0.039	0.015	1.74	0.042	0.021	1.77	0.052	0.027
1.43	0.028	0.011	1.48	0.047	0.019	1.48	0.054	0.029	1.59	0.060	0.034
1.25	0.032	0.014	1.37	0.052	0.022	1.19	0.071	0.044	1.36	0.073	0.045
1.02	0.044	0.021	1.25	0.057	0.026	1.03	0.090	0.059	1.14	0.096	0.064
0.79	0.068	0.033	1.15	0.063	0.031	0.88	0.118	0.080	1.01	0.119	0.082
0.67	0.091	0.046	0.99	0.082	0.041	0.73	0.152	0.116	0.91	0.143	0.100
0.61	0.108	0.055	0.91	0.091	0.049	0.68	0.176	0.133	0.84	0.159	0.117
0.55	0.123	0.067	0.74	0.118	0.075	0.63	0.193	0.154	0.79	0.175	0.135
0.52	0.135	0.076	0.61	0.151	0.109	0.58	0.222	0.186	0.74	0.193	0.153
0.49	0.144	0.087	0.54	0.178	0.140	0.54	0.244	0.212	0.68	0.220	0.179
0.43	0.169	0.112	0.49	0.212	0.175	0.52	0.255	0.231	0.62	0.254	0.216
0.37	0.195	0.152	0.39	0.292	0.276	0.50	0.271	0.254	0.59	0.272	0.241
0.33	0.234	0.188	0.35	0.376	0.363	0.47	0.290	0.281	0.54	0.316	0.288
0.30	0.282	0.237	0.32	0.413	0.427	0.45	0.335	0.318	0.49	0.364	0.349
0.26	0.328	0.306	0.30	0.470	0.514	0.43	0.369	0.355	0.47	0.403	0.388
0.23	0.417	0.431	0.27	0.545	0.631	0.40	0.398	0.403	0.45	0.447	0.439
0.21	0.500	0.555	0.25	0.700	0.831	0.37	0.489	0.503	0.43	0.493	0.492
0.18	0.652	0.822	0.25	0.700	0.831	0.34	0.581	0.608	0.40	0.580	0.579
0.18	0.652	0.822	0.25	0.700	0.831	0.32	0.796	0.787	0.40	0.580	0.579

Total Error =0.12

Table A3.5 Numerical values for Figure 4.5 From Mechanism 7
K_1=700, K_8=0.15, $K_{4/8}$=9, K_{LH}=25, K_{17}=0.09, T=210°C

%N_2O=0.303			%N_2O=0.57			%N_2O=0.85			%N_2O=1.15		
%CO	X_e	X_c	%CO	X_e	X_c	%CO	X_e	X_c	%CO	X_e	X_c
1.83	0.021	0.016	1.88	0.032	0.029	1.99	0.036	0.041	1.98	0.046	0.056
1.65	0.023	0.018	1.69	0.039	0.033	1.74	0.042	0.048	1.77	0.052	0.064
1.43	0.028	0.021	1.48	0.047	0.038	1.48	0.054	0.058	1.59	0.060	0.072
1.25	0.032	0.025	1.37	0.052	0.042	1.19	0.071	0.076	1.36	0.073	0.087
1.02	0.044	0.032	1.25	0.057	0.047	1.03	0.090	0.091	1.14	0.096	0.108
0.79	0.068	0.043	1.15	0.063	0.052	0.88	0.118	0.111	1.01	0.119	0.127
0.67	0.091	0.053	0.99	0.082	0.062	0.73	0.152	0.145	0.91	0.143	0.144
0.61	0.108	0.059	0.91	0.091	0.070	0.68	0.176	0.158	0.84	0.159	0.161
0.55	0.123	0.069	0.74	0.118	0.092	0.63	0.193	0.176	0.79	0.175	0.177
0.52	0.135	0.075	0.61	0.151	0.121	0.58	0.222	0.203	0.74	0.193	0.194
0.49	0.144	0.083	0.54	0.178	0.145	0.54	0.244	0.224	0.68	0.220	0.217
0.43	0.169	0.101	0.49	0.212	0.171	0.52	0.255	0.240	0.62	0.254	0.250
0.37	0.195	0.129	0.39	0.292	0.246	0.50	0.271	0.259	0.59	0.272	0.273
0.33	0.234	0.152	0.35	0.376	0.310	0.47	0.290	0.281	0.54	0.316	0.314
0.30	0.282	0.184	0.32	0.413	0.359	0.45	0.335	0.310	0.49	0.364	0.370
0.26	0.328	0.230	0.30	0.470	0.430	0.43	0.369	0.341	0.47	0.403	0.406
0.23	0.417	0.315	0.27	0.545	0.535	0.40	0.398	0.382	0.45	0.447	0.456
0.21	0.500	0.405	0.25	0.700	0.774	0.37	0.489	0.472	0.43	0.493	0.512
0.18	0.652	0.637	0.25	0.700	0.774	0.34	0.581	0.583	0.40	0.580	0.621
0.18	0.652	0.637	0.25	0.700	0.774	0.32	0.796	0.984	0.40	0.580	0.621

Total Error = 0.15

Table A3.6 Numerical values for Figure 4.6 from Mechanism 8
$K_1=100$, $K_8=0.01$, $K_{4/8}=5$, $K_{LH}=5.6$, $K_{18}=1.5$, T=210°C

%N_2O=0.303			%N_2O=0.57			%N_2O=0.85			%N_2O=1.15		
%CO	X_e	X_c	%CO	X_e	X_c	%CO	X_e	X_c	%CO	X_e	X_c
1.83	0.021	0.014	1.88	0.032	0.026	1.99	0.036	0.036	1.98	0.046	0.049
1.65	0.023	0.017	1.69	0.039	0.030	1.74	0.042	0.043	1.77	0.052	0.056
1.43	0.028	0.020	1.48	0.047	0.036	1.48	0.054	0.053	1.59	0.060	0.064
1.25	0.032	0.024	1.37	0.052	0.039	1.19	0.071	0.072	1.36	0.073	0.079
1.02	0.044	0.031	1.25	0.057	0.044	1.03	0.090	0.087	1.14	0.096	0.100
0.79	0.068	0.044	1.15	0.063	0.050	0.88	0.118	0.109	1.01	0.119	0.119
0.67	0.091	0.056	0.99	0.082	0.061	0.73	0.152	0.145	0.91	0.143	0.137
0.61	0.108	0.064	0.91	0.091	0.069	0.68	0.176	0.160	0.84	0.159	0.154
0.55	0.123	0.075	0.74	0.118	0.094	0.63	0.193	0.179	0.79	0.175	0.171
0.52	0.135	0.082	0.61	0.151	0.126	0.58	0.222	0.209	0.74	0.193	0.188
0.49	0.144	0.092	0.54	0.178	0.154	0.54	0.244	0.232	0.68	0.220	0.213
0.43	0.169	0.114	0.49	0.212	0.185	0.52	0.255	0.250	0.62	0.254	0.248
0.37	0.195	0.148	0.39	0.292	0.273	0.50	0.271	0.271	0.59	0.272	0.271
0.33	0.234	0.177	0.35	0.376	0.347	0.47	0.290	0.295	0.54	0.316	0.314
0.30	0.282	0.217	0.32	0.413	0.402	0.45	0.335	0.327	0.49	0.364	0.369
0.26	0.328	0.273	0.30	0.470	0.479	0.43	0.369	0.360	0.47	0.403	0.404
0.23	0.417	0.376	0.27	0.545	0.586	0.40	0.398	0.403	0.45	0.447	0.451
0.21	0.500	0.480	0.25	0.700	0.777	0.37	0.489	0.493	0.43	0.493	0.499
0.18	0.652	0.714	0.25	0.700	0.777	0.34	0.581	0.590	0.40	0.580	0.580
0.18	0.652	0.714	0.25	0.700	0.777	0.32	0.796	0.744	0.40	0.580	0.580

Total Error =0.07

Table A3.7 Numerical values for Figure 4.7 from Mechanism 9
$K_1=700$, $K_a=1.0$, $K_{4/8}=12$, $K_{LH}=16$, $\mu=1.0$, $T=210°C$

%N_2O=0.303			%N_2O=0.57			%N_2O=0.85			%N_2O=1.15		
%CO	X_e	X_c	%CO	X_e	X_c	%CO	X_e	X_c	%CO	X_e	X_c
1.83	0.021	0.005	1.88	0.032	0.009	1.99	0.036	0.012	1.98	0.046	0.017
1.65	0.023	0.006	1.69	0.039	0.011	1.74	0.042	0.016	1.77	0.052	0.021
1.43	0.028	0.008	1.48	0.047	0.014	1.48	0.054	0.022	1.59	0.060	0.026
1.25	0.032	0.011	1.37	0.052	0.017	1.19	0.071	0.034	1.36	0.073	0.035
1.02	0.044	0.016	1.25	0.057	0.020	1.03	0.090	0.045	1.14	0.096	0.050
0.79	0.068	0.025	1.15	0.063	0.024	0.88	0.118	0.062	1.01	0.119	0.064
0.67	0.091	0.035	0.99	0.082	0.032	0.73	0.152	0.091	0.91	0.143	0.079
0.61	0.108	0.042	0.91	0.091	0.038	0.68	0.176	0.105	0.84	0.159	0.092
0.55	0.123	0.052	0.74	0.118	0.058	0.63	0.193	0.122	0.79	0.175	0.107
0.52	0.135	0.059	0.61	0.151	0.085	0.58	0.222	0.149	0.74	0.193	0.122
0.49	0.144	0.067	0.54	0.178	0.110	0.54	0.244	0.170	0.68	0.220	0.144
0.43	0.169	0.088	0.49	0.212	0.138	0.52	0.255	0.187	0.62	0.254	0.176
0.37	0.195	0.119	0.39	0.292	0.223	0.50	0.271	0.206	0.59	0.272	0.197
0.33	0.234	0.148	0.35	0.376	0.298	0.47	0.290	0.229	0.54	0.316	0.239
0.30	0.282	0.189	0.32	0.413	0.355	0.45	0.335	0.262	0.49	0.364	0.294
0.26	0.328	0.246	0.30	0.470	0.435	0.43	0.369	0.295	0.47	0.403	0.331
0.23	0.417	0.355	0.27	0.545	0.549	0.40	0.398	0.338	0.45	0.447	0.381
0.21	0.500	0.467	0.25	0.700	0.780	0.37	0.489	0.435	0.43	0.493	0.435
0.18	0.652	0.732	0.25	0.700	0.780	0.34	0.581	0.546	0.40	0.580	0.535
0.18	0.652	0.732	0.25	0.700	0.780	0.32	0.796	0.838	0.40	0.580	0.535

Total Error =0.28

Table A3.8 Numerical values for Figure 4.8 from Mechanism 10

$K_1=225$, $K_a=0.25$, $K_{4/8}=2.4$, $K_{LH}=8.75$, $N_{CO}=1.03$, T=210°C

$\%N_2O=0.303$			$\%N_2O=0.57$			$\%N_2O=0.85$			$\%N_2O=1.15$		
%CO	X_e	X_c	%CO	X_e	X_c	%CO	X_e	X_c	%CO	X_e	X_c
1.83	0.021	0.025	1.88	0.032	0.036	1.99	0.036	0.041	1.98	0.046	0.048
1.65	0.023	0.028	1.69	0.039	0.040	1.74	0.042	0.048	1.77	0.053	0.055
1.43	0.028	0.033	1.48	0.047	0.047	1.48	0.054	0.059	1.59	0.060	0.063
1.25	0.032	0.039	1.37	0.052	0.052	1.19	0.071	0.078	1.36	0.073	0.076
1.02	0.044	0.049	1.25	0.057	0.058	1.03	0.090	0.094	1.14	0.096	0.096
0.79	0.068	0.065	1.15	0.063	0.064	0.88	0.118	0.115	1.01	0.119	0.115
0.67	0.091	0.079	0.99	0.082	0.076	0.73	0.152	0.150	0.91	0.143	0.132
0.61	0.108	0.088	0.91	0.091	0.085	0.68	0.176	0.165	0.84	0.159	0.148
0.55	0.123	0.100	0.74	0.118	0.112	0.63	0.193	0.184	0.79	0.175	0.164
0.52	0.135	0.109	0.61	0.151	0.145	0.58	0.222	0.213	0.74	0.193	0.180
0.49	0.144	0.119	0.54	0.178	0.173	0.54	0.244	0.236	0.68	0.220	0.204
0.43	0.169	0.142	0.49	0.212	0.203	0.52	0.255	0.253	0.62	0.254	0.238
0.37	0.195	0.176	0.39	0.292	0.288	0.50	0.271	0.273	0.59	0.272	0.261
0.33	0.234	0.204	0.35	0.376	0.360	0.47	0.290	0.296	0.54	0.316	0.304
0.30	0.282	0.242	0.32	0.413	0.414	0.45	0.335	0.329	0.49	0.364	0.362
0.26	0.328	0.296	0.30	0.470	0.491	0.43	0.369	0.362	0.47	0.403	0.401
0.23	0.417	0.391	0.27	0.545	0.603	0.40	0.398	0.406	0.45	0.447	0.454
0.21	0.500	0.488	0.25	0.700	0.850	0.37	0.489	0.504	0.43	0.493	0.514
0.18	0.652	0.723	0.25	0.700	0.850	0.34	0.581	0.623	0.40	0.580	0.632
0.18	0.652	0.723	0.25	0.700	0.850	0.32	0.796	1.000	0.40	0.580	0.632

Total Error = 0.10

Table A3.9 Numerical values for Figure 4.14 from Mechanism 11
$k_{-1}=0.050$, $k_4=0.40$, $k_8=1000$, $k_{12}=0.9$, $T=210°C$

%N_2O=0.303		%N_2O=0.57		%N_2O=0.85		%N_2O=1.15	
%CO	X_n	%CO	X_n	%CO	X_n	%CO	X_n
2.000	.02103	2.000	.03824	2.000	.05505	2.000	.07176
1.200	.03688	1.200	.06624	1.200	.09426	1.202	.12130
0.742	.06464	0.864	.09624	0.937	.12426	0.984	.15130
0.547	.09464	0.690	.12624	0.780	.15426	0.843	.18130
0.445	.12464	0.424	.24624	0.677	.18426	0.745	.21130
0.382	.15464	0.395	.27624	0.510	.27426	0.674	.24130
0.339	.18464	0.352	.33624	0.477	.30426	0.620	.27130
0.265	.27464	0.337	.36624	0.452	.33426	0.519	.36130
0.250	.30464	0.305	.45624	0.431	.36426	0.497	.39130
0.219	.39464	0.298	.48624	0.414	.39426	0.480	.42130
0.212	.42464	0.288	.54624	0.379	.48426	0.454	.48130
0.207	.45464	0.282	.60624	0.372	.51426	0.437	.54130
0.194	.54464	0.281	.63624	0.359	.60426	0.432	.57130
0.192	.57464	0.281	.66624	0.358	.63426	0.429	.60130
0.188	.66464	0.282	.69624	0.358	.66426	0.427	.63130
0.188	.69464	0.284	.72624	0.359	.69426	0.427	.66130
0.188	.72464	0.287	.75624	0.362	.72426	0.429	.69130
0.190	.75464	0.292	.78624	0.367	.75426	0.433	.72130
0.192	.78464	0.299	.81624	0.375	.78426	0.440	.75130
0.195	.81464	0.308	.84397	0.398	.84426	0.449	.78130
0.199	.84269	0.318	.86983	0.415	.87148	0.461	.81130
0.204	.86777	0.330	.89161	0.433	.89415	0.478	.84130
0.209	.88957	0.342	.91001	0.452	.91287	0.499	.86846
0.221	.92508	0.354	.92561	0.472	.92843	0.524	.89308
0.226	.93840	0.368	.93889	0.491	.94073	0.550	.91300
0.231	.94861	0.380	.94952	0.510	.95070	0.576	.92842

Table A3.9 Numerical values for Figure 4.14 from Mechanism 11
$k_{-1}=0.050$, $k_4=0.40$, $k_8=1000$, $k_{12}=0.9$, T=210°C

$\%N_2O=0.303$		$\%N_2O=0.57$		$\%N_2O=0.85$		$\%N_2O=1.15$	
%CO	X_n	%CO	X_n	%CO	X_n	%CO	X_n
0.236	.95650	0.392	.95779	0.526	.95830	0.601	.94069
0.240	.96273	0.402	.96418	0.541	.96421	0.624	.94993
0.243	.96775	0.411	.96920	0.554	.96889	0.645	.95705
0.246	.97186	0.418	.97323	0.565	.97264	0.662	.96265
0.249	.97528	0.425	.97650	0.575	.97569	0.678	.96711
0.251	.97816	0.431	.97918	0.582	.97819	0.691	.97072
0.253	.98061	0.435	.98142	0.593	.98195	0.702	.97366
0.255	.98271	0.439	.98328	0.596	.98336	0.711	.97607
0.256	.98453	0.442	.98485	0.597	.98451	0.717	.97805
0.257	.98611	0.444	.98617	0.597	.98541	0.721	.97968
0.258	.98748	0.446	.98728	0.594	.98613	0.723	.98102
0.259	.98869	0.446	.98820	0.589	.98668	0.722	.98208
0.259	.98974	0.445	.98892	0.582	.98705	0.719	.98294
0.259	.99059	0.443	.98949	0.572	.98725	0.712	.98359
0.259	.99133	0.439	.98990	0.558	.98728	0.703	.98407
0.258	.99194	0.434	.99017	0.539	.98711	0.690	.98438
0.256	.99242	0.425	.99025	0.516	.98673	0.673	.98452
0.211	.99077	0.308	.98622	0.488	.98613	0.652	.98449
0.202	.99007	0.291	.98544	0.462	.98551	0.626	.98428
0.166	.98700	0.274	.98464	0.437	.98484	0.555	.98328
0.157	.98618	0.256	.98382	0.411	.98413	0.521	.98266
0.138	.98447	0.239	.98297	0.308	.98095	0.381	.97969
0.120	.98269	0.083	.97420	0.283	.98009	0.346	.97885
0.065	.97676	0.078	.97386	0.153	.97530	0.206	.97514
0.005	.96925	0.043	.97154	0.008	.96885	0.005	.96864

Table A3.10 Numerical values for Figure 4.15 from Mechanism 11
$k_{-1}=0.046$, $k_4=0.14$, $k_8=650$, $k_{12}=0.5$, $T=190°C$

%N_2O=0.20		%N_2O=0.406		%N_2O=0.70		%N_2O=1.035	
%CO	X_n	%CO	X_n	%CO	X_n	%CO	X_n
1.950	.00562	1.950	.01118	1.950	.01872	1.950	.02681
1.200	.00992	1.200	.01956	1.200	.03238	1.200	.04580
0.402	.03831	0.740	.03424	0.742	.05600	0.765	.07580
0.267	.06831	0.450	.06424	0.524	.08600	0.581	.10580
0.178	.12831	0.341	.09424	0.420	.11600	0.481	.13580
0.158	.15831	0.283	.12424	0.358	.14600	0.418	.16580
0.132	.21831	0.247	.15424	0.317	.17600	0.374	.19580
0.117	.27831	0.204	.21424	0.288	.20600	0.343	.22580
0.107	.33831	0.179	.27424	0.249	.26600	0.319	.25580
0.104	.36831	0.163	.33424	0.217	.35600	0.285	.31580
0.096	.45831	0.158	.36424	0.204	.41600	0.274	.34580
0.094	.48831	0.153	.39424	0.196	.47600	0.264	.37580
0.093	.51831	0.146	.45424	0.193	.50600	0.250	.43580
0.092	.54831	0.141	.51424	0.191	.53600	0.245	.46580
0.091	.57831	0.140	.54424	0.190	.56600	0.238	.52580
0.091	.60831	0.139	.60424	0.189	.59600	0.236	.55580
0.091	.63831	0.139	.63424	0.189	.62600	0.235	.58580
0.091	.69831	0.139	.66424	0.190	.65600	0.235	.61580
0.094	.75831	0.141	.69424	0.192	.68600	0.236	.64580
0.098	.81831	0.142	.72424	0.194	.71600	0.241	.70580
0.101	.84613	0.145	.75424	0.198	.74600	0.251	.76580

Table A3.10 Numerical values for Figure 4.15 from Mechanism 11
$k_{-1}=0.046$, $k_4=0.14$, $k_8=650$, $k_{12}=0.5$, T=190°C

$\%N_2O=0.20$		$\%N_2O=0.406$		$\%N_2O=0.70$		$\%N_2O=1.035$	
%CO	X_n	%CO	X_n	%CO	X_n	%CO	X_n
0.104	.87362	0.153	.81424	0.203	.77600	0.268	.82580
0.109	.89721	0.159	.84424	0.209	.80600	0.282	.85580
0.112	.91494	0.166	.87143	0.218	.83600	0.315	.90434
0.119	.93936	0.175	.89814	0.229	.86600	0.332	.92093
0.123	.94798	0.185	.91781	0.242	.89166	0.362	.94301
0.125	.95500	0.201	.94342	0.257	.91286	0.375	.95053
0.128	.96080	0.208	.95200	0.270	.92838	0.387	.95652
0.130	.96565	0.215	.95879	0.283	.94005	0.396	.96135
0.132	.96976	0.226	.96871	0.305	.95607	0.411	.96851
0.134	.97326	0.231	.97239	0.322	.96621	0.419	.97336
0.136	.97627	0.238	.97802	0.329	.96991	0.421	.97516
0.137	.97888	0.241	.98020	0.339	.97547	0.420	.97661
0.138	.98115	0.244	.98359	0.342	.97756	0.417	.97778
0.139	.98314	0.245	.98490	0.345	.98071	0.412	.97870
0.140	.98488	0.244	.98595	0.344	.98184	0.405	.97939
0.140	.98641	0.243	.98680	0.341	.98274	0.395	.97985
0.140	.98871	0.240	.98748	0.307	.98419	0.382	.98010
0.137	.99033	0.208	.98798	0.220	.98099	0.183	.97224
0.129	.99108	0.115	.98043	0.150	.97567	0.132	.96784
0.033	.97284	0.023	.95881	0.039	.95845	0.055	.95806

Table A3.11 Numerical values for Figure 4.16 from Mechanism 11
$k_{-1}=0.058$, $k_4=2.2$, $k_8=2000$, $k_{12}=2.3$, T=246°C

%CO=0.399		%CO=0.564		%CO=0.705		%CO=0.85		%CO=0.97	
%N_2O	X_n	%N_2O	X_n	%N_2O	X_n	%N_2O	X_n	%N_2O	X_n
0.088	.1300	0.134	.1300	0.107	.0800	0.134	.080	0.058	.0300
0.108	.1600	0.165	.1600	0.148	.1100	0.185	.110	0.116	.0600
0.147	.2200	0.227	.2200	0.230	.1700	0.237	.140	0.176	.0900
0.167	.2500	0.257	.2500	0.312	.2300	0.341	.200	0.297	.1500
0.204	.3100	0.317	.3100	0.353	.2600	0.394	.230	0.421	.2100
0.223	.3400	0.346	.3400	0.434	.3200	0.499	.290	0.484	.2400
0.258	.4000	0.429	.4300	0.474	.3500	0.552	.320	0.547	.2700
0.274	.4300	0.455	.4600	0.551	.4100	0.604	.350	0.611	.3000
0.306	.4900	0.503	.5200	0.588	.4400	0.706	.410	0.674	.3300
0.321	.5200	0.525	.5500	0.657	.5000	0.755	.440	0.738	.3600
0.348	.5800	0.545	.5800	0.688	.5300	0.802	.470	0.800	.3900
0.371	.6400	0.563	.6100	0.744	.5900	0.889	.530	0.862	.4200
0.397	.7300	0.594	.6700	0.768	.6200	0.928	.560	0.979	.4800
0.404	.7600	0.606	.7000	0.806	.6800	0.995	.620	1.034	.5100
0.409	.7900	0.616	.7300	0.820	.7100	1.022	.650	1.085	.5400
0.416	.8500	0.628	.7900	0.830	.7400	1.059	.710	1.132	.5700
0.417	.8800	0.629	.8200	0.835	.7700	1.074	.770	1.174	.6000
0.416	.9084	0.628	.8481	0.837	.8000	1.072	.800	1.210	.6300
0.415	.9294	0.625	.8763	0.834	.8280	1.064	.827	1.240	.6600
0.414	.9435	0.618	.9045	0.827	.8559	1.049	.855	1.264	.6900
0.413	.9537	0.611	.9284	0.815	.8839	1.029	.883	1.280	.7200
0.412	.9612	0.604	.9444	0.800	.9117	1.002	.910	1.288	.7500
0.411	.9670	0.599	.9554	0.770	.9512	0.970	.937	1.288	.7800
0.410	.9716	0.595	.9633	0.761	.9607	0.951	.951	1.279	.8100
0.410	.9754	0.592	.9693	0.754	.9676	0.936	.960	1.262	.8376
0.409	.9810	0.588	.9775	0.749	.9728	0.925	.967	1.238	.8652
0.409	.9831	0.585	.9828	0.742	.9800	0.917	.973	1.205	.8927

Table A3.11 Numerical values for Figure 4.16 from Mechanism 11
$k_{-1}=0.058$, $k_4=2.2$, $k_8=2000$, $k_{12}=2.3$, T=246°C

%CO=0.399		%CO=0.564		%CO=0.705		%CO=0.85		%CO=0.97	
%N_2O	X_n	%N_2O	X_n	%N_2O	X_n	%N_2O	X_n	%N_2O	X_n
0.408	.9850	0.584	.9848	0.737	.9847	0.910	.977	1.164	.9201
0.408	.9866	0.582	.9879	0.735	.9864	0.905	.980	1.124	.9424
0.408	.9880	0.581	.9892	0.733	.9879	0.900	.982	1.100	.9546
0.408	.9893	0.581	.9903	0.731	.9902	0.897	.984	1.081	.9633
0.408	.9903	0.580	.9912	0.730	.9911	0.894	.986	1.067	.9697
0.408	.9913	0.580	.9920	0.730	.9926	0.892	.988	1.056	.9745
0.408	.9922	0.580	.9927	0.730	.9932	0.888	.990	1.047	.9782
0.408	.9930	0.580	.9934	0.730	.9937	0.887	.991	1.041	.9812
0.408	.9943	0.580	.9939	0.730	.9941	0.886	.991	1.035	.9836
0.408	.9948	0.581	.9944	0.731	.9944	0.886	.992	1.031	.9855
0.409	.9952	0.581	.9948	0.733	.9947	0.886	.993	1.027	.9871
0.409	.9955	0.582	.9950	0.735	.9948	0.887	.993	1.022	.9896
0.410	.9957	0.583	.9953	0.745	.9947	0.888	.993	1.020	.9905
0.412	.9958	0.586	.9953	0.755	.9943	0.889	.994	1.019	.9913
0.414	.9957	0.590	.9952	0.773	.9935	0.892	.994	1.018	.9920
0.418	.9955	0.596	.9949	0.858	.9912	0.897	.994	1.018	.9925
0.432	.9943	0.605	.9944	0.938	.9901	0.904	.994	1.019	.9930
0.451	.9930	0.622	.9935	1.034	.9893	0.916	.993	1.020	.9933
0.579	.9895	0.659	.9921	1.153	.9887	0.938	.993	1.022	.9936
0.645	.9889	0.718	.9907	1.304	.9882	1.037	.991	1.026	.9937
0.672	.9887	0.788	.9898	1.331	.9881	1.134	.990	1.075	.9929
0.882	.9878	0.874	.9890	1.537	.9878	1.395	.988	1.113	.9921
1.046	.9875	0.981	.9885	1.817	.9875	1.578	.988	1.381	.9894
1.285	.9872	1.023	.9883	1.987	.9875	1.922	.987	1.727	.9882
1.665	.9870	1.376	.9876	1.987	.9875	1.922	.987	1.911	.9879
1.908	.9868	1.663	.9873	1.987	.9875	1.922	.987	1.911	.9879
1.908	.9868	2.102	.9781	1.987	.9875	1.922	.987	1.911	.9879

APPENDIX 4. EXPERIMENTAL DATA FOR THE NO+CO REACTION

The experimental data for the NO+CO reaction are located in this appendix. Because of the complexity of this reaction system, the results have to be expressed by many measurements, such as CO conversion, NO conversion, N_2O concentration and selectivity. N_2O and CO_2 concentrations in the effluent were detected by IR. The other quantities were calculated by mass balance equations.

Table A4.1 Experimental Data for the NO+CO reaction at a Temperature of 150°C, Total Flow Rate of 138 μmol/s

Table A4.1.1 NO Feed Composition: 1.355% vol.

CO% Feed	CO Conv.	NO Conv.	Rate[*]	CO_2%	N_2O%	N_2%	S[**]
1.130	2.7	3.9	2.05	0.030	0.023	0.0035	6.6
0.960	3.2	4.1	2.12	0.031	0.025	0.0030	8.3
0.675	4.4	4.1	2.05	0.030	0.025	0.0025	11.6
0.500	6.2	4.3	2.12	0.031	0.027	0.0020	13.5
0.330	11.5	5.3	2.60	0.038	0.034	0.0020	17.0
0.285	14.0	5.6	2.74	0.040	0.036	0.0020	18.0
0.260	15.4	5.6	2.74	0.040	0.036	0.0020	18.0
0.226	18.6	5.8	2.88	0.042	0.037	0.0025	14.8
0.205	22.0	6.3	3.08	0.045	0.040	0.0025	16.0
0.175	28.5	6.9	3.36	0.049	0.045	0.0020	22.5
0.155	33.5	7.5	3.56	0.052	0.050	0.0010	50.0
0.138	43.6	8.4	4.11	0.060	0.054	0.0030	18.0
0.126	57.1	10.2	4.93	0.072	0.066	0.0030	22.0
-	-	-	-	-	-	-	-
0.073	82.2	8.3	4.11	0.060	0.053	0.0035	15.1
0.079	84.8	9.2	4.59	0.067	0.057	0.005	11.4
0.096	82.9	10.8	5.48	0.080	0.066	0.0070	9.4
0.132	81.8	14.6	7.40	0.108	0.090	0.0090	10.
0.161	84.9	18.1	9.25	0.135	0.110	0.0125	8.8
0.195	83.1	21.5	11.10	0.162	0.13	0.0160	8.1
0.200	86.0	22.7	11.78	0.172	0.135	0.0185	7.3
0.210	83.3	23.6	11.99	0.175	0.145	0.0150	9.7
0.220	84.5	24.5	12.74	0.186	0.136	0.0300	4.5

[*] Rate nmole/gcat·s

[**] Selectivity defined to be $[N_2O]/[N_2]$

Table A4.1.2   NO Feed Composition: 0.956% vol.

CO% Feed	CO Conv.	NO Conv.	Rate*	CO_2%	N_2O%	N_2%	S**
1.130	2.6	5.2	2.05	0.030	0.02	0.005	4.0
0.960	3.1	5.2	2.05	0.030	0.02	0.005	4.0
0.785	4.8	6.3	2.60	0.038	0.022	0.008	2.8
0.560	7.1	7.3	2.74	0.040	0.030	0.005	6.0
0.305	8.9	7.9	2.88	0.042	0.034	0.004	8.5
0.260	13.8	8.4	3.01	0.044	0.036	0.004	9.0
0.205	21.5	8.5	3.01	0.044	0.037	0.0035	10.6
0.182	24.2	9.0	3.01	0.044	0.042	0.001	42.
0.167	26.3	9.4	3.15	0.046	0.044	0.001	44
0.149	33.6	10.3	3.42	0.050	0.048	0.001	48
0.138	39.1	10.9	3.70	0.054	0.05	0.002	25.
-	-	-	-	-	-	-	-
0.059	84.7	8.9	3.42	0.05	0.035	0.0075	4.7
0.0905	79.6	13.8	4.93	0.072	0.06	0.006	10.
0.114	78.9	17.3	6.16	0.09	0.075	0.0075	10.
0.126	79.4	18.8	6.85	0.10	0.08	0.010	8.0
0.149	85.9	24.2	8.77	0.128	0.103	0.0125	8.2
0.172	91.3	29.3	10.75	0.157	0.123	0.017	7.2
0.190	89.5	31.9	11.64	0.17	0.135	0.0175	7.7
0.200	93.5	34.4	12.81	0.187	0.142	0.0225	6.3
0.210	95.2	36.4	13.70	0.20	0.148	0.026	5.7

Table A4.1.3 NO Feed Composition: 0.628% vol.

CO% Feed	CO Conv.	NO Conv.	Rate[*]	CO_2%	N_2O%	N_2%	S[**]
1.130	2.6	7.3	1.99	0.029	0.017	0.006	2.8
0.960	3.1	8.0	2.05	0.030	0.020	0.005	4.0
0.675	4.6	8.4	2.12	0.031	0.022	0.0045	4.9
0.445	7.9	9.6	2.40	0.035	0.025	0.005	5.0
0.330	12.1	10.7	2.74	0.040	0.027	0.0065	4.2
0.215	14.4	9.2	2.53	0.037	0.027	0.005	5.4
0.172	22.1	11.1	2.60	0.038	0.032	0.003	10.7
0.149	28.9	12.7	2.95	0.043	0.037	0.003	12.3
0.1375	36.4	14.6	3.42	0.050	0.042	0.004	10.5
0.126	46.0	16.9	3.97	0.058	0.048	0.005	9.6
-	-	-	-	-	-	-	-
0.032	93.8	8.3	2.05	0.030	0.022	0.004	5.5
0.067	86.6	16.9	3.97	0.058	0.048	0.005	9.6
0.102	78.4	23.2	5.48	0.080	0.066	0.007	8.6
0.137	80.3	31.8	7.53	0.110	0.090	0.010	9.0
0.161	83.2	38.2	9.18	0.134	0.105	0.015	7.0
0.180	88.5	42.7	10.82	0.158	0.110	0.024	4.6

Table A4.1.4 NO Feed Composition: 0.337% vol.

CO% Feed	CO Conv.	NO Conv.	Rate[*]	CO_2%	N_2O%	N_2%	S[**]
1.00	2.0	9.5	1.37	0.020	0.012	0.004	3.0
0.810	2.5	9.5	1.37	0.020	0.012	0.004	3.0
0.6157	3.7	11.6	1.57	0.023	0.016	0.0035	4.6
0.445	5.6	12.2	1.71	0.025	0.016	0.0045	3.6
0.273	11.0	15.4	2.05	0.030	0.022	0.004	5.5
0.215	14.4	16.6	2.12	0.031	0.025	0.003	8.3
0.172	23.3	19.9	2.74	0.040	0.027	0.0065	4.2
0.1305	32.2	22.0	2.88	0.042	0.032	0.005	6.4
0.126	38.1	24.9	3.29	0.048	0.036	0.006	6.0
–	–	–	–	–	–	–	–
0.026	96.2	13.6	1.71	0.025	0.021	0.002	10.5
0.0556	78.2	25.2	2.95	0.043	0.041	0.0015	41
0.090	80.0	38.6	4.93	0.072	0.058	0.007	8.3
0.126	77.8	51.6	6.71	0.098	0.075	0.012	6.5
0.149	80.5	60.6	8.22	0.120	0.086	0.017	5.1
0.167	80.8	67.1	9.25	0.135	0.090	0.023	4.0

Table A4.2 Experimental Data for the NO+CO reaction at a Temperature of 170°C, Total Flow Rate of 138 μmol/s

Table A4.2.1 NO Feed Composition: 1.19% vol.

CO% Feed	CO Conv.	NO Conv.	Rate*	CO$_2$%	N$_2$O%	N$_2$%	S**
1.146	6.1	8.7	4.79	0.070	0.033	0.019	1.78
0.9595	7.5	9.4	4.93	0.072	0.040	0.016	2.5
0.829	9.3	10.1	5.27	0.077	0.042	0.018	2.4
0.671	11.9	10.8	5.48	0.080	0.048	0.016	3.0
0.539	15.2	11.3	5.62	0.082	0.051	0.016	3.3
0.449	19.2	11.8	5.89	0.086	0.053	0.017	3.2
0.358	27.9	13.9	6.85	0.10	0.065	0.018	3.7
0.323	33.4	14.8	7.40	0.108	0.068	0.020	3.4
0.298	36.2	15.0	7.40	0.108	0.070	0.019	3.68
0.275	42.2	16.1	7.94	0.116	0.075	0.021	3.66
0.253	55.3	19.3	9.59	0.140	0.090	0.025	3.6
-	-	-	-	-	-	-	-
0.115	95.7	16.1	7.53	0.11	0.082	0.014	5.86
0.205	92.7	27.9	13.15	0.192	0.14	0.026	5.38
0.298	96.6	41.3	19.73	0.288	0.204	0.042	4.86
0.357	95.5	49.1	23.35	0.341	0.242	0.050	4.89
0.403	100	56.8	27.74	0.405	0.270	0.068	4.00
0.426	98.6	59.2	28.90	0.422	0.282	0.070	4.03
0.450	97.1	60.8	29.99	0.437	0.286	0.076	3.79

Table A4.2.2 NO Feed Composition: 0.899% vol.

CO% Feed	CO Conv.	NO Conv.	Rate*	CO_2%	N_2O%	N_2%	S**
1.146	5.1	9.7	3.97	0.058	0.030	0.014	2.1
0.936	6.2	10.2	3.97	0.058	0.033	0.013	2.6
0.822	7.1	10.2	3.97	0.058	0.034	0.012	2.8
0.7373	8.1	10.7	4.11	0.060	0.035	0.013	2.8
0.5656	12.0	12.0	4.66	0.068	0.040	0.014	2.9
0.500	14.0	12.8	4.79	0.070	0.045	0.013	3.6
0.4141	18.8	14.2	5.34	0.078	0.050	0.014	3.6
0.355	22.5	15.1	5.48	0.080	0.056	0.012	4.7
0.333	25.8	15.3	5.89	0.086	0.052	0.017	3.1
0.305	31.5	17.9	6.58	0.096	0.065	0.016	4.1
0.275	36.4	17.8	6.85	0.10	0.060	0.020	3.0
0.228	65.8	27.4	10.27	0.15	0.095	0.028	3.4
-	-	-	-	-	-	-	-
0.102	98.0	18.0	6.85	0.10	0.062	0.019	3.3
0.172	93.0	31.1	10.96	0.16	0.120	0.020	6.0
0.238	89.0	40.8	14.52	0.212	0.155	0.0285	5.4
0.289	88.2	47.3	17.46	0.255	0.170	0.0425	4.0
0.333	90.1	54.7	20.55	0.30	0.192	0.054	3.6
0.370	86.5	61.2	21.92	0.32	0.200	0.075	2.7
0.399	86.0	61.0	23.49	0.343	0.205	0.069	3.0

Table A4.2.3 NO Feed Composition: 0.601% vol.

CO% Feed	CO Conv.	NO Conv.	Rate*	CO_2%	N_2O%	N_2%	S**
1.086	4.6	12.5	3.42	0.050	0.025	0.0125	2.0
0.926	5.5	12.5	3.42	0.050	0.025	0.0125	2.0
0.783	6.4	12.8	3.42	0.050	0.027	0.0115	2.3
0.730	7.0	13.5	3.49	0.051	0.030	0.0105	2.8
0.615	8.5	14.0	3.54	0.052	0.032	0.010	3.2
0.50	10.6	14.8	3.63	0.053	0.036	0.0085	4.2
0.426	14.1	16.6	4.11	0.060	0.040	0.010	4.0
0.355	18.9	18.5	4.59	0.067	0.044	0.0115	3.8
0.322	21.7	19.1	4.79	0.070	0.045	0.0125	3.6
0.273	28.6	21.3	5.34	0.078	0.050	0.014	3.6
0.240	35.0	21.7	5.75	0.084	0.047	0.0185	2.50
0.217	41.5	23.6	6.16	0.090	0.052	0.019	2.63
0.196	62.6	31.1	8.36	0.122	0.065	0.0285	2.30
-	-	-	-	-	-	-	-
0.076	100	23.0	5.48	0.08	0.057	0.012	4.96
0.127	96.1	34.4	8.36	0.122	0.085	0.019	4.59
0.206	98.5	54.6	13.90	0.203	0.125	0.039	3.21
0.240	98.3	62.6	16.16	0.236	0.140	0.048	2.92
0.293	92.8	71.9	18.63	0.272	0.160	0.056	2.86
0.305	91.1	72.5	19.04	0.278	0.158	0.060	2.63
0.333	85.6	74.9	19.52	0.285	0.165	0.060	2.75

Table A4.2.4 NO Feed Composition: 0.294% vol.

CO% Feed	CO Conv.	NO Conv.	Rate*	CO_2%	N_2O%	N_2%	S**
1.1211	2.7	14.3	2.05	0.030	0.012	0.009	1.3
0.9696	3.1	14.3	2.05	0.030	0.012	0.009	1.3
0.795	3.8	15.0	2.05	0.030	0.014	0.008	1.75
0.644	5.1	17.0	2.26	0.033	0.016	0.009	1.88
0.495	6.7	17.0	2.26	0.033	0.016	0.009	1.88
0.333	12.	20.4	2.74	0.040	0.020	0.010	2.0
0.275	17.5	23.8	3.29	0.048	0.022	0.013	1.7
0.2293	21.4	25.2	3.36	0.049	0.024	0.013	1.90
0.205	24.4	25.9	3.42	0.050	0.025	0.013	2.0
0.196	25.5	25.9	3.42	0.050	0.026	0.012	2.2
0.180	30.6	29.3	3.77	0.055	0.030	0.013	2.4
0.162	35.8	30.6	3.97	0.058	0.032	0.013	2.5
0.145	46.9	36.7	4.66	0.068	0.040	0.014	2.8
-	-	-	-	-	-	-	-
0.0798	100	51.7	6.71	0.098	0.055	0.021	2.6
0.139	100	73.5	10.48	0.153	0.064	0.044	1.4
0.184	100	91.2	13.36	0.192	0.074	0.060	1.2
0.217	100	99.3	15.27	0.223	0.070	0.076	0.92
0.240	100	100.0	16.16	0.236	0.072	0.082	0.88

Table A4.3 Experimental Data for the NO+CO reaction at a Temperature of 190°C, Total Flow Rate of 138 μmol/s

Table A4.3.1 NO Feed Composition: 1.25% vol.

CO% Feed	CO Conv.	NO Conv.	Rate*	CO_2%	N_2O%	N_2%	S**
1.146	8.70	11.6	6.85	0.100	0.045	0.0275	1.6
0.9595	11.0	12.3	7.25	0.106	0.048	0.029	1.7
0.796	13.6	12.5	7.39	0.108	0.047	0.031	1.5
0.644	17.1	13.2	7.53	0.110	0.055	0.0275	2.0
0.497	24.5	14.7	8.35	0.122	0.062	0.030	2.1
0.425	29.9	15.4	8.70	0.127	0.065	0.031	2.1
0.357	42.0	17.9	10.27	0.150	0.074	0.038	1.9
0.333	48.6	19.2	11.10	0.162	0.078	0.042	1.86
0.309	64.7	24.0	13.70	0.200	0.100	0.050	2.0
-	-	-	-	-	-	-	-
0.115	83.4	14.1	6.58	0.096	0.080	0.008	10.0
0.228	90.4	28.6	14.11	0.206	0.152	0.027	5.6
0.309	92.5	38.9	19.59	0.286	0.200	0.043	4.7
0.438	93.6	54.4	28.01	0.41	0.27	0.070	3.9
0.529	94.5	64.8	34.24	0.50	0.31	0.095	3.3
0.566	95.7	69.0	37.05	0.541	0.32	0.111	2.9
0.600	100	74.6	41.09	0.60	0.332	0.134	2.5
0.622	96.4	74.9	41.09	0.60	0.335	0.133	2.5
0.638	95.3	75.5	41.64	0.608	0.336	0.136	2.5

Table A4.3.2 NO Feed Composition: 0.94% vol.

CO% Feed	CO Conv.	NO Conv.	Rate*	CO_2%	N_2O%	N_2%	S**
1.146	7.4	13.2	5.75	0.084	0.040	0.022	1.8
1.02	8.2	13.2	5.75	0.084	0.040	0.022	1.8
0.892	9.6	13.6	5.89	0.086	0.042	0.022	1.9
0.765	11.5	13.9	6.03	0.088	0.043	0.0225	1.9
0.637	14.4	14.6	6.30	0.092	0.045	0.0235	1.9
0.56	17.5	15.4	6.30	0.098	0.047	0.0255	1.8
0.467	23.3	17.8	7.47	0.109	0.054	0.0275	2.0
0.41	27.1	17.8	7.60	0.111	0.056	0.0275	2.0
0.37	33.8	20.0	8.56	0.125	0.063	0.031	2.0
0.333	42.0	22.3	9.59	0.140	0.070	0.035	2.0
0.309	50.8	25.2	10.75	0.157	0.080	0.0385	2.1
0.293	62.0	29.5	12.47	0.182	0.090	0.0435	2.2
–	–	–	–	–	–	–	–
0.104	100	21.9	7.12	0.120	0.086	0.0170	5.1
0.217	96.8	37.8	14.38	0.210	0.145	0.0325	4.5
0.333	97.9	55.4	22.33	0.326	0.195	0.0655	3.0
0.426	96.2	66.7	28.08	0.41	0.217	0.0965	2.3
0.472	94.9	73.2	30.68	0.448	0.240	0.104	2.3
0.507	93.7	76.6	32.53	0.475	0.245	0.115	2.1
0.5404	91.6	78.9	33.90	0.495	0.247	0.124	2.0

Table A4.3.3 NO Feed Composition: 0.64% vol.

CO% Feed	CO Conv.	NO Conv.	Rate[*]	CO_2%	N_2O%	N_2%	S[**]
1.146	7.0	18.0	5.48	0.080	0.035	0.0225	1.6
0.914	8.8	18.1	5.48	0.080	0.036	0.0220	1.6
0.775	10.6	19.1	5.62	0.082	0.040	0.0210	1.9
0.675	14.1	20.8	6.16	0.090	0.043	0.0235	1.8
0.550	17.3	22.3	6.51	0.095	0.048	0.0235	2.0
0.495	19.6	22.2	6.64	0.097	0.045	0.0260	1.7
0.380	26.8	23.3	6.98	0.102	0.047	0.0275	1.7
0.310	35.8	25.2	7.60	0.111	0.050	0.0305	1.6
0.275	43.3	27.0	8.15	0.119	0.054	0.0325	1.7
0.253	47.0	27.0	8.15	0.119	0.054	0.0325	1.7
-	-	-	-	-	-	-	-
0.127	89	29.5	7.74	0.113	0.076	0.0185	4.1
0.216	92.6	51.6	13.70	0.20	0.13	0.035	3.7
0.275	91.6	63.1	17.26	0.252	0.152	0.050	3.0
0.323	93	73.1	20.55	0.30	0.168	0.066	2.5
0.358	90.5	78.0	22.19	0.324	0.175	0.0745	2.3
0.38	93.7	83.8	24.38	0.356	0.18	0.088	2.0
0.403	100	92.2	28.56	0.417	0.173	0.122	1.4
0.425	98.8	91.2	28.77	0.42	0.165	0.127	1.3
0.438	98.2	93.4	29.45	0.43	0.167	0.132	1.27
0.4596	96.2	95.2	30.27	0.442	0.167	0.1375	1.2
0.483	95.2	97.7	31.51	0.46	0.165	0.1475	1.1

Table A4.3.4 NO Feed Composition: 0.33% vol.

CO% Feed	CO Conv.	NO Conv.	Rate*	CO_2%	N_2O%	N_2%	S**
1.133	6.4	27.0	4.59	0.067	0.022	0.0225	0.98
0.876	7.6	27.0	4.59	0.067	0.022	0.0225	0.98
0.6565	10.5	28.5	4.73	0.069	0.025	0.022	1.14
0.495	14.1	28.5	4.79	0.070	0.024	0.023	1.04
0.356	19.9	30.9	4.86	0.071	0.030	0.021	1.46
0.298	24.2	32.1	4.93	0.072	0.033	0.020	1.69
0.251	31.87	34.5	5.48	0.080	0.034	0.023	1.48
0.216	43.98	40.0	6.51	0.095	0.037	0.029	1.3
-	-	-	-	-	-	-	-
0.0758	93.3	33.9	4.79	0.07	0.042	0.014	3.0
0.150	93.3	63.6	9.59	0.14	0.070	0.035	2.0
0.216	85.6	87.9	12.67	0.185	0.085	0.060	1.7
0.275	85.8	91.2	16.16	0.236	0.065	0.0855	0.76
0.298	85.6	93.3	17.46	0.255	0.052	0.102	0.51
0.323	88.2	100	19.52	0.285	0.045	0.12	0.38
0.330	96.1	100	21.71	0.317	0.030	0.144	0.21
0.358	92.7	100.	22.74	0.332	0.030	0.151	0.20

Table A4.4 Experimental Data for the NO+CO reaction at a Temperature of 170°C, Total Flow Rate of 69 μmol/s

Table A4.4.1 NO Feed Composition: 1.24% vol.

CO% Feed	CO Conv.	NO Conv.	Rate*	CO_2%	N_2O%	N_2%	S**
0.185	91.9	23.8	5.82	0.17	0.125	0.0225	5.6
0.301	93.7	38.6	9.65	0.282	0.197	0.0425	4.6
0.394	93.9	50.0	12.67	0.37	0.25	0.060	4.2
0.529	94.5	65.7	17.12	0.50	0.315	0.0925	3.4
0.620	95.2	71.2	20.20	0.59	0.348	0.0937	3.7
0.693	95.2	82.5	22.60	0.66	0.363	0.1485	2.4
0.737	95.7	86.1	24.14	0.705	0.363	0.171	2.1
–	–	–	–	–	–	–	–
2.50	5.8	15.7	4.97	0.145	0.050	0.0475	1.05
1.95	9.2	19.1	6.16	0.180	0.057	0.0615	0.93
1.73	10.4	19.2	6.16	0.18	0.058	0.061	0.95
1.5	12.0	19.5	6.16	0.18	0.062	0.059	1.05
1.2	15.0	19.5	6.16	0.18	0.062	0.059	1.05
1.24	15.1	21.5	6.40	0.187	0.080	0.0535	1.5
1.08	17.7	21.0	6.40	0.187	0.074	0.0565	1.3
0.901	21.1	21.3	6.51	0.190	0.075	0.0575	1.3
0.739	27.1	23.4	6.85	0.20	0.090	0.055	1.6
0.620	34.4	25.6	7.29	0.213	0.105	0.054	1.9
0.574	36.6	25.6	7.19	0.21	0.107	0.0515	2.1
0.529	39.7	25.6	7.19	0.21	0.107	0.0515	2.1
0.448	46.9	25.6	7.19	0.21	0.107	0.0515	2.1
0.394	68.5	34.3	9.25	0.27	0.155	0.0575	2.7

Table A4.4.2   NO Feed Composition: 0.955% vol.

CO% Feed	CO Conv.	NO Conv.	Rate[*]	CO_2%	N_2O%	N_2%	S[**]
0.171	91.2	28.9	5.34	0.156	0.12	0.018	6.7
0.289	84.4	44.4	8.36	0.244	0.18	0.032	5.6
0.392	86.7	59.7	11.64	0.34	0.23	0.055	4.2
0.485	87.6	71.2	14.55	0.425	0.255	0.085	3.0
0.529	88.5	77.1	16.03	0.468	0.267	0.101	2.7
0.576	89.1	81.7	17.57	0.513	0.267	0.123	2.2
0.634	89.4	84.8	19 42	0.567	0.242	0.163	1.5
0.652	90.5	90.1	20.27	0.592	0.267	0.163	1.5
-	-	-	-	-	-	-	-
2.40	4.5	15.6	3.73	0.109	0.04	0.0345	1.16
2.00	5.5	15.8	3.73	0.109	0.042	0.0335	1.25
1.70	6.6	16.5	3.87	0.113	0.045	0.034	1.32
1.361	11.0	20.5	5.14	0.15	0.045	0.053	0.86
1.01	15.0	21.6	5.21	0.152	0.054	0.049	1.1
0.700	22.0	23.0	5.31	0.155	0.065	0.045	1.4
0.596	26.8	24.7	5.48	0.16	0.075	0.043	1.8
0.505	37.6	28.9	6.51	0.19	0.085	0.053	1.6
0.434	47.3	31.4	7.02	0.205	0.094	0.056	1.7
0.405	50.6	31.6	7.02	0.205	0.096	0.055	1.8
0.394	53.3	32.3	7.19	0.21	0.099	0.0555	1.8
0.368	62.5	36.6	7.88	0.23	0.12	0.055	2.2

Table A4.4.3 NO Feed Composition: 0.64% vol.

CO% Feed	CO Conv.	NO Conv.	Rate*	CO_2%	N_2O%	N_2%	S**
0.084	100	25.0	3.08	0.09	0.07	0.010	7.0
0.183	93.9	45.0	5.89	0.172	0.115	0.029	4.0
0.278	92.1	64.4	8.77	0.256	0.155	0.051	3.1
0.348	91.9	75.0	10.96	0.32	0.16	0.080	2.0
0.414	91.8	86.6	13.01	0.38	0.168	0.109	1.5
0.459	91.9	90.9	14.45	0.422	0.163	0.128	1.3
0.485	84.5	88.4	14.04	0.410	0.155	0.128	1.2
0.505	84.8	91.9	14.66	0.428	0.16	0.134	1.2
-	-	-	-	-	-	-	-
2.45	3.1	15.9	2.64	0.077	0.025	0.026	0.96
1.73	4.5	15.9	2.64	0.077	0.025	0.026	0.96
1.485	6.7	20.2	3.42	0.100	0.029	0.0355	0.82
1.116	9.4	22.2	3.60	0.105	0.037	0.034	1.09
0.899	12.2	23.9	3.73	0.109	0.043	0.0335	1.28
0.737	14.9	24.2	3.77	0.110	0.045	0.0325	1.38
0.598	19.4	26.7	3.97	0.116	0.055	0.0305	1.8
0.505	26.7	30.9	4.62	0.135	0.063	0.036	1.75
0.410	36.6	34.4	5.14	0.150	0.075	0.035	2.0
0.337	42.5	32.5	4.79	0.140	0.068	0.036	1.9
0.323	48.6	35.9	5.38	0.157	0.072	0.043	1.7
0.308	55.2	39.4	5.82	0.17	0.082	0.044	1.9
0.296	74.6	57.5	7.57	0.221	0.147	0.037	0.4

Table A4.4.4 NO Feed Composition: 0.35% vol.

CO% Feed	CO Conv.	NO Conv.	Rate*	CO_2%	N_2O%	N_2%	S**
0.065	92.3	29.7	2.05	0.060	0.043	0.009	5.1
0.112	87.5	45.7	3.36	0.098	0.061	0.019	3.3
0.147	87.1	59.3	4.38	0.128	0.080	0.024	3.3
0.23	81.7	80.6	6.44	0.188	0.093	0.048	2.0
0.301	81.1	92.6	8.36	0.244	0.080	0.082	0.98
0.347	82.4	99.4	9.79	0.286	0.061	0.113	0.54
0.356	80.3	99.4	9.79	0.286	0.060	0.113	0.54
-	-	-	-	-	-	-	-
2.27	2.6	22.9	2.05	0.06	0.020	0.020	1.0
1.95	3.1	24.3	2.23	0.065	0.020	0.023	0.89
1.586	5.4	29.7	2.91	0.085	0.018	0.034	0.54
1.406	6.0	29.7	2.91	0.085	0.018	0.034	0.54
1.199	7.3	30.8	3 01	0.088	0.020	0.034	0.59
1.02	8.9	33.1	3.12	0.091	0.024	0.034	0.72
0.854	11.4	34.9	3.32	0.097	0.025	0.036	0.69
0.663	14.8	36.6	3.36	0.098	0.030	0.034	0.88
0.529	19.3	39.4	3.49	0.102	0.036	0.033	1.1
0.436	25.2	42.9	3.77	0.11	0.040	0.035	1.1
0.368	33.4	48.0	4.21	0.123	0.044	0.040	1.1
0.349	36.1	49.1	4.31	0.126	0.046	0.040	1.2
0.325	38.8	48.0	4.31	0.126	0.042	0.042	1.0
0.301	44.2	52.6	4.55	0.133	0.050	0.042	1.2
0.278	53.96	58.9	5.14	0.15	0.055	0.048	1.2
0.267	57.7	60.6	5.27	0.154	0.057	0.049	1.2
0.255	65.5	66.3	5.72	0.167	0.065	0.051	1.3

Table A4.5 Experimental Data for the NO+CO reaction at a Temperature of 170°C, Total Flow Rate of 276 μmol/s

Table A4.5.1 NO Feed Composition: 1.495% vol.

CO% Feed	CO Conv.	NO Conv.	Rate*	CO_2%	N_2O%	N_2%	S**
1.97	2.1	4.9	5.64	0.041	0.032	0.0045	7.1
1.51	2.8	5.2	5.91	0.043	0.034	0.0045	7.6
1.25	3.4	5.2	5.77	0.042	0.035	0.0035	10.0
0.885	5.4	5.9	6.60	0.048	0.040	0.004	10.0
0.713	7.0	6.6	6.87	0.050	0.041	0.0045	11.1
0.509	11.4	7.4	7.79	0.058	0.048	0.005	9.6
0.365	19.7	12.5	9.90	0.072	0.055	0.0085	6.5
0.279	29.4	14.0	11.27	0.082	0.063	0.0095	6.6
0.20	41.0	10.2	11.27	0.082	0.071	0.0055	12.9
0.1775	53.5	11.4	13.06	0.095	0.075	0.010	7.5
-	-	-	-	-	-	-	-
0.045	95.6	5.7	5.91	0.043	0.043	0.00	
0.086	90.7	10.2	10.72	0.078	0.075	0.0015	50
0.125	89.6	13.4	15.40	0.112	0.088	0.012	7.3
0.16	90.6	16.8	19.93	0.145	0.106	0.0195	5.4
0.188	95.6	21.4	24.74	0.18	0.14	0.02	7.0
0.20	95.0	22.4	26.12	0.19	0.146	0.022	6.6
0.205	97.6	23.8	27.49	0.20	0.155	0.023	6.9
0.228	92.1	25.8	28.87	0.21	0.175	0.018	10.
0.245	91.8	27.0	30.93	0.225	0.178	0.0235	7.6
0.263	90.1	27.9	32.58	0.237	0.180	0.0285	6.3

Table A4.5.2 NO Feed Composition: 1.134% vol.

CO% Feed	CO Conv.	NO Conv.	Rate[*]	CO_2%	N_2O%	N_2%	S[**]
2.03	1.3	5.6	3.85	0.028	0.032	0.000	
1.795	1.6	5.6	3.85	0.028	0.032	0.000	
1.485	1.9	5.6	3.85	0.028	0.032	0.000	
1.25	2.3	6.0	3.99	0.029	0.034	0.000	
1.00	3.0	5.8	4.12	0.030	0.033	0.000	
0.7375	4.6	6.0	4.67	0.034	0.034	0.000	
0.538	7.4	6.3	5.50	0.040	0.037	0.0015	24.7
0.453	10.6	7.9	6.60	0.048	0.042	0.003	14.0
0.337	16.3	9.0	7.56	0.055	0.047	0.004	11.75
0.267	21.7	9.4	7.97	0.058	0.049	0.0045	11.9
0.211	23.2	11.0	9.62	0.070	0.055	0.0075	9.3
0.1775	43.9	12.6	10.72	0.078	0.065	0.0065	10.0
0.160	51.9	13.8	11.41	0.083	0.073	0.005	14.6
0.150	64.0	15.5	13.18	0.096	0.080	0.008	10.0
-	-	-	-	-	-	-	-
0.0395	86.1	7.2	4.67	0.034	0.041		
0.0925	90.3	14.2	12.10	0.088	0.073	0.0075	9.7
0.1365	82.1	18.7	15.40	0.112	0.10	0.006	16.8
0.1775	88.5	22.4	21.58	0.157	0.126	0.0155	8.1
0.188	85.1	25.9	21.99	0.160	0.134	0.013	10.3
0.200	85.0	27.3	223.3	0.17	0.140	0.015	9.3
0.217	86.6	29.6	25.84	0.188	0.148	0.020	7.4
0.234	81.6	29.9	26.25	0.191	0.148	0.0215	6.9

Table A4.5.3 NO Feed Composition: 0.731% vol.

CO% Feed	CO Conv.	NO Conv.	Rate*	CO_2%	N_2O%	N_2%	S**
1.96	1.0	8.6	2.74	0.020	0.016	0.002	8.0
1.538	1.3	8.6	2.74	0.020	0.017	0.0015	11.3
1.025	2.0	8.6	2.74	0.020	0.018	0.0010	18.0
0.71	2.8	8.6	2.74	0.020	0.025	0.0065	
0.565	4.4	8.6	3.42	0.025	0.025	0.0065	
0.4515	8.4	9.3	5.22	0.038	0.030	0.004	7.5
0.36	10.6	9.3	5.22	0.038	0.030	0.004	7.5
0.2768	13.7	9.6	5.22	0.038	0.032	0.003	10.7
0.205	19.5	10.4	5.22	0.040	0.036	0.002	18.0
0.1775	27.0	12.0	5.49	0.048	0.040	0.004	10.0
0.153	34.6	13.0	7.28	0.053	0.042	0.0055	7.0
0.126	46.0	14.4	7.96	0.058	0.047	0.0055	8.5
-	-	-	-	-	-	-	-
0.045	73.3		4.53	0.033	0.041		
0.0863	81.1	18.2	9.61	0.070	0.063	0.0035	18.0
0.1195	82.8	23.9	13.59	0.099	0.076	0.0115	6.6
0.14	80.7	27.8	15.52	0.113	0.090	0.0115	7.8
0.1535	78.2	29.1	16.48	0.12	0.095	0.0125	7.6
0.177	83.6	34.7	20.32	0.148	0.106	0.021	5.05

Table A4.5.4 NO Feed Composition: 0.337% vol.

CO% Feed	CO Conv.	NO Conv.	Rate*	CO_2%	N_2O%	N_2%	S**
1.96	1.0	10.7	2.7	0.02	0.016	0.002	8.0
1.485	1.3	10.7	2.7	0.02	0.016	0.002	8.0
0.965	2.1	10.7	2.7	0.02	0.016	0.002	8.0
0.765	2.6	10.7	2.7	0.02	0.016	0.002	8.0
0.565	3.5	10.7	2.7	0.02	0.016	0.002	8.0
0.389	5.1	10.7	2.7	0.02	0.016	0.002	8.0
0.325	6.2	11.3	2.7	0.02	0.018	0.001	18.0
0.24	8.8	11.6	2.9	0.021	0.018	0.0015	12.0
0.1925	10.9	11.6	2.9	0.021	0.018	0.0015	12.0
0.142	15.5	12.5	3.0	0.022	0.020	0.001	20.0
0.125	18.4	13.3	3.2	0.023	0.022	0.0005	44.0
0.1135	20.3	13.4	3.2	0.023	0.022	0.0005	44.0
0.0975	26.6	15.1	3.6	0.026	0.025	0.0005	52.0
0.0805	37.3		4.1	0.030	0.030	0.000	
0.075	42.7		4.4	0.032	0.030	0.000	
-	-	-	-	-	-	-	-
0.0395	76.9		4.12	0.03	0.035		
0.0745	80.5	32.6	8.24	0.06	0.050	0.005	10.0
0.0925	80.0	40.4	10.7	0.078	0.058	0.010	5.8
0.131	76.3	48.4	13.7	0.10	0.063	0.0185	3.4

APPENDIX 5. BALANCE EQUATIONS FOR N_2O+CO

The species balance equations for the mechanisms presented in Chapter 4 are summarized in this appendix. The computer solution of these sets of equations was performed using the programs contained in Appendix 7. For all of the sets of equations examined in Chapter 4, the gas-phase CO and N_2O concentrations are related via:

$$[CO]_o - [CO] = [N_2O]_o - [N_2O] \tag{A5.1}$$

Mechanism 4.1

$$k_1[CO](L-[CO\text{-}M]) - k_{-1}[CO\text{-}M] - k_9[N_2O][CO\text{-}M] = 0 \tag{A5.2}$$

$$Q([N_2O]_o-[N_2O]) - ak_9[N_2O][CO\text{-}M] = 0 \tag{A5.3}$$

Mechanism 4.2

$$\begin{aligned}k_1[CO](L-[CO\text{-}M]-[O\text{-}M]) &- k_{-1}[CO\text{-}M]\\ &- k_8[CO\text{-}M][O\text{-}M] = 0\end{aligned} \tag{A5.4}$$

$$k_4[N_2O](L-[CO\text{-}M]-[O\text{-}M]) - k_8[CO\text{-}M][O\text{-}M] = 0 \tag{A5.5}$$

$$Q([N_2O]_o-[N_2O]) - ak_4[N_2O](L-[CO\text{-}M]-[O\text{-}M]) = 0 \tag{A5.6}$$

Mechanism 4.3

$$\begin{aligned}k_1[CO](L-[CO\text{-}M]-[O\text{-}M]) &- k_{-1}[CO\text{-}M] - k_8[CO\text{-}M][O\text{-}M]\\ &- k_9[N_2O][CO\text{-}M] = 0\end{aligned} \tag{A5.7}$$

$$k_4[N_2O](L-[CO\text{-}M]-[O\text{-}M]) - k_8[CO\text{-}M][O\text{-}M] = 0 \tag{A5.5}$$

$$\begin{aligned}Q([N_2O]_o-[N_2O]) &- ak_4[N_2O](L-[CO\text{-}M]-[O\text{-}M])\\ &- ak_9[N_2O][CO\text{-}M] = 0\end{aligned} \tag{A5.8}$$

Mechanism 4.4

$$\begin{aligned} &k_1[CO](L-[CO-M]-[O-M]) - k_{-1}[CO-M] \\ &\qquad - k_8[CO-M][O-M] = 0 \end{aligned} \tag{A5.4}$$

$$\begin{aligned} &k_4[N_2O](L-[CO-M]-[O-M]) - k_8[CO-M][O-M] \\ &\qquad - k_{10}[CO][O-M] = 0 \end{aligned} \tag{A5.9}$$

$$Q([N_2O]_o-[N_2O]) - ak_4[N_2O](L-[CO-M]-[O-M]) = 0 \tag{A5.6}$$

Mechanism 4.5

$$\begin{aligned} &k_1[CO](L-[CO-M]-[O-M]) - k_{-1}[CO-M] - k_8[CO-M][O-M] \\ &\qquad - k_9[N_2O][CO-M] = 0 \end{aligned} \tag{A5.7}$$

$$\begin{aligned} &k_4[N_2O](L-[CO-M]-[O-M]) - k_8[CO-M][O-M] \\ &\qquad - k_{10}[CO][O-M] = 0 \end{aligned} \tag{A5.9}$$

$$\begin{aligned} &Q([N_2O]_o-[N_2O]) - ak_4[N_2O](L-[CO-M]-[O-M]) \\ &\qquad - ak_9[N_2O][CO-M] = 0 \end{aligned} \tag{A5.8}$$

Mechanism 4.6

$$\begin{aligned} &k_1[CO](L-[CO-M]-[O-M]) - k_{-1}[CO-M] - k_8[CO-M][O-M] \\ &\qquad - k_{16}[CO-M][CO-M] = 0 \end{aligned} \tag{A5.10}$$

$$k_4[N_2O](L-[CO-M]-[O-M]) - k_8[CO-M][O-M] = 0 \tag{A5.5}$$

$$Q([N_2O]_o-[N_2O]) - ak_4[N_2O](L-[CO-M]-[O-M]) = 0 \tag{A5.6}$$

Mechanism 4.7

$$\begin{aligned} &k_1[CO](L-[CO-M]-[O-M]) - k_{-1}[CO-M] - k_8[CO-M][O-M] \\ &\qquad - k_{17}[CO][CO-M] = 0 \end{aligned} \tag{A5.11}$$

$$k_4[N_2O](L-[CO-M]-[O-M]) - k_8[CO-M][O-M] = 0 \tag{A5.5}$$

$$Q([N_2O]_o-[N_2O]) - ak_4[N_2O](L-[CO-M]-[O-M]) = 0 \tag{A5.6}$$

Mechanism 4.8

$$k_1[CO](L-[CO\text{-}M]-[O\text{-}M]) - k_{-1}[CO\text{-}M] - k_8[CO\text{-}M][O\text{-}M] - k_{18}[N_2O][CO\text{-}M] = 0 \qquad (A5.12)$$

$$k_4[N_2O](L-[CO\text{-}M]-[O\text{-}M]) - k_8[CO\text{-}M][O\text{-}M] + k_{18}[N_2O][CO\text{-}M] = 0 \qquad (A5.13)$$

$$Q([N_2O]_o-[N_2O]) - ak_4[N_2O](L-[CO\text{-}M]-[O\text{-}M]) - ak_{18}[N_2O][CO\text{-}M] = 0 \qquad (A5.14)$$

Mechanism 4.9

$$k_1[CO](L-[CO\text{-}M]-[O\text{-}M]) - k_{-1}EXP(\mu[CO\text{-}M]/L)[CO\text{-}M] - k_8[CO\text{-}M][O\text{-}M] = 0 \qquad (A5.15)$$

$$k_4[N_2O](L-[CO\text{-}M]-[O\text{-}M]) - k_8[CO\text{-}M][O\text{-}M] = 0 \qquad (A5.5)$$

$$Q([N_2O]_o-[N_2O]) - ak_4[N_2O](L-[CO\text{-}M]-[O\text{-}M]) = 0 \qquad (A5.6)$$

Mechanism 4.10

$$k_1[CO](L-[CO\text{-}M]-[O\text{-}M])\frac{L-N_{CO}[CO\text{-}M]}{L-[CO\text{-}M]} - k_{-1}[CO\text{-}M] - k_8[CO\text{-}M][O\text{-}M] = 0 \qquad (A5.16)$$

$$k_4[N_2O](L-[CO\text{-}M]-[O\text{-}M]) - k_8[CO\text{-}M][O\text{-}M] = 0 \qquad (A5.5)$$

$$Q([N_2O]_o-[N_2O]) - ak_4[N_2O](L-[CO\text{-}M]-[O\text{-}M]) = 0 \qquad (A5.6)$$

Mechanism 4.11

$$k_1[CO](L-[CO\text{-}M]-[O\text{-}M])\frac{L-N_{CO}[CO\text{-}M]}{L-[CO\text{-}M]} - k_{-1}[CO\text{-}M] - k_8[CO\text{-}M][O\text{-}M] = 0 \qquad (A5.16)$$

$$k_4[N_2O](L-[CO\text{-}M]-[O\text{-}M]) - k_8[CO\text{-}M][O\text{-}M] - k_{10}[CO][O\text{-}M] = 0 \qquad (A5.9)$$

$$Q([N_2O]_o-[N_2O]) - ak_4[N_2O](L-[CO\text{-}M]-[O\text{-}M]) = 0 \qquad (A5.6)$$

Nomenclature

a : catalyst surface area, m^2

CO-M : adsorbed CO surface species

k_i : adsorption, or reaction, rate constant (value of i refers to the number of the corresponding step in the mechanism)

k_{-i} : desorption rate constant (value of i refers to the number of the corresponding step in the mechanism)

L : number of active sites per square meter

M : active site on catalyst surface

N_{CO} : a CO self-exclusion factor

O-M : adsorbed oxygen surface species

Q : total flow rate to the reactor

μ : parameter used in Mechanism 4.9

Subscript

$_o$: feed conditions

APPENDIX 6. BALANCE EQUATIONS FOR NO+CO

The species balance equations for the mechanisms presented in Chapter 6 are summarized in this appendix. The computer solution of these sets of equations was performed using the programs contained in Appendix 7. For all of the sets of equations examined in Chapter 6, the gas-phase CO, NO and N_2 concentrations are related via the balance equations:

$$[CO] = [CO]_o - [CO_2] \tag{A6.1}$$

$$[NO] = [NO]_o - [CO_2] - [N_2O] \tag{A6.2}$$

$$[N_2] = ([CO_2] - [N_2O])/2 \tag{A6.3}$$

Mechanism 6.1

$$k_1[CO](L-[CO\text{-}M]-[NO\text{-}M]-[O\text{-}M])\frac{L-N_{CO}[CO\text{-}M]}{L-[CO\text{-}M]} - k_{-1}[CO\text{-}M] - k_3[CO\text{-}M][O\text{-}M] = 0 \tag{A6.4}$$

$$k_5[NO](L-[CO\text{-}M]-[NO\text{-}M]-[O\text{-}M]) - k_{-5}[NO\text{-}M] - k_6[NO][NO\text{-}M] = 0 \tag{A6.5}$$

$$k_2[N_2O](L-[CO\text{-}M]-[NO\text{-}M]-[O\text{-}M]) - k_3[CO\text{-}M][O\text{-}M] - k_4[CO][O\text{-}M] + k_6[NO][NO\text{-}M] = 0 \tag{A6.6}$$

$$Q_o[NO]_o - Q[NO] - ak_5[NO](L-[CO\text{-}M]-[NO\text{-}M]-[O\text{-}M]) + ak_{-5}[NO\text{-}M] - ak_6[NO][NO\text{-}M] = 0 \tag{A6.7}$$

$$-Q[N_2O] - ak_2[N_2O](L-[CO\text{-}M]-[NO\text{-}M]-[O\text{-}M]) + ak_6[NO][NO\text{-}M] = 0 \tag{A6.8}$$

Mechanism 6.2

$$k_1[CO](L-[CO\text{-}M]-[NO\text{-}M]-[O\text{-}M])\frac{L-N_{CO}[CO\text{-}M]}{L-[CO\text{-}M]} - k_{-1}[CO\text{-}M] - k_3[CO\text{-}M][O\text{-}M] = 0 \tag{A6.4}$$

$$\begin{aligned} &k_5[NO](L-[CO\text{-}M]-[NO\text{-}M]-[O\text{-}M]) - k_{-5}[NO\text{-}M] \\ &\qquad - 2k_7[NO\text{-}M][NO\text{-}M] = 0 \end{aligned} \tag{A6.9}$$

$$\begin{aligned} &k_2[N_2O](L-[CO\text{-}M]-[NO\text{-}M]-[O\text{-}M]) - k_3[CO\text{-}M][O\text{-}M] \\ &\qquad - k_4[CO][O\text{-}M] + k_7[NO\text{-}M][NO\text{-}M] = 0 \end{aligned} \tag{A6.10}$$

$$\begin{aligned} &Q_o[NO]_o - Q[NO] - ak_5[NO](L-[CO\text{-}M]-[NO\text{-}M]-[O\text{-}M]) \\ &\qquad + ak_{-5}[NO\text{-}M] = 0 \end{aligned} \tag{A6.11}$$

$$\begin{aligned} &-Q[N_2O] - ak_2[N_2O](L-[CO\text{-}M]-[NO\text{-}M]-[O\text{-}M]) \\ &\qquad + ak_7[NO\text{-}M][NO\text{-}M] = 0 \end{aligned} \tag{A6.12}$$

Mechanism 6.3

$$\begin{aligned} &k_1[CO](L-[CO\text{-}M]-[N\text{-}M]-[NO\text{-}M]-[O\text{-}M])\frac{L-N_{CO}[CO\text{-}M]}{L-[CO\text{-}M]} \\ &\qquad - k_{-1}[CO\text{-}M] - k_3[CO\text{-}M][O\text{-}M] \\ &\qquad - k_{10}[CO\text{-}M][NO\text{-}M] = 0 \end{aligned} \tag{A6.13}$$

$$k_{10}[CO\text{-}M][NO\text{-}M] - k_8[N\text{-}M][NO\text{-}M] = 0 \tag{A6.14}$$

$$\begin{aligned} &k_5[NO](L-[CO\text{-}M]-[N\text{-}M]-[NO\text{-}M]-[O\text{-}M]) - k_{-5}[NO\text{-}M] \\ &\qquad - k_8[NO\text{-}M][N\text{-}M] - k_{10}[CO\text{-}M][NO\text{-}M] = 0 \end{aligned} \tag{A6.15}$$

$$\begin{aligned} &k_2[N_2O](L-[CO\text{-}M]-[N\text{-}M]-[NO\text{-}M]-[O\text{-}M]) \\ &\qquad - k_3[CO\text{-}M][O\text{-}M] - k_4[CO][O\text{-}M] = 0 \end{aligned} \tag{A6.16}$$

$$\begin{aligned} &Q_o[NO]_o - Q[NO] - ak_5[NO](L-[CO\text{-}M]-[N\text{-}M]-[NO\text{-}M]-[O\text{-}M]) \\ &\qquad + ak_{-5}[NO\text{-}M] = 0 \end{aligned} \tag{A6.17}$$

$$\begin{aligned} &-Q[N_2O] - ak_2[N_2O](L-[CO\text{-}M]-[N\text{-}M]-[NO\text{-}M]-[O\text{-}M]) \\ &\qquad + ak_8[NO\text{-}M][N\text{-}M] = 0 \end{aligned} \tag{A6.18}$$

Mechanism 6.4

$$\begin{aligned} &k_1[CO](L-[CO\text{-}M]-[N\text{-}M]-[NO\text{-}M]-[O\text{-}M])\frac{L-N_{CO}[CO\text{-}M]}{L-[CO\text{-}M]} \\ &\qquad - k_{-1}[CO\text{-}M] - k_3[CO\text{-}M][O\text{-}M] = 0 \end{aligned} \tag{A6.19}$$

$$k_9[NO\text{-}M](L-[CO\text{-}M]-[N\text{-}M]-[NO\text{-}M]-[O\text{-}M]) - k_{-9}[N\text{-}M][O\text{-}M]$$

$$- k_8[N\text{-}M][NO\text{-}M] - 2k_{11}[N\text{-}M][N\text{-}M] = 0 \tag{A6.20}$$

$$\begin{aligned} & k_5[NO](L-[CO\text{-}M]-[N\text{-}M]-[NO\text{-}M]-[O\text{-}M]) \\ & \quad - k_{-5}[NO\text{-}M] - k_8[NO\text{-}M][N\text{-}M] + k_{-9}[N\text{-}M][O\text{-}M] \\ & \quad - k_9[NO\text{-}M](L-[CO\text{-}M]-[N\text{-}M]-[NO\text{-}M]-[O\text{-}M]) = 0 \end{aligned} \tag{A6.21}$$

$$\begin{aligned} & k_2[N_2O](L-[CO\text{-}M]-[N\text{-}M]-[NO\text{-}M]-[O\text{-}M]) - k_3[CO\text{-}M][O\text{-}M] \\ & \quad - k_4[CO][O\text{-}M] + k_8[NO\text{-}M][N\text{-}M] - k_{-9}[N\text{-}M][O\text{-}M] \\ & \quad + k_9[NO\text{-}M](L-[CO\text{-}M]-[N\text{-}M]-[NO\text{-}M]-[O\text{-}M]) = 0 \end{aligned} \tag{A6.22}$$

$$\begin{aligned} & Q_o[NO]_o - Q[NO] - ak_5[NO](L-[CO\text{-}M]-[N\text{-}M]-[NO\text{-}M]-[O\text{-}M]) \\ & \quad + ak_{-5}[NO\text{-}M] = 0 \end{aligned} \tag{A6.23}$$

$$\begin{aligned} & -Q[N_2O] - ak_2[N_2O](L-[CO\text{-}M]-[N\text{-}M]-[NO\text{-}M]-[O\text{-}M]) \\ & \quad + ak_8[NO\text{-}M][N\text{-}M] = 0 \end{aligned} \tag{A6.18}$$

Nomenclature

a : catalyst surface area, m^2

CO-M : adsorbed CO surface species

k_i : adsorption, or reaction, rate constant (value of i refers to the number of the corresponding step in the mechanism)

k_{-i} : desorption rate constant (value of i refers to the number of the corresponding step in the mechanism)

L : number of active sites per square meter

M : active site on catalyst surface

N-M : adsorbed nitrogen surface species

NO-M : adsorbed NO surface species

N_{CO} : a CO self-exclusion factor

O-M : adsorbed oxygen surface species

Q : total flow rate

Subscript

$_o$: feed conditions

APPENDIX 7. COMPUTER PROGRAMS

This appendix contains listings of the computer programs and associated subroutines used for data fitting. The programs are written for the FORTRANVS compiler available on MTS. The main functions of the programs and subroutines are:

Program COMP21:

used to estimate CO conversions in the low conversion region for nitrous oxide reduction by carbon monoxide for mechanisms 2 to 11. It contains the following SUBROUTINES:

XVSCO: used to plot the results.

DATAA: contains the experimental data of N_2O+CO at 190°C.

DATAB: contains the experimental data of N_2O+CO at 210°C.

ROOT: used to find the roots of an equation.

Program COMP22:

used to solve nonlinear equations. It can evaluate conversions, surface coverages and other variables for both the N_2O+CO and the NO+CO reaction systems, when different kinetic parameters and mathematical equations are used. The major SUBROUTINES are:

DERPAR: obtaining dependence of solutions X(ALFA) of equations F(X,ALFA)=0.

FCN: equations to be solved, F(X,ALFA)=0.

NUJACX: numerical Jacobian matrix.

GAUSE: solution of N linear equations for N+1 unknowns with one of the unknowns specified.

HSBG: convert to upper almost triangular form.

ATEIG: eigenvalue calculations.

OUTPUT: print results.

```
      PROGRAM COMP21

      IMPLICIT REAL*4(K)
      PARAMETER (NDATA=20,NSET=4)
      CHARACTER*1 YESNO
      REAL*4 FEEDCO(NDATA+2,NSET),CONEXP(NDATA+2,NSET),
     *  FDN2O(NSET)
      REAL*4 CONCAL(NDATA+2,NSET),SUMERR(NSET),N2O
      WRITE(*,800)
 800  FORMAT('Read the Reaction Temperature. (190 or2 10)')
        READ(*,*)  NTEM
        IF (NTEM.EQ.190) THEN

        ELSEIF (NTEM.EQ.210) THEN
        DATA FDN2O/0.303,0.57,0.85,1.15/
        DATA FEEDCO/1.826,1.65,1.43,1.25,1.015,0.794,
     *  0.6696,0.611,0.552,0.518,0.485,0.427,0.369,
     *  0.333,.298,.265,.228,.206,.18,.18,0.,0.,
     *  1.875,1.69,1.475,1.37,1.25,1.146,.993,.908,.737,
     *  0.611,.54,.485,0.39,.346,.322,.298,.275,
     *  0.255,0.255,0.255,0.255,0.,
     *  1.99,1.745,1.475,1.185,1.027,0.878,.726,.68,
     *  0.633,.576,0.541,.518,.495,.472,.447,
     *  0.426,.402,.368,.344,.323,0.,0.,
     *  1.975,1.77,1.59,1.365,1.144,1.005,.911,.842,
     *  0.785,.737,.682,.621,.589,.541,.494,
     *  0.472,.447,.426,.4,0.4,0.,0./

        DATA CONEXP/.021,.023,.028,.032,.044,.068,.091,
     * 0.108,.123,.135,.144,.169,.195,.234,
     * 0.282,.328,.417,.50,.652,0.652,0.,0.,
     * 0.032,.039,.047,.052,.057,.063,.082,.091,
     * 0.118,.151,.178,.212,
     * 0.292,.376,.413,.47,.545,.7,.70,.70,.70,0.,.036,
     * 0.042,.054,.071,.090,.118,.152,.176,.193,.222,.244,
     * 0.255,.271,.29,.335,.369,.398,.489,.581,.796,0.,0.,
     * 0.046,.052,.06,.073,.096,.119,.143,.159,.175,.193,
     * 0.22, 0.254, 0.272,.316,
     * 0.364,.403,.447,.493,.580,0.58,0.,0./

         ELSEIF (NTEM.EQ.246) THEN

         ENDIF
CC
      OPEN(UNIT=15,FILE='D.210',STATUS='UNKNOWN')
CC
      READ(15,*) MODEL
      IF(MODEL.EQ.2) THEN
         READ(15,*) K1, K3, K37, KLH
         RNCO=1.0D0
      ELSEIF(MODEL.EQ.3) THEN
         READ(15,*) K1, K3, K37, KLH, KERN2O
      ELSEIF(MODEL.EQ.5) THEN
         READ(15,*) K1, K3, K37, KLH, KERN2O,KERCO
      ELSEIF(MODEL.EQ.6) THEN
         READ(15,*) K1, K3, K37, KLH, K11
      ELSEIF(MODEL.EQ.7) THEN
         READ(15,*) K1, K3, K37, KLH, KER
      ELSEIF(MODEL.EQ.8) THEN
         READ(15,*) K1, K3, K37, KLH, K13
      ELSEIF(MODEL.EQ.9) THEN
         READ(15,*) K1, K3,K37, KLH, AA
      ELSEIF(MODEL.EQ.10) THEN
         READ(15,*) K1, K3, K37, KLH, RNCO
      ENDIF
      DO 200 IRUN=1,1000
        DO 20 ISET=1,NSET
           SUMERR(ISET)=0.0
  20    CONTINUE
        DO 190 IDATA=1,NDATA
           DO 170 ISET=1,NSET
      N2O=FDN2O(ISET)-CONEXP(IDATA,ISET)*FEEDCO(IDATA,ISET)
      CO=FEEDCO(IDATA,ISET)*(1.-CONEXP(IDATA,ISET))

              IF(MODEL.EQ.2) THEN
              CONCAL(IDATA,ISET)=(1./FEEDCO(IDATA,ISET))*
     *         KLH*N2O*(K1*CO-(K3+K37)*N2O)/((K1*CO-K3*N2O)
     *         *(1.+K1*CO-K3*N2O))

              ELSEIF(MODEL.EQ.3) THEN
                 K5=K3*KERN2O/KLH
             CONCAL(IDATA,ISET)=(1./FEEDCO(IDATA,ISET))*(
     *         KLH*N2O*(1.+K5*N2O)*(K1*CO-(K3+K37)*N2O
     *         -K5*K37*N2O**2)/((K1*CO-K3*N2O)
     *         *(1.+K1*CO+(K5-K3)*N2O))+KERN2O
     *         *N2O*(K1*CO-(K3+K37)*N2O-K5*K37*N2O**2)
     *         /(1.+K1*CO+(K5-K3)*N2O)     )

              ELSEIF(MODEL.EQ.5) THEN
                 K5=K3*KERN2O/KLH
                 K8=K3*KERCO/KLH
                 K7=K3/K37
                 AA=(K7*K1-K8)*CO-K7*K3*N2O
                 BB=-K3*N2O*(1.*K5*N2O)-K7*(K1*CO-K3*N2O)
     *                          -K8*CO*(1.+K1*CO+K5*N2O)
                 CC=K3*N2O*(1.+K5*N2O)
                 TO=(-BB+SQRT(BB*BB-4.*AA*CC))/(2.*AA)
                 TCO=((K1*CO-K3*N2O)*(1.-TO)+K8*CO*TO)
     *                   /(1.+K5*N2O+K1*CO-K3*N2O)
                 IF((TO.LT.0.0) .OR. (TO.GT.1.0)
     *              .OR. (TCO.LT.0.0) .OR. (TCO.GT.1.0)
     *              .OR. ((TCO+TO).GT.1.)) THEN
                    TO=(-BB-SQRT(BB*BB-4.*AA*CC))/(2.*AA)
                    TCO=((K1*CO-K3*N2O)*(1.-TO)+K8*CO*TO)
     *                   /(1.+K5*N2O+K1*CO-K3*N2O)
                 ENDIF
              CONCAL(IDATA,ISET)=(1./FEEDCO(IDATA,ISET))*(
     *            KLH*N2O*(1.-TCO-TO) +KERN2O*N2O*TCO)

              ELSEIF(MODEL.EQ.6) THEN
                 K7=K3/K37
                 AA=K7*K11
                 BB=K11*K3*N2O+K7*(K1*CO-K3*N2O+1.)
                 CC=K3*N2O-K7*(K1*CO-K3*N2O)
                 TCO=(-BB+SQRT(BB*BB-4.*AA*CC))/(2.*AA)
                 TO=((K1*CO-K3*N2O)*(1.-TCO)-TCO-K11*TCO
     *               *TCO)/(K1*CO-K3*N2O)
                 IF((TO.LT.0.0) .OR. (TO.GT.1.0)
     *              .OR. (TCO.LT.0.0) .OR. (TCO.GT.1.0)
     *              .OR. ((TCO+TO).GT.1.)) THEN
              TCO=(-BB-SQRT(BB*BB-4.*AA*CC))/(2.*AA)
              TO=((K1*CO-K3*N2O)*(1.-TCO)-TCO-K11*TCO*TCO)
     *                  /(K1*CO-K3*N2O)
                 ENDIF
              CONCAL(IDATA,ISET)=(1./FEEDCO(IDATA,ISET))*
     *        KLH*N2O*(1.0-TCO-TO)
              ELSEIF(MODEL.EQ.7) THEN
                 K7=K3/K37
                 K12=KER*K3/KLH
                 TO=N2O*(K3*(1.+K12*N2O)+K12*K1*CO)
     *                    /(K7*(K1*CO-K3*N2O))
                 TCO=(K1*CO-K3*N2O)*(1.-TO)
     *                    /(1.+(2.*K12-K3)*N2O+K1*CO)
              CONCAL(IDATA,ISET)=(1./FEEDCO(IDATA,ISET))*(
     *               KLH*N2O*(1.-TCO-TO)+KER*N2O*TCO )

              ELSEIF(MODEL.EQ.8) THEN
                 K7=K3/K37
         TO=K3*N2O*(1.+K13*CO)/(K7*(K1*CO-K3*N2O))
         TCO=(K1*CO-K3*N2O)*(1.-TO)/(1.+(K13+K1)*CO-K3*N2O)
         CONCAL(IDATA,ISET)=(1./FEEDCO(IDATA,ISET))*(
     *                  KLH*N2O*(1.-TCO-TO))


              ELSEIF(MODEL.EQ.9) THEN
CC                   SOLVING TCO (surface coverage.)
                 K7=K3/K37
                 NR=1
                 RA=0.0
                 RH=0.02
                 RC=0.0
                 TCO=RA
                 Y0=(1.0-TCO)*(K1*CO-K7*K37*N2O)
     *                 - EXP(AA*TCO)*(TCO+K37*N2O)
   10            RC=RC + RH
                 TCO = RC
                 Y1=(1.0-TCO)*(K1*CO-K7*K37*N2O)
     *                 - EXP(AA*TCO)*(TCO+K37*N2O)
                    IF (Y0*Y1.LT.0.) GOTO 15
                    IF (Y1.EQ.0.) GOTO   15
                    IF (RC.GT.0.99) GOTO 15
                 Y0 = Y1
                 GOTO 10
   15            RA1=RC - RH
                 RB1=RC
                 TCO = RA1
                 Y0=(1.0-TCO)*(K1*CO-K7*K37*N2O)
     *               - EXP(AA*TCO)*(TCO+K37*N2O)
   30            RX = 0.5*(RA1+RB1)
                 TCO = RX
                 Y1=(1.0-TCO)*(K1*CO-K7*K37*N2O)
     *                    - EXP(AA*TCO)*(TCO+K37*N2O)
                   IF (Y1*Y0.GT.0.) RA1=RX
                   IF (Y1*Y0.LT.0.) RB1=RX
                 NR=NR+1
                 IF (NR.GT.90) GOTO 44
               FF=(ABS(Y1)+ABS(Y0))
                 IF (FF.LT.1.0)   GOTO 44
                    GOTO 30

  44             TCO =(RB1+RA1)/2.
                 TO= K37*N2O*(1.-TCO)/(TCO+K37*N2O)
            CONCAL(IDATA,ISET)=(1./FEEDCO(IDATA,ISET))*
     *                  KLH*N2O*(1.-TCO-TO)

              ELSEIF(MODEL.EQ.10) THEN
            CONCAL(IDATA,ISET)=(1./FEEDCO(IDATA,ISET))*
     *     KLH*N2O*(K1*CO-(K3+K37)*N2O)*
     *     (1.+(RNCO-1.)*K1*CO+K37*N2O)
     *     /((1.+RNCO*K1*CO-K3*N2O)*
     *     (K1*CO-K3*N2O+RNCO*K1*K37*CO*N2O-K3*K37*N2O**2))
              ENDIF
              IF(CONCAL(IDATA,ISET).LT.1.) THEN
                 SUMERR(ISET)=SUMERR(ISET)
     *      +(CONCAL(IDATA,ISET)-CONEXP(IDATA,ISET))**2
               ELSE
                  CONCAL(IDATA,ISET)=1.
              ENDIF
 170       CONTINUE
           WRITE(*,900) ((FEEDCO(IDATA,ISET),
     *   CONEXP(IDATA,ISET), CONCAL(IDATA,ISET)),ISET=1,4)
 900       FORMAT(4(F6.2,2F6.3))
 190       CONTINUE
CC
        SUMTOT=0.0
        DO 195 ISET=1,NSET
           SUMTOT=SUMTOT+SUMERR(ISET)
 195    CONTINUE
        WRITE(*,905) (SUMERR(ISET),ISET=1,NSET),SUMTOT
 905    FORMAT(5(1X,1PE10.3),/,'& Enter Model number:')
      MODSAV=MODEL
        READ(*,*) MODEL
        IF(MODEL.LE.0) THEN
           GO TO 210
```

```
         ELSEIF(MODEL.EQ.2) THEN
            WRITE(*,910) K1,K3,K37,KLH
 910     FORMAT(' K1=',1PD9.3,' K3=',1PD9.3,'K3/7=',1PD9.3,
     *         '  KLH=',1PD9.3,
     *          /,'& Enter new values for K1, K3, K3/7, KLH:')
            READ(*,*) K1,K3,K37,KLH
         ELSEIF(MODEL.EQ.3) THEN
            WRITE(*,920) K1,K3,K37,KLH,KERN2O
 920     FORMAT('K1=',1PD9.3,'K3=',1PD9.3,'K3/7=',1PD9.3,
     *    '  KLH=',1PD9.3,'  KERN2O=',1PD9.3,
     *    /,'& Enter new values for K1,K3,K3/7,KLH,KERN2O:')
            READ(*,*) K1,K3,K37,KLH,KERN2O
         ELSEIF(MODEL.EQ.5) THEN
            WRITE(*,930) K1,K3,K37,KLH,KERN2O,KERCO
 930     FORMAT(' K1=',1PD9.3,'K3=',1PD9.3,'K3/7=',1PD9.3,
     *   '  KLH=',1PD9.3,'KERN2O=',1PD9.3,'KERCO=',1PD9.3,
     *     /,'& Enter new values for
     *     K1, K3, K3/7, KLH, KERN2O, KERCO:')
            READ(*,*) K1,K3,K37,KLH,KERN2O,KERCO
         ELSEIF(MODEL.EQ.6) THEN
            WRITE(*,940) K1,K3,K37,KLH,K11
 940     FORMAT('K1=',1PD9.3,'K3=',1PD9.3,'K3/7=',1PD9.3,
     *       '  KLH=',1PD9.3,'  K11=',1PD9.3,
     *    /,'& Enter new values for K1, K3, K3/7, KLH, K11:')
           READ(*,*) K1,K3,K37,KLH,K11
         ELSEIF(MODEL.EQ.7) THEN
            WRITE(*,950) K1,K3,K37,KLH,KER
 950     FORMAT(' K1=',1PD9.3,'K3=',1PD9.3,'K3/7=',1PD9.3,
     *      '  KLH=',1PD9.3,'  KER=',1PD9.3,
     *    /,'& Enter new values for K1, K3, K3/7, KLH, KER:')
            READ(*,*) K1,K3,K37,KLH,KER
         ELSEIF(MODEL.EQ.8) THEN
            WRITE(*,960) K1,K3,K37,KLH,K13
 960       FORMAT(' K1=',1PD9.3,' K3=',1PD9.3,'K3/7=',1PD9.3,
     *       '  KLH=',1PD9.3,'  K13=',1PD9.3,
     *      /,'& Enter new values for K1, K3, K3/7, KLH, K13:')
            READ(*,*) K1,K3,K37,KLH,K13
         ELSEIF(MODEL.EQ.9) THEN
            WRITE(*,970) K1,K3,K37,KLH,AA
 970       FORMAT('K1=',1PD9.3,'K3=',1PD9.3,'K3/7=',1PD9.3,
     *           '  KLH=',1PD9.3,'  AA=',1PD9.3,
     *        /,'& Enter new values for
     *         K1, K3, K3/7, KLH, AA(1.or 0.):')
            READ(*,*) K1,K3,K37,KLH,AA
         ELSEIF(MODEL.EQ.10) THEN
            WRITE(*,980) K1,K3,K37,KLH,RNCO
 980     FORMAT(' K1=',1PD9.3,'K3=',1PD9.3,'K3/7=',1PD9.3,
     *          '  KLH=',1PD9.3,'  Nco=',1PD9.3,
     *  /,'& Enter new values for K1, K3,K3/7,KLH,Nco:')
            READ(*,*) K1,K3,K37,KLH,RNCO
         ENDIF
         IF (K1.LT.0.0) GO TO 210
 200   CONTINUE
 210   CONTINUE
```

```
      WRITE(*,999)
  999 FORMAT('& Do you wish to have a plot (Y/N)? ')
      READ(*,'(A1)') YESNO
      IF(YESNO.EQ.'y' .OR. YESNO.EQ.'Y') THEN
CC       WRITE(*,998)
CC 998   FORMAT('&  1=X vs CO,   2=Rate vs CO:')
CC         READ(*,*) ITYPE
CC       IF(ITYPE.EQ.1) THEN
            CALL XVSCO(FEEDCO,CONCAL,NDATA,NSET,MODSAV)
CC       ELSEIF(ITYPE.EQ.2) THEN
CC           CALL RVSCO(PLTCO,PLTCON,NPLOT,NN2OI)
CC         ENDIF
      ENDIF
      STOP
      END
CC
CC
       SUBROUTINE XVSCO(XCALC,YCALC,NCALC,NSET,MODEL)
       REAL*4 XCALC(NCALC+2,NSET),YCALC(NCALC+2,NSET)
       INTEGER NSYM(4),NDATA(4)
       REAL*4 XDATA(20,4),YDATA(20,4)
       DATA XDATA/1.826,1.65,1.43,1.25,1.015,0.794,0.6696,
     *  0.611, 0.552,0.518,0.485,
     *  0.427,0.369,.333,.298,.265,.228,.206,.18,0.,
     *  1.875,1.69,1.475,1.37,1.25,1.146,.993,.908,.737,
     *  0.611,.54,.485,.39,.346,.322,.298,.275,.255,0.,0.,
     *  1.99,1.745,1.475,1.185,1.027,0.878,.726,.68,
     *  0.633,.576, .541,.518,.495,0.472,.447,
     *  .426,.402,.368,.344,.323,1.975,1.77,
     *  1.59,1.365,1.144,1.005,.911,.842,.785,.737,
     * .682,.621,.589,.541,.494,.472,.447,.426,.4,0./

       DATA YDATA/.021,.023,.028,.032,.044,.068,.091,
     * .108,.123,.135,.144,.169,.195,
     * .234,.282,.328,.417,.50,.652,0.,0.032,.039,.047,
     * .052,.057,.063,.082,.091,.118,.151,.178,.212,
     * .292,.376,.413,.47,.545,.7,.0,.0,.036,
     * .042,.054,.071,.090,.118,.152,.176,.193,.222,.244,
     * .255,.271,.29,.335,.369,.398,.489,.581,.796,.046,
     * .052,.06,.073,.096,.119,.143,.159,.175,.193,.22,.254,
     * .272,.316,.364,.403,.447,.493,.580,0./
       DATA NDATA/19,18,20,19/,NSYM/4,2,6,1/
CC
      XLEN=10.
      YLEN=6.
      XSCALE=2./XLEN
      YSCALE=1./YLEN
      DO 5 I=1,NSET
      XCALC(NDATA(I)+1,I)=0.
      XCALC(NDATA(I)+2,I)=XSCALE
      YCALC(NDATA(I)+1,I)=0.
      YCALC(NDATA(I)+2,I)=YSCALE
  5   CONTINUE
      CALL PLOTS
      CALL METRIC(0)
      CALL PLOT(3.0,3.,-3)
      TEXTHT=0.25
        DO 20 I=1,4
          DO 10 J=1,NDATA(I)
           CALL SYM(XDATA(J,I)/XSCALE,YDATA(J,I)/YSCALE,
     *         TEXTHT*0.5,NSYM(I))
  10      CONTINUE
  20    CONTINUE
        DO 40 IP=1,NSET
       CALL FLINE(XCALC(1,IP),YCALC(1,IP),-NDATA(IP),1,0,1)
  40    CONTINUE
CC
      CALL AXIS(0.,0.,XLEN,0.,10,0,2,1,3,TEXTHT*0.9,1.)
      CALL AXIS(0.,YLEN,-XLEN,0.,10,0,2,1,3,-TEXTHT*0.9,1.)
      CALL AXIS(0.,0.,-YLEN,90.,10,0,1,1,4,TEXTHT*0.9,1.)
      CALL AXIS(XLEN,0.,YLEN,90.,10,0,1,1,4,-TEXTHT*0.9,1.)
      CALL TEXT(2.4,-1.2,TEXTHT,0.,'Percent CO in the Feed')
      CALL TEXT(-1.5,1.5,TEXTHT,90.,'CO Conversion')
      CALL TEXT(-1.,-2.3,TEXTHT*1.1,0.,
     *'Carbon Monoxide Oxidation with Nitrous Oxide')
      XLABEL=XLEN-2.
      YLABEL=4.
      YDEL=0.6
      CALL TEXT(XLABEL,YLABEL,TEXTHT,0.,'%N\Y2\ZO')
      CALL TEXT(XLABEL,YLABEL-YDEL,TEXTHT,0.,'0.303')
      CALL TEXT(XLABEL,YLABEL-2*YDEL,TEXTHT,0.,'0.57')
      CALL TEXT(XLABEL,YLABEL-3*YDEL,TEXTHT,0.,'0.85')
      CALL TEXT(XLABEL,YLABEL-4*YDEL,TEXTHT,0.,'1.15')
      CALL SYM(XLABEL-0.5,YLABEL-YDEL,TEXTHT*0.7,NSYM(1))
      CALL SYM(XLABEL-0.5,YLABEL-2*YDEL,TEXTHT*0.7,NSYM(2))
      CALL SYM(XLABEL-0.5,YLABEL-3*YDEL,TEXTHT*0.7,NSYM(3))
      CALL SYM(XLABEL-0.5,YLABEL-4*YDEL,TEXTHT*0.7,NSYM(4))

      IF(MODEL.EQ.2) THEN
      CALL TEXT(XLABEL-0.7,5.,TEXTHT,0.,'Mechanism No.2')
      ELSEIF(MODEL.EQ.3) THEN
      CALL TEXT(XLABEL-0.7,5.,TEXTHT,0.,'Mechanism No.3')

      ELSEIF(MODEL.EQ.5) THEN
      CALL TEXT(XLABEL-0.7,5.,TEXTHT,0.,'Mechanism No.5')
      ELSEIF(MODEL.EQ.6) THEN
      CALL TEXT(XLABEL-0.7,5.,TEXTHT,0.,'Mechanism No.6')
      ELSEIF(MODEL.EQ.7) THEN
      CALL TEXT(XLABEL-0.7,5.,TEXTHT,0.,'Mechanism No.7')
      ELSEIF(MODEL.EQ.8) THEN
      CALL TEXT(XLABEL-0.7,5.,TEXTHT,0.,'Mechanism No.8')
      ELSEIF(MODEL.EQ.9) THEN
      CALL TEXT(XLABEL-0.7,5.,TEXTHT,0.,'Mechanism No.9')
      ELSEIF(MODEL.EQ.10) THEN
      CALL TEXT(XLABEL-0.7,5.,TEXTHT,0.,'Mechanism No.10')
      ENDIF
      CALL PLOT(0.,0.,999)
        RETURN
```

END

```
      PROGRAM COMP22

      IMPLICIT REAL*8(A-H,K,O-Z)
      PARAMETER (NX=7)
C
C   MODEL FOR NO REACTION WITH CO ON PLATINUM
C        MECHANISM 4

      REAL*8 X(NX+1),XLOW(NX+1),XUPP(NX+1),W(NX+1),
     * PREF(NX+1),OUT(100,NX+2),F(NX),WKAREA(NX+1,3),
     * B(NX+1),BETA(NX+1),J(NX,NX+1),DXDT(NX+1),HMAX(NX+1)
      INTEGER NDIR(NX+1),IAREA(NX+1,2)
      CHARACTER MARK(NX+1)
      COMMON /TOL/ABSDX,RELDX
      READ(5,*)(X(I),I=1,NX+1)
      READ(5,*)(XLOW(I),I=1,NX+1)
      READ(5,*)(XUPP(I),I=1,NX+1)
      READ(5,*)(W(I),I=1,NX+1)
      READ(5,*)(HMAX(I),I=1,NX+1)
      READ(5,*)(PREF(I),I=1,NX+1)
      READ(5,*)(NDIR(I),I=1,NX+1)
      READ(5,*)EPS,HH,E
      READ(5,*)NCORR,NCRAD,MAXOUT,NPRNT,INITAL,ITIN
      READ(5,*)ABSDX,RELDX
      CALL INPUT(NX)

      CALL DERPAR(NX,X,XLOW,XUPP,EPS,W,INITAL,ITIN,HH,
     *         HMAX,PREF,NDIR,E,NCORR,NCRAD,NOUT,
     *         OUT,MAXOUT,NPRNT,MARK,
     *         WKAREA,IAREA,B,F,J,BETA,DXDT)
      WRITE(6,300)ITIN,NOUT,MAXOUT
  300 FORMAT('ITIN = ',I5,'NOUT = ',I5,'MAXOUT = ',I5)
      STOP
      END
      SUBROUTINE INPUT(N)
      IMPLICIT REAL*8(A-H,K,O-Z)
      REAL*8 XX(N+1),F(N)
      REAL*8 PF(3),P(29),NCO,NOP
      CHARACTER MARK(N+1)
      EQUIVALENCE (P(1),COP),(P(2),RKM1PE),(P(3),E1R),
     *(P(4),RK2PE),(P(5),E2R),(P(6),RK3PE),(P(7),E3R),
     *(P(8),RK4PE),(P(9),E4R),(P(10),NCOP),(P(11),RKM5PE),
     *(P(12),E5R),(P(13),RK8PE),(P(14),E8R),(P(15),RK9PE),
     *(P(16),E9R),(P(17),RKM9PE),(P(18),EM9R),
     *(P(19),RK11PE),(P(20),EM11R),(P(21),A),(P(22),V),
     *(P(23),RL),(P(24),TO),(P(25),PO),(P(26),QSC),
     *(P(27),FNO),(P(28),FCO),(P(29),NCO)

      DATA PF/3*0.D0/
      COMMON /TOL/ABSDX,RELDX
  900 FORMAT(//,3D40.16,/)
  901 FORMAT(//,2D40.16,/)
```

```
905  FORMAT(//,I20,I50,/)
906   FORMAT(/,D40.16)

     READ(5,900) COP,RKM1PE,E1R
     READ(5,901) RK2PE,E2R
     READ(5,901) RK3PE,E3R
     READ(5,901) RK4PE,E4R
     READ(5,900) NOP,RKM5PE,E5R
     READ(5,901) RK8PE,E8R
     READ(5,901) RK9PE,E9R
     READ(5,901) RKM9PE,EM9R
     READ(5,901) RK11PE,E11R

     READ(5,900) A,V,RL
     READ(5,900) TO,PO,QSC
     READ(5,901) FNO,FCO
     READ(5,905) IPAR,IPF
     READ(5,906) NCO
     PF(IPF)=1.D0
     RETURN

     ENTRY FCN(N,XX,F)
     XCO=XX(1)
     XNO=XX(2)
     XN2O=XX(3)
     SCO=XX(4)
     SNO=XX(5)
     SO=XX(6)
     SN=XX(7)
     SE=1.D0-SCO-SO-SNO-SN
     IF(SE.LT.0.0D0) SE=0.0D0
     P(IPAR)=PF(1)*DEXP(XX(N+1))+PF(2)*XX(N+1)
    *  +PF(3)*DLOG(XX(N+1))
     QO=QSC*(TO/294.15D0)*(0.101325D+06/PO)*(1.D-06/60.D0)

     CONCT=PO/(8.314D0*TO)

     RK1=6.87D0*COP*DSQRT(TO)/RL
     RKM1=RKM1PE*EXP(-E1R/TO)
     RK2=RK2PE*EXP(-E2R/TO)
     RK3=RK3PE*EXP(-E3R/TO)
     RK4=RK4PE*EXP(-E4R/TO)

     RK5=6.637D0*NOP*DSQRT(TO)/RL
     RKM5=RKM5PE*EXP(-E5R/TO)
     RK8=RK8PE*EXP(-E8R/TO)
     RK9=RK9PE*EXP(-E9R/TO)
     RKM9=RKM9PE*EXP(-EM9R/TO)
     RK11=RK11PE*EXP(-E11R/TO)

C        CO(g):
       F(1)=  QO*FCO*CONCT*XCO/(A*RL)
    *  - RK1*FCO*CONCT*(1.D0-XCO)*SE*(1.D0-NCO*SCO)
    *  /(1.D0-SCO)
```

```
     *  + RKM1*SCO -RK4*FCO*CONCT*(1.D0-XCO)*SO

C        NO(g)
        F(2) = QO*FNO*CONCT*XNO/(A*RL)
     *   -RK5*FNO*CONCT*(1.D0-XNO)*SE + RKM5*SNO

C        N2O(g)
        F(3) = - QO*XN2O*CONCT/(A*RL) + RK8*SNO*RL*SN
     *   - RK2*XN2O*CONCT*SE

C        CO-M
        F(4)=  RK1*FCO*CONCT*(1.D0-XCO)*SE*(1.D0-NCO*SCO)
     *  /(1.D0-SCO)- RKM1*SCO - RK3*SCO*SO*RL

C        NO-M
        F(5)= RK5*FNO*CONCT*(1D0-XNO)*SE -RKM5*SNO
     *  -RK8*RL*SNO*SN -RK9*SNO*SE*RL+RKM9*SN*SO*RL

C        O-M:
       F(6)= RK2*XN2O*CONCT*SE - RK3*SCO*SO*RL
     *  - RK4*FCO*CONCT*(1.D0-XCO)*SO+RK9*SNO*SE*RL
     *  -RKM9*SN*SO*RL

C        N-M
       F(7)= -RK8*SNO*SN*RL - 2.D0*RK11*SN*SN*RL
     *   + RK9*SNO*SE*RL - RKM9*SN*SO*RL


      RETURN
      ENTRY OUTPUT(XX,SQUAR,MARK,NPRP,IK,IWRITE)
      DO 160 I=1,N+1
      MARK(I)=' '
  160 CONTINUE
       MARK(IK) ='*'
       ALPHA=PF(1)*DEXP(XX(N+1))+PF(2)*XX(N+1)
     *   +PF(3)*DLOG(XX(N+1))
       OO= XX(3) - XX(2)*FNO/2.
       SELECT=-XX(3)/OO
       IF (OO.GT.0.0)  SELECT=0.0
       WRITE(6,800)NPRP,ALPHA,(XX(I),I=1,N),SELECT
 800  FORMAT(I2,1PD10.3,7(1PD9.2),1PD7.1)
      RETURN
      END

      SUBROUTINE DERPAR(N,X,XLOW,XUPP,EPS,W,INITAL,ITIN,HH,
     * HMAX,PREF,NDIR,E,NCORR,NCRAD,NOUT,OUT,
     * MAXOUT,NPRNT,MARK,WKAREA,IAREA,B,
     * F,G,BETA,DXDT)
      IMPLICIT REAL*8(A-H,O-Z)
      DIMENSION X(N+1),XLOW(N+1),XUPP(N+1),W(N+1),HMAX(N+1),
     * PREF(N+1),NDIR(N+1),OUT(100,N+2),F(N),G(N,N+1),
     * BETA(N+1),DXDT(N+1),B(N+1),WKAREA(N+1,3),
     * IAREA(N+1,2),X2(4)
      COMMON /TOL/ABSDX,RELDX
      CHARACTER MARK(N+1)
C OBTAINING OF DEPENDENCE OF SOLUTION X(ALFA) OF EQUATION
C F ( X ,ALFA ) = 0
C ON PARAMETER ALFA BY MODIFIED METHOD OF DIFFERENTIATION
C WITH RESPECT TO PARAMETER
C N - NUMBER OF UNKNOWNS X(I)
C X(1),...,X(N) - INITIAL VALUES OF X(I),AFTER RETURN
C                 FINAL VALUES OF X(I)
C X(N+1) - INITIAL VALUE OF PARAMETER ALFA,AFTER RETURN
C          FINAL VALUE OF ALFA
C XLOW(1),...,XLOW(N) - LOWER BOUNDS FOR X(I)
C XUPP(1),...,XUPP(N) - UPPER BOUNDS FOR X(I)
C XLOW(N+1),XUPP(N+1) - LOWER AND UPPER BOUNDS FOR ALFA
C    IF XLOW OR XUPP IS EXCEEDED,THEN END OF DERPAR
C    AND MAXOUT=-2 AFTER RETURN
C EPS - ACCURACY DESIRED IN NEWTON ITERATION FOR
C    SUM OF (W(I)*DABS(XNEW(I)-XOLD(I))),I=1,...,N+1
C W(1),...,W(N+1) - WEIGHTS USED IN TERMINATION CRITERION
C                   OF NEWTON PROCESS
C INITAL - IF (INITAL.NE.0) THEN SEVERAL STEPS IN NEWTON
C          ITERATION ARE MADE BEFORE COMPUTATION IN ORDER
C           TO INCREASE ACCURACY OF INITIAL POINT-
C     IF (INITAL.EQ.1.AND.EPS-ACCURACY IS NOT FULFILLED
C     IN ITIN ITERATIONS) THEN RETURN. IF (INITAL.EQ.2)
C     THEN ALWAYS RETURN
C     AFTER INITIAL NEWTON ITERATION,RESULTS ARE IN X.
C   IF (INITAL.EQ.3)
C         THEN CONTINUE IN DERPAR AFTER INITIAL NEWTON.
C   IF (INITAL.EQ.0)
C         THEN NO INITIAL NEWTON ITERATION IS USED.
C ITIN - MAXIMAL NUMBER OF INITIAL NEWTON ITERATIONS. IF
C    EPS-ACCURACY IS NOT FULFILLED IN ITIN ITERATIONS THEN
C       ITIN=-1 AFTER RETURN.
C HH - INTEGRATION STEP ALONG ARC LENGTH OF SOLUTION LOCUS
C HMAX(1),...,HMAX(N+1) - UPPER BOUNDS FOR INCREMENTS OF
C       X(I) IN ONE INTEGRATION STEP (APPROXIMATION ONLY)
C PREF(1),...,PREF(N+1) - PREFERENCE NUMBERS (EXPLANATION
C                         SEE IN SUBR.GAUSE)
C NDIR(1),...,NDIR(N+1) - INITIAL CHANGE OF X(I)
                          IS POSITIVE ALONG
C     SOLUTION LOCUS (CURVE) IF NDIR(I)=1 AND NEGATIVE IF
C     NDIR(I)=-1.
C E - CRITERION FOR TEST ON CLOSED CURVE,IF
C  (SUM OF (W(I)*DABS(X(I)-XINITIAL(I))),I=1,..,N+1).LE.E)
C    THEN CLOSED CURVE MAY BE EXPECTED.
C MXADMS - MAXIMAL ORDER OF ADAMS-BASHFORTH FORMULA,
C          1.LE.MXADMS.LE.4.
C NCORR - MAXIMAL NUMBER OF NEWTON CORRECTIONS AFTER
C   PREDICTION  BY ADAMS-BASHFORTH METHOD.
C NCRAD - IF (NCRAD.NE.0) THEN ADDITIONAL NEWTON CORRECTION
C    WITHOUT NEW COMPUTATION OF JACOBIAN MATRIX IS USED.
C NOUT - AFTER RETURN NUMBER OF CALCULATED POINTS ON THE
C        CURVE X(ALFA),NOUT.LE.MAXOUT.
C OUT(J,1),OUT(J,2),...,OUT(J,N+1) - J-TH POINT X(1),...,
C    X(N),ALFA ON CURVE X(ALFA)
C OUT(J,N+2) - VALUE OF DSQRT(SUM OF SQUARES OF F).
C    IF (OUT(J,N+2).LT.0.D0) THEN  DABS(OUT(J,N+2))
C    CORRESPONDS TO X AND ALFA NOT EXACTLY,
C    BECAUSE ADDITIONAL NEWTON CORRECTION WAS
C    USED (NCRAD.NE.0).
C    VALUES F(I) ARE NOT COMPUTED FOR X AND ALFA PRINTED
C    AND/OR STORED AND THEREFORE
C    LAST TIME COMPUTED VALUE OF DSQRT(SUM OF
C    SQUARES OF F) IS ON OUR DISPOSAL ONLY.
C  MAXOUT - MAXIMAL NUMBER OF CALCULATED POINTS
C                        ON CURVE X(ALFA).
C    IF MAXOUT AFTER RETURN EQUALS TO-
C      -1 - THEN CLOSED CURVE X(ALFA) MAY BE EXPECTED
C      -2 - THEN BOUND XLOW OR XUPP WAS EXCEEDED
C      -3 - THEN SINGULAR JACOBIAN MATRIX OCCURRED,
C              ITS RANK IS .LT. N.
C NPRNT - IF (NPRNT.EQ.3) THEN RESULTING POINTS
C    ON CURVE X(ALFA) ARE IN ARRAY OUT( ,) AFTER RETURN.
C    IF (NPRNT.EQ.1) THEN THESE POINTS ARE PRINTED ONLY.
C      IF (NPRNT.EQ.2) THEN THESE POINTS ARE
C    BOTH PRINTED AND IN ARRAY OUT.
C SUBROUTINE FCTN MUST BE PROGRAMMED IN FOLLOWING FORM -
C   SUBROUTINE FCTN(N,X,F,G)
C   DIMENSION X(11),F(10),G(10,11)
C   F(I)= FI (X(1),X(2),...,X(N),ALFA) FOR I=1,...,N
C   G(I,J)= D FI (X(1),...,X(N),
C                       ALFA)/ D X(J) FOR I,J=1,...,N
C   G(I,N+1)= D FI (X(1),...,X(N),
C                       ALFA)/ D ALFA  FOR I=1,...,N
C   RETURN
C   END
C LW IS PRINTER DEVICE NUMBER
      N1 = N + 1
      LW = 6
      IF (INITAL) 10,60,10
C INITIAL NEWTON ITERATIONS
   10 DO 40 L=1,ITIN
        CALL FCN(N,X,F)
        CALL NUJACX(FCN,X,N,G,ABSDX,RELDX,WKAREA,IFLAG)
      IF(IFLAG.GT.0) WRITE(6,9000) IFLAG
 9000 FORMAT(' ',20X,'WARNING:    IFLAG FROM NUJACX = ',I2)
        SQUAR = 0.D0
        DO 20 I=1,N
          SQUAR = SQUAR + F(I)**2
   20   CONTINUE
        LL = L - 1
        SQUAR = DSQRT(SQUAR)
       IF (NPRNT.NE.3) WRITE (LW,99999) LL,
     *    (X(I),I=1,N1),SQUAR
        CALL GAUSE(N,G,F,B,M,PREF,BETA,K,WKAREA,IAREA)
        IF (M.EQ.0) GO TO 310
        P = 0.D0
        DO 30 J=1,N1
```

```
          X(J) = X(J) - B(J)
          P = P + DABS(B(J))*W(J)
   30   CONTINUE
        IF (P.LE.EPS) GO TO 50
   40 CONTINUE
      WRITE (LW,99998) ITIN
      ITIN = -1
      IF (INITAL.EQ.1) RETURN
   50 IF (NPRNT.NE.3) WRITE (LW,99997) (X(I),I=1,N1)
      IF (INITAL.EQ.2) RETURN
C AFTER INITIAL NEWTON ITERATIONS
   60 IF (NPRNT.NE.3) WRITE (LW,99996)
      KOUT = 0
      NOUT = 0
      MADMS = 0
      NC = 1
      K1 = 0
  70    CALL FCN(N,X,F)
        CALL NUJACX(FCN,X,N,G,ABSDX,RELDX,WKAREA,IFLAG)
      IF(IFLAG.GT.0) WRITE(6,9000) IFLAG
      SQUAR = 0.D0
      DO 80 I=1,N
        SQUAR = SQUAR + F(I)**2
   80 CONTINUE
        CALL GAUSE(N,G,F,B,M,PREF,BETA,K,WKAREA,IAREA)
      IF (M.EQ.0) GO TO 310
      IF (K1.EQ.K) GO TO 90
C CHANGE OF INDEPENDENT VARIABLE (ITS INDEX = K NOW)
      MADMS = 0
      K1 = K
   90 SQUAR = DSQRT(SQUAR)
      IF (NCRAD.EQ.1) SQUAR = -SQUAR
      P = 0.D0
      DO 100 I=1,N1
        P = P + W(I)*DABS(B(I))
  100 CONTINUE
      IF (P.LE.EPS) GO TO 130
      IF (NC.GE.NCORR) GO TO 120
      DO 110 I=1,N1
        X(I) = X(I) - B(I)
  110 CONTINUE
C ONE ITERATION IN NEWTON METHOD
      NC = NC + 1
      GO TO 70
  120 IF (NCORR.EQ.0) GO TO 130
      WRITE (LW,99995) NCORR,P
  130 NC = 1
      IF (NCRAD.EQ.0) GO TO 150
C ADDITIONAL NEWTON CORRECTION
      DO 140 I=1,N1
        X(I) = X(I) - B(I)
  140 CONTINUE
  150 NOUT = NOUT + 1
        CALL NUJACX(FCN,X,N,G,ABSDX,RELDX,WKAREA,IFLAG)
      IF(IFLAG.GT.0) WRITE(6,9000) IFLAG
      CALL HSBG(N,G,N)
      CALL ATEIG(N,G,WKAREA(1,1),WKAREA(1,2),IAREA,N)
      NPRP=0
      DO 165 I=1,N
          IF(WKAREA(I,1).GT.0.D0)NPRP=NPRP+1
 165  CONTINUE
 163  IF (NPRNT.EQ.3) GO TO 170
C     WRITE (LW,99994)
      CALL OUTPUT(X,SQUAR,MARK,NPRP,K,IWRITE)
  170 IF (NPRNT.EQ.1) GO TO 200
      IF (NOUT.LE.100) GO TO 180
      WRITE (LW,99992)
      RETURN
  180 DO 190 I=1,N1
          OUT(NOUT,I)=X(I)
 190  CONTINUE
      OUT(NOUT,N+2)=SQUAR
      GO TO 210
  200 IF (NOUT.EQ.1) GO TO 180
  210 IF (NOUT.GE.MAXOUT) RETURN
      DO 220 I=1,N1
      IF (X(I).LT.XLOW(I) .OR. X(I).GT.XUPP(I)) GO TO 300
  220 CONTINUE
      IF (NOUT.LE.3) GO TO 240
      P = 0.D0
      DO 230 I=1,N1
        P = P + W(I)*DABS(X(I)-OUT(1,I))
  230 CONTINUE
      IF (P.LE.E) GO TO 290
C CLOSED CURVE MAY BE EXPECTED
  240 DXK2 = 1.D0
      DO 250 I=1,N1
        DXK2 = DXK2 + BETA(I)**2
  250 CONTINUE
      DXDT(K) = 1.D0/DSQRT(DXK2)*DFLOAT(NDIR(K))
C DERIVATIVE OF INDEPENDENT VARIABLE X(K)
C WITH RESPECT TO ARC LENGTH
C OF SOLUTION LOCUS IS COMPUTED HERE
      H = HH
      DO 270 I=1,N1
        NDIR(I) = 1
        IF (I.EQ.K) GO TO 260
        DXDT(I) = BETA(I)*DXDT(K)
  260   IF (DXDT(I).LT.0.D0) NDIR(I) = -1
        IF (H*DABS(DXDT(I)).LE.HMAX(I)) GO TO 270
        MADMS = 0
        H = HMAX(I)/DABS(DXDT(I))
  270 CONTINUE
      IF (NOUT.LE.KOUT+3) GO TO 280
      IF (H*DABS(DXDT(K)).LE.0.8D0*DABS(X(K)-OUT(1,K)))
     *     GO TO 280
      IF ((OUT(1,K)-X(K))*DFLOAT(NDIR(K)).LE.0.D0)
     *     GO TO 280
```

```
      MADMS = 0
      IF (H*DABS(DXDT(K)).LE.DABS(X(K)-OUT(1,K)))
     *     GO TO 280
      H = DABS(X(K)-OUT(1,K))/DABS(DXDT(K))
      KOUT = NOUT
 280  CONTINUE
      DO 239 III=1,N+1
          X(III)=DXDT(III)*H+X(III)
 239  CONTINUE
C 280 CALL ADAMS(N,DXDT,MADMS,H,X,MXADMS)
C 280 CALL RKF45(T,X,N,F2,H,DT,HMXFR,ABSER,RELER,IFLAG,
C    *    DXDT,K,BETA)
      GO TO 70
  290 WRITE (LW,99991)
      MAXOUT = -1
      RETURN
  300 MAXOUT = -2
      RETURN
  310 WRITE (LW,99990) (X(I),I=1,N1)
      MAXOUT = -3
      RETURN
99999 FORMAT (3X,7H DERPAR,I3,25H.INITIAL NEWTON
     * ITERATION/22X,11HX,ALFA,SQF=,8(1PD15.7))
99998 FORMAT (/16H DERPAR OVERFLOW,I5,2X,
     * 18HINITIAL ITERATIONS/)
99997 FORMAT (3X,39H DERPAR AFTER INITIAL NEWTON ITERATIONS,
     *  /22X 7HX,ALFA=,4X,5(1PD15.7)/(33X,5F15.7))
99996 FORMAT (/6X,45H DERPAR RESULTS (VARIABLE CHOSEN AS
     *  INDEPENDE,18HNT IS MARKED BY *)/)
99995 FORMAT (/37H DERPAR NUMBER OF NEWTON CORRECTIONS=,I5,
     * 31H  IS NOT SUFFICIENT,ERROR OF X=,1PD15.7/)
99994 FORMAT (6X,27H DERPAR RESULTS X,ALFA,SQF=)
99993 FORMAT(7(1PD12.5,A1),1X,1PD12.5,2X,I3)
99992 FORMAT (/28H DERPAR OUTPUT ARRAY IS FULL//)
99991 FORMAT (/36H DERPAR CLOSED CURVE MAY BE EXPECTED/)
99990 FORMAT (/48H DERPAR SINGULAR JACOBIAN MATRIX FOR X
     * AND ALFA=, 5F12.6/(48X,5F12.6))
      END
C        SUBROUTINE HSBG
C
C        PURPOSE
C TO REDUCE A REAL MATRIX INTO UPPER ALMOST TRIANGULAR FORM
C
C        USAGE
C           CALL HSBG(N,A,IA)
C
C        DESCRIPTION OF THE PARAMETERS
C   N   ORDER OF THE MATRIX
C   A   THE INPUT MATRIX, N BY N
C  IA   SIZE OF THE FIRST DIMENSION ASSIGNED TO THE ARRAY
C        A IN THE CALLING PROGRAM WHEN THE MATRIX IS IN
C        DOUBLE SUBSCRIPTED DATA STORAGE MODE.  IA=N WHEN
C        THE MATRIX IS IN SSP VECTOR STORAGE MODE.
C
```

```
C          REMARKS
C       THE HESSENBERG FORM REPLACES THE ORIGINAL MATRIX IN
THE
C             ARRAY A.
C
C      SUBROUTINES AND FUNCTION SUBPROGRAMS REQUIRED
C             NONE
C
C          METHOD
C     SIMILARITY TRANSFORMATIONS USING ELEMENTARY ELIMINATION
C           MATRICES, WITH PARTIAL PIVOTING.
C
C          REFERENCES
C      J.H. WILKINSON - THE ALGEBRAIC EIGENVALUE PROBLEM -
C      CLARENDON PRESS, OXFORD, 1965.
C
C        SEE IBM SSP MANUAL FOR ADDITIONAL INFORMATION
C
C .......................................................
C
      SUBROUTINE HSBG(N,A,IA)
      IMPLICIT REAL*8(A-H,O-Z)
      REAL*8 A(1)
      L=N
      NIA=L*IA
      LIA=NIA-IA
C
C          L IS THE ROW INDEX OF THE ELIMINATION
C
   20 IF(L-3) 360,40,40
   40 LIA=LIA-IA
      L1=L-1
      L2=L1-1
C
C          SEARCH FOR THE PIVOTAL ELEMENT IN THE LTH ROW
C
      ISUB=LIA+L
      IPIV=ISUB-IA
      PIV=DABS(A(IPIV))
      IF(L-3) 90,90,50
   50 M=IPIV-IA
      DO 80 I=L,M,IA
      T=DABS(A(I))
      IF(T-PIV) 80,80,60
   60 IPIV=I
      PIV=T
   80 CONTINUE
   90 IF(PIV) 100,320,100
  100 IF(PIV-DABS(A(ISUB))) 180,180,120
C
C          INTERCHANGE THE COLUMNS
C
  120 M=IPIV-L
      DO 140 I=1,L
      J=M+I
      T=A(J)
      K=LIA+I
      A(J)=A(K)
  140 A(K)=T
C
C        INTERCHANGE THE ROWS
C
      M=L2-M/IA
      DO 160 I=L1,NIA,IA
      T=A(I)
      J=I-M
      A(I)=A(J)
  160 A(J)=T
C
C        TERMS OF THE ELEMENTARY TRANSFORMATION
C
  180 DO 200 I=L,LIA,IA
  200 A(I)=A(I)/A(ISUB)
C
C        RIGHT TRANSFORMATION
C
      J=-IA
      DO 240 I=1,L2
      J=J+IA
      LJ=L+J
      DO 220 K=1,L1
      KJ=K+J
      KL=K+LIA
  220 A(KJ)=A(KJ)-A(LJ)*A(KL)
  240 CONTINUE
C
C        LEFT TRANSFORMATION
C
      K=-IA
      DO 300 I=1,N
      K=K+IA
      LK=K+L1
      S=A(LK)
      LJ=L-IA
      DO 280 J=1,L2
      JK=K+J
      LJ=LJ+IA
  280 S=S+A(LJ)*A(JK)*1.0D0
  300 A(LK)=S
C
C        SET THE LOWER PART OF THE MATRIX TO ZERO
C
      DO 310 I=L,LIA,IA
  310 A(I)=0.0D0
  320 L=L1
      GO TO 20
  360 RETURN
      END
```

```
C
C     ....................................................
C
C        SUBROUTINE ATEIG
C
C        PURPOSE
C              COMPUTE THE EIGENVALUES
C        OF A REAL ALMOST TRIANGULAR MATRIX
C
C        USAGE
C           CALL ATEIG(M,A,RR,RI,IANA,IA)
C
C      DESCRIPTION OF THE PARAMETERS
C  M   ORDER OF THE MATRIX
C  A   THE INPUT MATRIX, M BY M
C  RR  VECTOR CONTAINING THE REAL PARTS OF THE EIGENVALUES
C      ON RETURN
C  RI  VECTOR CONTAINING THE IMAGINARY PARTS OF THE EIGEN-
C      VALUES ON RETURN
C  IAN VECTOR WHOSE DIMENSION MUST BE GREATER THAN OR EQUAL
C      TO M, CONTAINING ON RETURN INDICATIONS ABOUT THE WAY
C      THE EIGENVALUES APPEARED (SEE MATH. DESCRIPTION)
C  IA  SIZE OF THE FIRST DIMENSION ASSIGNED TO THE ARRAY A
C      IN THE CALLING PROGRAM WHEN THE MATRIX IS IN DOUBLE
C      SUBSCRIPTED DATA STORAGE MODE.
C      IA=M WHEN THE MATRIX IS IN SSP VECTOR STORAGE MODE.
C
C        REMARKS
C           THE ORIGINAL MATRIX IS DESTROYED
C   THE DIMENSION OF RR AND RI MUST BE GREATER OR EQUAL TO M
C
C        SUBROUTINES AND FUNCTION SUBPROGRAMS REQUIRED
C           NONE
C
C        METHOD
C           QR DOUBLE ITERATION
C
C
C           SEE IBM SSP MANUAL FOR ADDITIONAL INFORMATION
C
C     ....................................................
C
      SUBROUTINE ATEIG(M,A,RR,RI,IANA,IA)
      IMPLICIT REAL*8(A-H,O-Z)
      REAL*8 A(1),RR(1),RI(1),PRR(2),PRI(2)
      INTEGER P,P1,Q,IANA(1)
C
      E8=1.0D-08
      E6=1.0D-06
      E10=1.0D-10
      DELTA=0.5D0
      MAXIT=30
C
C        INITIALIZATION
```

```
C
      N=M
   20 N1=N-1
      IN=N1*IA
      NN=IN+N
      IF(N1) 30,1300,30
   30 NP=N+1
C
C        ITERATION COUNTER
C
      IT=0
C
C  ROOTS OF THE 2ND ORDER MAIN SUBMATRIX AT THE PREVIOUS
C  ITERATION
C
      DO 40 I=1,2
      PRR(I)=0.0D0
   40 PRI(I)=0.0D0
C
C  LAST TWO SUBDIAGONAL ELEMENTS AT THE PREVIOUS ITERATION
C
      PAN=0.0D0
      PAN1=0.0D0
C
C        ORIGIN SHIFT
C
      R=0.0D0
      S=0.0D0
C
C        ROOTS OF THE LOWER MAIN 2 BY 2 SUBMATRIX
C
      N2=N1-1
      IN1=IN-IA
      NN1=IN1+N
      N1N=IN+N1
      N1N1=IN1+N1
   60 T=A(N1N1)-A(NN)
      U=T*T
      V=4.0D0*A(N1N)*A(NN1)
      IF(DABS(V)-U*E8) 100,100,65
   65 T=U+V
      IF(DABS(T)-DMAX1(U,DABS(V))*E6) 67,67,68
   67 T=0.0D0
   68 U=(A(N1N1)+A(NN))/2.0D0
      V=DSQRT(DABS(T))/2.0D0
      IF(T)140,70,70
   70 IF(U) 80,75,75
   75 RR(N1)=U+V
      RR(N)=U-V
      GO TO 130
   80 RR(N1)=U-V
      RR(N)=U+V
      GO TO 130
  100 IF(T)120,110,110
  110 RR(N1)=A(N1N1)
      RR(N)=A(NN)
      GO TO 130
  120 RR(N1)=A(NN)
      RR(N)=A(N1N1)
  130 RI(N)=0.0D0
      RI(N1)=0.0D0
      GO TO 160
  140 RR(N1)=U
      RR(N)=U
      RI(N1)=V
      RI(N)=-V
  160 IF(N2)1280,1280,180
C
C        TESTS OF CONVERGENCE
C
  180 N1N2=N1N1-IA
      RMOD=RR(N1)*RR(N1)+RI(N1)*RI(N1)
      EPS=E10*DSQRT(RMOD)
      IF(DABS(A(N1N2))-EPS)1280,1280,240
  240 IF(DABS(A(NN1))-E10*DABS(A(NN))) 1300,1300,250
  250 IF(DABS(PAN1-A(N1N2))-DABS(A(N1N2))*E6) 1240,1240,260
  260 IF(DABS(PAN-A(NN1))-DABS(A(NN1))*E6)1240,1240,300
  300 IF(IT-MAXIT) 320,1240,1240
C
C        COMPUTE THE SHIFT
C
  320 J=1
      DO 360 I=1,2
      K=NP-I
      IF(DABS(RR(K)-PRR(I))+DABS(RI(K)-PRI(I))
     *  -DELTA*(DABS(RR(K))+DABS(RI(K)))) 340,360,360
  340 J=J+I
  360 CONTINUE
      GO TO (440,460,460,480),J
  440 R=0.0D0
      S=0.0D0
      GO TO 500
  460 J=N+2-J
      R=RR(J)*RR(J)
      S=RR(J)+RR(J)
      GO TO 500
  480 R=RR(N)*RR(N1)-RI(N)*RI(N1)
      S=RR(N)+RR(N1)
C
C        SAVE THE LAST TWO SUBDIAGONAL
C        TERMS AND THE ROOTS OF THE
C        SUBMATRIX BEFORE ITERATION
C
  500 PAN=A(NN1)
      PAN1=A(N1N2)
      DO 520 I=1,2
      K=NP-I
      PRR(I)=RR(K)
  520 PRI(I)=RI(K)
C
C         SEARCH FOR A PARTITION OF THE MATRIX,
C         DEFINED BY P AND Q
C
      P=N2
      IF (N-3)600,600,525
  525 IPI=N1N2
      DO 580 J=2,N2
      IPI=IPI-IA-1
      IF(DABS(A(IPI))-EPS) 600,600,530
  530 IPIP=IPI+IA
      IPIP2=IPIP+IA
      D=A(IPIP)*(A(IPIP)-S)+A(IPIP2)*A(IPIP+1)+R
      IF(D)540,560,540
  540 IF(DABS(A(IPI)*A(IPIP+1))*(DABS(A(IPIP)+A(IPIP2+1)-S)
     *  +DABS(A(IPIP2+2))) -DABS(D)*EPS) 620,620,560
  560 P=N1-J
  580 CONTINUE
  600 Q=P
      GO TO 680
  620 P1=P-1
      Q=P1
      IF (P1-1) 680,680,650
  650 DO 660 I=2, P1
      IPI=IPI-IA-1
      IF(DABS(A(IPI))-EPS)680,680,660
  660 Q=Q-1
C
C         QR DOUBLE ITERATION
C
  680 II=(P-1)*IA+P
      DO 1220 I=P,N1
      II1=II-IA
      IIP=II+IA
      IF(I-P)720,700,720
  700 IPI=II+1
      IPIP=IIP+1
C
C         INITIALIZATION OF THE TRANSFORMATION
C
      G1=A(II)*(A(II)-S)+A(IIP)*A(IPI)+R
      G2=A(IPI)*(A(IPIP)+A(II)-S)
      G3=A(IPI)*A(IPIP+1)
      A(IPI+1)=0.0D0
      GO TO 780
  720 G1=A(II1)
      G2=A(II1+1)
      IF(I-N2)740,740,760
  740 G3=A(II1+2)
      GO TO 780
  760 G3=0.0D0
  780 CAP=DSQRT(G1*G1+G2*G2+G3*G3)
      IF(CAP)800,860,800
  800 IF(G1)820,840,840
  820 CAP=-CAP
  840 T=G1+CAP
      PSI1=G2/T
      PSI2=G3/T
      ALPHA=2.0D0/(1.0D0+PSI1*PSI1+PSI2*PSI2)
      GO TO 880
  860 ALPHA=2.0D0
      PSI1=0.0D0
      PSI2=0.0D0
  880 IF(I-Q)900,960,900
  900 IF(I-P)920,940,920
  920 A(II1)=-CAP
      GO TO 960
  940 A(II1)=-A(II1)
C
C        ROW OPERATION
C
  960 IJ=II
      DO 1040 J=I,N
      T=PSI1*A(IJ+1)
      IF(I-N1)980,1000,1000
  980 IP2J=IJ+2
      T=T+PSI2*A(IP2J)
 1000 ETA=ALPHA*(T+A(IJ))
      A(IJ)=A(IJ)-ETA
      A(IJ+1)=A(IJ+1)-PSI1*ETA
      IF(I-N1)1020,1040,1040
 1020 A(IP2J)=A(IP2J)-PSI2*ETA
 1040 IJ=IJ+IA
C
C        COLUMN OPERATION
C
      IF(I-N1)1080,1060,1060
 1060 K=N
      GO TO 1100
 1080 K=I+2
 1100 IP=IIP-I
      DO 1180 J=Q,K
      JIP=IP+J
      JI=JIP-IA
      T=PSI1*A(JIP)
      IF(I-N1)1120,1140,1140
 1120 JIP2=JIP+IA
      T=T+PSI2*A(JIP2)
 1140 ETA=ALPHA*(T+A(JI))
      A(JI)=A(JI)-ETA
      A(JIP)=A(JIP)-ETA*PSI1
      IF(I-N1)1160,1180,1180
 1160 A(JIP2)=A(JIP2)-ETA*PSI2
 1180 CONTINUE
      IF(I-N2)1200,1220,1220
 1200 JI=II+3
      JIP=JI+IA
      JIP2=JIP+II
      ETA=ALPHA*PSI2*A(JIP2)
      A(JI)=-ETA
      A(JIP)=-ETA*PSI1
      A(JIP2)=A(JIP2)-ETA*PSI2
 1220 II=IIP+1
      IT=IT+1
      GO TO 60
C
C        END OF ITERATION
C
 1240 IF(DABS(A(NN1))-DABS(A(N1N2))) 1300,1280,1280
C
C        TWO EIGENVALUES HAVE BEEN FOUND
C
 1280 IANA(N)=0
      IANA(N1)=2
      N=N2
      IF(N2)1400,1400,20
C
C        ONE EIGENVALUE HAS BEEN FOUND
C
 1300 RR(N)=A(NN)
      RI(N)=0.0D0
      IANA(N)=1
      IF(N1)1400,1400,1320
 1320 N=N1
      GO TO 20
 1400 RETURN
      END
      FUNCTION DET4(A,B,C,D)
      IMPLICIT REAL*8(A-H,K,O-Z)
      REAL*8 A(4),B(4),C(4),D(4)
      DET4=A(1)*DET3(B(2),C(2),D(2))
     *        -B(1)*DET3(A(2),C(2),D(2))
     *        +C(1)*DET3(A(2),B(2),D(2))
     *        -D(1)*DET3(A(2),B(2),C(2))
      RETURN
      END
      FUNCTION DET3(A,B,C)
      IMPLICIT REAL*8(A-H,K,O-Z)
      REAL*8 A(3),B(3),C(3)
      DET3=A(1)*DET2(B(2),C(2))
     *        -B(1)*DET2(A(2),C(2))
     *        +C(1)*DET2(A(2),B(2))
      RETURN
      END
      FUNCTION DET2(A,B)
      IMPLICIT REAL*8(A-H,K,O-Z)
      REAL*8 A(2),B(2)
      DET2=A(1)*B(2)-A(2)*B(1)
      RETURN
      END
      SUBROUTINE GAUSE(N,A,F,B,M,PREF,BETA,K,WKAREA,IAREA)
      IMPLICIT REAL*8(A-H,O-Z)
      DIMENSION A(N,N+1),B(N+1),PREF(N+1),BETA(N+1),
     * WKAREA(N+1,3),IAREA(N+1,2),F(N)
C SOLUTION OF N LINEAR EQUATIONS FOR N+1 UNKNOWNS
C BASED ON GAUSSIAN ELIMINATION WITH PIVOTING.
C N - NUMBER OF EQUATIONS
C A - N X (N+1) MATRIX OF SYSTEM
C B - RIGHT-HAND SIDES
C M - IF (M.EQ.0) AFTER RETURN THEN RANK(A).LT.N
C PREF(I) - PREFERENCE NUMBER FOR X(I)
C          TO BE INDEPENDENT VARIABLE,
C 0.D0.LE.PREF(I).LE.1.D0,THE LOWER IS PREF(I)
C          THE HIGHER IS
C PREFERENCE OF X(I).
C BETA(I) - COEFFICIENTS IN EXPLICIT DEPENDENCES
C          OBTAINED IN FORM
C          X(I)=B(I)+BETA(I)*X(K),I.NE.K.
C K - RESULTING INDEX OF INDEPENDENT VARIABLE
      N1 = N + 1
      ID = 1
      M = 1
      DO 10 I=1,N1
        IAREA(I,1) = 0
        IAREA(I,2) = 0
   10 CONTINUE
   20 IR = 1
      IS = 1
      AMAX = 0.D0
      DO 60 I=1,N
        IF (IAREA(I,2)) 60,30,60
   30   DO 50 J=1,N1
          P = PREF(J)*DABS(A(I,J))
          IF (P-AMAX) 50,50,40
   40     IR = I
          IS = J
          AMAX = P
   50   CONTINUE
   60 CONTINUE
      IF (AMAX.NE.0.D0) GO TO 70
C     THIS CONDITION FOR SINGULARITY OF
C       MATRIX MUST BE SPECIFIED
C MORE EXACTLY WITH RESPECT TO COMPUTER ACTUALLY USED
      M = 0
      GO TO 150
   70 IAREA(IR,2) = IS
      DO 90 I=1,N
        IF (I.EQ.IR .OR. A(I,IS).EQ.0.D0) GO TO 90
        P = A(I,IS)/A(IR,IS)
        DO 80 J=1,N1
          A(I,J) = A(I,J) - P*A(IR,J)
   80   CONTINUE
        A(I,IS) = 0.D0
        F(I) = F(I) - P*F(IR)
   90 CONTINUE
```

```
      ID = ID + 1
      IF (ID.LE.N) GO TO 20
      DO 100 I=1,N
        IR = IAREA(I,2)
        WKAREA(IR,1) = F(I)/A(I,IR)
        IAREA(IR,1) = 1
  100 CONTINUE
      DO 110 K=1,N1
        IF (IAREA(K,1).EQ.0) GO TO 120
  110 CONTINUE
  120 DO 130 I=1,N
        IR = IAREA(I,2)
        WKAREA(IR,2) = -A(I,K)/A(I,IR)
  130 CONTINUE
      DO 140 I=1,N1
        B(I) = WKAREA(I,1)
        BETA(I) = WKAREA(I,2)
  140 CONTINUE
      B(K) = 0.D0
      BETA(K) = 0.D0
  150 RETURN
      END
      SUBROUTINE NUJACX(FOFX,X,NX,J,ABSDX,
     *      RELDX,WKAREA,IFLAG)
      IMPLICIT REAL*8(A-H,K,O-Z)
      REAL*8 X(NX+1),J(NX,NX+1),WKAREA(NX+1,3)
      IFLAG=0
      P=1.D-13
      DO 10 IX=1,NX+1
     WKAREA(IX,1)=(DABS(X(IX))*RELDX+DABS(ABSDX))/2.D0
  10  CONTINUE
      DO 30 JCOL=1,NX+1
         XSAVE=X(JCOL)
         X(JCOL)=XSAVE-WKAREA(JCOL,1)
         CALL FOFX(NX,X,WKAREA(1,2))
         X(JCOL)=XSAVE+WKAREA(JCOL,1)
         CALL FOFX(NX,X,WKAREA(1,3))
         X(JCOL)=XSAVE
         DO 20 JROW=1,NX
         J(JROW,JCOL)=(WKAREA(JROW,3)-WKAREA(JROW,2))/
     *            (2.D0*WKAREA(JCOL,1))
          IF((DABS(WKAREA(JROW,3)-WKAREA(JROW,2)).LT.
     * P*DMAX1(DABS(WKAREA(JROW,3)),DABS(WKAREA(JROW,2))))
     * .AND.(WKAREA(JROW,3).NE.WKAREA(JROW,2)))
     * IFLAG=JROW
  20     CONTINUE
  30  CONTINUE
      RETURN
      END
      SUBROUTINE NUJAC(FOFX,X,NX,J,ABSDX,RELDX,WKAREA,IFLAG)
      IMPLICIT REAL*8(A-H,K,O-Z)
      REAL*8 X(NX),J(NX,NX),WKAREA(NX,3)
      IFLAG=0
      P=1.D-13
```

```
    DO 10 IX=1,NX
       WKAREA(IX,1)=(DABS(X(IX))*RELDX+DABS(ABSDX))/2.D0
10  CONTINUE
    DO 30 JCOL=1,NX
       XSAVE=X(JCOL)
       X(JCOL)=XSAVE-WKAREA(JCOL,1)
       CALL FOFX(NX,X,WKAREA(1,2))
       X(JCOL)=XSAVE+WKAREA(JCOL,1)
       CALL FOFX(NX,X,WKAREA(1,3))
       X(JCOL)=XSAVE
       DO 20 JROW=1,NX
       J(JROW,JCOL)=(WKAREA(JROW,3)-WKAREA(JROW,2))/
   *                     (2.D0*WKAREA(JCOL,1))
      IF((DABS(WKAREA(JROW,3)-WKAREA(JROW,2)).LT.
   *  P*DMAX1(DABS(WKAREA(JROW,3)),DABS(WKAREA(JROW,2))))
   * .AND.(WKAREA(JROW,3).NE.WKAREA(JROW,2)))
   *  IFLAG=JROW
20     CONTINUE
30  CONTINUE
    RETURN
    END
```